

# Oceanologia

Official Journal of the Polish Academy of Sciences: Institute of Oceanology and Committee on Maritime Research



## EDITOR-IN-CHIEF

Janusz Pempkowiak  
Institute of Oceanology Polish Academy of Sciences, Sopot, Poland

## MANAGING EDITOR

Agata Bielecka - abielecka@iopan.gda.pl

## Editorial Office Address

Institute of Oceanology Polish Academy of Sciences (IO PAN)  
Powstańców Warszawy 55  
81-712 Sopot, Poland  
Mail: pempa@iopan.gda.pl

## THEMATIC EDITORS

Alicja Kosakowska – Institute of Oceanology Polish Academy of Sciences, Sopot, Poland  
Stanisław Massel – Institute of Oceanology Polish Academy of Sciences, Sopot, Poland  
Jan Marcin Węśławski – Institute of Oceanology Polish Academy of Sciences, Sopot, Poland  
Marek Zajączkowski – Institute of Oceanology Polish Academy of Sciences, Sopot, Poland  
Tymon Zieliński – Institute of Oceanology Polish Academy of Sciences, Sopot, Poland

## ADVISORY BOARD

### Prof. Jerzy Dera

Institute of Oceanology Polish Academy of Sciences (IO PAN), Sopot, Poland

### Prof. Howard Gordon

Dept. of Physics, University of Miami, USA

### Prof. Genrik Sergey Karabashev

P.P. Shirshov Institute of Oceanology RAS, Moscow, Russia

### Prof. Zygmunt Kowalik

Institute of Marine Science, School of Fisheries and Ocean Sciences, University of Alaska Fairbanks (UAF), USA

### Prof. Matti Leppäranta

Department of Physics, University of Helsinki, Finland

### Prof. Gennady Matishov

Murmansk Marine Biological Institute KSC, Russian Academy of Sciences (MMBI KSC RAS), Russia

### Prof. Sergej Olenin

Coastal Research and Planning Institute, Klaipeda University CORPI, Lithuania

### Prof. Anders Omstedt

University of Gothenburg, Dept. Earth Sciences: Oceanography, Gothenburg, Sweden

### Prof. Janusz Pempkowiak

Institute of Oceanology Polish Academy of Sciences (IO PAN), Sopot, Poland

### Prof. Marcin Pliński

Institute of Oceanography, University of Gdańsk, Gdynia, Poland

### Prof. Xosé Antón Álvarez Salgado

Department of Oceanography, Marine Research Institute, Spanish Research Council (CSIC), Spain

### Prof. Tarmo Soomere

Institute of Cybernetics, Tallinn University of Technology, Tallinn, Estonia

### Prof. Hans von Storch

Institute for Coastal Research, Helmholtz Zentrum Geesthacht, Germany

### Prof. Dariusz Stramski

Marine Physical Laboratory, Scripps Institution of Oceanography, University of California, San Diego, USA

### Prof. Juergen Suendermann

Institut für Meereskunde, Universität Hamburg, Hamburg, Germany

### Prof. Piotr Szefer

Department of Food Sciences, Medical University of Gdańsk, Gdańsk, Poland

### Prof. Antoni Śliwiński

Institute of Experimental Physics, University of Gdańsk, Gdańsk, Poland

### Prof. David Turner

Department of Chemistry and Molecular Biology, University of Gothenburg, Sweden

### Prof. Bogdan Woźniak

Institute of Oceanology Polish Academy of Sciences (IO PAN), Sopot, Poland

### Prof. Ronald Zaneveld

Western Environmental Technology Laboratories, Philomath, USA

This journal is supported by the Ministry of Science and Higher Education, Warsaw, Poland

Indexed in: ISI Journal Master List, Science Citation Index Expanded, Scopus, Current Contents, Zoological Record, Thomson Scientific SSCI, Aquatic Sciences and Fisheries Abstracts, DOAJ

IMPACT FACTOR ANNOUNCED FOR 2014 IN THE 'JOURNAL CITATION REPORTS' IS 1.000; 5-year IF – 1.346

## Publisher

Elsevier Sp. z o.o. 4/59,  
02-796 Warsaw, Poland  
Tel. +48 22 546 38 20, Fax. +48 22 546 38 21

## Director of Journals Publishing

Ewa Kittel-Prejs

## Publishing Manager

Agnieszka Pawłowska  
a.pawlowska@elsevier.com

## Marketing & Promotion Manager

Anna Szkolūt  
a.szkolūt@elsevier.com  
48 22 546 38 40, 48 515 090 174

## Publishing Editor

Joanna Lewczuk  
j.lewczuk@elsevier.com  
48 515 082 585, 48 22 546 38 24

## Subscription and Distribution Manager

Jacek Sołtyk  
prenumerata@elsevier.com  
48 22 546 38 27, 48 510 134 282

## Advertising Pharma Solutions

Monika Giergiełewicz  
m.giergielewicz@elsevier.com  
48 519 130 280

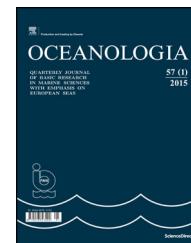
ISSN 0078-3234



Available online at [www.sciencedirect.com](http://www.sciencedirect.com)

ScienceDirect

journal homepage: [www.elsevier.com/locate/oceano](http://www.elsevier.com/locate/oceano)



ORIGINAL RESEARCH ARTICLE

# New simple statistical formulas for estimating surface concentrations of suspended particulate matter (SPM) and particulate organic carbon (POC) from remote-sensing reflectance in the southern Baltic Sea<sup>☆</sup>

Sławomir B. Woźniak<sup>a,\*</sup>, Mirosław Darecki<sup>a</sup>, Monika Zabłocka<sup>a</sup>,  
Dorota Burska<sup>b</sup>, Jerzy Dera<sup>a</sup>

<sup>a</sup> Institute of Oceanology, Polish Academy of Sciences, Sopot, Poland

<sup>b</sup> Institute of Oceanography, University of Gdańsk, Gdynia, Poland

Received 8 January 2016; accepted 25 March 2016

Available online 15 April 2016

## KEYWORDS

Remote-sensing reflectance;  
Light backscattering;  
Suspended particulate matter;  
Particulate organic carbon;  
Empirical formulas;  
Southern Baltic surface water

**Summary** In a step taken towards improving the new system for the satellite monitoring of the Baltic Sea environment, officially started in Poland recently (*SatBałtyk System*, see <http://www.satbaaltyk.pl>), a new set of simple statistical formulas was derived. These combine the empirically determined spectral values of remote-sensing reflectance  $R_{rs}(\lambda)$  with the mass concentrations of suspended particulate matter (SPM) and particulate organic carbon (POC) in southern Baltic surface waters. The new formulas are based on 73 empirical data sets gathered during 4 research cruises on board r/v *Oceania* during spring and late summer in the open waters of the southern Baltic and coastal regions of the Gulf of Gdańsk. Correlations of SPM and POC concentrations with reflectance or reflectance ratios in various spectral bands were tested. Several variants of candidate statistical relationships, which can be used later in the construction of simple local remote sensing algorithms for the waters in question, are introduced here. These relationships utilise either absolute values of  $R_{rs}$  at a selected waveband, mostly from the yellow, red or near

<sup>☆</sup> Financial support for this research was provided by the 'SatBałtyk' project funded by the European Union through the European Regional Development Fund (contract No. POIG.01.01.02-22-011/09 entitled 'The Satellite Monitoring of the Baltic Sea Environment'), and by Statutory Research Programme at the Institute of Oceanology, Polish Academy of Sciences (themes No. I.1 and II.5).

\* Corresponding author at: Institute of Oceanology, Polish Academy of Sciences, Powstańców Warszawy 55, 81-712 Sopot, Poland. Tel.: +48 58 7311812.

E-mail address: [woznjr@iopan.gda.pl](mailto:woznjr@iopan.gda.pl) (S.B. Woźniak).

Peer review under the responsibility of Institute of Oceanology of the Polish Academy of Sciences.



Production and hosting by Elsevier

<http://dx.doi.org/10.1016/j.oceano.2016.03.002>

0078-3234/© 2016 Institute of Oceanology of the Polish Academy of Sciences. Production and hosting by Elsevier Sp. z o.o. This is an open access article under the CC BY-NC-ND license (<http://creativecommons.org/licenses/by-nc-nd/4.0/>).

infrared part of the light spectrum, or  $R_{rs}$  ratios for two different wavebands, mostly ratios of blue to yellow, blue to red and blue to infrared or green to yellow and green to red spectral band. From the numerous simple approximate relationships established, the following two, characterised by large correlation coefficients  $r^2$  and small standard error factors  $X$ , may serve as examples: SPM [ $\text{g m}^{-3}$ ] =  $1480(R_{rs}(710))^{0.902}$  (with the factors  $r^2 = 0.86$ ;  $X = 1.26$ ) (the unit of  $R_{rs}(\lambda)$  is [ $\text{sr}^{-1}$ ]) and POC [ $\text{g m}^{-3}$ ] =  $0.814(R_{rs}(555)/R_{rs}(589))^{-4.42}$  ( $r^2 = 0.75$ ;  $X = 1.37$ ). From the practical standpoint, taking into consideration light wavelengths that are close to or concurrent with the currently available spectral bands used in satellite observations of the Baltic Sea, another two formulas (using the same spectral ratio) are worth pointing out: SPM [ $\text{g m}^{-3}$ ] =  $2.6(R_{rs}(490)/R_{rs}(625))^{-1.29}$  ( $r^2 = 0.86$ ;  $X = 1.25$ ) and POC [ $\text{g m}^{-3}$ ] =  $0.774(R_{rs}(490)/R_{rs}(625))^{-1.18}$  ( $r^2 = 0.66$ ;  $X = 1.44$ ). The paper also presents a number of intermediate statistical relationships between SPM and POC concentrations,  $R_{rs}$  spectra and light backscattering coefficients in order to illustrate the simplified physical justification for some of the observed direct statistical relationships, presented as the main content of this work.

© 2016 Institute of Oceanology of the Polish Academy of Sciences. Production and hosting by Elsevier Sp. z o.o. This is an open access article under the CC BY-NC-ND license (<http://creativecommons.org/licenses/by-nc-nd/4.0/>).

## 1. Introduction

In recent decades there has been significant progress in passive remote-sensing techniques that retrieve information on seawater composition imprinted in the colour of oceans and seas (see, for example, a series of reports by [International Ocean-Colour Coordination Group – IOCCG Report 16 \(2015\)](#) or earlier reports and the references cited therein). To make full use of the potential of these techniques, there is obviously a need to mathematically relate the quantity that describes sea colour precisely, i.e. the remote-sensing reflectance, with the various biogeochemical characteristics describing the concentrations and composition of substances present in surface waters. In practice this can be done in many ways, either directly or indirectly by using the water's inherent optical properties (IOPs) as a “link” between the sea's colour and biogeochemistry. One of the biogeochemical characteristics most often studied with remote sensing techniques is the concentration of chlorophyll  $a$ , the quantity used as the basic measure of phytoplankton biomass. Other substances that are also important indicators of different processes taking place in seawater and at the same time influence its colour include phytoplankton pigments other than chlorophyll  $a$ , chromophoric dissolved organic matter (CDOM), suspended particulate matter (SPM) of both organic and inorganic origin, and the main chemical elements from which organic matter is constructed, e.g. carbon. Hence it is mainly the relationships between the concentrations of these substances/elements and the remote-sensing reflectance, often specific to particular seas, that are investigated.

The application of remote-sensing techniques in the Baltic region started in the 1970s (when the first oceanographic satellites became available) and has intensified in the last 20 years. This problem has been addressed by different scientific groups from many countries, not just from states around the Baltic Sea (detailed literature surveys on this topic can be found, for example, in book chapters by [Siegel and Gerth \(2008\)](#), [Berthon et al. \(2008\)](#) or [Kratzer et al. \(2011\)](#); see also [Arst \(2003\)](#)). The brackish waters of the semi-enclosed shelf basin of the Baltic Sea are optically very complex. These waters belong to a broad category of Case

2 waters (according to the classification of [Morel and Prieur \(1977\)](#)), the optical properties of which do not depend only on phytoplankton and its by-products. In Case 2 waters an important role may be also played by suspended matter and CDOM, which generally do not co-vary with chlorophyll  $a$  concentration. Indeed, Baltic waters are an exceptional example of Case 2 waters, since they are much richer in both allogenic and autogenic CDOM than other shelf seas (see e.g. [Kowalczyk \(1999\)](#)). Consequently, optical relationships, models and algorithms derived as being either universal/global, or even local but for other marine environments, are often unsuitable for Baltic Sea remote sensing (see e.g. a work by [Darecki and Stramski \(2004\)](#), in which the performances of different chlorophyll  $a$  algorithms in the Baltic Sea are compared). The derivation of local algorithms thus appears to be indispensable. In the last 10 years or so, the application of neural network algorithms has become a common practical approach to the remote sensing of the Baltic and other European seas (see e.g. [Doerffer and Schiller \(2006\)](#)). Such algorithms use the artificial neural network inversion procedure to derive various independently varying in-water constituents, such as chlorophyll  $a$  (or pigment index), SPM and CDOM. The input for such algorithms is usually multispectral information (specific to the satellite sensors under consideration) on either top of atmosphere radiances or remote sensing reflectances. Recent evaluations and comparisons of different variants of such algorithms applied to Baltic data acquired using a medium resolution imaging spectrometer (MERIS) can be found, for example, in [Beltran-Abaunza et al. \(2014\)](#) or [D'Alimonte et al. \(2014\)](#). Another observation from the literature survey may be that particulate organic carbon (POC) has not yet become a common ocean colour data product for the Baltic Sea region, despite the already demonstrated fact that SPM can be treated as its effective tracer ([Ferrari et al., 2003](#)).

In common with many other scientific groups and institutions working on the optics of Baltic Sea waters, a group of scientists from Poland has also been deeply involved in this topic in recent decades ([Dera and B. Woźniak, 2010](#) and the extensive list of citations therein). The Polish team has also undertaken comprehensive studies with the aim of developing

practical methods for the remote sensing of this demanding marine environment (see e.g. Darecki et al., 2008; B. Woźniak et al., 2008, 2011a,b; M. Woźniak et al., 2014). The *SatBaltyk System*<sup>1</sup>, a new complex system for the satellite monitoring of the Baltic Sea developed by this research team (B. Woźniak et al., 2011a,b), was officially inaugurated in Poland recently. In order to expand the set of its existing algorithm formulas, new studies focusing on different characteristics of suspended matter are being conducted by the authors of this and a previous paper (S.B. Woźniak, 2014). The latter paper presented the first set of simple local empirical formulas for the southern Baltic area. Among other things, these formulas enable the mass concentration of suspended particulate matter (SPM) or particulate organic carbon (POC) to be estimated as a function of selected seawater IOPs, such as the coefficient of light backscattering by suspended particles  $b_{bp}(\lambda)$  or the coefficient of light absorption by the sum of all substances suspended and dissolved in seawater  $a_n(\lambda)$ . Such formulas can be applied as the final step in a local empirical multistage algorithm for estimating the biogeochemical characteristics of suspended substances. Obviously, coefficients  $b_{bp}$  and/or  $a_n$  have first to be estimated from remote-sensing reflectance spectra  $R_{rs}(\lambda)$ . In the previous work (S.B. Woźniak, 2014) it was suggested that SPM and POC concentrations could be estimated in a relatively simple way as direct functions of  $R_{rs}(\lambda)$ , mostly for red wavelengths of light. But this suggestion was based solely on analyses of modelled reflectance spectra obtained as a result of simplified radiative energy transfer modelling. Moreover, these analyses were performed only for a limited number of light wavebands.

The main objective of the current work was to use the newly acquired empirical data to establish a new, improved set of statistical formulas that would enable SPM and also POC concentrations in southern Baltic Sea surface waters to be estimated simply and directly on the basis of spectral values of the remote-sensing reflectance  $R_{rs}(\lambda)$  at chosen wavelength or from reflectance spectral ratio. The  $R_{rs}(\lambda)$  data used for these analyses are determined from in situ optical measurements performed at over a dozen of spectral bands covering the range from UV, through visible, to near infrared. The analyses presented here are not limited only to the bands corresponding to current or past satellite sensors. On the contrary, all the available spectral information is used. The new simple statistical formulas established in this way, together with our earlier results (S.B. Woźniak et al., 2014), can later serve as elements for constructing new local empirical remote sensing algorithms.

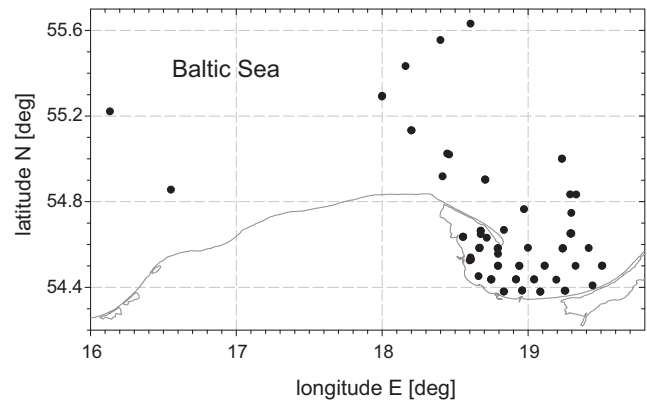


Figure 1 Location of the sampling stations in the southern Baltic Sea.

## 2. Material and methods

The empirical measurements used in this work were performed during 4 research cruises of *r/v Oceania* in spring and late summer (April and September 2011, September 2012 and May 2013), at 73 sampling stations. The positions of these sampling stations in the open waters of the southern Baltic Sea and in the Gulf of Gdańsk are shown in Fig. 1.

### 2.1. Analyses of SPM and POC concentrations

Discrete water samples for laboratory analyses of the biogeochemical properties of suspended matter were taken from the surface layer (ca 1 m depth) in 20 L Niskin bottles. In general, we applied the same laboratory methods as those we had used and described previously (see S.B. Woźniak et al. (2011, 2014)). The concentration of suspended particulate matter (SPM), defined as the dry mass of particles per unit volume of seawater and expressed in  $[g\ m^{-3}]$ , was determined using a standard gravimetric technique. We used specially prepared GF/F filters (25 mm diameter) pre-combusted at 450°C for 4 h, pre-washed with pure deionised and particle-free water (to prevent the loss of filter material during the filtration of the main sample), then dried and pre-weighed. Measured volumes of seawater (generally between 150 and 1000 mL) were filtered immediately after sample collection. At the end of filtration, the filters were rinsed with about 30 mL of deionised water to remove sea salt (the salinity of our samples was on average 6.7, and did not exceed 7.3). The filters together with their particle load were dried and stored in a freezer for later analysis at the land-based laboratory. The dry mass of particles collected on the filters was measured with a Radwag WAX110 microbalance (resolution 0.01 mg). Three replicate filters were measured in each sample. The reproducibility of replicates (defined as the ratio of the standard deviation to the average value and expressed as a percentage) was on average 6%; for 90% of individual samples it was no greater than 13%.

The concentration of particulate organic carbon (POC), expressed in  $[g\ m^{-3}]$ , was determined by high temperature combustion. Samples were collected at sea by filtration in the same way as for the SPM analyses, by using separate sets of pre-combusted GF/F filters (three replicates per water sample). The filters were dried and stored until later analysis at

<sup>1</sup> The *SatBaltyk System* has been developed within the framework of the project entitled “The Satellite Monitoring of the Baltic Sea Environment” (Project No. POIG.01.01.02-22-011/09). The project is being implemented within the framework of the Innovative Economy Operational Programme, Priority axis 1: Research and development of modern technologies, Action 1.1: Supported scientific research for the construction of a knowledge-based economy. Executors of the project are the Institute of Oceanology, Polish Academy of Sciences, Sopot (coordinator); the Institute of Oceanography, University of Gdańsk; the University of Szczecin; and the Pomeranian Academy, Słupsk.

the land-based laboratory with a Perkin Elmer CHN 2400 instrument. The reproducibility of the POC replicate measurements was on average 11%; for 90% of individual samples it was no greater than 26%.

## 2.2. Determination of remote-sensing reflectance

Values of the remote-sensing reflectance  $R_{rs}(\lambda)$  [ $\text{sr}^{-1}$ ] were obtained from vertical profiles of the spectral upward radiance  $L_u(z, \lambda)$  (measured in water) and the spectral downward irradiance  $E_d(0^+, \lambda)$  (above the sea surface) measured simultaneously. These quantities were measured in 17 spectral channels (centred at wavelengths  $\lambda$  of 340, 380, 395, 412, 443, 465, 490, 510, 532, 555, 565, 589, 625, 665, 683, 710 and 765 nm) with a Compact Optical Profiling System (C-OPS) (Biospherical Instruments Inc.).  $R_{rs}(\lambda)$  was calculated as the ratio of the water-leaving radiance just above the water surface  $L_w(0^+, \lambda)$  to the downward irradiance measured above the water  $E_d(0^+, \lambda)$ . The water-leaving radiance  $L_w(0^+, \lambda)$  was obtained from estimated values of the upward radiance just below the water surface  $L_u(0^-, \lambda)$ , which were propagated through the water–air interface using a factor of 0.544 calculated from the “ $n^2$  law for radiance” (see e.g. Mobley (1994)). Thus, the practical formula for  $R_{rs}(\lambda)$  is as follows:

$$R_{rs}(\lambda) = \frac{L_w(0^+, \lambda)}{E_d(0^+, \lambda)} = 0.544 \frac{L_u(0^-, \lambda)}{E_d(0^+, \lambda)}. \quad (1)$$

To obtain  $L_u(0^-, \lambda)$ , measurements of the profiles of upwelling radiance  $L_u(z, \lambda)$  were extrapolated from a subsurface layer of 0.5–2 m to a depth “just below the sea surface” (“0<sup>-</sup>”) using the attenuation coefficient for upward radiance  $K_{Lu}(z, \lambda)$ , calculated as the local slope of  $\ln[L_u(z, \lambda)]$  measured over a depth interval spanning a few metres in the surface layer. The thickness of this depth interval depended on the extent to which the surface layer was homogeneous (typically about 3 m). The correction for the self-shading effect in the upward radiance just below the sea surface  $L_u(0^-, \lambda)$  was also applied to all data according to Gordon and Ding (1992) and Zibordi and Ferrari (1995). The C-OPS system was equipped with a shadow band radiometer, and ratios of the direct to diffuse light used in the self-shading corrections were determined using this system as well.

## 2.3. Light backscattering measurements

The light backscattering coefficients of  $b_b(\lambda)$  [ $\text{m}^{-1}$ ] were estimated from in situ measurements performed in the surface layer (ca 1 m depth) using a spectral backscattering meter (HOBI Labs Hydroscat-4 instrument) at four light wavelengths (420, 488, 550 and 620 nm). The raw data from the instrument, i.e. the volume scattering functions at an angle of 140°, were used for estimating  $b_b(\lambda)$  according to the method described in Maffione and Dana (1997) and Dana and Maffione (2002). A correction for the incomplete recovery of backscattered light in highly attenuating waters (the so-called sigma-correction) was applied in accordance with the instrument User’s Manual (HOBI Labs, 2008) using data on absorption and attenuation coefficients measured with a separate instrument (WET Labs ac-9). To obtain the backscattering coefficients of particles,  $b_{bp}(\lambda)$  [ $\text{m}^{-1}$ ], the

theoretical values of the backscattering coefficient of pure water were subtracted according to Morel (1974).

## 2.4. Measurements of additional biogeochemical parameters

This work also refers to biogeochemical parameters describing the variability of the seawater samples other than SPM and POC concentrations. They are the concentration of the organic fraction of SPM, i.e. particulate organic matter (POM) and the concentration of the main photosynthetic pigment, chlorophyll *a* (Chl *a*) (additional measurements also followed protocols described in more detail in S.B. Woźniak et al. (2011)). To determine the POM concentration, the same GF/F filters utilised earlier for SPM concentration analyses were placed in a furnace, kept there for 4 h at a temperature of 450°C and then re-weighed. The POM concentration was calculated from the loss of mass of the sample retained by the filter. Here, the total chlorophyll *a* concentration (Chl *a*) was represented by the sum of chlorophyll *a*, allomer and epimer, chlorophyllide *a* and phaeophytin *a*; it was determined with the use of high performance liquid chromatography (HPLC).

## 2.5. Statistical analyses

The empirical data were statistically analysed, as a result of which approximate relationships between the target quantities were obtained. These simple relationships take the form of best-fit power functions ( $y = C_1 x^{C_2}$ ), found using least square linear regression applied to log-transformed variables. For each formula established in this way we give the square of the correlation coefficient  $r^2$  calculated for log-transformed variables and also a set of the standard statistical descriptors of estimation errors, such as the root mean square error between observed and predicted values (RMSE), the mean normalised bias (MNB) and the normalised root mean square error (NRMSE). All these standard descriptors will be given later in the relevant tables for readers who would like to compare our results with others published in the literature. But since the fitting was performed on log-transformed variables, when discussing the quality of the fit we also present and pay special attention to another statistical quantity, the standard error factor  $X$ . Being an element of so-called logarithmic statistics, this can be determined according to the formula:

$$X = 10^{\sigma_{\log}}; \sigma_{\log} = \left[ \frac{1}{n-1} \sum_{i=1}^n \left( \log \left( \frac{P_i}{O_i} \right) - \frac{1}{n} \sum_{j=1}^n \log \left( \frac{P_j}{O_j} \right) \right)^2 \right]^{1/2}, \quad (2)$$

where  $P_i$  stands for values predicted using the approximate formula,  $O_i$  represents empirical values and  $n$  is the number of samples. The standard error factor  $X$  allows one to quantify the range of the statistical error calculated according to logarithmic statistics. This range extends from the value of  $\sigma_- = (1/X) - 1$  to the value of  $\sigma_+ = X - 1$ . Note also, that because of the method used for data approximation (linear regression applied to the log-transformed variables), the systematic error according to logarithmic statistics is always equal to 0; for this reason we make no further mention of it.

**Table 1** Variability ranges of selected biogeochemical characteristics of suspended particulate matter in surface water samples and selected optical properties of water at stations from the southern Baltic Sea analysed in this paper.

Quantity	Minimum value	Maximum value	Average value	Standard deviation (coefficient of variation)	Number of samples
SPM [ $\text{g m}^{-3}$ ]	0.568	9.81	1.77	1.59 (90%)	73
POC [ $\text{g m}^{-3}$ ]	0.145	2.37	0.555	0.438 (79%)	73
POM [ $\text{g m}^{-3}$ ]	0.447	5.39	1.41	0.961 (68%)	73
Chl <i>a</i> [ $\text{mg m}^{-3}$ ]	0.442	36.1	5.79	7.39 (128%)	71
POC/SPM [g:g]	0.16	0.563	0.322	0.073 (23%)	73
POM/SPM [g:g]	0.506	1.05	0.859	0.127 (15%)	73
Chl <i>a</i> /SPM [g:g]	$6.94 \times 10^{-4}$	$9.19 \times 10^{-3}$	$3.02 \times 10^{-3}$	$1.56 \times 10^{-3}$ (52%)	71
$b_{bp}(488)$ [ $\text{m}^{-1}$ ]	$2.7 \times 10^{-3}$	$8.58 \times 10^{-2}$	$1.27 \times 10^{-2}$	$1.27 \times 10^{-2}$ (100%)	73
$b_{bp}(620)$ [ $\text{m}^{-1}$ ]	$2.06 \times 10^{-3}$	$8.17 \times 10^{-2}$	$1.03 \times 10^{-2}$	$1.19 \times 10^{-2}$ (115%)	73
$R_{rs}(490)$ [ $\text{sr}^{-1}$ ]	$1.12 \times 10^{-3}$	$2.84 \times 10^{-3}$	$1.71 \times 10^{-3}$	$3.47 \times 10^{-4}$ (20%)	73
$R_{rs}(625)$ [ $\text{sr}^{-1}$ ]	$4.12 \times 10^{-4}$	$5.12 \times 10^{-3}$	$1.19 \times 10^{-3}$	$7.44 \times 10^{-4}$ (62%)	73
$R_{rs}(710)$ [ $\text{sr}^{-1}$ ]	$1.63 \times 10^{-4}$	$4.11 \times 10^{-3}$	$5.81 \times 10^{-4}$	$6.08 \times 10^{-4}$ (105%)	73

### 3. Results and discussion

#### 3.1. General characterisation of the empirical dataset

The empirical material, though not large in terms of sample number ( $n = 73$ ) and having been acquired only in spring and late summer, is characterised by a relatively large variability in the target biogeochemical and optical quantities (see Table 1) (this is undoubtedly a consequence of measurements and water sampling performed over different coastal and open sea areas). Both the absolute mass concentration of suspended particulate matter (SPM) and the concentration of organic carbon (POC), the latter an important constituent of the organic fraction of suspended matter, varied over more than one order of magnitude in terms of the maximum to minimum range. The corresponding coefficients of variation CV (defined as the ratio of the standard deviation to the average value) were 90% for SPM and 79% for POC. The concentration of chlorophyll *a* (Chl *a*) in our samples varied even more: the CV was almost 130%. In contrast, the changes in the proportions (ratios) of these biogeochemical quantities were relatively small. Such ratios may help to characterise the variability in suspended matter composition. For example, the average ratio of POC to SPM was 0.32, but its variability, characterised by CV, was only 23%. In the case of the POM to SPM ratio, the average value was 0.86, and the corresponding CV was 15%. These values show that in all the water samples, SPM was dominated by matter of organic origin. This is characteristic of the surface waters of the southern Baltic Sea (see e.g. S.B. Woźniak et al. (2011)). The variability of the optical quantities was also significant: that of the backscattering coefficients of particles  $b_{bp}(\lambda)$  was substantial over the entire spectral range. For  $\lambda = 488$  nm the maximum to minimum variation was more than 30-fold, while for  $\lambda = 620$  nm it was more than 40-fold. The corresponding CVs were 100% and 115% respectively. The variability of the remote-sensing reflectance  $R_{rs}(\lambda)$ , a quantity influenced by both suspended and dissolved substances in seawater, was spectrally diverse: it was the smallest in the bands of the blue part of the spectrum (e.g. CV = 20% for  $R_{rs}(490)$ ), and distinctively larger in the bands of the red and infrared parts of

the spectrum (e.g. CV of 62% for  $R_{rs}(625)$  and 105% for  $R_{rs}(710)$ ). The complete set of remote-sensing reflectance spectra that we registered in the southern Baltic Sea is presented in Fig. 2a. An important observation regarding the nature of the spectral variability of  $R_{rs}(\lambda)$  may be made if we normalise the values of that quantity by dividing them by SPM concentration or the coefficient  $b_{bp}$ . Two sets of curves normalised in this way are presented in panels b and c in Fig. 2. While the absolute values of  $R_{rs}(\lambda)$  varied mostly in the  $\lambda > 600$  nm range, the variability of the normalised curves within that spectral range was the smallest. For example, the CVs calculated for the normalised value of  $R_{rs}(\lambda)/\text{SPM}$  at bands 625 and 710 nm were only 27% and 23%, whereas at 490 nm CV was as high as 45%. All this generally agrees with the qualitative expectation that in the spectral range of red and infrared light, the SPM concentration should exert the greatest influence on the absolute values of reflectance  $R_{rs}$  (through light backscattering), whereas the influence of light absorption by CDOM in this spectral range is small and negligible. Hence, the spectral bands from the red and infrared parts of the spectrum should be the most suitable for establishing simple statistical relationships between  $R_{rs}$  and  $b_{bp}$  or SPM concentration.

#### 3.2. Statistical formulas

The statistical analyses yielded two separate sets of several different spectral variants of formulas, which enable the SPM and POC concentrations to be roughly estimated on the basis of either the absolute values of remote-sensing reflectance or the reflectance ratios at two spectral bands. These formulas are presented in tabular form and will be discussed in detail later in the text. At this point, it should be mentioned that these tables contain not only the best spectral variants from the statistical point of view, but also other ones, slightly inferior but still, we believe, acceptably accurate. This has been done deliberately, in order to give potential users of our formulas the opportunity to select the spectral variant in accordance with the measurement or data collection techniques that are available to them.

Table 2 contains formulas that permit a rough estimate of SPM and POC concentrations based on absolute values of the

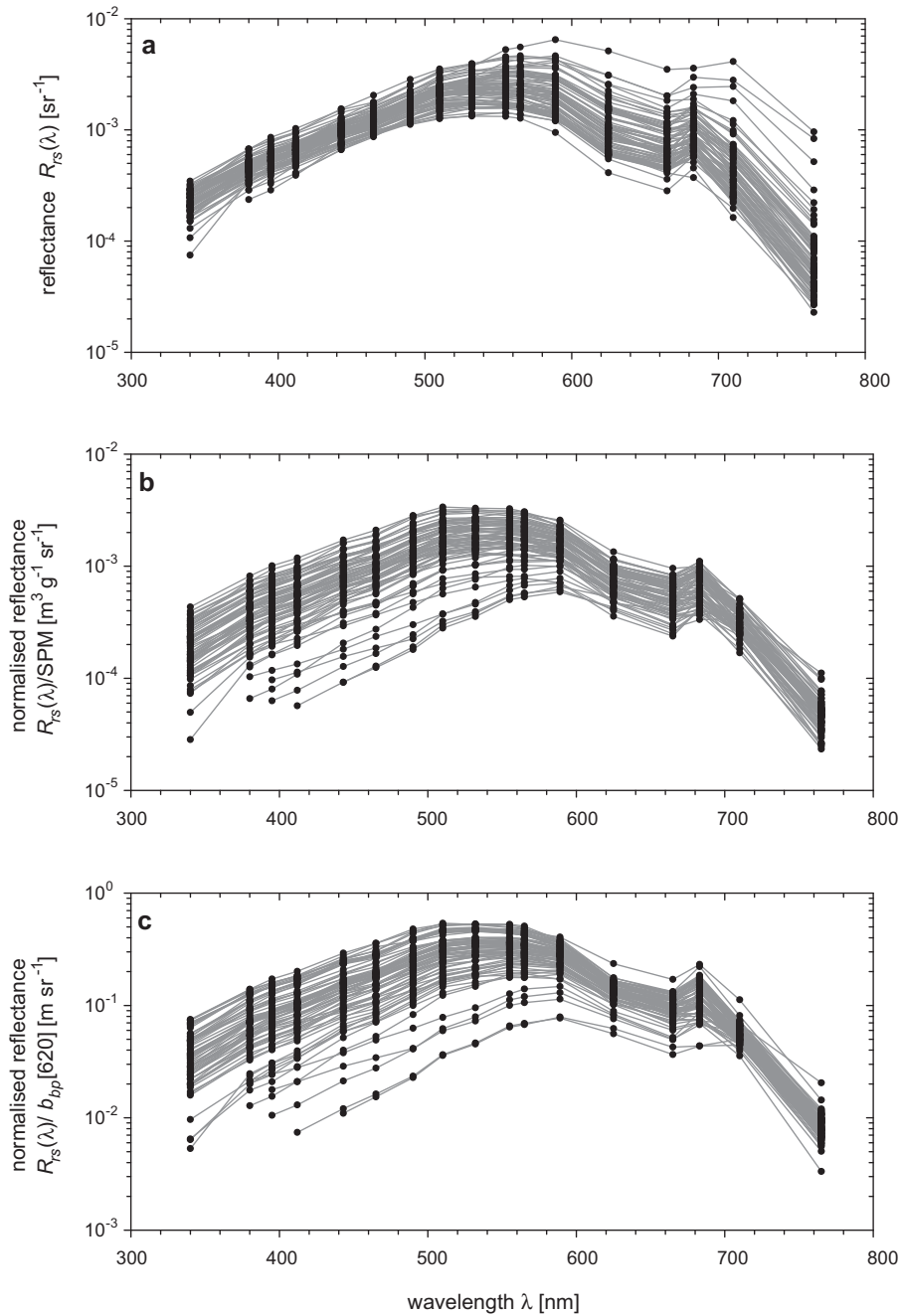


**Figure 2** Empirically derived spectra of remote-sensing reflectance  $R_{rs}(\lambda)$  (a) and the same spectra normalised to values of SPM (b) or  $b_{bp}(620)$  (c) for all ( $n = 73$ ) the sampling stations analysed in this work.

remote-sensing reflectance  $R_{rs}(\lambda_i)$  at the chosen spectral band. The different spectral variants in Table 2 all satisfy the following condition: the correlation coefficient  $r^2$  calculated for the relationship between the logarithms of the empirical variables under consideration (e.g. between  $\log(\text{SPM})$  and  $\log(R_{rs}(555))$ ) has to be equal to or greater than 0.5. Based on this criterion, we obtained a listing suggesting that for rough estimates of the SPM concentration one can use as many as 8 of the 17 spectral bands analysed. These are all bands available from the 555–765 nm range. The corresponding standard error factors  $X$  for these formulas range from 1.26 to 1.51. The same criterion applied to POC vs.  $R_{rs}(\lambda_i)$  relationships leads to the selection of only 4 spectral

variants, which use bands of 589, 625, 710 and 765 nm. The standard error factors  $X$  for the latter formulas lie between 1.47 and 1.53. Four examples selected from among all the formulas in Table 2 are presented graphically in Fig. 3. The first two examples (Fig. 3a and c) represent formulas using the spectral band at 710 nm. These formulas have the highest correlation coefficients  $r^2$  and the lowest standard error factors  $X$  within each group:

$$\text{SPM} = 1480(R_{rs}(710))^{0.902} \quad (r^2 = 0.86; X = 1.26), \quad (3)$$

$$\text{POC} = 222(R_{rs}(710))^{0.807} \quad (r^2 = 0.63; X = 1.47). \quad (4)$$

**Table 2** The best-fit power functions ( $y = C_1 x^{C_2}$ ) between the concentration of suspended particulate matter SPM or the concentration of particulate organic carbon POC and the absolute magnitude of remote-sensing reflectance  $R_{rs}(\lambda)$  for different spectral bands. The square of the correlation coefficient  $r^2$  (between the log-transformed variables), root mean square error RMSE<sup>a</sup>, mean normalised bias MNB<sup>b</sup>, normalised root mean square error NRMSE<sup>c</sup>, standard error factor  $X$  and number of samples  $n$  are also given for each fitted function. Examples discussed in more detail in the text are marked in bold.

Relationship	$C_1$	$C_2$	$r^2$	RMSE [ $\text{g m}^{-3}$ ]	MNB [%]	NRMSE [%]	$X$	$n$
SPM vs. $R_{rs}(555)$	$7.52 \times 10^3$	1.42	0.54	1.23	7.9	39.3	1.51	73
SPM vs. $R_{rs}(565)$	$7.66 \times 10^5$	1.42	0.60	1.15	7.0	37.6	1.47	73
SPM vs. $R_{rs}(589)$	$4.94 \times 10^3$	1.32	0.74	0.915	4.7	31.4	1.36	73
<b>SPM vs. <math>R_{rs}(625)</math></b>	$2.51 \times 10^3$	1.09	<b>0.78</b>	0.72	3.9	28.8	<b>1.33</b>	73
SPM vs. $R_{rs}(665)$	$4.22 \times 10^3$	1.11	0.72	0.813	4.9	32.1	1.38	73
SPM vs. $R_{rs}(683)$	$7.33 \times 10^3$	1.23	0.73	0.697	4.9	32.3	1.37	73
<b>SPM vs. <math>R_{rs}(710)</math></b>	$1.48 \times 10^3$	0.902	<b>0.86</b>	0.383	3.6	22.9	<b>1.26</b>	73
SPM vs. $R_{rs}(765)$	$2 \times 10^3$	0.754	0.83	0.502	3.0	24.5	1.29	73
POC vs. $R_{rs}(589)$	$6.97 \times 10^2$	1.19	0.55	0.3	9.6	51.8	1.53	73
<b>POC vs. <math>R_{rs}(625)</math></b>	$3.46 \times 10^2$	0.97	<b>0.57</b>	0.281	9.1	50.1	<b>1.51</b>	73
<b>POC vs. <math>R_{rs}(710)</math></b>	$2.22 \times 10^2$	0.807	<b>0.63</b>	0.239	7.6	43.0	<b>1.47</b>	73
POC vs. $R_{rs}(765)$	$2.85 \times 10^2$	0.672	0.61	0.246	8.0	44.3	1.49	73

$$^a \text{RMSE} = \left[ \frac{1}{n-1} \sum_{i=1}^n (P_i - O_i)^2 \right]^{1/2}$$

$$^b \text{MNB} = \frac{1}{n} \sum_{i=1}^n \left( \frac{P_i - O_i}{O_i} \right)$$

$$^c \text{NRMSE} = \left[ \frac{1}{n-1} \sum_{i=1}^n \left( \frac{P_i - O_i}{O_i} - \text{MNB} \right)^2 \right]^{1/2} \text{ where } P_i \text{ and } O_i \text{ are predicted and observed values, respectively.}$$

The other two examples represent the 625 nm band (Fig. 3b and d). They have slightly inferior statistical parameters compared to formulas (3) and (4) but are still the best if we consider only the visible part of the light spectrum:

$$\text{SPM} = 2510(R_{rs}(625))^{1.09} \quad (r^2 = 0.78; X = 1.33), \quad (5)$$

$$\text{POC} = 346(R_{rs}(625))^{0.97} \quad (r^2 = 0.57; X = 1.51). \quad (6)$$

The other form of the simple formulas we have determined here are the formulas for estimating SPM and POC concentrations based on the so-called colour ratios, i.e. ratios of  $R_{rs}$  values at two spectral bands ( $R_{rs}(\lambda_i)/R_{rs}(\lambda_j)$ ). The colour ratios are often used in satellite data processing. If the bands are appropriately chosen, more information on the optical properties of seawater constituents “concealed” in the signal reaching the satellite sensor can be used, and also, the influence of potential errors resulting from imperfect atmospheric corrections is minimised to some extent. The available empirical material contained  $R_{rs}(\lambda_i)$  data for 17 different spectral bands: 136 different combinations of the  $R_{rs}(\lambda_i)/R_{rs}(\lambda_j)$  ratio (where  $\lambda_j > \lambda_i$ ) could thus be analysed. For all of these combinations we calculated the correlation coefficients  $r^2$  for the relationships between the logarithms of SPM or POC concentration and the logarithms of  $R_{rs}(\lambda_i)/R_{rs}(\lambda_j)$ . With the  $r^2$  values, additionally presented here in Tables 3 and 4, a group of “statistically promising” spectral combinations of bands was chosen at which the approximate formulas could be established. A selection of the best candidate formulas is presented in Table 5. Among these formulas are 12 variants from which the SPM concentration can be estimated. They have correlation coefficients  $r^2$  ranging between 0.84 and 0.89, and standard error factors

$X$  from 1.23 to 1.28. These formulas generally use ratios of the reflectance at blue or green bands (443, 465, 490, 510 or 532 nm) to the reflectance at either yellow (589 nm), red (625 nm) or infrared (710 nm) bands. With regard to the formulas for estimating POC concentration, another 12 promising examples are presented in the lower part of Table 2. These examples have lower correlation coefficients  $r^2$ , in the range between 0.66 and 0.75, and higher standard error factors  $X$ , ranging from 1.37 to 1.45. Apart from the formulas that use a combination of spectral bands similar to that for estimating SPM concentration, a few different formulas have also appeared in this group. The latter formulas use the following bands in the spectral ratio numerator: 555, 565 and 683 nm (see the last four rows in Table 5). Four examples from the 24 formulas in Table 5 are presented in Fig. 4. The first two examples (Fig. 4a and c) represent two formulas that are characterised by the best statistical parameters within each group:

$$\text{SPM} = 0.95(R_{rs}(490)/R_{rs}(589))^{-1.74} \quad (r^2 = 0.89; X = 1.23), \quad (7)$$

$$\text{POC} = 0.814(R_{rs}(555)/R_{rs}(589))^{-4.42} \quad (r^2 = 0.75; X = 1.37). \quad (8)$$

The other two examples (Fig. 4b and d) are arbitrarily chosen formulas that use the reflectance ratio of  $R_{rs}(490)/R_{rs}(625)$ :

$$\text{SPM} = 2.6(R_{rs}(490)/R_{rs}(625))^{-1.29} \quad (r^2 = 0.86; X = 1.25), \quad (9)$$

$$\text{POC} = 0.774(R_{rs}(490)/R_{rs}(625))^{-1.18} \quad (r^2 = 0.66; X = 1.44). \quad (10)$$



**Table 4** The correlation coefficients  $r^2$  calculated for the relationships between log-transformed POC and the log-transformed spectral remote-sensing reflectance ratio of  $R_{rs}(\lambda_i)/R_{rs}(\lambda_j)$ . Examples of the relatively high  $r^2$  values are marked in bold.

$\lambda_i$ [nm]	$\lambda_j$ [nm]															
	380	395	412	443	465	490	510	532	555	565	589	625	665	683	710	765
340 ( $n = 65$ )	0.12	0.13	0.11	0.07	0.06	0.07	0.12	0.15	0.18	0.19	0.30	0.30	0.24	0.21	0.35	0.34
380 ( $n = 69$ )	–	0.04	0.04	0.02	0.02	0.04	0.10	0.15	0.21	0.24	0.38	0.38	0.30	0.27	0.44	0.43
395 ( $n = 71$ )		–	0.01	0.01	0.01	0.02	0.10	0.16	0.26	0.29	0.44	0.45	0.37	0.35	0.53	0.52
412 ( $n = 72$ )			–	0.01	0.01	0.03	0.16	0.25	0.35	0.38	0.52	0.53	0.44	0.41	0.58	0.57
443 ( $n = 73$ )				–	0.03	0.10	0.37	0.45	0.52	0.54	<b>0.66</b>	0.63	0.55	0.47	0.63	0.61
465 ( $n = 73$ )					–	0.05	0.37	0.52	0.59	0.61	<b>0.72</b>	<b>0.67</b>	0.59	0.50	<b>0.66</b>	0.63
490 ( $n = 73$ )						–	0.61	0.61	0.60	0.61	<b>0.71</b>	<b>0.66</b>	0.57	0.45	0.63	0.61
510 ( $n = 73$ )							–	0.44	0.51	0.53	<b>0.68</b>	0.63	0.52	0.36	0.60	0.57
532 ( $n = 73$ )								–	0.51	0.54	<b>0.72</b>	0.65	0.52	0.33	0.60	0.57
555 ( $n = 73$ )									–	0.55	<b>0.75</b>	<b>0.66</b>	0.46	0.19	0.58	0.55
565 ( $n = 73$ )										–	<b>0.70</b>	0.63	0.40	0.14	0.57	0.53
589 ( $n = 73$ )											–	0.45	0.08	0.00	0.47	0.44
625 ( $n = 73$ )												–	0.39	0.17	0.39	0.38
665 ( $n = 73$ )													–	0.04	0.56	0.49
683 ( $n = 73$ )														–	<b>0.68</b>	0.58
710 ( $n = 73$ )															–	0.21

**Table 5** The best-fit power functions ( $y = C_1 x^{C_2}$ ) between the concentration of suspended particulate matter SPM or the concentration of particulate organic carbon POC and the remote-sensing reflectance ratios  $R_{rs}(\lambda_i)/R_{rs}(\lambda_j)$ . The statistical parameters (as in Table 2) are also given for each fitted function. Examples discussed in more detail in the text are marked in bold.

Relationship	$C_1$	$C_2$	$r^2$	RMSE [ $\text{g m}^{-3}$ ]	MNB [%]	NRMSE [%]	X	n
SPM vs. $R_{rs}(443)/R_{rs}(589)$	0.438	–1.52	0.84	0.625	2.7	22.9	1.27	73
SPM vs. $R_{rs}(443)/R_{rs}(625)$	1.3	–1.17	0.84	0.582	2.8	23.1	1.28	73
SPM vs. $R_{rs}(443)/R_{rs}(710)$	2.79	–0.885	0.84	0.492	2.8	23.4	1.28	73
SPM vs. $R_{rs}(465)/R_{rs}(589)$	0.559	–1.65	0.86	0.616	2.5	22.1	1.26	73
SPM vs. $R_{rs}(465)/R_{rs}(625)$	1.68	–1.25	0.85	0.527	2.6	22.0	1.26	73
SPM vs. $R_{rs}(465)/R_{rs}(710)$	3.49	–0.925	0.84	0.458	2.3	23.1	1.27	73
<b>SPM vs. <math>R_{rs}(490)/R_{rs}(589)</math></b>	0.95	–1.74	<b>0.89</b>	0.483	2.0	19.7	<b>1.23</b>	73
<b>SPM vs. <math>R_{rs}(490)/R_{rs}(625)</math></b>	2.60	–1.29	<b>0.86</b>	0.429	2.4	21.5	<b>1.25</b>	73
SPM vs. $R_{rs}(510)/R_{rs}(589)$	1.42	–2.11	0.87	0.536	2.4	21.5	1.25	73
SPM vs. $R_{rs}(510)/R_{rs}(625)$	3.98	–1.48	0.84	0.434	2.8	23.5	1.27	73
SPM vs. $R_{rs}(532)/R_{rs}(589)$	1.78	–2.64	0.87	0.512	2.4	21.7	1.25	73
SPM vs. $R_{rs}(532)/R_{rs}(625)$	5.46	–1.71	0.84	0.41	2.9	24.1	1.28	73
POC vs. $R_{rs}(443)/R_{rs}(589)$	0.151	–1.4	0.66	0.265	6.7	38.1	1.45	73
POC vs. $R_{rs}(465)/R_{rs}(589)$	0.183	–1.57	0.72	0.242	5.5	34.0	1.4	73
POC vs. $R_{rs}(465)/R_{rs}(625)$	0.52	–1.16	0.67	0.253	6.4	37.1	1.44	73
POC vs. $R_{rs}(465)/R_{rs}(710)$	1.02	–0.854	0.66	0.247	6.5	36.3	1.45	73
POC vs. $R_{rs}(490)/R_{rs}(589)$	0.306	–1.63	0.71	0.218	5.6	34.3	1.4	73
<b>POC vs. <math>R_{rs}(490)/R_{rs}(625)</math></b>	0.774	–1.18	<b>0.66</b>	0.236	6.7	38.3	<b>1.44</b>	73
POC vs. $R_{rs}(510)/R_{rs}(589)$	0.445	–1.95	0.68	0.218	6.2	36.4	1.43	73
POC vs. $R_{rs}(532)/R_{rs}(589)$	0.554	–2.51	0.72	0.205	5.4	33.7	1.4	73
<b>POC vs. <math>R_{rs}(555)/R_{rs}(589)</math></b>	0.814	–4.42	<b>0.75</b>	0.205	4.7	30.6	<b>1.37</b>	73
POC vs. $R_{rs}(555)/R_{rs}(625)$	2.84	–2.22	0.66	0.241	6.9	40.0	1.45	73
POC vs. $R_{rs}(565)/R_{rs}(589)$	0.826	–5.32	0.7	0.24	5.6	33.9	1.41	73
POC vs. $R_{rs}(683)/R_{rs}(710)$	2.14	–2.17	0.68	0.234	6.6	40.0	1.43	73

These latter formulas, although characterised by statistical parameters inferior to formulas (7) and (8), use spectral bands which are close to or concurrent with bands potentially available for satellite observations of the southern Baltic Sea

(compare, for example, with the spectral bands of MODIS Aqua/Terra). But obviously, the final choice of spectral variants from the different formulas listed in Table 5 should depend on the demands and constraints of potential future users.

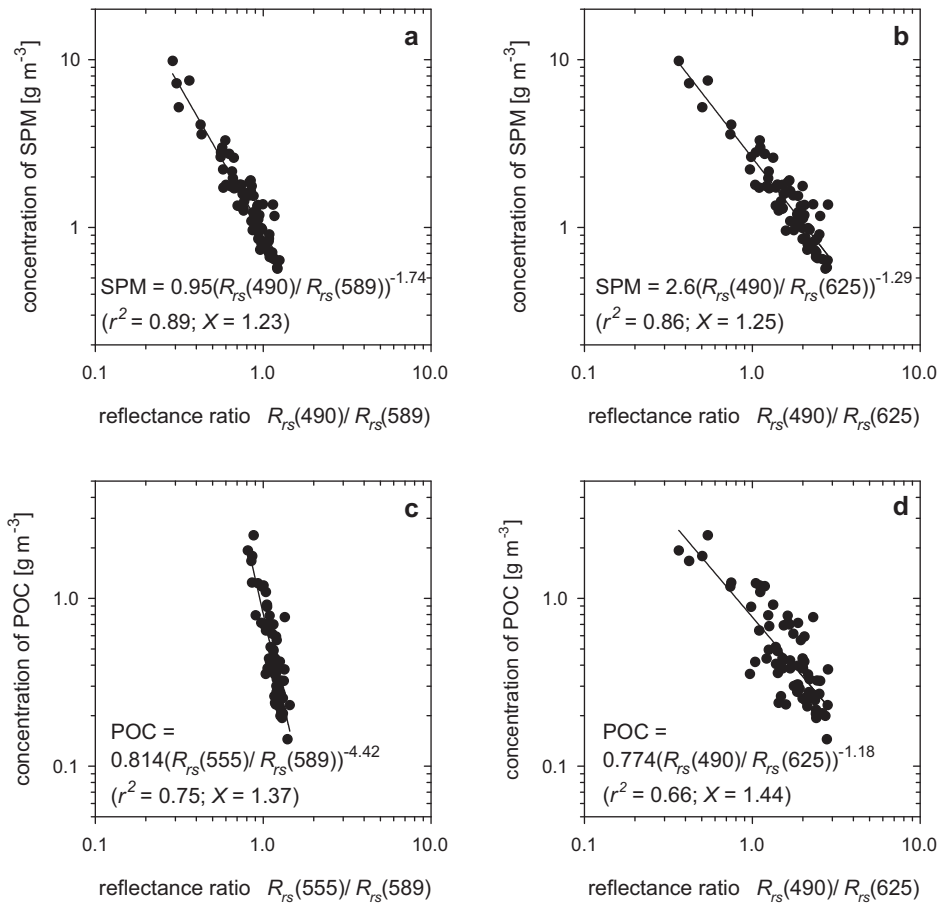


**Figure 4** Examples of empirical relationships between: (a) SPM concentration and the remote-sensing reflectance ratio of  $R_{rs}(490)/R_{rs}(589)$ ; (b) SPM and  $R_{rs}(490)/R_{rs}(625)$ ; (c) POC and  $R_{rs}(555)/R_{rs}(589)$ ; and (d) POC and  $R_{rs}(490)/R_{rs}(625)$ . The black lines represent the best-fit power functions; the formulas and the statistical parameters are given in each panel. For further similar formulas for other spectral variants of remote-sensing reflectance ratios, see Table 5.

### 3.3. Discussion

One can give a simplified physical explanation for some of the formulas presented above, i.e. those which use absolute reflectance values from the red and near infrared spectral

bands, and illustrate it with examples of intermediate statistical relationships. Such relationships between the target quantities and the coefficients describing light backscattering in seawater are presented in the next two figures. Fig. 5 illustrates two correlations between  $R_{rs}(710)$  or  $R_{rs}(625)$  and

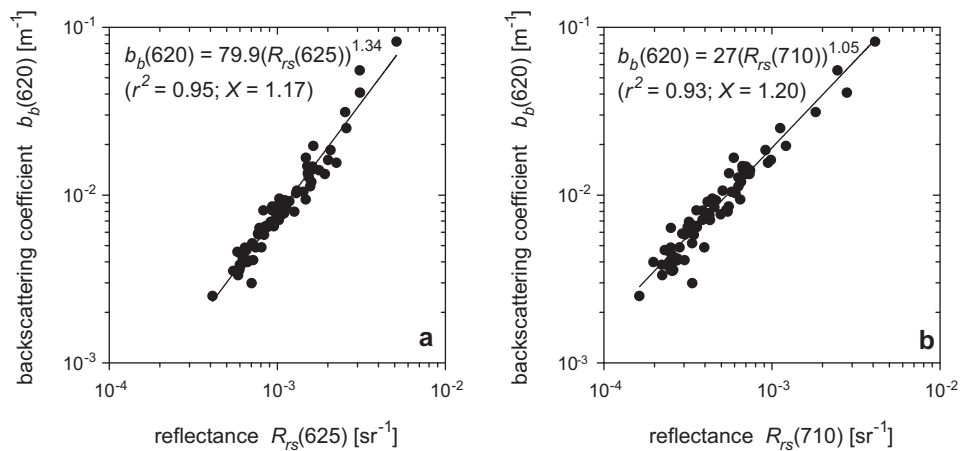


**Figure 5** Examples of empirical relationships between the light backscattering coefficient  $b_b(620)$  and the remote-sensing reflectance  $R_{rs}$  for spectral bands (a) 625 nm and (b) 710 nm. The black lines represent the best-fit power functions; the formulas and the statistical parameters are given in each panel.

light backscattering coefficients in seawater measured in situ at the closest spectral band, i.e.  $b_b(620)$  (the approximation formulas of these relationships are shown in the panels in Fig. 5). The appearance of such correlations is in general agreement with the well-known approximate relation linking  $R_{rs}(\lambda)$  with seawater IOPs, which takes the form:  $R_{rs}(\lambda) \propto b_b(\lambda)/(a(\lambda) + b_b(\lambda))$  (see e.g. Gordon et al., 1988; Lee et al., 1996). Obviously, the light absorption coefficients in seawater  $a(\lambda)$  in the bands from the red and infrared parts of the spectrum are mainly dominated by absorption due to pure molecular water. Hence, this relationship for the particular bands under consideration can be reduced to  $R_{rs}(\lambda) \propto b_b(\lambda)$ . Fig. 6 illustrates relationships between the light backscattering coefficients of particles  $b_{bp}(620)$  (which in southern Baltic conditions is only slightly less than  $b_b(620)$ , due to the relatively small contribution of light backscattering by pure seawater) and SPM and POC concentrations. Comparison of the statistical parameters of all the fits presented in Fig. 6 shows that the approximate relationship POC vs.  $b_{bp}(\lambda)$  (Fig. 6b) is related to the occurrence of stronger relationships between  $b_{bp}(\lambda)$  and the SPM concentration (presented in Fig. 6a as the SPM vs.  $b_b(\lambda)$  relation), and the additional statistical relationship between the concentrations of POC and SPM (Fig. 6c). The latter “local” relationship occurs because southern Baltic surface waters are usually

dominated by suspended matter of organic origin (see e.g. S. B. Woźniak et al., 2011). Here, it is important to stress that the approximate functional relationships presented here are strong and considerable simplifications made in order to achieve practical goals. Detailed analyses of the complicated relationships between light scattering characteristics and the concentration, composition and size distribution of suspended matter can be found in our other works (see e.g. S.B. Woźniak et al., 2010, 2014).

In the case of other approximate statistical relationships, i.e. those which use spectral reflectance ratios, an attempt to give a physical explanation would be much more complicated. In order to do this one would need to perform both qualitative and quantitative analyses using the full physical spectral model of remote-sensing reflectance formation. Such analyses would have to account not only for the influence of light backscattering on reflectance spectra, but also the strongly spectrally diverse influence of the light absorption coefficient, which occurs in different proportions with regard to suspended and dissolved seawater constituents. To carry out such complicated analyses is beyond the scope of this particular work, which is mainly of a statistical nature. Nevertheless, it is worth mentioning one certain fact at this point. The statistical analyses suggest that when SPM concentrations are estimated, the application of colour ratio

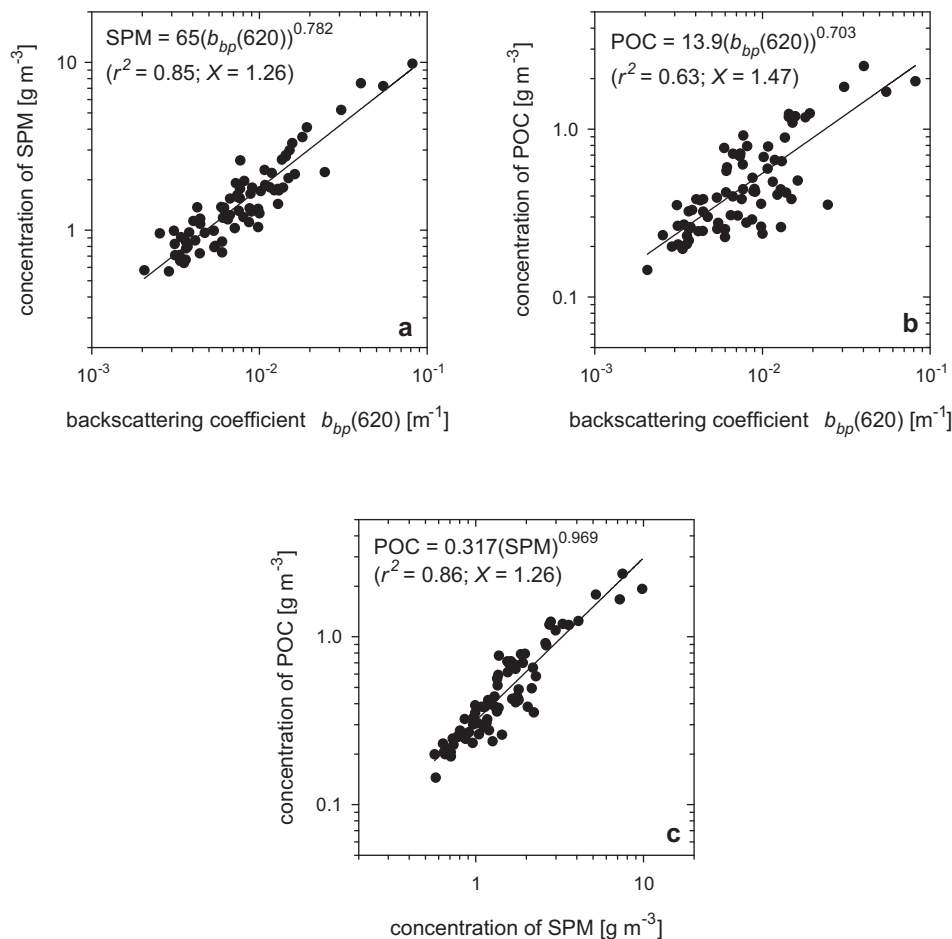


**Figure 6** Examples of empirical relationships between: (a) SPM concentration and coefficient of light backscattering by particles  $b_{bp}(620)$ ; (b) POC and  $b_{bp}(620)$ ; and (c) POC and SPM. The black lines represent the best-fit power functions; the formulas and the statistical parameters are given in each panel.

formulas instead of formulas based on the absolute reflectance at one spectral band alters the accuracy of such an estimate only slightly (compare e.g. the statistical parameters for formulas (3) and (7)). In contrast, when POC is estimated, the differences between these two kinds of formulas are decidedly in favour of colour ratio formulas (compare e.g. the statistical parameters for formulas (4) and (8)). This appears to be in agreement with our earlier observations that in the Baltic Sea conditions POC concentrations exhibit slightly stronger statistical relationships with the light absorption coefficient in the chosen spectral bands than with the light backscattering coefficient (see S.B. Woźniak, 2014).

Among the formulas hitherto shown to be the best examples from the statistical point of view, only a few are directly and quantitatively comparable with the formulas found in the subject literature. One such example is formula (5), which can be compared with the formula given by Ahn et al. (2001). The original formula given by these authors for coastal regions of the Korean peninsula takes the form:  $\text{SPM} [\text{g m}^{-3}] = 647.8(R_{rs}(625))^{0.86}$  (see the additional dashed line in Fig. 3b). The possibility of using the 625 nm band for estimating SPM concentrations agrees qualitatively with our

observations. However, quantitative comparison shows that the formula of Ahn et al., when applied to our Baltic data, predicts slightly different values than our formula (5). In extreme cases (i.e. for the minimum and maximum values of  $R_{rs}(625)$  that we registered) these predictions are up to 1.55 times higher and up to 2.41 times smaller, respectively. In the subject literature there are other works suggesting the possibility of using “red” reflectance bands for estimating SPM concentrations, which also concurs qualitatively with our new results; such citations were given in our earlier work (S.B. Woźniak, 2014).

Further comparisons, albeit done for different variants of new formulas, not those already presented as being the best from the statistical point of view, are shown in Fig. 7. The few formulas presented there combine the SPM concentration with the reflectance ratios of  $R_{rs}(510)/R_{rs}(665)$  or  $R_{rs}(490)/R_{rs}(665)$ , and POC concentration with reflectance ratios of  $R_{rs}(443)/R_{rs}(555)$  or  $R_{rs}(490)/R_{rs}(555)$ . The explicit forms of the new formulas obtained for our data are given in the panels of Fig. 7. They can be compared with the following reflectance ratio based formulas given by other authors, which we have found in the literature: (1) the formula for

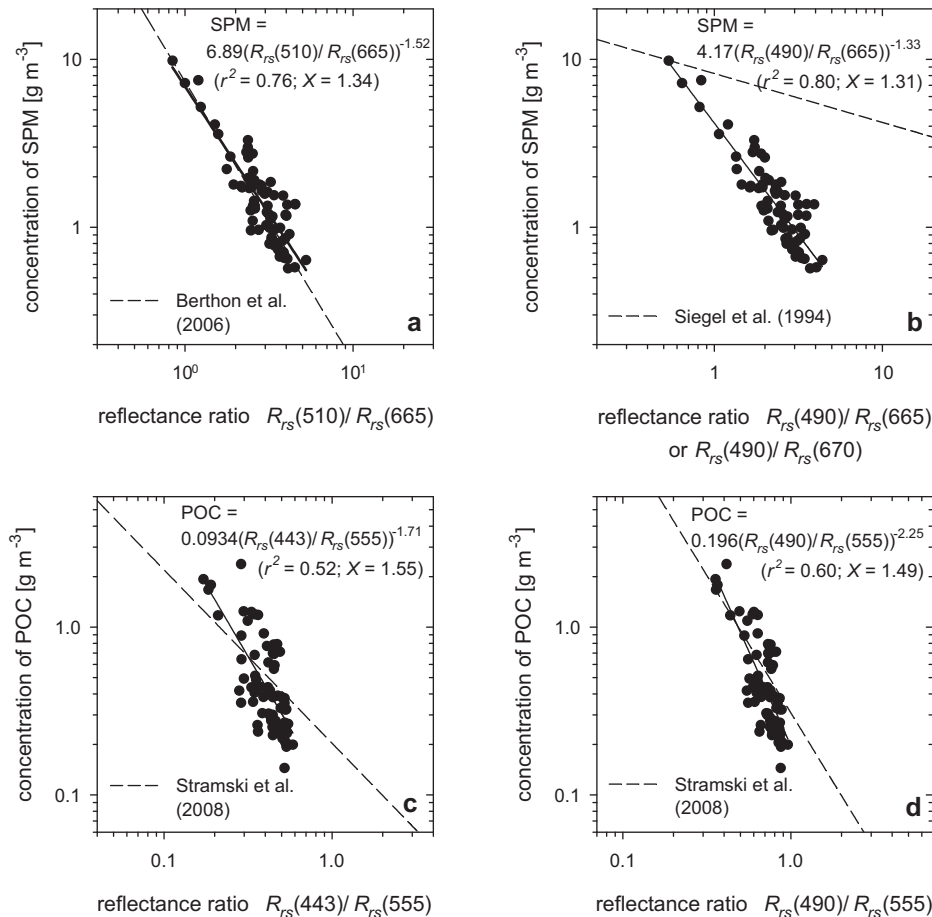


**Figure 7** Selected examples of empirical relationships obtained in this work compared with formulas from the literature: (a) relationship between SPM and reflectance ratio of  $R_{rs}(510)/R_{rs}(665)$ ; (b) relationship between SPM and  $R_{rs}(490)/R_{rs}(665)$ ; (c) relationship between POC and  $R_{rs}(443)/R_{rs}(555)$ ; and (d) relationship between POC and  $R_{rs}(490)/R_{rs}(555)$ . The black solid lines represent the best-fit power functions of our southern Baltic Sea data; the formulas and the statistical parameters are given in each panel. The dashed lines in all panels represent formulas from the literature: in panel a it is a formula given for the Baltic Sea by Berthon et al. (2006), in panel b it is a formula given for the Baltic Sea by Siegel et al. (1994), in panels c and d these are the formulas for the southern Pacific and eastern Atlantic Oceans given by Stramski et al. (2008) (for details of the literature formulas, see text).

the Baltic Sea given by Berthon et al. (2006), which after conversion takes the form:  $SPM [g m^{-3}] = 7.396(R_{rs}(510)/R_{rs}(670))^{-1.665}$  (note that this particular formula uses the reflectance ratio of the two spectral bands also pointed out recently by D'Alimonte et al. (2014) as being an effective selection for the simplified neural network inversion of SPM based on MERIS data in the Baltic); (2) the formula also developed for the Baltic Sea by Siegel et al. (1994) but for spectral bands similar to though not identical with ours:  $SPM [g m^{-3}] = 8.22045(R_{rs}(490)/R_{rs}(670))^{-0.29065}$ ; and (3) formulas for POC obtained for the southern Pacific and eastern Atlantic Oceans according to Stramski et al. (2008):  $POC [g m^{-3}] = 0.2032(R_{rs}(443)/R_{rs}(555))^{-1.034}$  and  $POC [g m^{-3}] = 0.3083(R_{rs}(490)/R_{rs}(555))^{-1.639}$ . Comparison of the new SPM formula according to our data with the formula according to Berthon et al. (2006) shows good agreement. Fig. 7a exhibits only small differences in the slopes of the relevant curves. Even in extreme cases, the quantitative differences in predicted SPM values do not exceed a factor of 1.2. In contrast, a marked difference in the slope of the curves can be observed in Fig. 7b when other variant of new formula according to our data is compared with the formula given by Siegel et al. (1994). This difference, unless it is an incorrect interpretation of the literature data on our part, would, in extreme cases, lead to a more than 9-fold difference in predicted SPM values. Other variants of formulas, also given in Siegel et al. (1994), are those for estimating SPM concentration based on colour ratios of 520 to 550 nm, 520 to 670 nm or 665 to 710 nm. Using such (or similar) colour ratios, a rough estimate of the SPM concentration is possible (compare the correlation coefficients  $r^2$  given in Table 3), but they are definitely not the colour ratios that should be regarded as optimal for the Baltic Sea environment in the context of our empirical material. The other two examples presented in Fig. 7 (see panels c and d) relate to the POC concentration calculated with the formulas according to Stramski et al. (2008). Although these formulas were developed for a marine environment different from that of the Baltic Sea, even in extreme cases they show differences of no more than a factor of 1.5. Taking into account these few cases of directly comparable examples, it can be concluded overall that there is a qualitative consistency in the fact that certain reflectance spectral bands can be used for roughly estimating SPM and POC concentrations. In the context of our results, however, the spectral reflectance ratios proposed in the literature often do not seem to be optimal for this purpose in the southern Baltic Sea environment. Nevertheless, for the majority of presented examples (with one notable exception) the quantitative differences even in extreme cases do not exceed a factor of 2.

Finally, one more question should be commented. Even though the variability in the biogeochemical characteristics recorded by us was large (see Section 3.1), it should not be forgotten that the data used here for the derivation of simple statistical formulas were gathered only during two limited periods of the annual phytoplankton activity cycle. The first period was in April and May, when the main annual spring phytoplankton bloom of diatoms and dinoflagellates normally occurs in the Baltic, and the second was in September, which is distinct from the typical occurrence of the important summer annual cyanobacteria bloom (see e.g. discussions in Siegel and Gerth, 2008 or Kratzer et al., 2011 and also the

“classic” work in the Baltic literature by Voipio (1981)). Thus, it is possible that the relationships between SPM, POC and optical properties may differ to some extent at the height of summer or during periods of low phytoplankton activity in autumn and winter. Addressing this problem remains a future task for our group.

#### 4. Final remarks

The new results presented here are in general agreement with earlier observations of other researchers, and also with our own results obtained with the aid of theoretical modelling (see S.B. Woźniak, 2014), that for estimating the concentration of suspended particulate matter (SPM) in surface waters of the southern Baltic Sea one can use simple, direct relationships between that concentration and either absolute values of  $R_{rs}$  at a selected waveband, or alternatively  $R_{rs}$  ratios for two different wavebands (colour ratios). Based on our regionally acquired dataset, we find that the most suitable single bands are those from the long-wave part of the visible light spectrum and from the near infrared (e.g.  $R_{rs}(625)$  or  $R_{rs}(710)$ ), and the most suitable colour ratios are those relating reflectance from the short-wave part of the visible light spectrum to the reflectance from the long-wave part (e.g. ratios of  $R_{rs}(490)/R_{rs}(589)$  or  $R_{rs}(490)/R_{rs}(625)$ ). The standard error factor  $X$  related to such estimates, for the empirical material analysed here, is relatively low, even as low as 1.23. We also find that the use of statistical relationships of a similar form also permits the POC concentration to be roughly estimated for typical southern Baltic conditions. Nevertheless, one should expect that the accuracy of these latter estimates will be inferior compared to the estimated SPM (for the empirical material available here the lowest value of the standard error factor  $X$  was 1.37). Regardless of the relatively small number of empirical data available, we believe that in view of the large variability of our dataset, our quantitative formulas may already adequately describe the approximate relationships that can be established at this level of simplification between SPM and POC concentrations and in situ measured remote-sensing reflectance  $R_{rs}(\lambda)$ , at least for the situations typical of the spring and late summer in the southern Baltic. We consider that both our earlier empirical IOP-based formulas (S.B. Woźniak, 2014) and the new empirical reflectance-based formulas presented here should henceforth be used as a basis for deriving different variants of simple local algorithms for analysing satellite data from the southern Baltic Sea. Once such new algorithms have been derived, they should then be validated against an independent dataset and their performance should be confronted with that of existing algorithms. This will then allow us to make a conscious choice of the most suitable algorithms for the southern Baltic region. This task is especially important in view of the potential input that improved methods of optical remote sensing may have on studies of the dynamics and spatial distribution of organic matter, a topic of major interest to the scientific community studying the Baltic Sea environment (see e.g. Maciejewska and Pempkowiak, 2014, 2015, and the works cited there). Finally, it has to be stressed that potential users of the estimates obtained in the way we propose here should always bear in mind their limited accuracy, which are a consequence of the many simplifications adopted.

## Acknowledgements

The authors thank their colleagues from IO PAN, especially Sławomir Sagan and Joanna Stoń-Egiert, for their help in collecting the empirical material presented in this work.

## References

- Ahn, Y.-H., Moon, J.-E., Gallegos, S., 2001. Development of suspended particulate matter algorithms for ocean color remote sensing. *Korean J. Remote Sens.* 17 (4), 285–295.
- Arst, H., 2003. *Optical Properties and Remote Sensing of Multicomponental Water Bodies*. Springer-Verlag, Berlin, Heidelberg, New York, 234 pp.
- Beltran-Abauza, J.M., Kratzer, S., Brockmann, C., 2014. Evaluation of MERIS products from Baltic Sea coastal waters rich in CDOM. *Ocean Sci.* 10, 377–396, <http://dx.doi.org/10.5194/os-10-377-2014>.
- Berthon, J.-F., Melin, F., Zibordi, G., 2008. Ocean colour remote sensing of the optically complex European Seas. In: Barale, V., Gade M., M. (Eds.), *Remote Sensing of the European Seas*. Springer, Berlin, 35–52.
- Berthon, J.-F., Zibordi, G., Van Der Linde, D., Canuti, E., Eker-Develi, E., 2006. *Regional Bio-optical Relationships and Algorithms for the Adriatic Sea, the Baltic Sea and the English Channel/North Sea Suitable for Ocean Colour Sensors*. European Commission, Directorate-General Joint Research Centre, EUR 22188 EN, 43 pp.
- Dana, D.R., Maffione, R.A., 2002. Determining the backward scattering coefficient with fixed-angle backscattering sensors – revisited. In: *Ocean Optics XVI Conference*. Santa Fe, New Mexico, USA 9 pp.
- Darecki, M., Ficek, D., Krężel, A., Ostrowska, M., Majchrowski, R., Woźniak, S.B., Bradtke, K., Dera, J., Woźniak, B., 2008. Algorithm for the remote sensing of the Baltic ecosystem (DESAMBEM), Part 2: Empirical validation. *Oceanologia* 50 (4), 509–538.
- Darecki, M., Stramski, D., 2004. An evaluation of MODIS and SeaWiFS bio-optical algorithms in the Baltic Sea. *Remote Sens. Environ.* 89 (3), 326–350, <http://dx.doi.org/10.1016/j.rse.2003.10.012>.
- Dera, J., Woźniak, B., 2010. Solar radiation in the Baltic Sea. *Oceanologia* 52 (4), 533–582, <http://dx.doi.org/10.5697/oc.52-4.533>.
- Doerffer, R., Schiller, H., 2006. The MERIS neural network algorithm. In: Lee, Z.P. (Ed.), *Remote Sensing of Inherent Optical Properties: Fundamentals, Tests of Algorithms, and Applications*. IOCCG Report Series, No. 5. International Ocean Colour Coordinating Group, Dartmouth, Canada (Chapter 6), 126 pp.
- D'Alimonte, D., Zibordi, G., Kajiyama, T., Berthon, J.-F., 2014. Comparison between MERIS and regional high-level products in European seas. *Remote Sens. Environ.* 140, 378–395, <http://dx.doi.org/10.1016/j.rse.2013.07.029>.
- Ferrari, G.M., Bo, F.G., Babin, M., 2003. Geo-chemical and optical characterizations of suspended matter in European coastal waters. *Estuar. Coast. Shelf Sci.* 57, 17–24, [http://dx.doi.org/10.1016/S0272-7714\(02\)00314-1](http://dx.doi.org/10.1016/S0272-7714(02)00314-1).
- Gordon, H.R., Brown, O.B., Evans, R.H., Brown, J.W., Smith, R.C., Baker, K.S., Clark, D.K., 1988. A semianalytic radiance model of ocean colour. *J. Geophys. Res.* 93, 10909–10924, <http://dx.doi.org/10.1029/JD093iD09p10909>.
- Gordon, H.R., Ding, K., 1992. Self-shading of in-water instruments. *Limnol. Oceanogr.* 37 (3), 491–500, <http://dx.doi.org/10.4319/lo.1992.37.3.0491>.
- HOBILabs (Hydro-Optics, and Instrument. Lab. Inc.), 2008. *HydroScat-4 Spectral Backscattering Sensor, User's Manual, Rev. 4*, June 15 2008, 65 pp.
- IOCCG, 2015. *Ocean colour remote sensing in polar seas*. In: Babin, M., Arriago, K., Bélanger, S., Forget, M.-H. (Eds.), IOCCG Report Series, No. 16. International Ocean Colour Coordinating Group, Dartmouth, Canada, 130 pp.
- Kowalczyk, P., 1999. Seasonal variability of yellow substance absorption in the surface layer of the Baltic Sea. *J. Geophys. Res.* 104 (12), 30047–30058, <http://dx.doi.org/10.1029/1999JC900198>.
- Kratzer, S., Ebert, K., Sørensen, K., 2011. Monitoring the bio-optical state of the Baltic Sea ecosystem with remote sensing and autonomous in situ techniques. In: Harff, J., Björck, S., Hoth, P. (Eds.), *The Baltic Sea Basin. Central and Eastern European Development Studies (CEEDES)*. Springer, Heidelberg, 407–435, (Chapter 20).
- Lee, P., Carder, L., Peacock, T.G., Davis, C.O., Mueller, J.L., 1996. Method to derive ocean absorption coefficients from remote-sensing reflectance. *Appl. Opt.* 35 (3), 453–462, <http://dx.doi.org/10.1364/AO.35.000453>.
- Maciejewska, A., Pempkowiak, J., 2014. DOC and POC in the southern Baltic. Part I. Evaluation of factors influencing sources distribution and dynamics of organic matter. *Oceanologia* 56 (3), 523–548, <http://dx.doi.org/10.5697/oc.56-3.523>.
- Maciejewska, A., Pempkowiak, J., 2015. DOC and POC in the southern Baltic Sea. Part II. Evaluation of factors affecting organic matter concentrations using multivariate statistical methods. *Oceanologia* 57 (2), 168–176, <http://dx.doi.org/10.1016/j.ocean.2014.11.003>.
- Maffione, R.A., Dana, D.R., 1997. Instruments and methods for measuring the backward-scattering coefficient of ocean waters. *Appl. Opt.* 36 (24), 6057–6067, <http://dx.doi.org/10.1364/AO.36.006057>.
- Mobley, C.D., 1994. *Light and Water; Radiative Transfer in Natural Waters*. Academic Press, San Diego, 592 pp.
- Morel, A., 1974. Optical properties of pure water and pure sea water. In: Jerlov, N.G., Steemann Nielsen, E. (Eds.), *Optical Aspects of Oceanography*. Academic Press, London, 1–24.
- Morel, A., Prieur, L., 1977. Analysis of variations in ocean color. *Limnol. Oceanogr.* 22, 709–722, <http://dx.doi.org/10.4319/lo.1977.22.4.0709>.
- Siegel, H., Gerth, M., 2008. Optical remote sensing applications in the Baltic Sea. In: Barale, V., Gade M., M. (Eds.), *Remote Sensing of the European Seas*. Springer, Berlin, 91–102.
- Siegel, H., Gerth, M., Beckert, M., 1994. The variation of optical properties in the Baltic Sea and algorithms for the application of remote sensing data. *Ocean Optics XII. Proc. SPIE Int. Soc. Opt. Eng.* 2258, 894–905.
- Stramski, D., Reynolds, R.A., Babin, M., Kaczmarek, S., Lewis, M.R., Röttgers, R., Sciandra, A., Stramska, M., Twardowski, M.S., Franz, B.A., Claustre, H., 2008. Relationships between the surface concentration of particulate organic carbon and optical properties in the eastern South Pacific and eastern Atlantic Oceans. *Biogeosciences* 5 (1), 171–201, <http://dx.doi.org/10.5194/bg-5-171-2008>.
- Voipio, A. (Ed.), 1981. *The Baltic Sea*. Elsevier Scientific Publishing Company, Amsterdam, Oxford, New York, 418 pp.
- Woźniak, B., Bradtke, K., Darecki, M., Dera, J., Dudzińska-Nowak, J., Dzierzbicka-Głowacka, L., Ficek, D., Furmańczyk, K., Kowalewski, M., Krężel, A., Majchrowski, R., Ostrowska, M., Paszkuta, M., Stoń-Egiert, J., Stramska, M., Zapadka, T., 2011a. SatBaltic – a Baltic environmental satellite remote sensing system – an ongoing Project in Poland. Part 1: Assumptions, scope and operating range. *Oceanologia* 53 (4), 897–924, <http://dx.doi.org/10.5697/oc.53-4.897>.
- Woźniak, B., Bradtke, K., Darecki, M., Dera, J., Dudzińska-Nowak, J., Dzierzbicka-Głowacka, L., Ficek, D., Furmańczyk, K., Kowalewski, M., Krężel, A., Majchrowski, R., Ostrowska, M., Paszkuta, M., Stoń-Egiert, J., Stramska, M., Zapadka, T., 2011b. SatBaltic – a Baltic environmental satellite remote sensing system – an ongoing Project in Poland. Part 2: Practical applicability and preliminary results. *Oceanologia* 53 (4), 925–958, <http://dx.doi.org/10.5697/oc.53-4.925>.

- Woźniak, B., Krężel, A., Darecki, M., Woźniak, S.B., Majchrowski, R., Ostrowska, M., Kozłowski, Ł., Ficek, D., Olszewski, J., Dera, J., 2008. Algorithm for the remote sensing of the Baltic ecosystem (DESAMBEM). Part 1: Mathematical apparatus. *Oceanologia* 50 (4), 451–508.
- Woźniak, M., Bradtke, K.M., Krężel, A., 2014. Comparison of satellite chlorophyll *a* algorithms for the Baltic Sea. *J. Appl. Remote Sens.* 8 (1), 083605, <http://dx.doi.org/10.1117/1.JRS.8.083605>.
- Woźniak, S.B., 2014. Simple statistical formulas for estimating biogeochemical properties of suspended particulate matter in the southern Baltic Sea potentially useful for optical remote sensing applications. *Oceanologia* 56 (1), 7–39, <http://dx.doi.org/10.5697/oc.56-1.007>.
- Woźniak, S.B., Meler, J., Lednicka, B., Zdun, A., Stoń-Egiert, J., 2011. Inherent optical properties of suspended particulate matter in the southern Baltic Sea. *Oceanologia* 53 (3), 691–729, <http://dx.doi.org/10.5697/oc.53-3.691>.
- Woźniak, S.B., Sagan, S., Stoń-Egiert, J., Burska, D., Zabłocka, M., 2014. Light backscattering and scattering by marine particles in relation to particle concentration, composition and size distribution in the southern Baltic Sea. In: *Ocean Optics XXII Conference. Portland, Maine, USA* 12 pp.
- Woźniak, S.B., Stramski, D., Stramska, M., Reynolds, R.A., Wright, V. M., Miksic, E.Y., Cichocka, M., Cieplak, A.M., 2010. Optical variability of seawater in relation to particle concentration, composition, and size distribution in the nearshore marine environment at Imperial Beach, California. *J. Geophys. Res. Oceans* 115, C08027, <http://dx.doi.org/10.1029/2009JC005554>.
- Zibordi, G., Ferrari, G.M., 1995. Instrument self-shading in underwater optical measurements: experimental data. *Appl. Opt.* 34 (2), 2750–2754, <http://dx.doi.org/10.1364/AO.34.002750>.



ORIGINAL RESEARCH ARTICLE

# The impact of surface currents and sea level on the wave field evolution during St. Jude storm in the eastern Baltic Sea<sup>☆</sup>

Marili Viitak<sup>a,\*</sup>, Ilja Maljutenko<sup>a</sup>, Victor Alari<sup>b,1</sup>, Ülo Suursaar<sup>c</sup>, Sander Rikka<sup>a</sup>, Priidik Lagemaa<sup>a,d</sup>

<sup>a</sup> Tallinn University of Technology, Marine Systems Institute, Tallinn, Estonia

<sup>b</sup> Helmholtz-Zentrum Geesthacht, Centre for Material and Coastal Research, Geesthacht, Germany

<sup>c</sup> University of Tartu, Estonian Marine Institute, Estonia

<sup>d</sup> Estonian Environment Agency, Estonian Weather Service, Estonia

Received 5 October 2015; accepted 29 January 2016

Available online 16 February 2016

## KEYWORDS

SWAN;  
Wave–current–surge  
interaction;  
Extreme storm;  
Hindcast;  
SAR

**Summary** A third generation numerical wave model SWAN (Simulating WAVes Nearshore) was applied to study the spatio-temporal effect of surface currents and sea level height on significant wave height; and to describe the mechanisms responsible for wave–current interaction in the eastern Baltic Sea. Simulation results were validated by comparison with in situ wave measurements in deep and shallow water, carried out using the directional wave buoy and RDGP respectively, and with TerraSAR-X imagery. A hindcast period from 23 to 31 October 2013 included both a period of calm to moderate weather conditions and a severe North-European windstorm called St. Jude. The prevailing wind directions were southerly to westerly. Four simulations with SWAN were made: a control run with dynamical forcing by wind only; and simulations with additional inputs of surface currents and sea level, both separately and combined. A clear effect of surface currents and sea level on the wave field evolution was found. It manifested itself as an increase or decrease of significant wave height of up to 20%. The strength of the interaction was

<sup>☆</sup> This study was financially supported by the Estonian Science Foundation Grant 9278, by institutional research funding IUT19-6 of the Estonian Ministry of Education and Research and by the Estonian Research Council grant PUT595.

\* Corresponding author at: Tallinn University of Technology, Marine Systems Institute, Akadeemia tee 15a, 12618 Tallinn, Estonia. Tel.: +372 53803824.

E-mail address: [viitak.marili@gmail.com](mailto:viitak.marili@gmail.com) (M. Viitak).

<sup>1</sup> Current address: Marine Systems Institute at Tallinn University of Technology, Estonia.

Peer review under the responsibility of Institute of Oceanology of the Polish Academy of Sciences.



Production and hosting by Elsevier

influenced by the propagation directions of waves and surface currents and the severity of weather conditions. An increase in the wave height was mostly seen in shallower waters and in areas where waves and surface currents were propagating in opposite directions. In deeper parts of the eastern Baltic Sea and in case of waves and surface currents propagating in the same direction a decrease occurred.

© 2016 Institute of Oceanology of the Polish Academy of Sciences. Production and hosting by Elsevier B.V. This is an open access article under the CC BY-NC-ND license (<http://creativecommons.org/licenses/by-nc-nd/4.0/>).

## 1. Introduction

In the event of a storm at sea, rough wave and severe surge conditions may lead to significant coastal and property damage or even to loss of life (e.g. Feser et al., 2015). Correct quantification of met-ocean parameters of a storm using numerical models and forecasting systems helps to reduce the storm related risks and mitigate consequences. Because in nature there is a feedback system between processes, detailed information about different interactions would provide us with a better understanding and improved predictability of hydrodynamic conditions at sea. For instance, an important feedback occurs between slowly-varying currents and highly varying waves. So far, the issue is little studied in the Baltic Sea.

The groundbreaking work of wave–current interaction was done by Longuet-Higgins and Stewart in a series of papers (1960, 1961, 1964). They described the interaction using radiation stress and demonstrated the energy transfer between waves and currents. Bretherton and Garrett (1968) introduced the idea of action conservation. Since then numerous papers have been published on the application of the theory including those by Wolf and Prandle (1999), Guedes Soares and de Pablo (2006) and Van der Westhuysen (2012). Alari (2013) studied the local storm surge effect on wave field in Pärnu Bay, Baltic Sea. He showed that sea level has a significant effect on wave field during extreme weather conditions. However, the effect of surface currents on wave field in the eastern Baltic Sea has had little attention.

The objectives of the present study were firstly, to assess the one-way interaction between waves, surface currents and sea level in almost tideless (up to 10 cm (Feistel et al., 2008)) coastal areas. We tried to find out the mechanisms by which surface currents and sea level rise influence the evolution of significant wave height under stormy conditions. This could help to improve modelling systems and see if it is worth further investigating the coupling of wave and hydrodynamic models in the Baltic Sea. Secondly, we studied the effect of spatial variability of surface currents and sea level on wave field. This would also indicate in which sea areas these interactions might be important during severe storms.

The paper is structured as follows: In Section 2 data and methods are presented including the description of measured and remotely sensed data and the description of numerical models and their set-ups. Section 3 presents the calculation results and discussion. The main conclusions and recommendations for further studies are summed up in Section 4.

## 2. Data and methods

### 2.1. Investigation area and measurements

The area of investigation is the eastern Baltic Sea, which is shown in Fig. 1. It includes two large gulfs – the Gulf of Finland and the Gulf of Riga. Water depth varies between 0 and 170 m. The Eastern section of the Baltic Sea, including the Gulf of Finland and Gulf of Riga, are extremely prone to storm surge (e.g. Wolski et al., 2014). The Gulf of Finland is connected with Baltic Proper with no barrier to the propagation of the waves, which allows, under certain meteorological conditions, long and high waves to enter the region (Leppäranta and Myrberg, 2009). According to Kahma and Petterson (1993) the mean significant wave height in spring is 0.5 m with peak period of 3.8 s and in winter 1.3 m with period of 5.3 s. Higher waves are produced in storm conditions (Soomere et al., 2008). In the Gulf of Riga wave propagation and growth are limited by shallow and narrow straits. Annual average wave height is between 0.25 and 0.5 m (Suursaar et al., 2012). According to Raudsepp et al. (2011) the peak period ranges between 2.3 and 8 s.

In Fig. 1 red and black squares show the stations where the measurements were taken for comparison with the simulations. Measurements in the Gulf of Finland (Fig. 1, station A) were conducted by the Finnish Meteorological Institute (FMI) at a site where water depth is 43 m. The device used was the

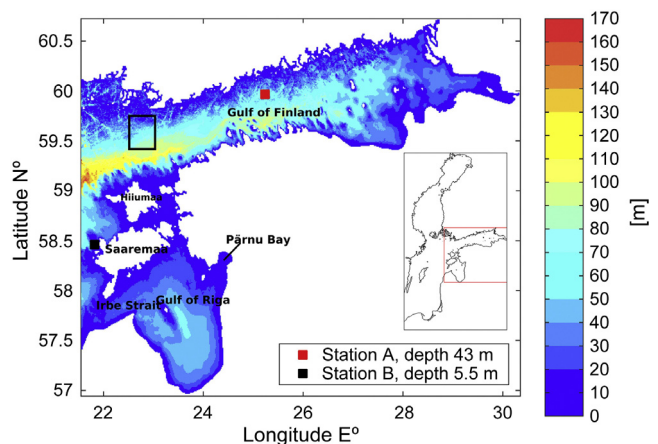


**Figure 1** Eastern Baltic Sea bathymetry with grid resolution of 0.5 nautical miles. This area also represents the nested grid area. The black rectangle is the area of SAR measurements.

WAVERIDER MKIII directional wave buoy, which measures surface acceleration. Waves with period of 1.6 s and higher were registered. Measurements close to Saaremaa Island (Fig. 1, Station B) were conducted by the Estonian Marine Institute (Suursaar, 2013). The water depth at the measurement site was 5.5 m. The measurements were taken with a bottom mounted RDCP-600 (Recording Doppler Current Profiler), which measured the instantaneous dynamic pressure above its sensor. The pressure was further converted to surface elevation spectra with linear wave theory. Due to the attenuation of the pressure signal, there was a high-frequency cut-off and only waves with period of 2.6 s and bigger were measurable. As a result the realistic significant wave height can be higher than measured.

For remotely sensed data, a TerraSAR-X multi-look ground range detect (MGD) Stripmap product was used. The image was acquired with VV polarization and the pixel size was 1.25 m. Here the image acquired for the morning of 29 October 2013 (at 04:57 UTC) was used, which coincided with the storm maximum. The area of the image is shown on Fig. 1 as a black rectangle.

## 2.2. Numerical model

The SWAN model used in this study is a third-generation numerical wave model developed at the Delft University of Technology, in The Netherlands (Booij et al., 1999). Waves are described with the two-dimensional wave action density spectrum. The action density spectrum  $N$  is considered instead of the energy density spectrum  $E$  because in the presence of ambient currents, action density is conserved, but energy density is not. Action density is related to energy density through the relative frequency  $\sigma$  (Whitham, 1974):

$$N(\sigma, \theta) = \frac{E(\sigma, \theta)}{\sigma}. \quad (1)$$

Relative frequency is observed in a frame of reference moving with the current velocity, and  $\theta$  is the wave propagation direction (the direction normal to the wave crest of each spectral component). SWAN solves the spectral action balance equation without any *a priori* restrictions on the spectrum for the evolution of wave growth (Booij et al., 1999). The action balance equation in Cartesian coordinates reads:

$$\frac{\partial N}{\partial t} + (c_g \rightarrow + \mathbf{u} \rightarrow) \nabla_{x,y} N + \frac{\partial c_\sigma N}{\partial \sigma} + \frac{\partial c_\theta N}{\partial \theta} = \frac{S_{wind} + S_{nl3} + S_{nl4} + S_{wc} + S_{bot} + S_{db}}{\sigma}. \quad (2)$$

On the left-hand side of Eq. (2) the first term represents the local rate of change of action density in time; the second term denotes the propagation of wave energy in two dimensional geographical space, where  $c_g \rightarrow$  is the group velocity and  $\mathbf{u}$  is the ambient current. The third term represents the shifting of the relative frequency due to variations in depths and currents (with propagation velocity  $c_\sigma$  in  $\sigma$  space). The fourth term represents depth induced and current-induced refraction (with propagation velocity  $c_\theta$  in  $\theta$  space). On the right-hand side of the action balance equation is the source term that represents all physical processes which generate, redistribute or dissipate wave energy. These terms denote, respectively, wave growth by the wind  $S_{wind}$ , non-linear

transfer of wave energy through three-wave  $S_{nl3}$  and four-wave interactions  $S_{nl4}$  and wave dissipation due to white-capping  $S_{wc}$ , bottom friction  $S_{bot}$  and depth-induced wave breaking  $S_{db}$  (The SWAN team, 2013a).

## 2.3. Accounting for currents and sea level in SWAN

The SWAN is not capable of calculating surface currents and sea levels. In order to take them into account they have to be presented as input. If there is no current or sea level input data, they are assumed to be zero (The SWAN team, 2013b).

### 2.3.1. Wind

Two mechanisms are used to describe the transfer of wind energy to waves – a resonance mechanism and a feed-back mechanism. For a more precise description see Phillips (1957) and Miles (1957). Wave growth is the sum of linear (A) and exponential (B) growth:

$$S_{wind}(\sigma, \theta) = A + BE(\sigma, \theta), \quad (3)$$

in which A and B depend on wave frequency and direction, and wind speed and direction. Linear wave growth contributes to the initial stages of wave growth. As the waves grow they start to affect the wind induced pressure field, which results in a larger energy transfer from the wind as the waves grow.

To account for the currents the apparent local wind speed and directions are used (The SWAN team, 2013a). In the presence of surface currents travelling opposite to the wave direction the transfer of wind energy to the waves is stronger and vice versa.

### 2.3.2. Kinematic effects

In Eq. (2) the kinematic effects are presented with left-side terms, except the time derivative term. As stated by Whitham (1974), wave energy propagation velocities in spatial and spectral space can be described by the kinematics of a wave train. In spatial space it reads:

$$\frac{d\vec{x}}{dt} = c_g \rightarrow + \vec{u} = \frac{1}{2} \left( 1 + \frac{2|\vec{k}|d}{\sinh(2|\vec{k}|d)} \right) \frac{\sigma \vec{k}}{|\vec{k}|^2} + \vec{u}, \quad (4)$$

where  $k$  is wave number vector and  $d$  is the total water depth.

In spectral space:

$$c_\sigma = \frac{\partial \sigma}{\partial d} \left( \frac{\partial d}{\partial t} + \vec{u} \nabla_{x,y} d \right) - c_g \vec{k} \frac{\partial \vec{u}}{\partial s}, \quad (5)$$

$$c_\theta = \frac{-1}{k} \left( \frac{\partial \sigma}{\partial d} \frac{\partial d}{\partial m} + \vec{k} \frac{\partial \vec{u}}{\partial m} \right), \quad (6)$$

where  $s$  is the space coordinate in the wave propagation direction of  $\theta$  and  $m$  is a coordinate perpendicular to  $s$  (The SWAN team, 2013a).

From kinematics in spatial space and spectral space (Eqs. (4)–(6)) it is observed that, when waves and currents are propagating in opposite directions, the second left-side term will be smaller in value in Eq. (2). This will result in an increase in the wave energy and therefore also in the wave

height. With waves and currents propagating in the same direction the effect is reversed.

As the sea level changes the total water depth influences the height of the waves. In nearshore regions, the group velocity decreases with decreasing water depth. To maintain a constant flux of energy transport an increase in the energy density occurs. This results in an increase of the wave height. With varying surface current and sea level refraction occurs (Eq. (6)).

### 2.3.3. Depth-induced wave breaking

Sea level will determine the maximum height of the waves beyond which the waves will start to break. Energy dissipation due to depth-induced wave breaking follows the analogy of breaking of a bore applied to random waves (Battjes and Janssen, 1978):

$$S_{db}(\sigma, \theta) = \frac{D_{tot}}{E_{tot}} E(\sigma, \theta), \quad (7)$$

where  $D_{tot} = -\alpha_{BJ} Q_b \tilde{\sigma} H_{max}^2 (8\pi)^{-1}$  is the mean rate of energy dissipation per unit horizontal area due to wave breaking,  $\alpha_{BJ} = 1$ ,  $\tilde{\sigma}$  is the mean frequency,  $Q_b$  is the fraction of breaking waves and  $H_{max}^2 = \gamma d$  is the maximum wave height that can exist at the given depth  $d$  where  $\gamma$  is the breaker parameter (set to 0.73).  $E_{tot}$  is the total wave energy integrated over all directions and frequencies (The SWAN team, 2013a).

During a surge the water depth deepens and the fraction of breaking waves reduces. This has the effect of moving the breaking zone towards the coast and increasing wave heights in coastal areas.

### 2.3.4. Whitecapping

Whitecapping is represented by the pulse-based model of Hasselmann (1974):

$$S_{wc}(\sigma, \theta) = -\Gamma \tilde{\sigma} \frac{k}{k} E(\sigma, \theta), \quad (8)$$

where  $\tilde{k}$  is the mean wave number. The coefficient  $\Gamma$  depends on the overall wave steepness (The SWAN team, 2013a). In the presence of opposing currents waves experience enhanced whitecapping, because with opposing current wave number and wave steepness increases.

### 2.3.5. Bottom friction

The empirical model of JONSWAP (Hasselmann et al., 1973) is used to express bottom friction

$$S_{bot} = -C_b \frac{\sigma^2}{g^2 \sinh^2(kd)} E(\sigma, \theta), \quad (9)$$

where  $C_b = 0.038 \text{ m}^2 \text{ s}^{-3}$  is the bottom friction coefficient (The SWAN team, 2013a).

As the surface currents affect the spectral wave energy, the bottom friction will also experience change. Bottom friction will increase with increasing wave energy e.g. in the case of an opposite current.

## 2.4. Model set-up and dynamical forcing

A nine-day period was chosen for the simulations, from 23.10.2013 to 31.10.2013. This includes calm to moderate weather conditions and a storm. In order to achieve realistic

**Table 1** Description of SWAN simulations.

r1 – simulation 1	(Reference simulation) wind
r2 – simulation 2	Wind and surface currents
r3 – simulation 3	Wind and sea level
r4 – simulation 4	Wind, surface currents and sea level

results in coastal areas, a nesting approach was used. The whole Baltic Sea region was simulated with a resolution of 1 nautical mile (nm). From there boundary conditions were obtained for the eastern Baltic Sea area, which had a resolution of 0.5 nm. The area of the 0.5 nm grid is shown in Fig. 1.

SWAN was forced with a 10 m wind field from the atmospheric model HIRLAM (Unden et al., 2002) interpolated on a model grid. HIRLAM wind fields had a spatial resolution of 11 km and a temporal resolution of 1 h. Additionally, input of surface currents and sea level were taken from the HIROMB model (Funkquist and Kleine, 2007; Lagema, 2012). Current values for the 1 nm grid were taken at a depth of 2 m. For the 0.5 nm grid the depth was 1.5 m. The SWAN computational grid and HIROMB horizontal grid were defined to be identical in order to avoid interpolation errors.

For bathymetry the Baltic Sea Bathymetry Database data was used (Baltic Sea Hydrographic Commission, 2013). Bathymetry was interpolated to the SWAN computational grid which was identical to HIROMB horizontal grid.

The integration time step for SWAN simulations was 10 min with directional bin width of  $10^\circ$ . Input fields of wind, currents and sea level to the wave model had a time step of 1 h. Output of SWAN was also requested once per hour.

Four simulations with SWAN were made using different dynamical forcings. Wind, surface currents and sea level were considered. In Table 1 there is a description of all the simulations. First a reference simulation with SWAN where there was only forcing by wind. On the second simulation, in addition to the wind, surface currents were included. With the third simulation, wind and sea level impact were taken into account. Finally, in the fourth simulation, all the dynamical forcings were present.

In this study it is assumed that the current and sea level are not affected by the wave field.

## 2.5. Wave parameters and statistics

The main focus of this study is to investigate the effects of hydrodynamics on significant wave height ( $H_s$ ), which is defined as the mean height of the highest third of waves. In SWAN it is expressed as  $H_s = 4 \sqrt{\int \int E(\omega, \theta) d\omega d\theta}$ , where  $\omega$  is the radian frequency.

To evaluate the performance of the model, four statistical parameters were calculated for simulations and measurements: the root mean square error (RMSE), the scatter index (SI), the mean deviation (BIAS) and the correlation coefficient:

$$RMSE = \sqrt{\frac{1}{N} \sum_{i=1}^N (a_i - b_i)^2}, \quad (10)$$

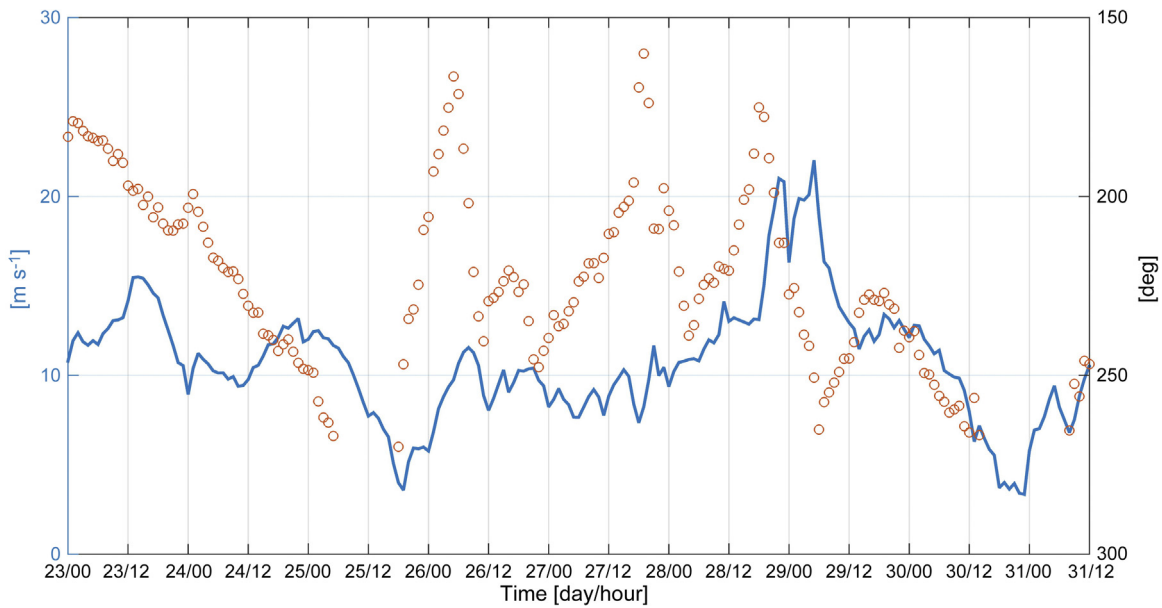


**Figure 2** A time series of HIRLAM mean wind speed (blue line) and direction (red circles) near station B from modelling period 23.10.2013 to 31.10.2013. (For interpretation of the references to colour in this figure legend, the reader is referred to the web version of this article.)

$$SI = \frac{RMSE}{\frac{1}{N} \sum_{i=1}^N b_i} \times 100\%, \quad (11)$$

$$BIAS = \frac{\sum_{i=1}^N (a_i - b_i)}{N}, \quad (12)$$

where  $a$  is the model data,  $b$  is the measurement and  $N$  is the number of elements.

In order to see the effects of different dynamical forcings, the significant wave height changes were studied by comparing the significant wave height of each model simulation ( $n = 2, 3, 4$ ) with the reference simulation  $n = 1$  at every time moment  $t$ :

$$\Delta Hs^n(t) = Hs^n(t) - Hs^1(t). \quad (13)$$

To see the maximum range of possible change in significant wave height, the maximum difference over the time period of the storm day (whole day 29.10.2013) was calculated. The maximum difference  $\Delta mHs^n$  for each grid point ( $lon, lat$ ) was found as:

$$\Delta mHs^n = \Delta Hs^n(t_{max}^n), \quad (14)$$

where  $t_{max}^n$  (Eq. (15)) is the time when the difference of significant wave height (Eq. (13)) is maximum:

$$t_{max}^n = \operatorname{argmax}(|\Delta Hs^n(t)|). \quad (15)$$

The maximum relative change was also calculated:

$$\Delta rHs^n = \frac{\Delta mHs^n}{Hs^1} \times 100\%, \quad (16)$$

where

$$Hs^1 = Hs^1(t_{max}^n), \quad (17)$$

and significant wave height of reference run r1  $Hs^1$  was found at time moment  $t_{max}^n$ .

### 3. Results and discussion

#### 3.1. Weather and sea state

A time series of HIRLAM 10 m mean wind speed and direction near the west coast of Saaremaa near measurement station B (see Fig. 1) is shown in Fig. 2.

From 23.10.2013 to 28.10.2013 mean wind speed ranges between 4 and 15 m s<sup>-1</sup> which is considered to be calm to moderate weather. The storm, named St. Jude, lasted three days. It arrived in Estonia in the evening of 28.10.2013 and reached its highpoint in the early morning of the 29th. The weather started to calm down at the beginning of the next day.

At the peak of the storm, on 29.10.2013 at 04.00 mean wind speed, current velocity, sea level and significant wave height are shown in Fig. 3. During the storm the mean wind speed reaches 22 m s<sup>-1</sup> (Fig. 3a). Wind was blowing from the sector S–SW, which is one of the most frequent wind directions in the Baltic Sea (Jaagus and Kull, 2011).

In Fig. 3b the simulated surface current velocities and propagation directions (every 10th vector is displayed) at the highpoint of the storm are displayed. Current speed reaches up to 195 cm s<sup>-1</sup> in the Irbe strait. In the Gulf of Finland, in Pärnu bay and around Hiiumaa and Saaremaa the highest currents are up to 90 cm s<sup>-1</sup>. The simulated surge reached up to 200 cm, compared to the model zero level (Fig. 3c). To the south east of Hiiumaa and Saaremaa, on the Finnish coast and in the Irbe strait the surge was up to 80 cm. In the deeper parts of the eastern Baltic it ranged from 80 to 100 cm. Simulated significant wave height (Fig. 3d) reached 6.5 m in the eastern Baltic Sea. Entering the Gulf of Finland and Gulf of Riga the wave height starts to decrease. Near the shore significant wave height is up to 2.5 m.

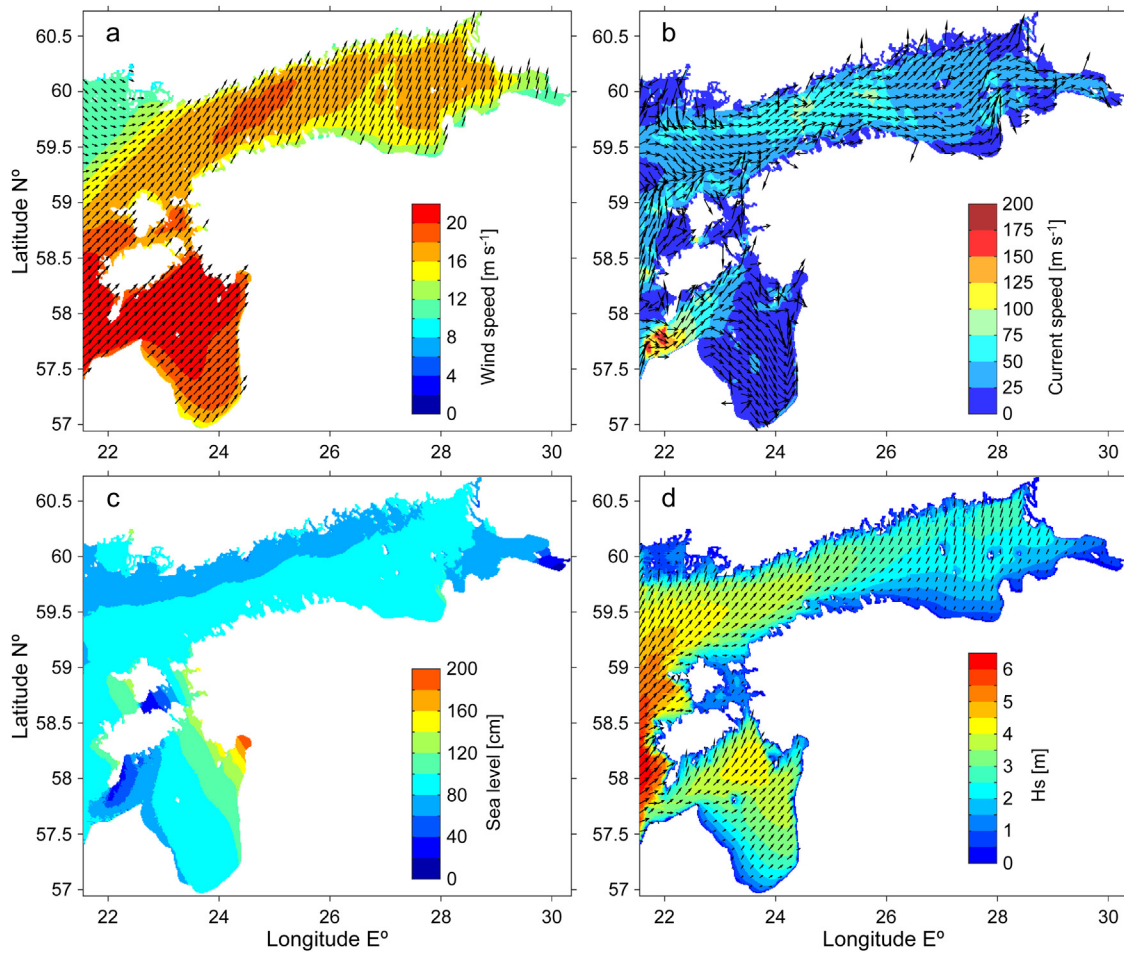


**Figure 3** On 29.10.2013 at 04:00: (a) mean wind speed and direction (from HIRLAM model); (b) current velocity and direction (from HIROMB model); (c) the increase in the sea level (from HIROMB model); and (d) significant wave height (from SWAN model).

### 3.2. Comparison to measurements

Significant wave height is compared with measurements taken in deep water (depth 43 m) and close to the shore

(measurement station A and B on Fig. 1, respectively). Wave direction is compared to SAR data. The model point chosen for comparison with station A is ca 200 m away with a water depth of 42.85 m.

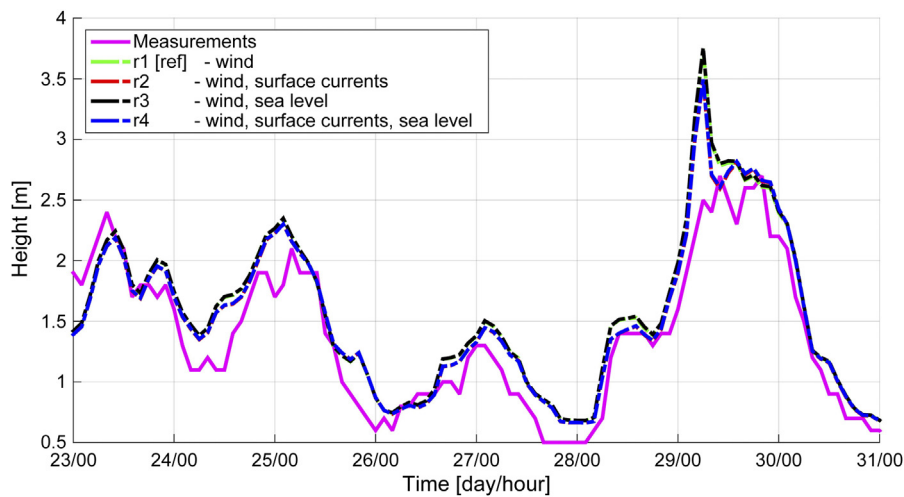


**Figure 4** Comparison of measurements of significant wave height taken in Gulf of Finland in station A and SWAN simulations r1 to r4.

**Table 2** RMSE, scatter index, BIAS and correlation coefficient are calculated from comparison of measurements in Gulf of Finland (measurement station A, Fig. 1) and model results. (a) In the time period from 23.10.2013 00.00 to 31.10.2013 23.00 – the whole modelling period. (b) Time period during the storm, 28.10.2013 00.00 to 30.10.2013 12.00.

	RMSE [cm]	Scatter index [%]	BIAS [cm]	Correlation coefficient
(a) 23.10.2013 00.00 to 31.10.2013 23.00				
Simulation 1	28	22	19	0.95
Simulation 2	25	19	15	0.95
Simulation 3	29	22	19	0.95
Simulation 4	25	19	16	0.95
(b) 28.10.2013 00.00 to 30.10.2013 12.00				
Simulation 1	36	21	26	0.95
Simulation 2	29	17	21	0.96
Simulation 3	37	22	27	0.95
Simulation 4	30	18	21	0.96

In Fig. 4, significant wave height from all four simulations (r1–r4) is compared. The time period for the validation in deep water covers the whole simulation period from 23.10.2013 to 31.10.2013. Simulated significant wave height follows the variability of the measurements well. In general the wave height is overestimated by the model in all runs. On 29.10.13 there is an unexpected overshoot in all the simulations. It is not caused by meteorological forcing time steps, as the wind is interpolated linearly over time for the model input. Simulations r2 and r4 show a slight improvement in the model results compared to r1 and r3.

Next the statistical parameters for significant wave height are calculated using Eqs. (10)–(12). Calculated over the period of 23.10.2013 00.00 to 31.10.2013 23.00 (Table 2a), the best results are produced with simulations r2 and r4, where surface currents are accounted for. RMSE for the reference simulation r1 is 28 cm, SI 22% and BIAS 19 cm. Taking into account currents (r2) RMSE decreases 3 cm, scatter index 3% and BIAS 4 cm. Considering only sea level

in the simulations has a negative impact on the results. This may be due to the fact that the measurement point is situated in deep water. The study of Alari (2013) shows that sea level plays a more significant role in shallower waters. Correlation between measurements and the model is reasonably good, 0.95 for all the simulations.

Now looking separately at the statistics for the storm period 28.10.2013 00.00 to 30.10.2013 12.00 (Table 2b), it is apparent that accounting for surface currents improves the comparison significantly. As the RMSE of reference simulation r1 in storm conditions is 36 cm, it decreases when taking account of currents by 7 cm. The scatter index and BIAS also show improvement. Correlation goes from 0.95 (r1 and r3) to 0.96 (r2 and r4).

The *ad hoc* measurements at station B near Saaremaa Island lasted from 26.10.2013 to 31.10.2013. Measurements were taken at a location where there were large gradients in water depth. In the model bathymetry the closest point to the measurement station had a depth of 21.10 m. Therefore another point in shallower water, with depth of 7.83 m, was chosen as a comparison point. The latter point is ca 1 km away from station B.

In Fig. 5 it can be seen that, as with the deeper water, the model again overestimates measurements. Reference simulation r1 is closest to the measured results. Taking currents into account (r2), the significant wave height is overestimated even more. Considering sea level and also surface currents, both increase the wave height compared to simulations r1 and r2. In the case of current being accounted for, the increase of significant wave height can be explained by the changes in the group velocity of waves. With a decrease in the group velocity in the case of opposing current, in order to maintain energy flux, the wave energy density has to increase.

Model deviations from measurements increase when more dynamical forcings are added to the simulations (Table 3). This can be caused by several factors. In shallow water bottom effects occur, making the balance between wind, surface currents and sea level quite complicated. For example, unknown local bathymetrical features not resolved by the model may be the cause of increasing errors (Tuomi et al., 2014). While the water depth at station B was 5.5 m only,

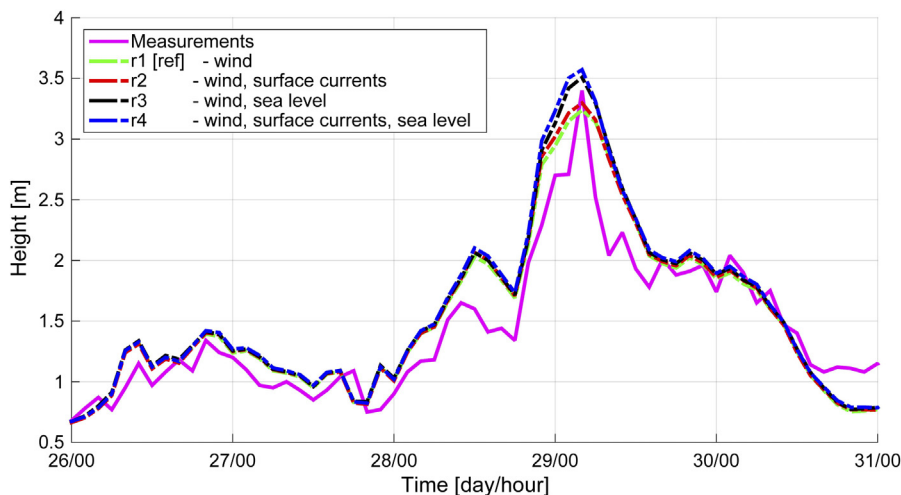


**Figure 5** Comparison of measurements of significant wave height taken close to Saaremaa at station B and SWAN simulations r1 to r4.

**Table 3** RMSE, scatter index, BIAS and correlation coefficient between measurements taken close to Saaremaa (measurement station B, Fig. 1) and model simulations.

Simulation	RMSE [cm]	Scatter index [%]	BIAS [cm]	Correlation coefficient
1	26	18	9	0.93
2	27	19	10	0.93
3	29	21	12	0.93
4	30	22	13	0.94

**Table 4** RMSE between SWAN and SAR peak directions.

RMSE [°]	Simulation			
	1	2	3	4
	47.10	49.01	47.08	48.94

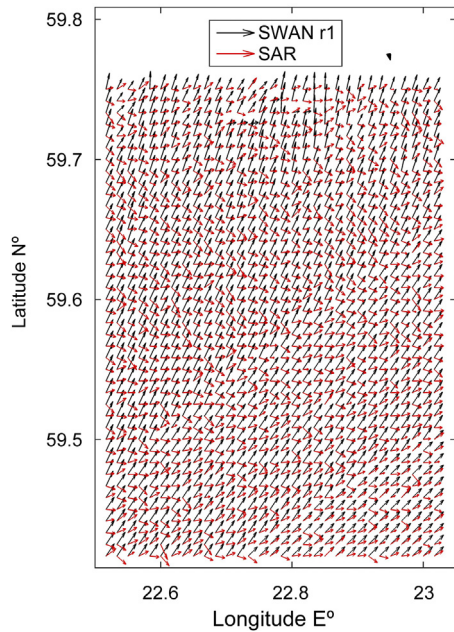


**Figure 6** SWAN peak direction in simulation 1 (black arrows) are compared with SAR image (red arrows) on 29.10.2013 at 05.00. (For interpretation of the references to colour in this figure legend, the reader is referred to the web version of this article.)

water depth at the model point was 7.83 m. This calls for higher-resolution simulations, which are outside the scope of the present study.

Peak wave peak directions calculated with SWAN were compared to results from SAR images. The area of validation is shown in Fig. 1. In Fig. 6 SWAN reference simulation peak directions (red arrows) and directions provided by SAR (black arrows) are displayed. A moderate difference between the directions can be seen. In Table 4 RMSE of direction for all four simulations is presented. It varies between 47.08 and 49.01°. Simulation 3, where water level was included in the simulation, produces the best result, with RMSE of 47.08°.

### 3.3. Spatio-temporal impact of currents and sea-level

In order to quantify the impact of different dynamical forcings, the maximum difference of significant wave height  $\Delta mHs^n$  and relative change  $\Delta rHs^n$  were found with Eqs. (13)–(17). It was seen from the validations that current and sea-level effects are most noticeable during the St. Jude storm. For this reason the day of 29.10.2013 was chosen to evaluate the spatial variability of the wave field.

In Fig. 7 the probability density functions of spatial  $\Delta mHs^n$  distribution are presented on a logarithmic scale. It shows the distribution of maximum difference of significant wave height. With simulation r2 (red line), where wind and surface currents were taken into account, there is a decrease in the wave height of up to 50 cm and an increase as big as 40 cm compared to r1. When taking account of wind and sea level (r3, black line) the difference ranges from –10 to 100 cm. With varying sea level the increase in the wave height is more evident. This should be the case, since with increased water

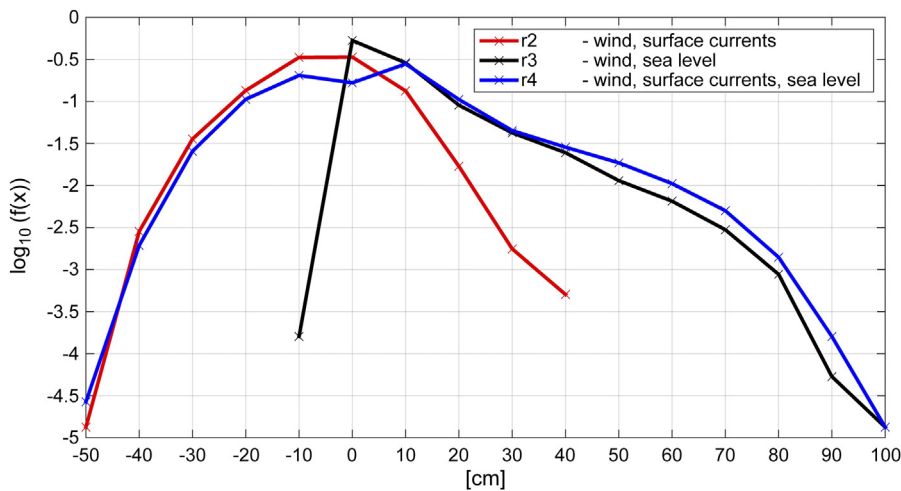


**Figure 7** Significant wave height maximum differences  $\Delta mHs^n$  logarithmical probability distribution for simulations r2, r3 and r4 on 29.10.2013.

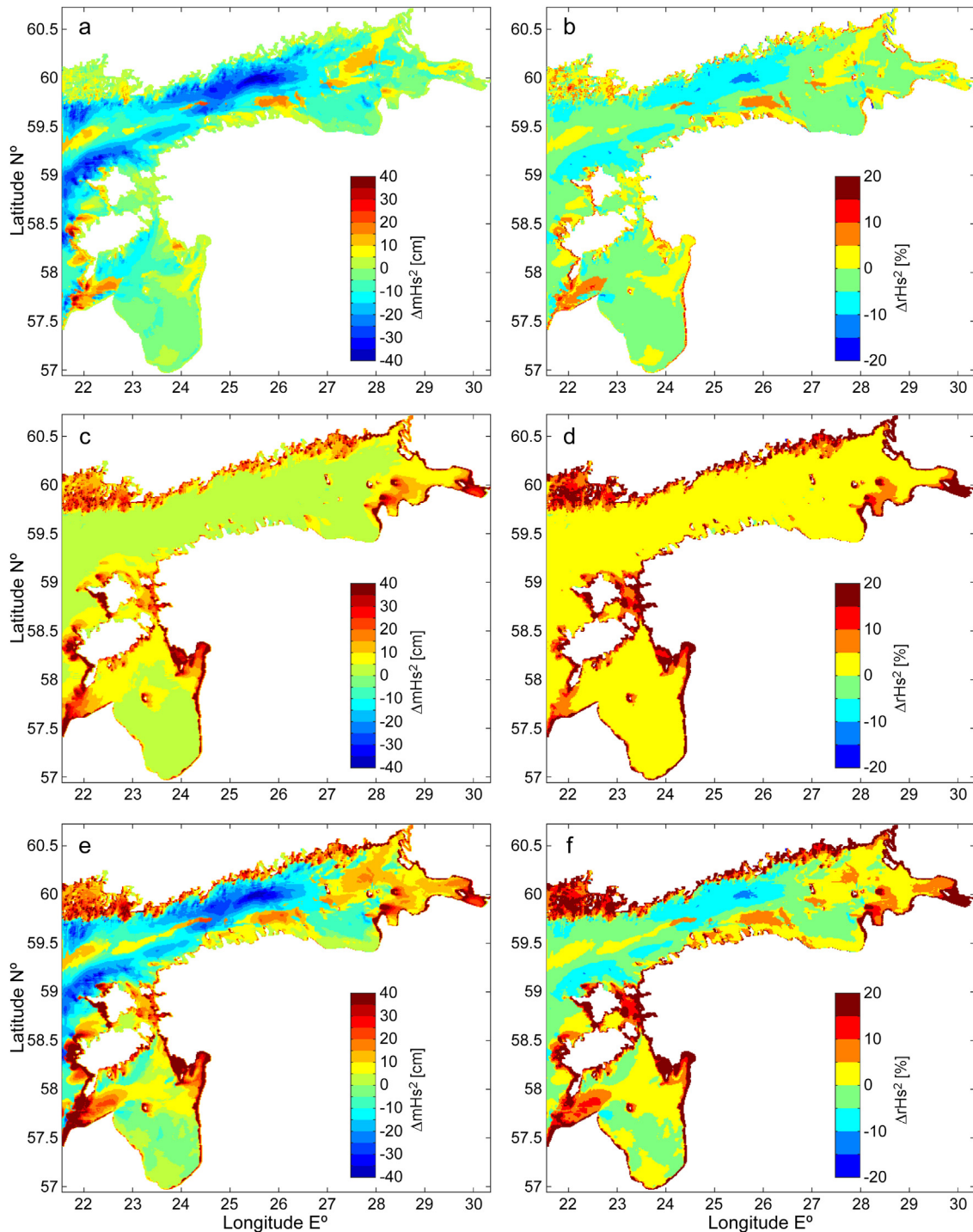


**Figure 8** Time maximum absolute difference  $\Delta mHs^n$  and relative difference  $\Delta rHs^n$  in the significant wave height. (a and b) for r2; (c and d) for r3; (e and f) for r4. Values in a range  $-40$  to  $40$  cm and  $-20$  to  $20\%$  are shown in the figure.

level the dissipation is less. Accounting for all the dynamical forcings, the difference of  $\Delta mHs^4$  ranges from  $-50$  to  $100$  cm.

Next the spatial variability of maximum difference of significant wave height  $\Delta mHs^n$  is shown in Fig. 8 on the left side and relative change  $\Delta rHs^n$  on the right side. The colour bar ranges from  $-40$  cm to  $40$  cm in the case of absolute differences and from  $-20\%$  to  $20\%$  for the relative changes.

In Fig. 8a and b the maximum absolute difference and relative change in the significant wave height when taking

account of surface currents (r2) is shown. Increase in the wave height is most evident near coasts and in narrow straits. In the southern part of the Gulf of Finland near the coast there is an increase of up to  $10$  cm ( $5\%$ ). In the north-east of the Gulf of Riga there is an increase of up to  $20$  cm ( $10\text{--}15\%$ ). Near the west coast of Hiiumaa wave height difference is about  $10\text{--}20$  cm (up to  $20\%$ ). In Saaremaa and in the Irbe strait the difference can reach as much as  $40$  cm (up to  $20\%$ ).

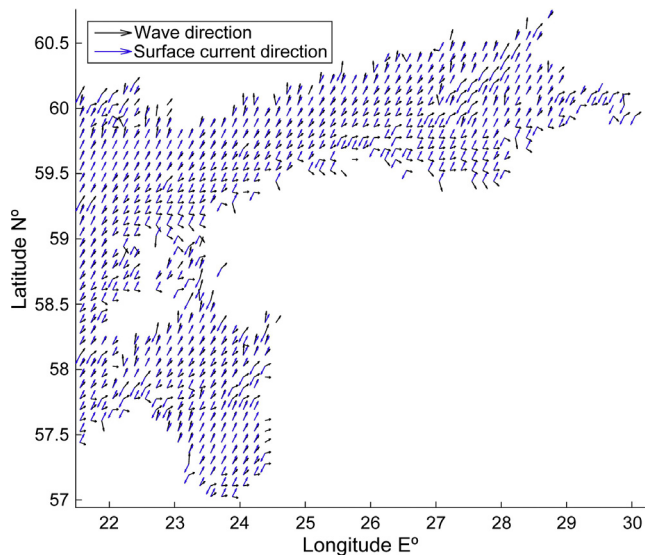


**Figure 9** Propagation directions for waves in run r2 and surface currents on the time moments of maximum differences on 29.10.2013. Every 10th vector is displayed.

In Fig. 9 every 10th vector of wave and current propagation direction at time moment  $t_{\max}$  (of simulation r2) are displayed. Wave directions are shown with black arrows and surface currents with blue arrows. As waves and surface currents approach opposite directions, currents have the effect of elevating wave height. For example in Fig. 9 in Pärnu bay, the Irbe strait and on the west coast of the islands Hiiumaa and Saaremaa the waves and surface currents are propagating in opposite directions (or the current direction is deflected right of the wave directions). This results in a greater wave height increase, seen also in Fig. 8a.

In the case of currents being accounted for, a decrease of the significant wave height occurs in deeper parts of the eastern Baltic Sea. In the Gulf of Riga and Gulf of Finland there is a decrease of up to 15 cm (5%). In the Gulf of Finland between 25–26°E and 58.8–60°N wave height decreases up to 40 cm (20%) (Fig. 8a and b). In Fig. 9 it is seen that in these areas waves and surface currents are propagating more or less in the same direction and this results in a decrease of significant wave height, which is also consistent with the theory.

It is likely that the maximum differences in significant wave height occur in a specific phase of the surface currents inertial oscillation. The magnitude of the increase and decrease of significant wave height is influenced by current velocity. For example in the Irbe strait the current velocity reaches up to 195 cm s<sup>-1</sup> (Fig. 3b) and from Fig. 8a and b it is seen that in this area the significant wave height is one of the things most strongly affected by the surface currents.

In Fig. 8c and d the maximum difference and relative change of significant wave height when considering wind and sea level in the run (r3) is shown. In deeper parts of the eastern Baltic Sea, where the waves are not affected by the sea bed, there is an increase in the significant wave height of about 5 cm with relative increase of 5%. Near the coast, where the bottom effects come into play, a bigger increase in

the wave height is noticeable. In coastal areas the maximum difference of significant wave height between reference run r1 and r3 is up to 40 cm (20%). Also in specific locations in the Gulf of Finland and in the Gulf of Riga there is a possible increase in wave height of 40%. It is seen that areas most significantly affected by sea-level are well exposed to the wind. This is also consistent with the work by Alari (2013).

In Fig. 8e and f it is shown the joint effect of surface currents and sea level on the wave field. On areas open to the wind the total impact of surface currents and sea level on wave height increases. For example in Pärnu bay when accounting for just currents the difference is up to 20 cm (10–15%), but the joint effect increases the wave height up to 40 cm (20%). The spatial variability patterns of surface current effects and sea level both remain. The decrease in the significant wave height remained more or less in the same areas where it was when there were just surface currents present.

#### 4. Conclusions

Analysis of spatio-temporal patterns of wave–current–surge interaction in the eastern Baltic Sea and the corresponding mechanisms showed the impact of surface currents and sea level to the evolution of significant wave height. In deep (>20 m) water, surface currents improved the model-data comparison, especially in storm conditions. Variations in sea level had a negligible effect in deep waters, but in shallower water the effect of sea level was even larger than that of the surface currents. The extra increase in wave height was most noticeable in storm conditions and in wind exposed areas. During extreme storms, the joint effect of currents and sea level produced changes in the significant wave height from lowering it by as much as 50 cm (mostly offshore), compared to the control run, to increasing it up to 100 cm (nearshore). The relative differences of up to 20% being distributed non-symmetrically. Considering the effect of surface currents only, the range was between –50 and 40 cm whereas the sea level induced changes were between –10 and 100 cm, compared to the control run. The differences in significant wave heights were favoured under a specific phase of inertial oscillation of the surface currents.

As the wave growth effect is concentrated in the narrow coastal zone, even a 0.5 nautical mile model grid was not accurate enough to capture all the local topographical features. For further studies of this kind, higher resolution models should be used and appropriate (directional) measurements in shallow water are needed for model validation.

#### Acknowledgment

We are grateful to Benjamin Matterson for providing language help.

#### References

- Alari, V., 2013. *Multi-scale wind wave modeling in the Baltic Sea*. (PhD Dissertation). Tallinn Univ. Technol., 134 pp.
- Baltic Sea Hydrographic Commission, 2013. Baltic Sea Bathymetry Database version 0.9.3, (Downloaded from <http://data.bshc.pro/> on 21.03.2015).

- Battjes, J.A., Janssen, J.P.F.M., 1978. Energy loss and set-up due to breaking of random waves. In: Proc. of the 16th International Conference on Coastal Engineering. 569–587, <http://dx.doi.org/10.1061/9780872621909.034>.
- Booij, N., Ris, R.C., Holthuijsen, L.H., 1999. A third-generation wave model for coastal regions: 1. Model description and validation. *J. Geophys. Res.* 104 (C4), 7649–7666, <http://dx.doi.org/10.1029/98JC02622>.
- Bretherton, F.P., Garrett, C.J.R., 1968. Wavetrains in inhomogeneous moving media. *Proc. Roy. Soc. A: Math. Phys.* 302 (1471), 529–554, <http://dx.doi.org/10.1098/rspa.1968.0034>.
- Feistel, R., Nausch, G., Wasmund, N., 2008. *State and Evolution of the Baltic Sea, 1952–2005: A Detailed 50-year Survey of Meteorology and Climate, Physics, Chemistry, Biology and Marine Environment*. John Wiley & Sons, Hoboken, 712 pp.
- Feser, F., Barcikowska, M., Krueger, O., Schenk, F., Weisse, R., Xia, L., 2015. Storminess over the North Atlantic and northwestern Europe – a review. *Q. J. Roy. Meteor. Soc.* 141 (687), 350–382, <http://dx.doi.org/10.1002/qj.2364>.
- Funkquist, L., Kleine, E., 2007. *An introduction to HIROMB, an operational baroclinic model for the Baltic Sea*. SMHI Rep. *Oceanogr.* 37, 1–39.
- Guedes Soares, C., de Pablo, H., 2006. Experimental study of the transformation of wave spectra by a uniform current. *Ocean Eng.* 33 (3–4), 293–310, <http://dx.doi.org/10.1016/j.oceaneng.2005.05.005>.
- Hasselmann, K., 1974. On the spectral dissipation of ocean waves due to whitecapping. *Bound.-Lay. Meteorol.* 6 (1), 107–127, <http://dx.doi.org/10.1007/BF00232479>.
- Hasselmann, K., Barnett, T.P., Bouws, E., Carlson, H., Cartwright, D. E., Enke, K., Ewing, J.A., Gienapp, H., Hasselmann, D.E., Kruseman, P., Meerburg, A., 1973. *Measurements of Wind-Wave Growth and Swell Decay During the Joint North Sea Wave Project (JONSWAP)*. Deutsches Hydrogr. Inst.
- Jaagus, J., Kull, A., 2011. Changes in surface wind directions in Estonia during 1966–2008 and their relationships with large-scale atmospheric circulation. *Est. J. Earth Sci.* 60 (4), 220–231, <http://dx.doi.org/10.3176/earth.2011.4.03>.
- Kahma, K.K., Petterson, H., 1993. *Wave Statistics from the Gulf of Finland*. Finnish Inst. Marine Rep., Intern. Rep. 1.
- Lagemaa, P., 2012. *Operational forecasting in Estonian marine waters*. (Ph.D. diss.). Tallinn Univ. Tech., 130 pp.
- Leppäranta, M., Myrberg, K., 2009. *Physical Oceanography of the Baltic Sea*. Springer-Verlag, Berlin, Heidelberg, 378 pp., <http://dx.doi.org/10.1007/978-3-540-79703-6>.
- Longuet-Higgins, M.S., Stewart, R.W., 1960. Changes in the form of short gravity waves on long waves and tidal currents. *J. Fluid Mech.* 8 (4), 565–583, <http://dx.doi.org/10.1017/S0022112060000803>.
- Longuet-Higgins, M.S., Stewart, R.W., 1961. The changes in amplitude of short gravity waves on steady non-uniform currents. *J. Fluid Mech.* 10 (4), 529–549, <http://dx.doi.org/10.1017/S0022112061000342>.
- Longuet-Higgins, M.S., Stewart, R.W., 1964. Radiation stresses in water waves; a physical discussion, with applications. *Deep Sea Res. Oceanogr. Abstr.* 11 (4), 529–562, [http://dx.doi.org/10.1016/0011-7471\(64\)90001-4](http://dx.doi.org/10.1016/0011-7471(64)90001-4).
- Miles, J.W., 1957. On the generation of surface waves by shear flows. *J. Fluid Mech.* 3 (2), 185–204, <http://dx.doi.org/10.1017/S0022112057000567>.
- Phillips, O.M., 1957. On the generation of waves by turbulent wind. *J. Fluid Mech.* 2 (5), 417–445, <http://dx.doi.org/10.1017/S0022112057000233>.
- Raudsepp, U., Laanemets, J., Haran, G., Alari, V., Pavelson, J., Kõuts, T., 2011. Flow, waves, and water exchange in the Suur Strait, Gulf of Riga, in 2008. *Oceanologia* 53 (1), 35–56, <http://dx.doi.org/10.5697/oc.53-1.035>.
- Soomere, T., Behrens, A., Tuomi, L., Nielsen, J.W., 2008. Wave conditions in the Baltic Proper and in the Gulf of Finland during windstorm Gudrun. *Nat. Hazards Earth Syst.* 8 (1), 37–46, <http://dx.doi.org/10.1016/j.ecss.2014.08.001>.
- Suursaar, Ü., 2013. Locally calibrated wave hindcasts in the Estonian coastal sea in 1966–2011. *Est. J. Earth Sci.* 62 (1), 42–56, <http://dx.doi.org/10.5697/oc.54-3.421>.
- Suursaar, Ü., Kullas, T., Aps, R., 2012. Currents and waves in the northern Gulf of Riga: measurements and long-term hindcast. *Oceanologia* 54 (3), 421–447, <http://dx.doi.org/10.5697/oc.54-3.421>.
- The SWAN team, 2013a. *SWAN: Scientific and Technical Documentation. Cycle III version 40.91*. Delft University of Technology, Department of Civil Engineering, The Netherlands.
- The SWAN team, 2013b. *SWAN: User Manual. Cycle III version 40.91*. Delft University of Technology, Department of Civil Engineering, The Netherlands.
- Tuomi, L., Pettersson, H., Fortelius, C., Tikka, K., Björkqvist, J.V., Kahma, K.K., 2014. Wave modelling in archipelagos. *Coast. Eng.* 83, 205–220, <http://dx.doi.org/10.1016/j.coastaleng.2013.10.011>.
- Uden, P., Rontu, L., Jarvinen, H., Lynch, P., Calvo, J., Cats, G., Cuxart, J., Eerola, K., Fortelius, C., Garcia-Moya, J.A., Jones, C., Lenderlink, G., McDonald, A., McGrath, R., Navascues, B., Nielsen, N.W., Odegaard, V., Rodriguez, E., Rummukainen, M.A., 2002. *HIRLAM-5 Scientific Documentation*. Swedish Meteorol. Hydrol. Inst., Sweden.
- Van der Westhuysen, A.J., 2012. Spectral modeling of wave dissipation on negative current gradients. *Coast. Eng.* 68, 17–30, <http://dx.doi.org/10.1016/j.coastaleng.2012.05.001>.
- Whitham, G.B., 1974. *Linear and Nonlinear Waves*. John Wiley, New York, 55 pp.
- Wolf, J., Prandle, D., 1999. Some observations of wave–current interaction. *Coast. Eng.* 37 (3), 471–485, [http://dx.doi.org/10.1016/S0378-3839\(99\)00039-3](http://dx.doi.org/10.1016/S0378-3839(99)00039-3).
- Wolski, T., Wiśniewski, B., Giza, A., Kowalewska-Kalkowska, H., Boman, H., Grabbi-Kaiv, S., Hammarklint, T., Holfort, J., Lydeikaite, Ž., 2014. Extreme sea levels at selected stations on the Baltic Sea coast. *Oceanologia* 56 (2), 259–290, <http://dx.doi.org/10.5697/oc.56-2.259>.



Available online at [www.sciencedirect.com](http://www.sciencedirect.com)

ScienceDirect

journal homepage: [www.elsevier.com/locate/oceano](http://www.elsevier.com/locate/oceano)



ORIGINAL RESEARCH ARTICLE

# Fisher–Shannon analysis of the time variability of remotely sensed sea surface temperature at the Brazil–Malvinas Confluence<sup>☆</sup>

Jorge O. Pierini<sup>a</sup>, Michele Lovallo<sup>b</sup>, Eduardo A. Gómez<sup>c</sup>, Luciano Telesca<sup>d,\*</sup>

<sup>a</sup> *Comisión de Investigaciones Científicas (CIC)–UCALP–CCT–BB (IADO–CONICET), CC 804, Bahía Blanca, Argentina*

<sup>b</sup> *ARPAB, Potenza, Italy*

<sup>c</sup> *CCT–BB (IADO–CONICET), UTN Facultad Regional Bahía Blanca, Bahía Blanca, Argentina*

<sup>d</sup> *National Research Council, Institute of Methodologies for Environmental Analysis, Tito, PZ, Italy*

Received 8 May 2015; accepted 12 February 2016

Available online 19 March 2016

## KEYWORDS

Brazil–Malvinas Confluence Zone; Fisher–Shannon method; Ocean

**Summary** The collision of the warm and salty southward flowing Brazil Current and the cold and relatively fresh northward flowing Malvinas Current produces a strong frontal zone known as the Brazil–Malvinas Confluence Zone (BMCZ). This is featured by intense presence of eddies and meanders and is one of the most energetic areas of the world oceans. We apply the statistical method of Fisher–Shannon (FS) to the time series of sea surface temperature, derived from the satellite Advanced Very High Resolution Radiometer (AVHRR) imagery, acquired from 1984 to 1999. The FS method consists of the joint application of Fisher information measure (FIM) and Shannon entropy (SE), measuring respectively the degree of organization and the disorder of a system. Our findings indicate that the FS method is able to locate very clearly the BMCZ, which corresponds to the less organized and more disordered area within the area of confluence between the Brazil and Malvinas Currents.

© 2016 Institute of Oceanology of the Polish Academy of Sciences. Production and hosting by Elsevier B.V. This is an open access article under the CC BY-NC-ND license (<http://creativecommons.org/licenses/by-nc-nd/4.0/>).

<sup>☆</sup> The study was supported by the 2014–2016 Bilateral Project Italy–Argentina “Use of satellite technologies for large-scale oceanographic and environmental studies over the Argentinean Continental Shelf” funded by MINCyT and MAECI.

\* Corresponding author at: National Research Council, Institute of Methodologies for Environmental Analysis, Tito, PZ, Italy  
E-mail address: [luciano.telesca@imaa.cnr.it](mailto:luciano.telesca@imaa.cnr.it) (L. Telesca).

Peer review under the responsibility of Institute of Oceanology of the Polish Academy of Sciences.



Production and hosting by Elsevier

<http://dx.doi.org/10.1016/j.oceano.2016.02.003>

0078-3234/© 2016 Institute of Oceanology of the Polish Academy of Sciences. Production and hosting by Elsevier B.V. This is an open access article under the CC BY-NC-ND license (<http://creativecommons.org/licenses/by-nc-nd/4.0/>).

## 1. Introduction

The South Atlantic's circulation presents several characteristics that are very significant for climate variability. In this region, which is the main source of equatorial surface and thermocline waters (Blanke et al., 1999; Matano et al., 1993; Speich et al., 2007), the circulation affects the climate of the surrounding continents by influencing the distribution of the sea surface temperature (SST) through lateral advection and/or by propagation of anomalies within the mixed layer (Kushnir et al., 2002). The South Atlantic is linked with the Indian and Pacific Oceans, and therefore it provides a gateway by which the Atlantic meridional overturns.

In the South Atlantic, the Brazil–Malvinas Confluence Zone (BMCZ) is crucial to understand circulation and heat transport processes (Wainer et al., 2000). The BMCZ is located off the coast of Argentina and Uruguay, at the convergence between the warm poleward flowing of the Brazil Current and the cold equatorward flowing of the Malvinas Current, between 35°S and 45°S latitude and 50°W to 70°W longitude. The confluence of these two currents originates a strong thermocline and the formation of many high energy eddies (Maamaatuaiahutapu et al., 1998) (Fig. 1).

The Brazil Current carries warm subtropical water with typical temperature values between 18 and 28°C. It generally

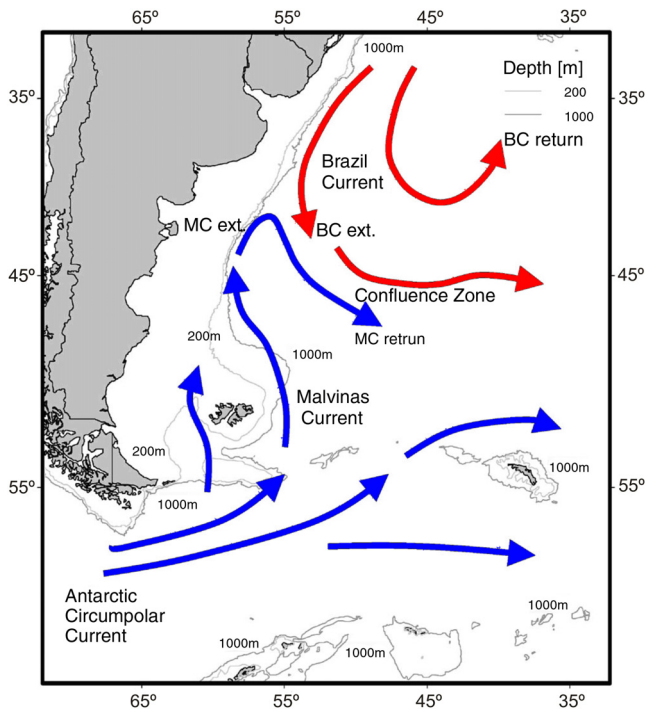


**Figure 1** Map of the Argentinean continental shelf with the warm poleward flowing Brazil Current (red) and the cold equatorward flowing Malvinas Current (blue). Also indicated are the Malvinas Current return (MC return), the Brazil Current extension (BC ext.) and the Brazil Current return (BC return). The continent and the shelf up to the 1000 m and 200 m isobath are indicated by dark gray and light gray line respectively. (For interpretation of the references to color in this figure legend, the reader is referred to the web version of this article.)

flows in the upper 600 m of the ocean and its volume transport at the confluence zone is upwards of 20 Sv with speeds over a half a meter per second (Evans et al., 1983; Memery et al., 2000; Peterson and Stramma, 1990). The Malvinas Current, a branch off of the Antarctic Circumpolar Current, carries cold and relatively fresh subantarctic water, between 60 and 90 Sv and speeds varying from about 0.5 m s<sup>-1</sup> to about 1 m s<sup>-1</sup>. Interestingly, the Malvinas Current extends all the way to the sea-floor, contrarily to the Brazil Current that is a surface current. The temperature ranges typically around 6°C (Vigan et al., 2000; Vivier and Provost, 1999).

After the collision with the Malvinas Current at around 38°S, the Brazil Current branches off into two different paths: the first path is redirected back to the equator creating a large anticyclonic eddy with the original Brazil Current; the second one, which is much stronger than the first one deflects about 45°E of its original tract poleward (Maamaatuaiahutapu et al., 1998). On the contrary, after the collision the surface flow for the Malvinas Current becomes much simpler, being redirected poleward, till about 50°S latitude where it once again is detached back up by the Antarctic Circumpolar Current and heads East (Matano, 1993).

The southeast deflected Brazil Current flows just east of the redirected Malvinas current at around 57.5°W and between 40°S and 45°S (Saraceno et al., 2004, 2006). In this region SST gradients can be as high as 1°C per kilometer. In this zone, which is characterized by very high energy among the world oceans (Gordon, 1989), the meanders, eddies, and filaments are extraordinary. The strong mixing processes cause high-speed cooling of subtropical waters conveyed by the Brazil Current, characterizing this area as very important for the circulation and heat transport processes (Wainer et al., 2000). Provost and Le Traon (1993) report the high inhomogeneity and anisotropy of the BMCZ at the mesoscale. At shorter frequencies, the Brazil–Malvinas Confluence variability is intense and is principally governed by the yearly and semi-annual cycles (Fu, 1996). Podesta et al. (1991) show that the yearly periodicity is responsible for the most of the SST variability in the southwestern Atlantic, and, in particular, of more than 80% of the SST variability on the continental shelf off the southwestern Atlantic Ocean. The eddies, extremely energetic, are featured by intense rotational velocity. Eight or nine different mesoscale eddies with many other microscale eddies could exist at any time. Even if many studies have been done on these high energy turbulent mixing areas, the deep knowledge of these mesoscale processes is still challenging and far from being completely understood (Tokinaga et al., 2005).

Joint use of advanced statistical techniques and satellite images have advanced our knowledge of the relevant scales and features of ocean properties (i.e., Denman and Abbott, 1994; Doney et al., 2003; Lentini et al., 2002; McClain et al., 1998; Stammer, 1997). The application of singularity analysis to SST images has recently suggested a different conceptual approach to the identification of flow patterns from satellite images (Isern-Fontanet et al., 2007; Turiel et al., 2005). Experimental studies of the chaotic properties of oceanic processes have been performed for several years; for instance, Osborne et al. (1986) and Brown and Smith (1990, 1991) investigated deeply the chaotic behavior of oceanic large and mesoscale motions.

Up to now, the majority of researches dealing with SST satellite images in the BMCZ have focused on the complexity of the mesoscale surface structures. Podesta et al. (1991) and Legeckis (1978), using National Oceanic and Atmospheric Administration (NOAA) Advanced Very High Resolution Radiometer (AVHRR) imagery, revealed the highly time variability of the southward extension of the Brazil Current and eddy generation.

In our study, we aim at describing quantitatively the temporal variations of the SST in the BMCZ by using a statistical approach, the so called Fisher–Shannon (FS) method, never used in the context of ocean dynamics and in particular to investigate the variability of the SST. The FS approach is based on the information content of the time series using the statistical measures of the Fisher information measure and the Shannon entropy, and is a powerful statistical method to gain insight into the inner dynamics of a complex system like the BMCZ.

## 2. Data

The SST data analyzed in the present study were part of those produced for the western South Atlantic Ocean on the base of the agreement between Servicio Meteorológico Nacional of Argentina (SMN) and the University of Miami's Rosenstiel School of Marine and Atmospheric Science (RSMAS). The SST fields were derived from data collected by the Advanced Very High Resolution Radiometer (AVHRR), (Olson et al., 1988; Podesta et al., 1991), an infrared radiometer flying onboard polar-orbiting satellites of the National Oceanic and Atmospheric Administration (NOAA). For more information on the AVHRR and NOAA satellites, the reader is referred to the Users' Guide available on [www.noaa.gov](http://www.noaa.gov). The data were recorded at the HRPT Receiving Station operated by SMN in Villa Ortúzar, Buenos Aires, Argentina.

The SST was subjected to atmospheric correction by measuring radiance from the same field of view at two wavelengths (Anding and Kauth, 1970; McClain et al., 1985).

The SST data were compared to in situ measurement for the investigated area (Bava, 2004; Bava et al., 2002; Kilpatrick et al., 2001; Lentini et al., 2001; Saraceno et al., 2004).

The time span is 15 years, from July 1984 to July 1999 and is constituted by 1080 5-day composite images with an approximately 4 km × 4 km resolution. The compositing is done by keeping the warmest pixel among all images available for the 5-day period; in this manner, if a pixel is cloud-contaminated, its temperature is generally lower than that of a pixel in open water. As clouds move within the compositing considered period, the same pixel on a subsequent image may be cloud-free and, consequently, will have a higher SST value. By keeping the warmest value in a series of images, one would decrease the cloud coverage effect in the composited image. However, despite the numbers of individual composite images, cloud coverage would persist over some areas at some times, causing that the SST retrievals for some pixels are not valid in some composite images (Bernstein and Chelton, 1985; Njoku, 1985; Njoku et al., 1985). Fig. 2 shows the spatial distribution of the mean SST value and, as an example, the time variation of five pixels in the BMCZ.

## 3. The Fisher information measure and the Shannon entropy

The Fisher information measure (FIM) and the Shannon entropy are statistical quantities well known in the context of information theory, efficiently used to investigate complex non-stationary signals. The FIM reveals how much organized or ordered is a time series, while the Shannon entropy informs on how much uncertain or disordered a system is.

The FIM was first introduced by Fisher (1925) in the context of estimation theory. Later, it was employed in large variety of applications. Frieden (1990) employed the FIM to represent the evolution laws of physical systems. Martin et al. (1999, 2001) applied it to distinguish the time variations of electroencephalograms (EEG) in order to emphasize significant dynamic changes. Complex phenomena in the field of geophysics and environmental sciences, such as continuous seismic signals measured in volcanic areas, electromagnetic signals related with the generation of earthquakes, and time series of atmospheric particulate matter were investigated by using the FIM to get information about the dynamical mechanisms governing their time variability and to detect precursory signatures of critical phenomena (Lovallo and Telesca, 2011; Telesca and Lovallo, 2011; Telesca et al., 2010, 2011, 2009).

Shannon entropy quantifies the uncertainty of the prediction of the outcome of a probabilistic event (Shannon, 1948), being, then, zero for a deterministic event. Instead of the Shannon entropy, the so-called Shannon power entropy  $N_X$  (defined below) is generally used to avoid the difficulty of negative information measures that can arise when the Shannon entropy is used with a continuous distribution function.

Let  $f(x)$  be the probability density of the SST time series, then its FIM is given by

$$\text{FIM} = \int_{-\infty}^{+\infty} \left( \frac{\partial}{\partial x} f(x) \right)^2 \frac{dx}{f(x)}, \quad (1)$$

and its Shannon entropy is defined as (Shannon, 1948):

$$H_X = - \int_{-\infty}^{+\infty} f_X(x) \log f_X(x) dx. \quad (2)$$

As specified above, the notion of Shannon entropy power will be used (Angulo et al., 2008)

$$N_X = \frac{1}{2\pi e} e^{2H_X}. \quad (3)$$

The quantitative value of the FIM and the Shannon entropy power depends on the right computation of the probability density function  $f(x)$ , estimation of which can be performed by using the kernel density estimator technique (Devroye, 1987; Janicki and Weron, 1994) as shown in Eq. (4)

$$\hat{f}_M(x) = \frac{1}{Mb} \sum_{i=1}^M K\left(\frac{x-x_i}{b}\right), \quad (4)$$

with  $b$  the bandwidth,  $M$  the number of data and  $K(u)$  the kernel function, which is a continuous non-negative and symmetric function satisfying the two following conditions

$$K(u) \geq 0 \quad \text{and} \quad \int_{-\infty}^{+\infty} K(u) du = 1. \quad (5)$$

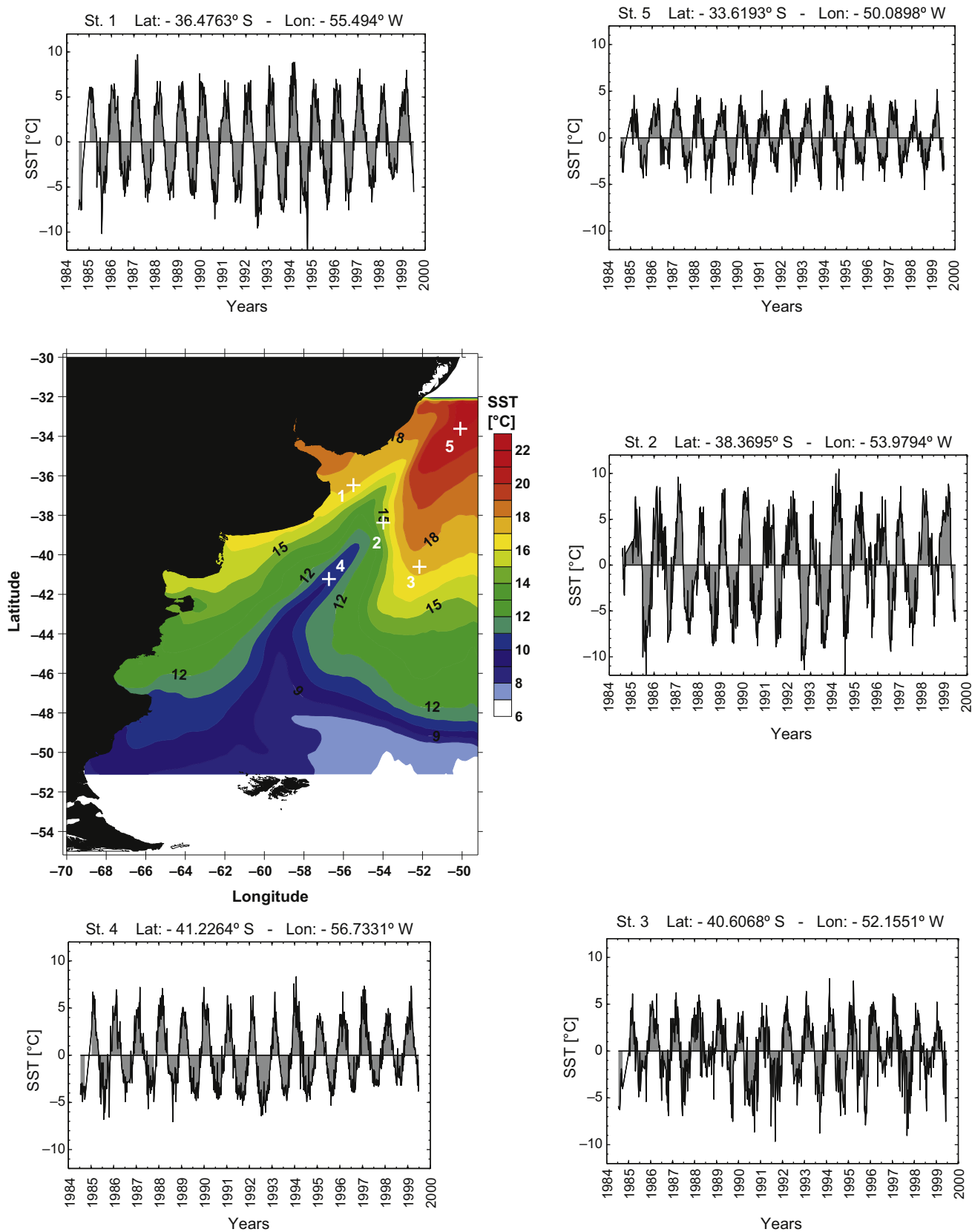


**Figure 2** Spatial distribution of the mean sea surface temperature (SST) value and, as an example, the time variation of five pixels in the Brazil Malvinas Confluence Zone (BMCZ). The SST spatial patterns clearly highlights the interactions between the warmer Brazil Current and the colder Malvinas Current.

In our study,  $f(x)$  was estimated by using Troudi et al.'s algorithm (2008) combined with Raykar and Duraiswami's method (2006), in which a Gaussian kernel with zero mean and unit variance is used:

$$\hat{f}_M(x) = \frac{1}{M\sqrt{2\pi}b^2} \sum_{i=1}^M e^{-\frac{(x-x_i)^2}{2b^2}} \quad (6)$$

### 4. Results and discussion

The strong contrast in sea-surface temperature over the southwest Atlantic makes satellite infrared and color images particularly appropriate tools for studying the BMCZ. We examined 15 years (1984–1999) of AVHRR images to analyze the structure of the collision region (i.e., between 52.5°W and 56°W and 36°S and 40°S) where the Malvinas and Brazil currents produce a very active front.

Because of the presence of some anomalous SST values, very probably due to errors, a data pre-processing was performed and all the SST values deviating from the mean of more than 3 standard deviations were filtered out.

As shown in Fig. 2, the pixel time variation is subjected to seasonal cycles that are necessary to be removed before applying the FS method and to avoid any cycle-induced effect on the results. Since the sampling time of the SST data is not always regular, the cycles were not removed by using the Fourier filtering, but calculating for each 5-day composite the anomaly  $SST_d = (SST - \langle SST \rangle)$  where the composite mean  $\langle SST \rangle$  is calculated for each calendar day, e.g., 1st January, by averaging over all years in the record. This filtering procedure for satellite data was already applied by Telesca and Lasaponara (2005, 2006). Fig. 3 shows the spatial distribution of the mean  $SST_d$ ; as it can be clearly seen, the mean  $SST_d$  is

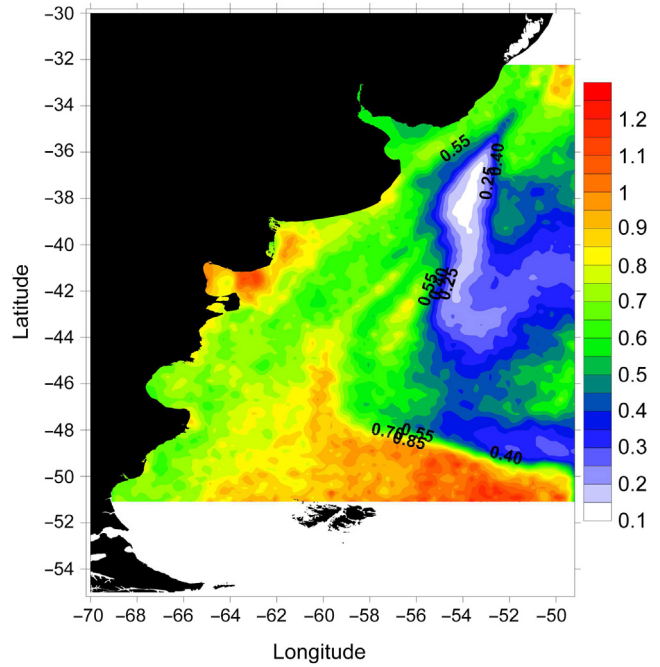


Figure 4 Spatial distribution of the Fisher information measure (FIM) of the  $SST_d$ . The BMCZ occupies the region with lower FIM.

very low and homogeneously spatially distributed in the investigated area. This indicates that the filtering procedure was correctly done and the time dynamics of each pixel is not influenced by any bias due to persistent relatively high or low mean value. To each  $SST_d$  time series the FS method was applied. Figs. 4 and 5 show the spatial distribution of the FIM and Shannon entropy, respectively.

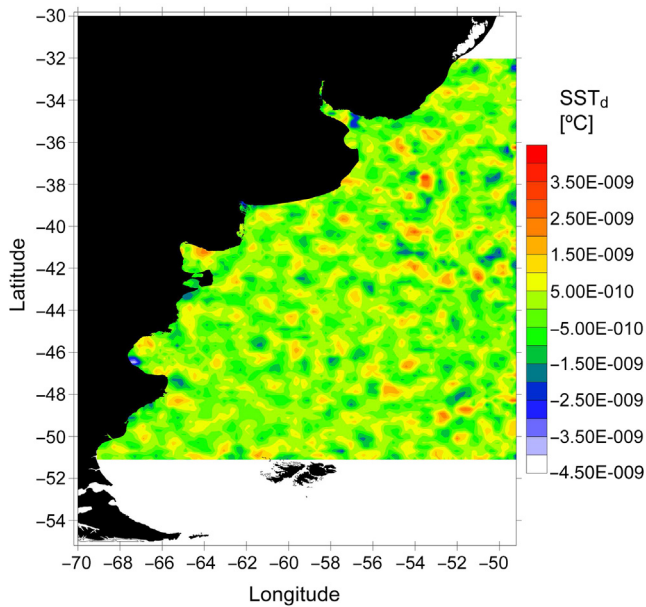


Figure 3 Spatial distribution of the mean sea surface temperature anomaly ( $SST_d$ ). The mean  $SST_d$  is very low and homogeneously spatially distributed in the investigated area, indicating that the time dynamics of each pixel is not influenced by any bias due to persistent relatively high or low mean value.

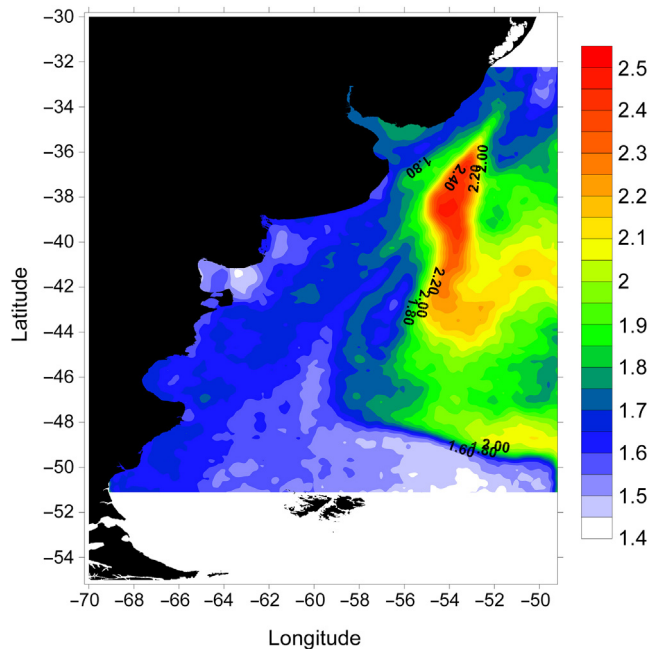
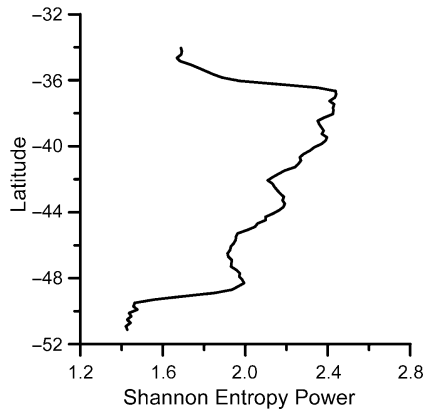
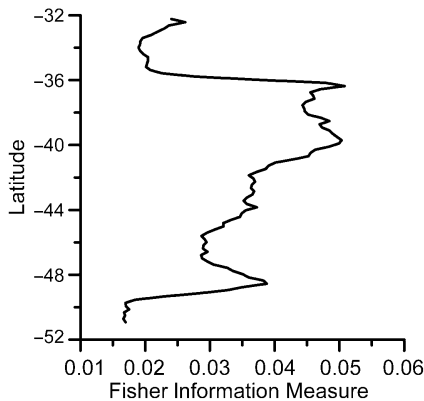


Figure 5 Spatial distribution of the Shannon entropy power of the sea surface temperature anomaly ( $SST_d$ ). The BMCZ occupies the region with higher Shannon entropy.

The FIM and Shannon entropy values can be used to classify the water masses at each pixel. What is striking here, is that the FS analysis suggests that the order/organization structure of the time series of the pixels within the zone occupied by the Brazil Current and of those occupied by the Malvinas Current is rather the same. For instance, comparing the pixels, at longitude  $-53.4^\circ\text{W}$  and varying the latitude, both the Shannon entropy (Fig. 6) and FIM (Fig. 7) show that the pixels at latitudes from  $-32^\circ\text{S}$  and  $-36^\circ\text{S}$  (where the Brazil Current flows) and those between  $-50^\circ\text{S}$  and  $-52^\circ\text{S}$  (where the Malvinas Current flows) are characterized by the same order/organization structures, being featured by high FIM and low Shannon entropy values. The same two sets of pixels, instead, are characterized by very different SST patterns, being the first set warmer than the second set (Fig. 8). It is clearly visible that the confluence occupies the region with higher Shannon entropy (Fig. 5) and lower FIM (Fig. 4) (as it can also be observed looking at the latitudinal variation of the FIM and Shannon entropy



**Figure 6** Profile of the Shannon entropy power at longitude  $53.4^\circ\text{W}$  and varying the latitude. The Shannon entropy shows that the pixels at latitudes from  $-32^\circ\text{S}$  and  $-36^\circ\text{S}$  (where the Brazil Current flows) and those between  $-50^\circ\text{S}$  and  $-52^\circ\text{S}$  (where the Malvinas Current flows) are characterized by the same order structure, being featured by high low Shannon entropy values.



**Figure 7** Profile of the Fisher information measure (FIM) at longitude  $53.4^\circ\text{W}$  and varying the latitude. The FIM shows that the pixels at latitudes from  $-32^\circ\text{S}$  and  $-36^\circ\text{S}$  (where the Brazil Current flows) and those between  $-50^\circ\text{S}$  and  $-52^\circ\text{S}$  (where the Malvinas Current flows) are characterized by the same organization structures, being featured by high FIM values.

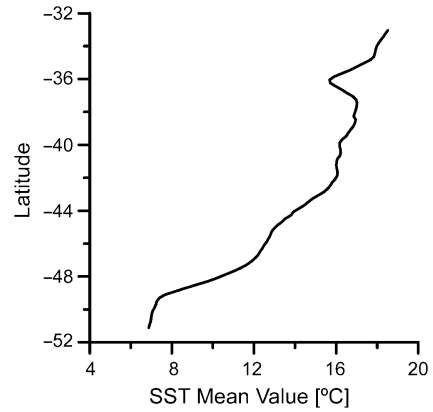


**Figure 8** Profile of the SST mean value at  $53.4^\circ\text{W}$  and varying the latitude. The SST profile increases as the latitude increases.

(Figs. 6 and 7)); therefore, the FS analysis of the spatial distribution of the  $\text{SST}_d$  reveals that the BMCZ can be quite precisely spatially located, because it is characterized by higher Shannon entropy and lower FIM.

These results point out to a peculiar dynamical characterization of the investigated area: the warmer water masses of the Brazil Current and the colder water masses of the Malvinas Current are dynamically similar in terms of order/organization structure of the time series of the SST; while, in the BMCZ, where the two currents converge, the level of disorder (organization) of the structure of the SST time series increases (decreases). Such increase of the level of disorder is associated with a higher uncertainty and higher irregularity of the time series of the pixels occupying the BMCZ. Since the FIM and Shannon entropy have the capability to discriminate between regular and chaotic trajectories (Martin et al., 2001), the higher value of the Shannon entropy or lower value of FIM in the BMCZ indicates the higher chaotic regime that governs the dynamics of SST in the BMCZ.

This result is in agreement with the findings of Morel et al. (2014), who applied to the BMCZ an analysis of specific Lagrangian patterns in an unsteady chaotic flow which organize the transport through the regional oceanic dynamic features. The spatial distribution of their finite-time Lyapunov exponent (FTLE) shows that the high-valued zone, which corresponds to a high-mixing and high-variability zone, coincides with the BMCZ. Even the spatial distribution of the largest finite-time Lyapunov exponent (L-FTLE), estimated by computing from the geostrophic velocities, shows that the most intense values are over the BMCZ, whose dynamics is associated to stirring processes that, in general, create filaments, which are stretched in progressively thinner structures and are eventually dispersed by small-scale turbulence.

We performed a complementary analysis on the  $\text{SST}_d$  time series calculating the mean  $\text{SST}_d$  gradient distribution. For each pixel, at a specified time, the gradient magnitude is calculated using centered differences as (Saraceno et al., 2004):

$$\|grad(\text{SST}_d(i))\| = \sqrt{\left(\frac{\text{SST}_d(ix+1) - \text{SST}_d(ix-1)}{dist(ix+1, ix-1)}\right)^2 + \left(\frac{\text{SST}_d(iy+1) - \text{SST}_d(iy-1)}{dist(iy+1, iy-1)}\right)^2}, \quad (7)$$

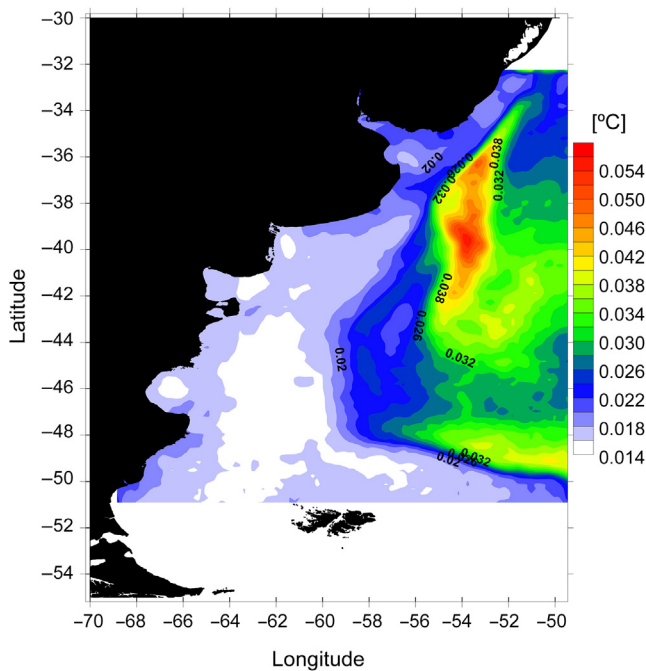


**Figure 9** Spatial distribution of the gradient of the sea surface temperature anomaly ( $SST_d$ ). Between 36°S and 40°S (respectively, the northern and southern limits of the Brazil-Malvinas Collision front), the mean  $SST_d$  gradient is characterized by the highest values correlating well with the Shannon entropy and FIM.

where  $(ix - 1)$  and  $(ix + 1)$  are the neighbors of the  $ix$ th pixel in the  $X$  (analogously in  $Y$ ) direction;  $dist$  is the distance in the  $X$  (analogously in  $Y$ ) direction. Then, the time average of all the gradients for each pixel is calculated and the mean  $SST_d$  gradient distribution is shown in Fig. 9. Alike the Shannon entropy (Fig. 5) (FIM (Fig. 4)) on the along-shelf section shows local maxima (minima), between 36°S and 40°S (which respectively correspond to the northern and southern limits of the Brazil-Malvinas Collision front), even the mean  $SST_d$  gradient presents the highest values between these limits (Fig. 9), and, thus, it correlates well with the Shannon entropy and FIM. The mean SST (Fig. 2) shows that the transition region from the colder subantarctic waters (8–12°C) to the warmer subtropical waters (>16°C) occurs within this zone. The inflection point in Fig. 2 is located near to 38.2°S, corresponding also to the latitude of the maximum in the mean  $SST_d$  gradient. Thus we associate this point (between 52.5°W and 56°W and 36°S and 40°S) to the time-averaged position of the Brazil-Malvinas Collision front along the section. The intersection between the along-shelf section and the coincident mean positions of the Subantarctic Front and Brazil Current Front as estimated by Saraceno et al. (2004) is in good agreement with our results. In fact, the mean  $SST_d$  gradient at the along-shelf section assumes the highest values within a range of about 500 km between 38.2°S and 40°S (Fig. 6). This range of migration coincides with separation between the frontal positions derived from SST frontal probability maps obtained by Saraceno et al. (2006, 2004).

The displacement of the front along the section is also observed between the same range of latitudes for the rest of

the available Shannon entropy data and for the remote sensing  $SST_d$  gradient data set.

## 5. Conclusions

The upper layers in the western Argentine Basin present intense current systems, such as the Brazil Current and the Malvinas Current, which are associated with strong thermocline fronts (Saraceno et al., 2004). Cross frontal mixing creates small-scale thermohaline structures (Bianchi et al., 1993, 2002), which may enhance the vertical stratification of subantarctic waters, and also lead to small-scale SST exchange (Brandini et al., 2000). In addition, current instabilities generate one of the most energetic regions of the world oceans due to the strong presence of eddies and meanders (Chelton et al., 1990). Such region is known as the Brazil–Malvinas Confluence Zone (BMCZ). For the first time, up to our knowledge, the SST time series derived from the AVHRR satellite imagery, were analyzed by using an advanced statistical method, the Fisher–Shannon method, which is capable of capturing the organizational features of a dynamical system. The calculation of the Fisher information measure (FIM) and the Shannon entropy power for all the pixel time series of SST covering the continental shelf has revealed that the most disordered and less organized structures in SST are located in correspondence with the BMCZ. This result is in good agreement with the most recent findings of chaotic behavior detected in the BMCZ.

## Acknowledgements

We are grateful to PhD Guillermo Podesta (Univ. of Miami). The data set of sea surface temperature (SST) fields were derived from NOAA Advanced Very High Resolution Radiometer.

## References

- Anding, D., Kauth, R., 1970. Estimation of sea surface temperature from space. *Rem. Sens. Environ.* 1, 217–220.
- Angulo, J.C., Antolin, J., Sen, K.D., 2008. Fisher–Shannon plane and statistical complexity of atoms. *Phys. Lett. A* 372 (5), 670–674.
- Bava, J., 2004. Metodologías de procesamiento de imágenes NOAA-AVHRR y su utilización en aplicaciones oceanográficas y biológico-pesqueras en el Atlántico Sudoccidental. (Ph.D. thesis). Univ. Buenos Aires, 142 pp.
- Bava, J., Gagliardini, D.A., Dogliotti, A.I., Lasta, C.A., 2002. Annual distribution and variability of remotely sensed sea surface temperature fronts in the southwestern Atlantic Ocean. In: 29th International Symposium on Remote Sensing of the Environment, *Int. Soc. Rem. Sens. Environ.*, Buenos Aires, 8–12.
- Bernstein, R.L., Chelton, D.B., 1985. Large-scale sea surface temperature variability from satellite and shipboard measurements. *J. Geophys. Res.* 90 (11), 619–630.
- Bianchi, A.A., Giulivi, C.F., Piola, A.R., 1993. Mixing in the Brazil–Malvinas Confluence. *Deep-Sea Res. Pt. I* 40 (7), 1345–1358.
- Bianchi, A.A., Piola, A.R., Collino, G.J., 2002. Evidence of double diffusion in the Brazil–Malvinas Confluence. *Deep-Sea Res. Pt. I* 49 (1), 41–52.
- Blanke, B., Arhan, M., Modec, G., Rocheet, S., 1999. Warm water paths in the equatorial Atlantic as diagnosed with a general circulation model. *J. Phys. Oceanogr.* 29 (11), 2453–2768.

- Brandini, F.P., Boltovskoy, D., Piola, A., Kocmur, S., Rottgers, R., Cesar Abreu, P., Mendes Lopes, R., 2000. Multiannual trends in fronts and distribution of nutrients and chlorophyll in the south-western Atlantic (30–62°S). *Deep-Sea Res. Pt. I* 47 (6), 1015–1033.
- Brown, M.G., Smith, K.B., 1990. Are SOFAR float trajectories chaotic? *J. Phys. Oceanogr.* 20 (1), 139–149.
- Brown, M.G., Smith, K.B., 1991. Ocean stirring and chaotic low-order dynamics. *Phys. Fluids* 3, 1186–1192.
- Chelton, D.B., Schlax, M.G., Witter, D.L., Richman, J.G., 1990. GEOSAT altimeter observations of the surface circulation of the Southern Ocean. *J. Geophys. Res.* 95 (C10), 17877–17903.
- Denman, K.L., Abbott, M.A., 1994. Time scales of pattern evolution from cross-spectrum analysis of advanced very high resolution radiometer and coastal zone color scanner imagery. *J. Geophys. Res.* 99 (C4), 7433–7442.
- Devroye, L.A., 1987. *Course on Density Estimation*. Birkhauser, Boston, 183 pp.
- Doney, S., Glover, D.M., McCue, S.J., Fuentes, M., 2003. Mesoscale variability of SeaWiFS satellite ocean color: global patterns and spatial scales. *J. Geophys. Res.* 108 (C2), 1–15.
- Evans, D.L., Signorini, S.S., Miranda, L.B., 1983. A note on the transport of the Brazil Current. *J. Phys. Oceanogr.* 23 (13), 1732–1738.
- Fisher, R.A., 1925. *Theory of statistical estimation*. Proc. Camb. Philos. Soc. 22, 700–725.
- Frieden, B.R., 1990. Fisher information, disorder, and the equilibrium distributions of physics. *Phys. Rev. A* 41 (8), 4265–4276.
- Fu, L.L., 1996. The circulation and its variability of the South Atlantic Ocean: first results from the TOPEX/POSEIDON mission. In: Wefer, G., Berger, W.H., Siedler, G., Webb, D.J. (Eds.), *The South Atlantic: Present and Past Circulation*, Springer-Verlag, Berlin, 63–82, 644 pp.
- Gordon, A.L., 1989. Brazil–Malvinas Confluence – 1984. *Deep-Sea Res. Pt. I* 36 (3), 359–384.
- Isern-Fontanet, J., Turiel, A., Garcia-Ladona, E., Font, J., 2007. Microcanonical multifractal formalism: application to the estimation of ocean surface velocities. *J. Geophys. Res.* 112 (C5), C05024, 18 pp.
- Janicki, A., Weron, A., 1994. *Simulation and Chaotic Behavior of Alpha-Stable Stochastic Processes*. Marcel Dekker, New York, 57 pp.
- Kilpatrick, K.A., Podesta, G.P., Evans, R., 2001. Overview of the NOAA/NASA Advanced Very High Resolution Radiometer Pathfinder algorithm for sea surface temperature and associated matchup database. *J. Geophys. Res.* 106 (C5), 9179–9197.
- Kushnir, Y., Robinson, W.A., Bladé, I., Hall, N.M.J., Peng, S., Sutton, R., 2002. Atmospheric GCM response to extratropical SST anomalies: synthesis and evaluation. *J. Climate* 15 (16), 2233–2256.
- Legeckis, R., 1978. A survey of worldwide sea surface temperature fronts detected by environmental satellites. *J. Geophys. Res.* 83 (C9), 4501–4522.
- Lentini, C., Olson, D., Podesta, G., 2002. Statistics of Brazil of current rings observed from AVHRR: 1993 to 1998. *Geophys. Res. Lett.* 29 (16), 1811–1814.
- Lentini, C.A.D., Podesta, G.P., Campos, E.J.D., Olson, D.B., 2001. Sea surface temperature anomalies on the western South Atlantic from 1982 to 1994. *Continent. Shelf Res.* 21 (1), 89–112.
- Lovullo, M., Telesca, L., 2011. Complexity measures and information planes of X-ray astrophysical sources. *J. Stat. Mech. Theory Exp.* P03029.
- Maamaatuaiahutapu, K., Garçon, V., Provost, C., Mercier, H., 1998. Transports of the Brazil and Malvinas Currents at their Confluence. *J. Mar. Res.* 56 (2), 417–438.
- Martin, M.T., Pennini, F., Plastino, A., 1999. Fisher's information and the analysis of complex signals. *Phys. Lett. A* 256 (2–3), 173–180.
- Martin, M.T., Perez, J., Plastino, A., 2001. Fisher information and nonlinear dynamics. *Physica A* 291 (1–4), 523–532.
- Matano, R.P., 1993. On the separation of the Brazil current from the coast. *J. Phys. Oceanogr.* 23 (1), 79–90.
- Matano, R.P., Schlax, M.G., Chelton, D.B., 1993. Seasonal variability in the South Atlantic. *J. Geophys. Res.* 98 (C10), 18027–18035.
- McClain, C.R., Cleave, M., Feldman, G., Gregg, W., Hooker, S., Kuring, N., 1998. Science quality SeaWiFS data for global biosphere research. *Sea Technol.* 39 (9), 10–14.
- McClain, E.P., Pichel, W.G., Walton, C.C., 1985. Comparative performance of AVHRR-based multichannel sea surface temperatures. *J. Geophys. Res.* 90 (C6), 11587–11601.
- Memery, L., Arhan, M., Alvarez-Salgado, X.A., Messias, M.-J., Mercier, H., Castro, C.G., Rios, A.F., 2000. The water masses along the western boundary of the south and equatorial Atlantic. *Prog. Oceanogr.* 47 (1), 69–98.
- Morel, X., Lucas, M.A., Dos Santos, F., 2014. A Lagrangian study of the Brazil–Malvinas confluence: Lagrangian coherent structures and several Lyapunov exponents. *J. Oper. Oceanogr.* 7 (2), 13–23.
- Njoku, E.G., 1985. Satellite-derived sea surface temperature: workshop comparisons. *Bull. Am. Meteorol. Soc.* 66 (3), 274–281.
- Njoku, E.G., Barnett, T.P., Laurs, R.M., Vastano, A.C., 1985. Advances in satellite sea surface temperature measurement and oceanographic applications. *J. Geophys. Res.* 90 (C6), 573–586.
- Olson, D.B., Podesta, G.P., Evans, R.H., Brown, O.B., 1988. Temporal variations in the separation of Brazil and Malvinas currents. *Deep Sea Res.* 35 (12), 1971–1990.
- Osborne, A.R., Kirwan, A.D., Provenzale, A., Bergamasco, L., 1986. A search for chaotic behavior in large and mesoscale motions in the Pacific Ocean. *Physica D* 23 (1–3), 75–83.
- Peterson, R.G., Stramma, L., 1990. Upper-level circulation in the South Atlantic Ocean. *Prog. Oceanogr.* 26 (1), 1–73.
- Podesta, G.P., Brown, O.B., Evans, R.H., 1991. The annual cycle of satellite-derived sea surface temperature in the southwestern Atlantic Ocean. *J. Climate* 4 (4), 457–467.
- Provost, C., Le Traon, P.Y., 1993. Spatial and temporal scales in altimetric variability in the Brazil–Malvinas Current Confluence region: dominance of the semiannual period and large spatial scales. *J. Geophys. Res.* 98 (C10), 18037–18051.
- Raykar, V.C., Duraiswami, R., 2006. Fast optimal bandwidth selection for kernel density estimation. In: *Proceedings of the Sixth SIAM International Conference on Data Mining*, Bethesda, April 2006, 524–528.
- Saraceno, M., Provost, C., Lebbah, M., 2006. Biophysical regions identification using an artificial neuronal network: a case study in the South Western Atlantic. *Adv. Space Res.* 37 (4), 793–805.
- Saraceno, M., Provost, C., Piola, A., Bava, J., Gagliardini, A., 2004. Brazil Malvinas frontal system as seen from 9 years of advanced very high resolution radiometer data. *J. Geophys. Res.* 109 (5), C05027, <http://dx.doi.org/10.1029/2003JC002127>.
- Shannon, C.E., 1948. *A mathematical theory of communication*. *Bell Syst. Tech. J.* 27, 379–423, 623–656.
- Speich, S., Blanke, B., Cai, W., 2007. Atlantic meridional overturning and the Southern Hemisphere supergyre. *Geophys. Res. Lett.* 34 (23), L23614, <http://dx.doi.org/10.1029/2007GL031583>.
- Stammer, D., 1997. Global characteristics of ocean variability estimated from regional TOPEX/POSEIDON altimeter measurements. *J. Phys. Oceanogr.* 27 (8), 1743–1769.
- Telesca, L., Lasaponara, R., 2005. Discriminating dynamical patterns in burned and unburned vegetational covers by using SPOT-VGT NDVI data. *Geophys. Res. Lett.* 32 (21), L21401, <http://dx.doi.org/10.1029/2005GL024391>.
- Telesca, L., Lasaponara, R., 2006. Pre- and post-fire behavioral trends revealed in satellite NDVI time series. *Geophys. Res. Lett.* 33 (14), L14401, <http://dx.doi.org/10.1029/2006GL026630>.
- Telesca, L., Lovullo, M., 2011. Analysis of the time dynamics in wind records by means of multifractal detrended fluctuation analysis and the Fisher–Shannon information plane. *J. Stat. Mech.* P07001, 31 pp.

- Telesca, L., Lovallo, M., Carniel, R., 2010. Time-dependent Fisher information measure of volcanic tremor before 5 April 2003 paroxysm at Stromboli volcano, Italy. *J. Volcanol. Geotherm. Res.* 195 (1), 78–82.
- Telesca, L., Lovallo, M., Hsu, H.-L., Chen, C.-C., 2011. Analysis of dynamics in magnetotelluric data by using the Fisher–Shannon method. *Physica A* 390 (7), 1350–1355.
- Telesca, L., Lovallo, M., Ramirez-Rojas, A., Angulo-Brown, F., 2009. A nonlinear strategy to reveal seismic precursory signatures in earthquake-related self-potential signals. *Physica A* 388 (10), 2036–2040.
- Tokinaga, H., Tanimoto, Y., Xie, S.P., 2005. SST-induced surface wind variations over the Brazil–Malvinas Confluence: satellite and in situ observations. *J. Climate* 18 (17), 3470–3482.
- Troudi, M., Alimi, A.M., Saoudi, S., 2008. Analytical plug-in method for kernel density estimator applied to genetic neutrality study. *EURASIP J. Adv. Signal Process.* 2008 Article ID 739082, 8 pp.
- Turiel, A., Isern-Fontanet, J., García-Ladona, E., Font, J., 2005. Multifractal method for the instantaneous evaluation of the stream function in geophysical flows. *Phys. Rev. Lett.* 95 (10), 104502.
- Vigan, X., Provost, C., Podesta, G., 2000. Sea surface velocities from sea surface temperature image sequences 2. Application to the Brazil–Malvinas Confluence area. *J. Geophys. Res.* 105 (C8), 19515–19534.
- Vivier, F., Provost, C., 1999. Volume transport of the Malvinas Current: can the flow be monitored by TOPEX/POSEIDON. *J. Geophys. Res.* 104 (C9), 21105–21122.
- Wainer, I., Gent, P., Goni, G., 2000. Annual cycle of the Brazil Malvinas Confluence region in the National Center for Atmospheric Research climate system model. *J. Geophys. Res.* 105 (C11), 167–177.



ORIGINAL RESEARCH ARTICLE

# First occurrence of thinlip grey mullet, *Liza ramada* (Risso, 1827) in the Odra River estuary (NW Poland): genetic identification

Remigiusz Panicz<sup>a,\*</sup>, Sławomir Keszka<sup>b,c</sup>

<sup>a</sup> Department of Meat Technology, Faculty of Food Sciences and Fisheries, West Pomeranian University of Technology, Szczecin, Poland

<sup>b</sup> Border Veterinary Inspection, Szczecin, Poland

<sup>c</sup> Division of Aquaculture, Faculty of Food Science and Fisheries, West Pomeranian University of Technology, Szczecin, Poland

Received 25 March 2015; accepted 10 February 2016

Available online 9 March 2016

## KEYWORDS

Non-native species;  
*Liza ramada*;  
Cytochrome c oxidase  
subunit 1;  
Rhodopsin gene;  
Mugilidae

**Summary** The presence of exotic fish species in the Baltic Sea and its tributaries poses a serious threat for native ichthyofauna, mainly due to the spread of new pathogens. As the accurate identification of species is essential for an effective assessment of changes related to the appearance of non-native species in an aquatic environment, in this paper we tested the usefulness of biometrics and molecular markers in identifying a specimen from the Mugilidae family found in the Odra estuary. The results demonstrated that unambiguous identification of the specimen using biometric features was impossible due to high morphological similarities shared by grey mullets. Unambiguous identification was possible only due to molecular markers, e.g. rhodopsin gene, which helped to identify the collected fish specimen as *Liza ramada* (Risso, 1827), the first specimen of this species found in the Odra River estuary. The presence of an *L. ramada* specimen in the Odra River – which could signal the expansion of non-native species into wider ranges – may be linked to climate change or human activity.

© 2016 Institute of Oceanology of the Polish Academy of Sciences. Production and hosting by Elsevier B.V. This is an open access article under the CC BY-NC-ND license (<http://creativecommons.org/licenses/by-nc-nd/4.0/>).

\* Corresponding author at: Department of Meat Technology, Faculty of Food Sciences and Fisheries, West Pomeranian University of Technology, Szczecin, ul. K. Królewicza 4, 71-550 Szczecin, Poland. Tel.: +48 914496664.

E-mail addresses: [rpanicz@zut.edu.pl](mailto:rpanicz@zut.edu.pl) (R. Panicz), [skeszka@zut.edu.pl](mailto:skeszka@zut.edu.pl) (S. Keszka).

Peer review under the responsibility of Institute of Oceanology of the Polish Academy of Sciences.



Production and hosting by Elsevier

<http://dx.doi.org/10.1016/j.oceano.2016.02.001>

0078-3234/© 2016 Institute of Oceanology of the Polish Academy of Sciences. Production and hosting by Elsevier B.V. This is an open access article under the CC BY-NC-ND license (<http://creativecommons.org/licenses/by-nc-nd/4.0/>).

## 1. Introduction

According to diverse estimates, the number of fish species in the seas surrounding Europe fluctuates between 40,000 and 48,000, constituting 15% of the estimated 230,000 marine species (Costello and Wilson, 2011). Based on the variety of available data (published papers, reports, grey literature, unpublished data), the Baltic Sea including Kattegat is host to at least 6065 species, including about 200 fish species (Ojaveer et al., 2010). The number of Baltic marine fish species gradually decreases eastwards from the Danish straits towards the Gulf of Finland (Nellen and Thiel, 1996), as for numerous fishes the conditions of the Baltic Sea are unfavorable, especially the salinity and temperature (Thiel et al., 1996). However, in recent years both rare and exotic species, for example the European seabass (*Dicentrarchus labrax*), the tub gurnard (*Chelidonichthys lucernus*), the Ballan wrasse (*Labrus bergylta*), the saithe (*Pollachius virens*) and the swordfish (*Xiphias gladius*) have been recorded in the southern Baltic and its estuaries (Keszka and Raczyński, 2002; Keszka et al., 2003; Krzykawski et al., 2001). Some species often occur unexpectedly in new regions following expansion of their natural range (Mohra, 1988; Nehring, 2002). One of these is the thicklip grey mullet (*Chelon labrosus* (Risso 1827)) which lives in the North Atlantic.

The Mugilidae family consists of more than 72 species from 17 fish genera with a worldwide distribution (Nelson, 2006). In the seas surrounding Europe, the Mugilidae family consists of 6 native and 1 exotic species in which only *Oedalechilus labeo* does not thrive in freshwater inland conditions (Kottelat and Freyhof, 2007). To date, *C. labrosus* has been the only Mugilidae species to be found in Polish marine areas (Czerniejewski et al., 2008; Grygiel, 2009). There are also two other Mugilidae species, i.e. *Liza aurata* and *Liza ramada*, that may potentially enter Polish sea waters from adjacent areas, e.g. North Sea (Winkler et al., 2000). Generally, grey mullets are easily recognized from other Acanthopterygii fishes by the two widely separated small dorsal fins (anterior fin with 4 slender spines and a soft-rayed posterior fin). While within the Mugilidae family it is cumbersome to identify grey mullets due to the high morphological similarities shared between the species (Menezes et al., 2010). Identification of the Mugilidae species occurring in European waters on the basis of external characteristics depends mainly on the combination of several measurable characters, the appearance of scales on the head or the number of scale rows around the caudal peduncle. It cannot be based on the body shape or color, which are very similar for all Mugilidae, especially for juvenile specimens (Kottelat and Freyhof, 2007). The main purpose of this study was to characterize and identify a Mugilidae specimen caught in Polish waters for the first time. Additionally, the aim was to compare the usefulness of biometric and molecular data applied in this study.

## 2. Material and methods

The study was carried out on a fish specimen caught with a fyke net during summer season in the Szczecin Lagoon near the town of Stepnica, GPS coordinates: 53°39'3.21"N,

14°36'39.34"E. The fish was measured with an electronic caliper and its mass was determined with the use of an Axis 3000 scale. Biometric data for 32 measurable and 7 countable characters was collected according to the methodology published by Brylińska (2000). The age of the fish was determined following the guidelines for fish age determination published by Glamuzina et al. (2007). The sex of the collected specimen was assessed based on gonad inspection.

### 2.1. Molecular analysis of RH1 and COI sequences

A fin clip of the grey mullet was excised and DNA extraction was performed with the use of a peqGOLD Tissue DNA Kit (PEQaLAB Biotechnologie). Purity and concentration of DNA eluates were assessed on a 1.5% agarose gel with the use of a Nanodrop ND-1000 spectrophotometer (Thermo Fisher Scientific Inc.). Genetic identification of the collected specimen was carried out based on the amplification of rhodopsin (RH1) and subunit I of cytochrome oxidase (COI) regions. The reactions were based on the primers Rod-F2W + Rod-R4n (Sevilla et al., 2007) and FishF2\_t1 + FishR2\_t1 (Ivanova et al., 2007) according to methodological guidelines provided by the respective authors. The results of each PCR were verified by separating the analyzed samples in 1.5% agarose gel, and then each PCR product was sequenced bidirectionally according to Sanger's method (Genomed, Poland). The results of sequence analysis were then analyzed with the following software: BLAST, MEGA5 and BioEdit (Altschul et al., 1990; Hall, 1999; Tamura et al., 2007).

## 3. Results

The Mugilidae fish specimen caught in the Szczecin Lagoon was a 5-year old male, characterized by the taxonomical formulae D<sub>1</sub> IV, D<sub>2</sub> I7, A III9, V I5, P14, I.I.41. The body is spindle-shaped and elongated, with two short dorsal fins; the head is strongly flattened. Morphometric characteristics of the thinlip grey mullet are presented in Fig. 1, as well as the detailed measurements are available as supplementary material (S1).



**Figure 1** Thinlip grey mullet, *Liza ramada* caught in the Odra River, lateral view.

**Table 1** Genetic distances between sequences based on Kimura's two-parameter model (K2P).

Liza_ramada (this_study)										
Liza_ramada	0.002									
Liza_ramada(2)	0.002	0.000								
Liza_ramada(3)	0.002	0.000	0.000							
Chelon_labrosus	0.004	0.007	0.007	0.007						
Chelon_labrosus(2)	0.004	0.007	0.007	0.007	0.000					
Chelon_labrosus(3)	0.004	0.007	0.007	0.007	0.000	0.000				
Liza_aurata	0.007	0.009	0.009	0.009	0.007	0.007	0.007			
Liza_aurata(2)	0.007	0.009	0.009	0.009	0.007	0.007	0.007	0.000		
Liza_aurata(3)	0.007	0.009	0.009	0.009	0.007	0.007	0.007	0.000	0.000	
Liza_saliens	0.007	0.009	0.009	0.009	0.002	0.002	0.002	0.009	0.009	0.009

### 3.1. Genetic identification of *Liza ramada*

Sequences obtained in this study were compared with records deposited in GenBank, resulting in a COI sequence similar with a record submitted for a thinlip grey mullet sample collected in Italy (EU392240). Screening of the GenBank sequence database resources with the RH1 sequence did not reveal entirely homological records, therefore the RH1 sequence was submitted and may be accessed as KM435345. Sequence analysis through the GenBank search for the COI sequence enabled correct assignment of the collected specimen as *L. ramada*. Comparison of the RH1 sequence derived in this study with those submitted in GenBank for *L. ramada* (JX298797.1, EU224158.1, EU224157.1) and related species, such as *Liza saliens* (Y18670.1), *L. aurata* (EF439127.1, Y18671.1, KF017144.1) or *C. labrosus* (DQ197837.1, Y18669.1, JX298796.1), revealed that this sequence may be used as a genetic marker. Genetic diversity among the aforementioned sequences ranged from 0.0% within the group of *L. ramada* sequences, up to 0.9% between *L. ramada* and *L. saliens* records (Table 1). Distances calculated between species pairs showed that the smallest differences (0.4%) existed between *L. ramada* and *C. labrosus*, whereas the highest between *L. ramada* specimen and *L. aurata* or *L. saliens* amounted to 0.7%.

## 4. Discussion

Correct assignment of Mugilidae species into one of the following genera: *Liza*, *Chelon* or *Mugil*, has been widely studied due to the significant morphological and genetic resemblances (Fraga et al., 2007; Semina et al., 2007). Results obtained by Heras et al. (2009) have shown that it is necessary to carry out additional genetic studies to provide reliable genetic markers for the species phylogeny description. In this study we analyzed the usefulness of two genetic markers, with only RH1 allowing the correct classification of the found *L. ramada* specimen. The selection of an appropriate molecular marker is particularly important for the Mugilidae family, consisting of a large number of species (Chauhan and Rajiv, 2010; Polyakova et al., 2013). Imsiridou et al. (2007) embarked on the task of genetic identification of six Mugilidae representatives (*M. cephalus*, *M. soiyu*, *C. labrosus*, *L. aurata*, *L. saliens* and *L. ramada*). For this purpose, they used the

5S rDNA marker, which provided interesting facts about the phylogeny of the Mugilidae family. According to the authors *L. ramada* and *L. aurata* are clustered together but *L. ramada* and *C. labrosus* differ significantly. In the present study, where the main aim was to identify a mullet specimen, the latter group had the highest similarity. Phylogenetic relationships among Mugilidae species are very complex and investigating them through carefully selected molecular markers is necessary to obtain reliable results. The 0.2% difference between the sequence from the collected specimen and that deposited at GenBank for the species *L. ramada* (JX298797.1, EU224158.1, EU224157.1) results from a sequencing error, the presence of Y (T or C) from the IUPAC code in those sequences. The sequence obtained in this study is free of errors and was submitted to GenBank (KM435345), and may be successfully used for species assignment within the Mugilidae family. In our opinion, the present study delivers a reliable molecular marker which might be used through amplification and sequencing. The authors of this paper do not support the idea of the interchangeable use of the genus name *Liza* or *Chelon* (Semina et al., 2007). Based on analysis of RH1 pairwise genetic distances we found 0.4% differences between *L. ramada* and *C. labrosus* sequences (Table 1). The results indicate that the smallest genetic distance between *L. ramada* and *C. labrosus* are consistent with the results obtained by Heras et al. (2009).

The natural range of a given species is often dictated by its optimal environment. According to Kottelat and Freyhof (2007), distribution of *L. ramada* includes the eastern Atlantic: from the coasts of southern Norway to Morocco, the Mediterranean and the Black Sea and as a landlocked population in the Fratel Reservoir, Portugal (Fig. 2). However, this euryhaline species can exploit fresh water habitats and tolerate abrupt changes in water salinity (Cardona, 2006; Thomson, 1990). The occurrence of thinlip grey mullet in northern Europe is not well known (Jonsson and Jonsson, 2008). The presence of an *L. ramada* specimen in the Odra River – which could signal the expansion of non-native species into wider ranges – may be linked to climate change or human activity (transport of fish in ballast water). According to Selgado et al. (2004) juveniles of thinlip grey mullet may often feed in intertidal creeks and small brooks in river deltas showing fast increase of population density, as it was reported for the Neretva River (Glamuzina et al., 2007). Additionally, exceptional water exchange between the Baltic Sea and the North Sea can result in the temporary occurrence

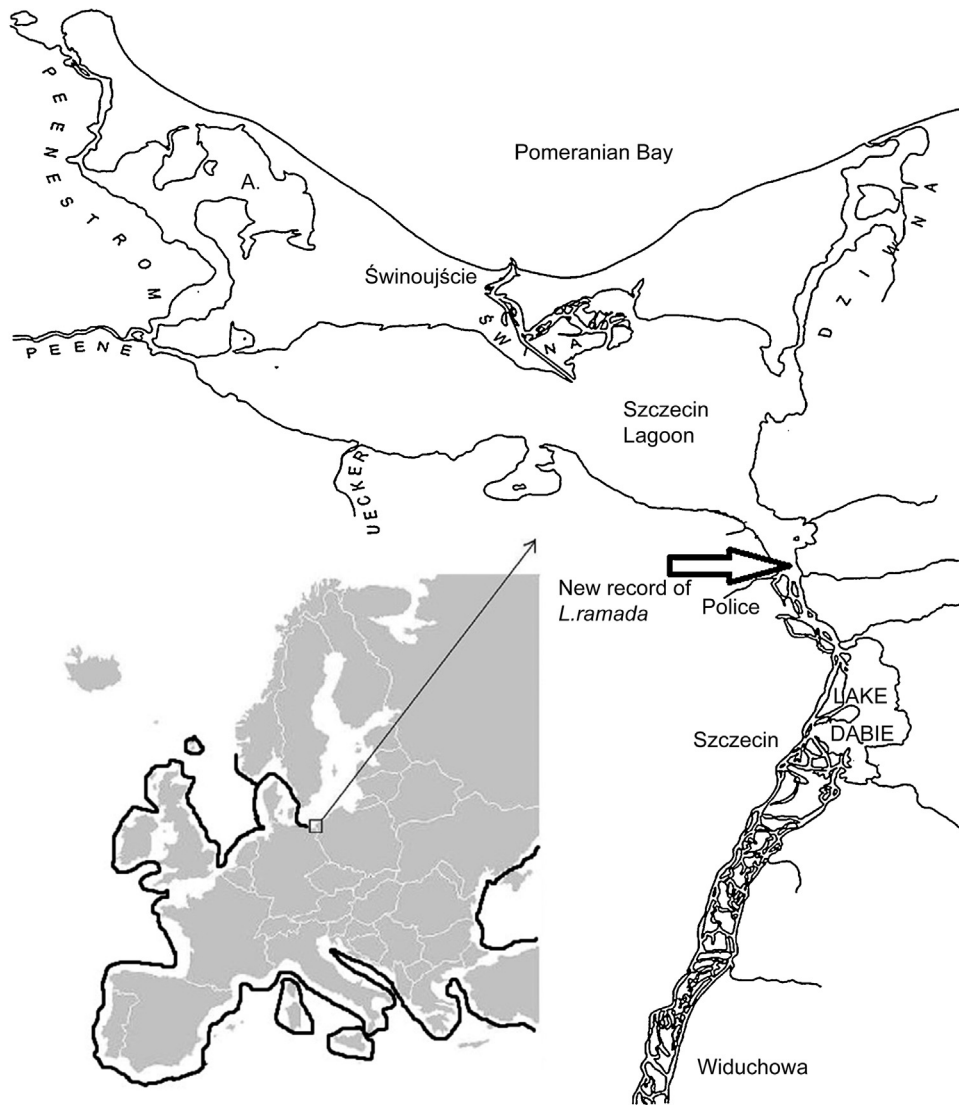


Figure 2 European distribution of *Liza ramada* including a new finding in the Odra River.

of species outside their normal ranges (Berge et al., 2005; Feistel et al., 2004).

In addition, the biology of European Mugilidae, including the alien species (especially the juveniles), prompts them to enter bays and lower reaches of rivers (Carvalho et al., 2007; Kottelat and Freyhof, 2007; Vieira, 1991). According to Gruszka (1999), the Odra River estuary belongs to those water bodies in the Baltic Sea area which are most exposed to immigration of alien species. Regardless of how the tested specimen reached the waters of NW Poland (Fig. 2), it is necessary to perform a detailed characteristic of the first recorded specimen, as it may constitute a serious threat to the biodiversity of the native fish fauna of the Odra River.

### Acknowledgments

We would like to thank Tomasz Zdanowicz, director of the fishery company from Stepnica for information concerning the history, localization and the great help with the mugil collection.

### Appendix A. Supplementary data

Supplementary data associated with this article can be found, in the online version, at [doi:10.1016/j.oceano.2016.02.001](https://doi.org/10.1016/j.oceano.2016.02.001).

### References

- Altschul, S.F., Gish, W., Miller, W., Myers, E.W., Lipman, D.J., 1990. Basic local alignment search tool. *J. Mol. Biol.* 215 (3), 403–410. [http://dx.doi.org/10.1016/S0022-2836\(05\)80360-2](http://dx.doi.org/10.1016/S0022-2836(05)80360-2).
- Berge, J., Johnsen, G., Nilsen, F., Gulliksen, B., Slagstad, D., 2005. Ocean temperature oscillations enable reappearance of blue mussels *Mytilus edulis* in Svalbard after a 1000 year absence. *Mar. Ecol. Prog. Ser.* 303, 167–175. <http://dx.doi.org/10.3354/meps303167>.
- Brylińska, M., 2000. *Ryby słodkowodne Polski*. PWN, Warszawa, 524 pp.
- Cardona, L., 2006. Habitat selection by grey mullets (Osteichthyes: Mugilidae) in Mediterranean estuaries: the role of salinity. *Sci. Mar.* 70 (3), 443–455.

- Carvalho, C.D., Corneta, C.M., Uieda, V.S., 2007. Schooling behavior of *Mugil curema* (Perciformes: Mugilidae) in an estuary in south-eastern Brazil. *Neotrop. Ichthyol.* 5 (1), 81–83, <http://dx.doi.org/10.1590/S1679-62252007000100012>.
- Chauhan, T., Rajiv, K., 2010. Molecular markers and their applications in fisheries and aquaculture. *Adv. Biosci. Biotechnol.* 1, 281–291, <http://dx.doi.org/10.4236/abb.2010.14037>.
- Costello, M.J., Wilson, S.P., 2011. Predicting the number of known and unknown species in European seas using rates of description. *Global Ecol. Biogeogr.* 20 (2), 319–330, <http://dx.doi.org/10.1111/j.1466-8238.2010.00603.x>.
- Czerniejewski, P., Keszka, S., Rybczyk, A., 2008. *Chelon labrosus* (Risso, 1827) – the first record from Lake Dąbie (Poland). *Oceanologia* 50 (2), 281–284.
- Feistel, R., Nausch, G., Heene, T., Piechura, J., Hagen, E., 2004. Evidence for a warm water inflow into the Baltic Proper in summer 2003. *Oceanologia* 46 (4), 581–598.
- Fraga, E., Schneider, H., Nirchio, M., Santa-Brigida, E., Rodrigues-Filho, L.F., Sampaio, I., 2007. Molecular phylogenetic analyses of mullets (Mugilidae, Mugiliformes) based on two mitochondrial genes. *J. Appl. Ichthyol.* 23 (5), 598–604, <http://dx.doi.org/10.1111/j.1439-0426.2007.00911.x>.
- Glamuzina, B., Dulčić, J., Conides, A., Bartulović, V., Matic-Skoko, S., Papaconstantinou, C., 2007. Some biological parameters of the thin-lipped mullet, *Liza ramada* (Pisces, Mugilidae) in the Neretva River delta (Eastern Adriatic, Croatian coast). *Vie et Millieu* 57 (3), 131–136.
- Gruszka, P., 1999. The River Odra estuary as a gateway for alien species immigration to the Baltic Sea basin. *Acta Hydrochim. Hydrobiol.* 27 (5), 374–382, [http://dx.doi.org/10.1002/\(SICI\)1521-401X\(199911\)27:5<374::AID-AHEH374>3.0.CO;2-V](http://dx.doi.org/10.1002/(SICI)1521-401X(199911)27:5<374::AID-AHEH374>3.0.CO;2-V).
- Grygiel, W., 2009. Niektóre obce i rzadkie gatunki ryb w polskich połowach na Bałtyku. *Wiad. Ryb.* 3–4 (168), 11–14.
- Hall, T.A., 1999. BioEdit: a user-friendly biological sequence alignment editor and analysis program for Windows 95/98/NT. *Nucl. Acids Symp. Ser.* 41, 95–98.
- Heras, S., Roldan, M.I., Castro, M.G., 2009. Molecular phylogeny of Mugilidae fishes revised. *Rev. Fish Biol. Fisheries* 19 (2), 217–231, <http://dx.doi.org/10.1007/s11160-008-9100-3>.
- Imsiridou, A., Minos, G., Katsares, V., Karaiskou, N., Tsiara, A., 2007. Genetic identification and phylogenetic inferences in different Mugilidae species using 5S rDNA markers. *Aquacult. Res.* 38 (13), 1370–1379, <http://dx.doi.org/10.1111/j.1365-2109.2007.01808.x>.
- Ivanova, N.V., Zemlak, T.S., Hanner, R.H., Hebert, P.D.N., 2007. Universal primer cocktails for fish DNA barcoding. *Mol. Ecol. Notes* 7 (4), 544–548, <http://dx.doi.org/10.1111/j.1471-8286.2007.01748.x>.
- Jonsson, B., Jonsson, N., 2008. Thinlip grey mullet *Liza ramada* (Mugilidae) caught in a small Norwegian stream. *Fauna Norv.* 26/27, 31–33.
- Keszka, S., Raczyński, M., 2002. Wargacz kniazik *Labrus bergylta* Ascanius, 1767 u wybrzeży polskich. *Kom. Ryb.* 5, 22–23.
- Keszka, S., Raczyński, M., Śmietana, P., 2003. Pojawienie się labraksa *Dicentrarchus labrax* (Linnaeus, 1758) w Zalewie Kamieńskim. *Kom. Ryb.* 5, 13–15.
- Kottelat, M., Freyhof, J., 2007. *Handbook of European Freshwater Fishes*. Kottelat, Cornol and Freyhof, Berlin, 646 pp.
- Krzykawski, S., Więcaszek, B., Keszka, S., 2001. A taxonomic review of representatives of extremely rare species in Polish waters collected in 1993–1999. *Folia Univ. Agric. Stetin.* 218 (18), 52–62.
- Menezes, N.A., de Oliveira, C., Nirchio, M., 2010. An old taxonomic dilemma: the identity of the western south Atlantic lebranche mullet (Teleostei: Perciformes: Mugilidae). *Zootaxa* 2519, 59–68.
- Mohra, H., 1988. Zur Biologie und fischereilichen Bedeutung der Meeräsche an der deutschen Nord- und Ostseeküste. *Protokolle zur Fischereitechnik*. Inst. Fangtechnik, Hamburg.
- Nehring, S., 2002. Biological invasions into German waters: an evaluation of the importance of different human-mediated vectors for nonindigenous macrozoobenthic species. In: Leppäkoski, E., Golasch, S., Olenin, S. (Eds.), *Invasive Aquatic Species of Europe: Distributions, Impacts and Management*. Kluwer Acad. Publ., Dordrecht, 373–383.
- Nellen, W., Thiel, R., 1996. Fische. In: Rheinheimer, G. (Ed.), *Meereskunde der Ostsee*. Heidelberg, Berlin, 190–196.
- Nelson, J.S., 2006. *Fishes of the World*, 4th ed. John Wiley & Sons, Inc., 601 pp.
- Ojaveer, H., Jaanus, A., MacKenzie, B.R., Martin, G., Olenin, S., Radziejewska, T., Telesh, I., Zettler, M.L., Zaiko, A., 2010. Status of biodiversity in the Baltic Sea. *PLoS ONE* 5 (9), e12467, <http://dx.doi.org/10.1371/journal.pone.0012467>.
- Polyakova, N., Boutin, A., Brykov, V., 2013. Barcoding and phylogenetic inferences in nine Mugilid species (Pisces, Mugiliformes). *Anim. Syst. Evol. Divers.* 29 (4), 272–278, <http://dx.doi.org/10.5635/ASED.2013.29.4.272>.
- Selgado, J., Costa, M.J., Cabral, H., Deegan, L., 2004. Comparison of the fish assemblages in tidal salt marsh creeks and in adjoining mudflat areas in the Tejo estuary (Portugal). *Cah. Biol. Mar.* 45 (3), 213–224.
- Semina, A.V., Polyakova, N.E., Brykov, V.A., 2007. Analysis of mitochondrial DNA: taxonomic and phylogenetic relationships in two fish taxa (Pisces: Mugilidae and Cyprinidae). *Biochemistry* 72 (12), 1349–1355, <http://dx.doi.org/10.1134/S0006297907120085>.
- Sevilla, R.G., Diez, A., Norén, M., Mouchel, O., Jérôme, M., Verrez-Bagnis, V., van Pelt, H., Favre-Krey, L., Krey, G., the Fishtrace Consortium, Bautista, J.M., 2007. Primers and polymerase chain reaction conditions for DNA barcoding teleost fish based on the mitochondrial cytochrome b and nuclear rhodopsin genes. *Mol. Ecol. Notes* 7 (5), 730–734, <http://dx.doi.org/10.1111/j.1471-8286.2007.01863.x>.
- Tamura, K., Dudley, J., Nei, M., Kumar, S., 2007. MEGA4: Molecular Evolutionary Genetics Analysis (MEGA) software version 4.0. *Mol. Biol. Evol.* 24 (8), 1596–1599, <http://dx.doi.org/10.1093/molbev/msm092>.
- Thiel, R., Sepulveda, A., Oesmann, S., 1996. Occurrence and distribution of twaite shad (*Alosa fallax* Lacépède) in the lower Elbe River, Germany. In: Kirchhofer, A., Hefti, D. (Eds.), *Conservation of Endangered Freshwater Fish in Europe*. Birkhäuser Verlag, Basel, 157–170.
- Thomson, J.M., 1990. Mugilidae. In: Quero, J.C., Hureau, J.C., Post, C.A., Saldanha, L. (Eds.), *Check-list of the Fishes of the Eastern Tropical Atlantic*, vol. II. UNESCO, Paris, 857–858.
- Vieira, J.P., 1991. Juvenile mullets (Pisces: Mugilidae) in the Estuary of Lagoa dos Patos, RS, Brazil. *Copeia* 2, 409–418.
- Winkler, H.M., Skóra, K., Repecka, R., Ploks, M., Neelov, A., Urho, L., Gushin, A., Jespersen, H., 2000. Checklist and status of fish species in the Baltic Sea. *ICES CM 2000/Mini:11*, 15 pp.



Available online at [www.sciencedirect.com](http://www.sciencedirect.com)

ScienceDirect

journal homepage: [www.elsevier.com/locate/oceano](http://www.elsevier.com/locate/oceano)



ORIGINAL RESEARCH ARTICLE

# Phytoplankton pigments and functional community structure in relation to environmental factors in the Pearl River Estuary<sup>☆</sup>

Chao Chai<sup>a,b</sup>, Tao Jiang<sup>b,\*</sup>, Jingyi Cen<sup>c</sup>, Wei Ge<sup>d</sup>, Songhui Lu<sup>c,\*\*</sup>

<sup>a</sup> Qingdao Engineering Research Center for Rural Environment, Qingdao Agricultural University, Qingdao, China

<sup>b</sup> Key Laboratory of Sustainable Development of Marine Fisheries, Ministry of Agriculture, Yellow Sea Fisheries Research Institute, Chinese Academy of Fishery Sciences, Qingdao, China

<sup>c</sup> Research Center for Harmful Algae and Marine Biology, Jinan University, Guangzhou, China

<sup>d</sup> College of Life Sciences, Qingdao Agricultural University, Qingdao, China

Received 11 April 2015; accepted 8 March 2016

Available online 31 March 2016

## KEYWORDS

Phytoplankton;  
Pigments;  
Functional community;  
HPLC;  
Pearl River Estuary

**Summary** Two cruises were undertaken in the Pearl River Estuary in November 2011 and March 2012 to analyze the distribution of phytoplankton pigments and to define the relationships of pigment indices and functional community structure with environmental factors. Among 22 pigments, 17 were detected by high-performance liquid chromatography. Chlorophyll *a* was found in all samples, with a maximum of  $7.712 \mu\text{g L}^{-1}$  in spring. Fucoxanthin was the most abundant accessory pigment, with mean concentrations of  $2.914 \mu\text{g L}^{-1}$  and  $0.207 \mu\text{g L}^{-1}$  in spring and autumn, respectively. Chlorophyll *a*, chlorophyll *c*<sub>2</sub>, fucoxanthin, diadinoxanthin, and diatoxanthin were high in the northern or northwest estuary in spring and in the middle-eastern and northeast estuary in autumn. Chlorophyll *b*, chlorophyll *c*<sub>3</sub>, prasinoxanthin, and peridinin were similarly distributed during the two cruises. Chlorophyll *a* and fucoxanthin positively correlated with nutrients in spring, whereas 19'-hex-fucoxanthin and 19'-but-fucoxanthin

<sup>☆</sup> Support for this study was partly provided by the projects 'National Natural Science Foundation of China (41476098), Special Scientific Research Funds for Central Non-profit Institutes, Yellow Sea Fisheries Research Institutes (20603022015002), and Open Foundation of Key Laboratory of South China Sea Fishery Resources Development and Utilization, Ministry of Agriculture (LSF2014-04)'.

\* Corresponding author at: Key Laboratory of Sustainable Development of Marine Fisheries, Ministry of Agriculture, Yellow Sea Fisheries Research Institute, Chinese Academy of Fishery Sciences, Qingdao 266071, China. Tel.: +86 53285806341.

\*\* Corresponding author at: Research Center for Harmful Algae and Marine Biology, Jinan University, Guangzhou 510632, China. Tel.: +86 2085222720.

E-mail address: [jiangtaophy@163.com](mailto:jiangtaophy@163.com) (T. Jiang).

Peer review under the responsibility of Institute of Oceanology of the Polish Academy of Sciences.



Production and hosting by Elsevier

<http://dx.doi.org/10.1016/j.oceano.2016.03.001>

0078-3234/© 2016 Institute of Oceanology of the Polish Academy of Sciences. Production and hosting by Elsevier B.V. This is an open access article under the CC BY-NC-ND license (<http://creativecommons.org/licenses/by-nc-nd/4.0/>).

negatively correlated. The biomass proportion of microphytoplankton ( $BP_m$ ) was higher in spring, whereas that of picophytoplankton ( $BP_p$ ) was higher in autumn.  $BP_m$  in spring was high in areas with salinity  $<30$ , but  $BP_p$  and the biomass proportion of nanophytoplankton ( $BP_n$ ) were high in areas with salinity  $>30$ .  $BP_m$  increased but  $BP_n$  reduced with the increase in nutrient contents. By comparison,  $BP_p$  reduced with the increase in nutrient contents in spring, but no relationship was found between  $BP_p$  and nutrient contents in autumn. The ratios of photosynthetic carotenoids to photoprotective carotenoids in the southern estuary approached unity linear relationship in spring and were under the unity line in autumn.

© 2016 Institute of Oceanology of the Polish Academy of Sciences. Production and hosting by Elsevier B.V. This is an open access article under the CC BY-NC-ND license (<http://creativecommons.org/licenses/by-nc-nd/4.0/>).

## 1. Introduction

The Pearl River Estuary (PRE) is situated in southern Guangdong Province, China, along the northern boundary of the South China Sea. It receives most of the outflow from the Pearl River, which is the third longest river in China and the 13th largest river by discharge in the world (Lerman, 1981). The Pearl River drains an area of 453,700 km<sup>2</sup>, and some of the most densely populated cities, such as Hong Kong, Macau, Shenzhen, Zhuhai, Guangzhou, are located on the Pearl River Delta. Approximately 19 billion tons of domestic, industrial, and agricultural effluents are annually discharged to the drainage basin of the Pearl River (Bulletin of Water Resources in the Pearl River Drainage, 2011, 2012). Therefore, the PRE has been experiencing deterioration of its aquatic environment (He et al., 2014; Qiu et al., 2010).

Phytoplankton is the base of food webs and the principal source of organic production in aquatic ecosystems. The biomass, composition, and community structure of phytoplankton can serve as indices to monitor aquatic environments (Paerl et al., 2003). Meanwhile, the distribution and succession of phytoplankton are the consequences of adaption to different environmental conditions, such as temperature, discharge, nutrients, and light intensity (Margalef, 1978).

Many studies have investigated the diversity, distribution, and seasonal variation of cell abundance of phytoplankton in the PRE (Huang et al., 2004; Li et al., 2014; Yin et al., 2000, 2001, 2004). Most previous studies have employed microscopy to identify and analyze phytoplankton quantitatively in the PRE. However, this method is time consuming and requires taxonomic knowledge (Naik et al., 2011). Moreover, picophytoplankton are typically not identified or counted with the use of this method (Jeffrey et al., 1997). Alternatively, photosynthetic pigments can be easily detected and can serve as biomarkers for particular classes or even genera of phytoplankton (Wright and Jeffrey, 2006). Pigment detection based on high-performance liquid chromatography (HPLC) methods enables quantification of over 50 phytoplankton pigments (Aneeshkumar and Sujatha, 2012; Jeffrey et al., 1997). Some photosynthetic pigments (e.g., fucoxanthin, peridinin, alloxanthin, zeaxanthin, chlorophyll *b*, 19'-hex-fucoxanthin, and 19'-but-fucoxanthin) can be considered diagnostic pigments (DP) of specific phytoplankton groups (diatoms, dinoflagellates, cryptophytes, cyanobacteria, chlorophytes, haptophytes, and pelagophytes, respectively) (Barlow et al., 2008; Paerl et al., 2003). Moreover, diatoxanthin and diadinoxanthin are generally found in diatoms and dinoflagellates, whereas prasinoxanthin, lutein, violaxanthin, and neoxanthin

are found in prasinophyceae and chlorophyceae. Chlorophyll *a*, *c*, and  $\beta,\beta$ -carotene are general indicators of total algal biomass. Phytoplankton cells are categorized into three groups according to their sizes (equivalent spherical diameter): microphytoplankton (20–200  $\mu\text{m}$ ), nanophytoplankton (2–20  $\mu\text{m}$ ), and picophytoplankton (0.2–2  $\mu\text{m}$ ) (Sieburth et al., 1978). The contribution of each group is also reflected by its pigment signatures (Vidussi et al., 2001). Therefore, photosynthetic pigment biomarkers are widely used in oceanography for quantifying phytoplankton biomass and assessing the structure of phytoplankton community (Paerl et al., 2003; Wright and Jeffrey, 2006).

Photosynthetic pigments also function as indicators of the physiological condition of a phytoplankton community, which may be affected by environmental and trophic conditions (Roy et al., 2006). Photoprotective carotenoids (PPCs) are more dominant in low productivity waters, whereas photosynthetic carotenoids (PSCs) are dominant in high productivity waters (Barlow et al., 2002; Gibb et al., 2000). In addition, intensive light increases the PPC:PSC ratio (Moreno et al., 2012; Vijayan et al., 2009). Thus, PPC:PSC ratio is considered a good indicator of environmental factors.

Estuarine environmental factors often vary markedly in spatial and temporal scales, thereby affecting phytoplankton physiology, biomass, and communities. The PRE has a complex estuarine environment in terms of freshwater input, turbidity and irradiance, nutrient content and composition, etc. However, few studies have observed the spatial and temporal distribution of phytoplankton pigments, as well as the functional community structure, in relation to environmental factors in the PRE. The present study aims to describe the spatial–temporal distribution of phytoplankton pigments in the PRE and to define the relationships of pigment indices and functional community structure with environmental factors.

## 2. Material and methods

### 2.1. Study area

The PRE is triangular and encompasses a large area of approximately 1900 km<sup>2</sup>. It is approximately 60 km long and 10 km wide at its head and 60 km at its mouth. The PRE is shallow, with a depth of 2–10 m (Harrison et al., 2008). It has a subtropical climate with a long summer and a short winter. The Pearl River mainly consists of three branches (Xi Jiang, Bei Jiang, and Dong Jiang) with eight outlets, four of which enter the estuary (Harrison et al., 2008). Its annual average

discharge is approximately  $10,000 \text{ m}^3 \text{ s}^{-1}$  (Zhai et al., 2005), with 20% occurring from October to March next year (the dry season) and 80% from April to September (the wet season) (Zhao, 1990).

## 2.2. Field sampling

Two surveys were conducted at 23 stations located in the PRE and in the adjacent area in November 2011 (autumn) and in March 2012 (spring) (Fig. 1). Water samples were collected at a depth of 0.5 m and analyzed for dissolved  $\text{O}_2$  (DO), pH, transparency, dissolved nutrients, and phytoplankton pigments. A filtered subsample with a pre-ignited Whatman GF/F filter was added with 0.3% chloroform (final concentration) to determine dissolved nutrients. The filtrate was stored at  $-20^\circ\text{C}$  in an 80 mL polycarbonate bottle for later analysis. A 1000 mL subsample was filtered on a Whatman GF/F filter with a vacuum pressure of less than 0.03 MPa under low light to analyze phytoplankton pigments. The filters were wrapped in aluminum foil and stored at  $-80^\circ\text{C}$  for later extraction and analysis of pigments.

## 2.3. Measurements of environment variables and pigments

Water temperature and salinity were measured using a multi-parameter water quality monitoring instrument (YSI 6600, Yellow Springs Instruments, USA). Dissolved oxygen (DO) was analyzed using the Winkler method and the pH with electrode method on board. Water transparency was determined using a Secchi disk. The concentrations of dissolved nutrients, including nitrate, nitrite, ammonium, phosphate, and silicate, were analyzed using a SKALAR flow analyzer in accordance with

standard methods (Grasshoff et al., 1983). Dissolved inorganic nitrogen (DIN) was calculated as the sum of nitrate, nitrite, and ammonium.

Pigment extraction and analysis were conducted according to the methods described by Zapata et al. (2000). The frozen filters were cut into small pieces and then extracted with 3 mL 95% methanol (v/v in deionized water) in a sonication bath with ice and water for 5 min under low light. The extract was then passed through a Teflon film with  $0.2 \mu\text{m}$  pore size to remove cellular debris. The methanol extract (1 mL) was mixed with 0.2 mL Milli-Q water, and then, a  $100 \mu\text{L}$  aliquot of the mixture was analyzed using reverse-phase HPLC.

The HPLC system was equipped with a C8 column (Eclipse XDB,  $150 \text{ mm} \times 4.6 \text{ mm}$ ,  $3.5 \mu\text{m}$  particle size, 1000 nm pore size). The column was maintained at  $25^\circ\text{C}$ , and the detection wavelengths of the Agilent diode array detector were set to 430, 440, and 450 nm. Eluent A comprised a methanol:acetonitrile:aqueous pyridine solution (50:25:25, v/v/v), and eluent B was composed of acetonitrile:acetone (80:20, v/v). Elution was performed at a rate of  $1.0 \text{ mL min}^{-1}$ .

Pigments were identified and quantified using pure pigment standards that contain the following 22 pigments commercially obtained from DHI Inc. (Denmark): chlorophyll *a* (Chl *a*), chlorophyll *b* (Chl *b*), chlorophyll *c*<sub>2</sub> (Chl *c*<sub>2</sub>), chlorophyll *c*<sub>3</sub> (Chl *c*<sub>3</sub>), fucoxanthin (Fuco), diadinoxanthin (Diadino), peridinin (Peri), violaxanthin (Viola), alloxanthin (Allo), diatoxanthin (Diato),  $\beta,\beta$ -carotene ( $\beta\beta$ -Car), prasinoxanthin (Pras), lutein (Lut), neoxanthin (Neo), zeaxanthin (Zea), 19'-hex-fucoxanthin (Hex-Fuco), 19'-but-fucoxanthin (But-Fuco), pheophorbide *a* (Pheide *a*), canthaxanthin (Cantha), divinyl chlorophyll *a* (DV-Chl *a*), pheophytin *a* (Phe *a*), and Mg-2,4-divinylpheoporphyryn (MgDVP). Chlorophylls and carotenoids were detected using a diode array detector at 350–750 nm, and chlorophylls were detected by fluorescence at 440 nm and 660 nm (excitation and emission). Absorbance chromatograms were extracted at wavelengths of 430, 440, and 450 nm.

## 2.4. Pigment indices

Pigment indices included PSC, PPC, and DP. PSC was the sum of Fuco, Peri, Hex-Fuco, But-Fuco, Viola, and Chl *b* (Gibb et al., 2001); and PPC was the sum of Allo, Diadino, Diato, Zea, and  $\beta\beta$ -Car (Jeffrey et al., 2005). DP was the sum of seven pigments (Zea, Chl *b*, Allo, Hex-Fuco, But-Fuco, Fuco, and Peri). Among these pigments, Zea and Chl *b* were the signatures of picophytoplankton; Allo, Hex-Fuco, and But-Fuco were those of nanophytoplankton; and Fuco and Peri were those of microphytoplankton. The biomass proportion (BP) of each size group, namely, BP<sub>m</sub> (microphytoplankton), BP<sub>n</sub> (nanophytoplankton), and BP<sub>p</sub> (picophytoplankton), was calculated as follows (Jeffrey et al., 2005):

$$\text{BP}_m = \frac{(\text{Fuco} + \text{Peri})}{\text{DP}} \times 100\%$$

$$\text{BP}_n = \frac{(\text{Allo} + \text{Hex-Fuco} + \text{But-Fuco})}{\text{DP}} \times 100\%$$

$$\text{BP}_p = \frac{(\text{Chl } b + \text{Zea})}{\text{DP}} \times 100\%$$

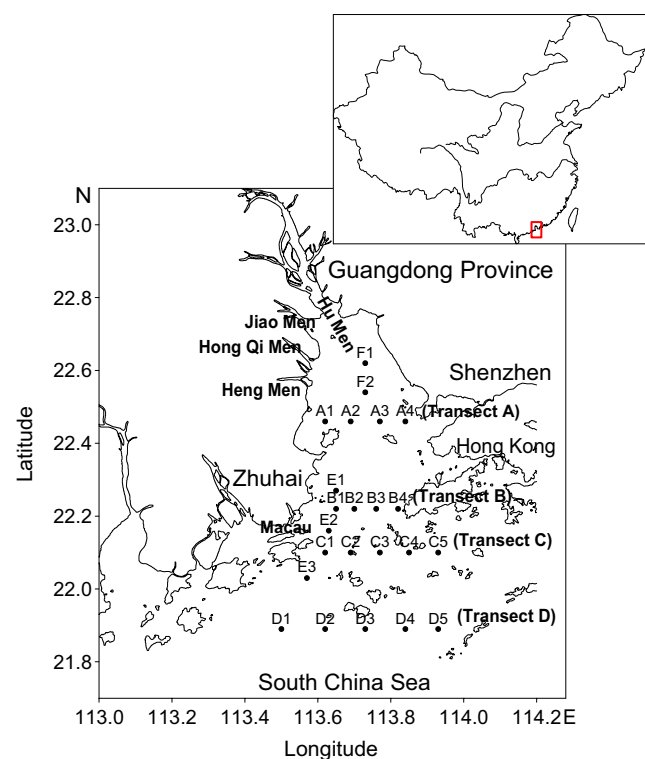


Figure 1 Sampling stations in the PRE in spring and autumn.

## 2.5. Statistical analysis

Principal component analysis (PCA) was applied using SPSS 16.0, and 11 variables (temperature, salinity, pH, DO, transparency, nitrate, nitrite, ammonium, DIN, phosphate, and silicate) were considered to elucidate the main environmental driving force in the PRE. All variables were log-transformed to normalize their distributions. Principal components (PCs) with an eigenvalue of more than 1 were extracted. A rotation of varimax with Kaiser normalization was used to achieve a simpler and more meaningful representation of the underlying PCs. The scores of the PCs and diagnostic pigments were subjected to stepwise multiple linear regression analysis to identify the influencing environmental factors. Correlation was analyzed with the Pearson correlation, and was performed at significance levels of  $P < 0.05$  and  $P < 0.01$ , which indicates that the correlation coefficient outstrips the critical value at the confidence intervals of 95% and 99%, respectively. Standard one-way ANOVA was used to completely randomize the experimental design, and significantly different means were separated ( $P = 0.05$ ).

## 3. Results

### 3.1. Hydrological parameters and nutrients

Water temperature was significantly lower but transparency was higher in the spring cruise than in the autumn cruise ( $P < 0.05$ , Table 1). No significant difference in DO and pH was detected between the two cruises ( $P > 0.05$ ). The mean of phosphate in spring was  $0.42 \mu\text{mol L}^{-1}$ , which was significantly lower than that in autumn ( $P < 0.05$ ). However, DIN ( $58.47\text{--}79.25 \mu\text{mol L}^{-1}$ ) and silicate ( $39.93\text{--}49.38 \mu\text{mol L}^{-1}$ ) did not present significant differences between the two cruises ( $P > 0.05$ ). The high N:P ratio suggested potential phosphorus limitation in the PRE. The distribution of salinity was low in the northwest but high in the southeast, both in spring and autumn (Fig. 2), whereas nitrate and silicate decreased from the northwest to the southeast in the two cruises. Phosphate presented a low concentration in the south in spring and in the middle in autumn.

By applying PCA, 90% and 70% of the variance contained in the original data set was explained by only two PCs in spring and autumn, respectively. Loadings of two PCs are displayed

**Table 1** Physio-chemical variables and pigment concentrations from the surface waters of the PRE in spring and autumn.

Physio-chemical variables and pigments	Spring				Autumn			
	AVE	SD	MIN	MAX	AVE	SD	MIN	MAX
<b>Physio-chemical variables</b>								
Temperature [ $^{\circ}\text{C}$ ]	17.19	0.3	16.49	17.82	23.95	0.36	23.15	24.66
Salinity	26.86	6.15	12.57	32.58	25.77	6.38	10.17	33.36
DO [ $\text{mg L}^{-1}$ ]	7.94	0.41	6.96	8.66	6.69	0.31	5.89	7.41
pH	8.13	0.17	7.76	8.33	7.81	0.14	7.46	8.03
Transparency [m]	1.2	0.9	0.2	3.2	0.8	0.3	0.5	2.0
Nitrate [ $\mu\text{mol L}^{-1}$ ]	35.17	28.38	3.76	93	60.28	49.97	4.81	177.18
Nitrite [ $\mu\text{mol L}^{-1}$ ]	6.62	5.76	0.56	19.91	13.06	7.52	2.49	32.02
Ammonium [ $\mu\text{mol L}^{-1}$ ]	16.67	12.61	0.27	32.7	5.9	3.26	2.26	14.71
DIN [ $\mu\text{mol L}^{-1}$ ]	58.47	44.21	4.65	140.75	79.25	55.63	12.62	201.27
Phosphate [ $\mu\text{mol L}^{-1}$ ]	0.42	0.3	0.08	0.98	0.82	0.41	0.35	2.46
Silicate [ $\mu\text{mol L}^{-1}$ ]	49.38	38.32	7.96	137.96	39.93	23.93	7.78	78.27
DIN:phosphate ratio	137.60	81.53	43.30	443.59	103.66	69.89	11.40	240.06
<b>Pigments</b>								
Chl <i>a</i> [ $\mu\text{g L}^{-1}$ ]	1.166	1.605	0.126	7.712	0.267	0.141	0.013	0.570
Chl <i>b</i> [ $\mu\text{g L}^{-1}$ ]	0.029	0.041	0.000	0.140	0.070	0.030	0.023	0.127
Chl <i>c</i> <sub>2</sub> [ $\mu\text{g L}^{-1}$ ]	0.859	0.710	0.143	3.437	0.040	0.029	0.000	0.096
Chl <i>c</i> <sub>3</sub> [ $\mu\text{g L}^{-1}$ ]	0.054	0.058	0.000	0.190	0.006	0.010	0.000	0.045
Fuco [ $\mu\text{g L}^{-1}$ ]	2.914	3.103	0.148	11.020	0.207	0.073	0.075	0.332
Diadino [ $\mu\text{g L}^{-1}$ ]	0.261	0.240	0.057	1.082	0.028	0.013	0.010	0.059
Peri [ $\mu\text{g L}^{-1}$ ]	0.208	0.157	0.027	0.565	0.061	0.029	0.017	0.123
Viola [ $\mu\text{g L}^{-1}$ ]	0.019	0.010	0.006	0.043	0.011	0.004	0.005	0.018
Allo [ $\mu\text{g L}^{-1}$ ]	0.131	0.082	0.050	0.328	0.052	0.028	0.003	0.107
Diato [ $\mu\text{g L}^{-1}$ ]	0.042	0.026	0.012	0.113	0.005	0.004	0.000	0.012
$\beta\beta$ -Car [ $\mu\text{g L}^{-1}$ ]	0.037	0.049	0.000	0.212	0.007	0.005	0.000	0.013
Pras [ $\mu\text{g L}^{-1}$ ]	0.023	0.015	0.000	0.056	0.011	0.007	0.002	0.029
Lut [ $\mu\text{g L}^{-1}$ ]	0.019	0.014	0.005	0.061	0.008	0.005	0.000	0.019
Neo [ $\mu\text{g L}^{-1}$ ]	0.016	0.011	0.000	0.037	0.012	0.005	0.002	0.026
Zea [ $\mu\text{g L}^{-1}$ ]	0.013	0.009	0.002	0.031	0.017	0.011	0.007	0.043
Hex-Fuco [ $\mu\text{g L}^{-1}$ ]	0.019	0.018	0.000	0.058	0.012	0.010	0.000	0.036
But-Fuco [ $\mu\text{g L}^{-1}$ ]	0.002	0.002	0.000	0.008	0.004	0.003	0.000	0.011

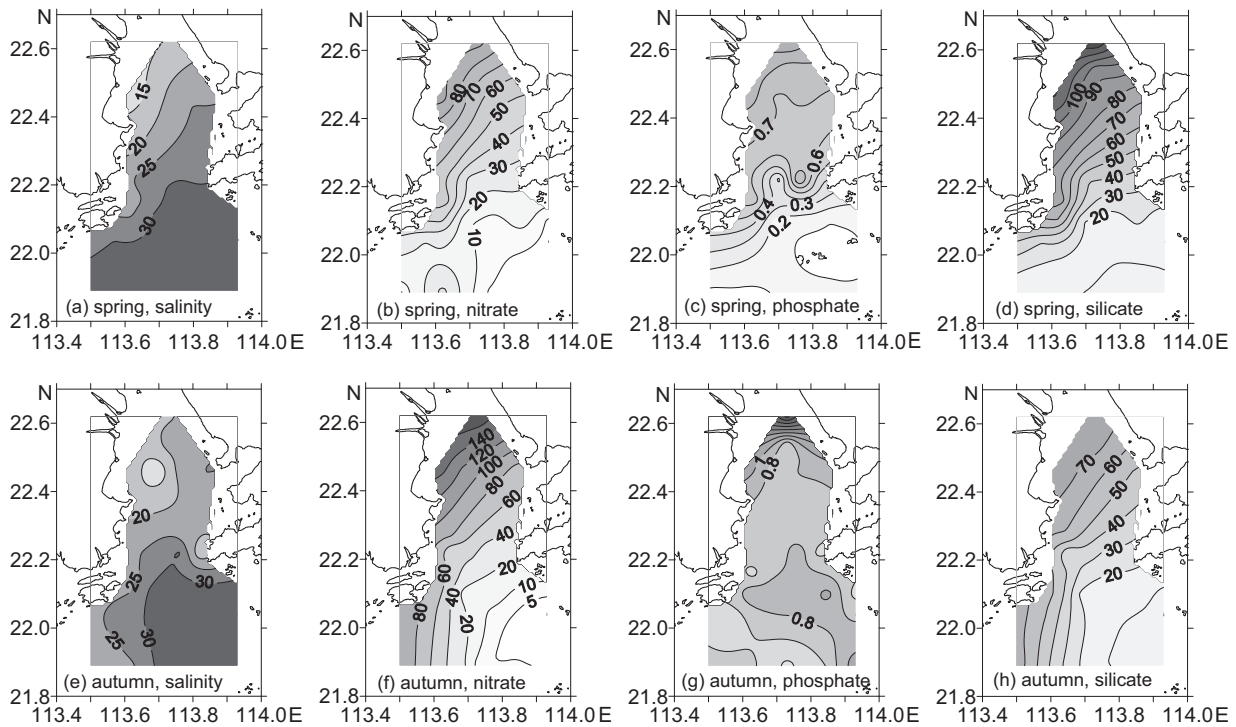


**Figure 2** Spatial distributions of salinity and nutrients [ $\mu\text{mol L}^{-1}$ ] in the PRE in spring and autumn.

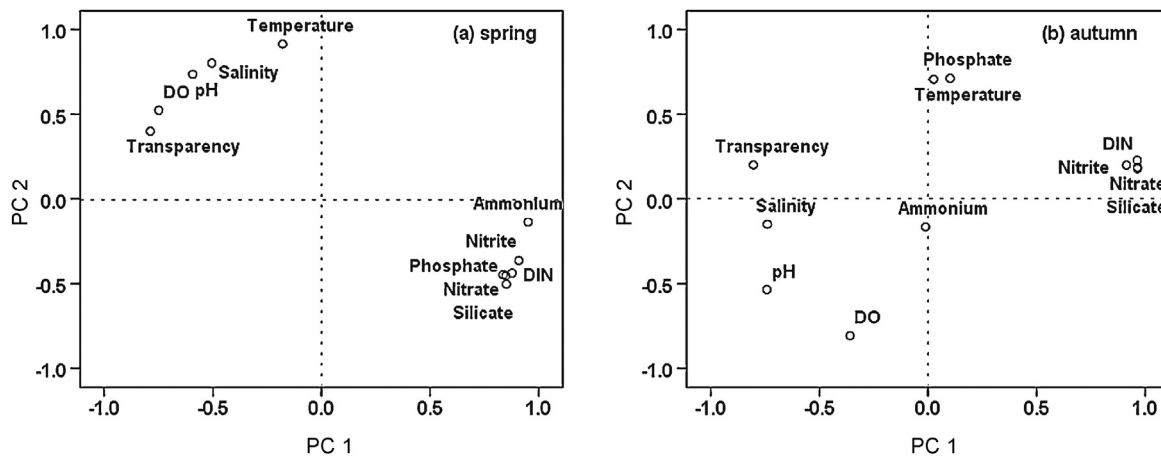


**Figure 3** Loadings of 11 variables on two rotated PCs in (a) spring and (b) autumn.

in Fig. 3. In spring, PC 1 was highly participated by nutrients, whereas PC 2 was mainly participated by water temperature, salinity, and pH. Similarly, PC 1 had a highly positive load of nitrogen and silicon in autumn, whereas PC 2 had load of water temperature and phosphate. The results from Pearson's correlation (Table 2) showed that all nutrients correlated most significantly with PC 1 in spring ( $r > 0.8$ ,  $P < 0.01$ ), whereas nitrogen and silicon correlated significantly with PC 1 in autumn ( $r > 0.9$ ,  $P < 0.01$ ). Thus, nutrients were the most important environmental driving element in the PRE. In addition, the high correlation coefficients between PC 2 and temperature and salinity in spring, as well as between PC 1 and transparency in autumn, indicated that these physical variables were also important.

### 3.2. Pigment concentrations and distributions

Among 22 pigments, 17 major pigments were detected in the PRE during the sampling periods (Table 1). Chl *a*, Fuco, and Chl *c*<sub>2</sub> were the most abundant pigments in spring, with mean values of 1.166, 2.914, and 0.859  $\mu\text{g L}^{-1}$ , respectively. By comparison, the concentrations of Diadino, Peri, and Allo were relatively low, i.e., 0.131–0.261  $\mu\text{g L}^{-1}$ ; the other 11 pigments were  $< 0.1 \mu\text{g L}^{-1}$  in concentration. In autumn, the mean values of Chl *a* and Fuco were higher than those of the other pigments, which were 0.267  $\mu\text{g L}^{-1}$  and 0.207  $\mu\text{g L}^{-1}$ , respectively. By contrast, the mean values of Chl *b*, Peri, and Allo were lower, i.e., 0.052–0.070  $\mu\text{g L}^{-1}$ . Other pigments had relatively low concentrations, with mean values generally

**Table 2** Pearson's correlation coefficients between the variables and PCs.

	Spring		Autumn	
	PC 1	PC 2	PC 1	PC 2
Temperature	−0.179	0.913**	0.026	0.705**
Salinity	−0.505*	0.800**	−0.740**	−0.151
DO	−0.749**	0.523*	−0.359	−0.735**
pH	−0.593**	0.735**	−0.742**	−0.535**
Transparency	−0.788**	0.399	−0.804**	0.200
Nitrate	0.849**	−0.453*	0.964**	0.187
Nitrite	0.878**	−0.438*	0.914**	0.199
Ammonium	0.951**	−0.137	−0.011	−0.166
DIN	0.909**	−0.364	0.963**	0.227
Phosphate	0.837**	−0.448*	0.102	0.711**
Silicate	0.852**	−0.503*	0.965**	0.178

\*  $P < 0.05$ .\*\*  $P < 0.01$ .

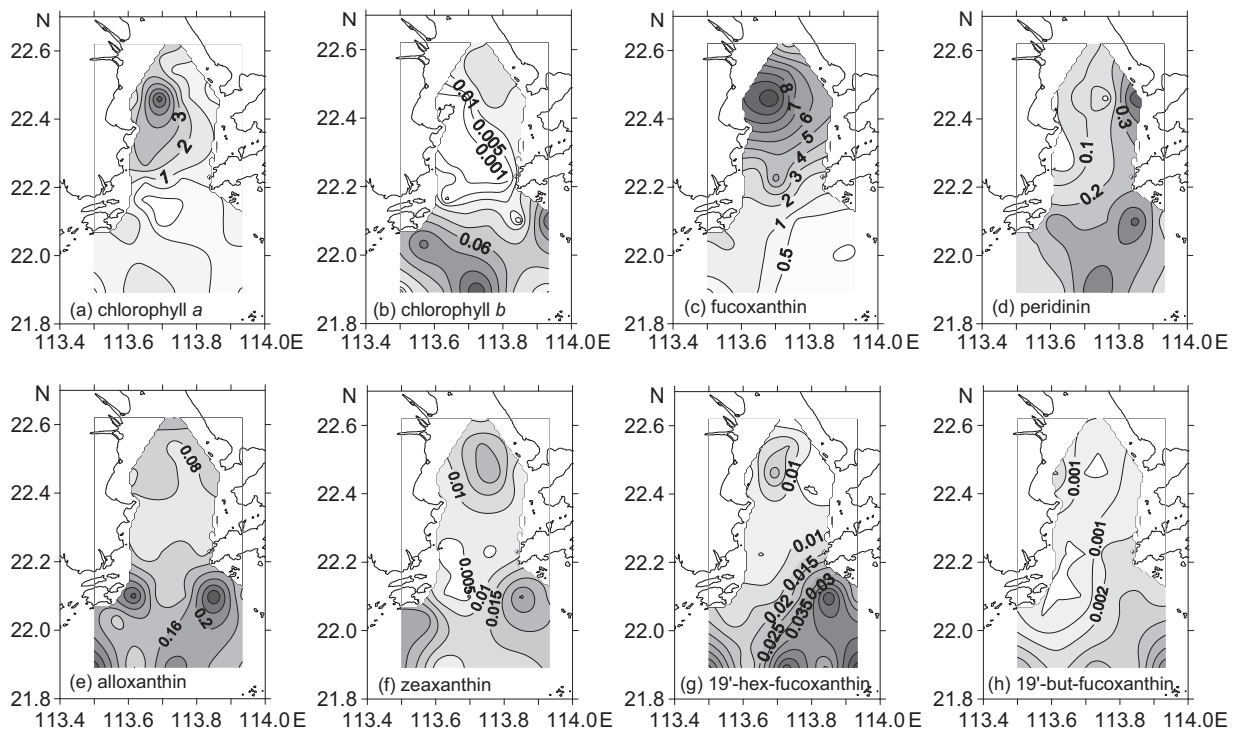
lower than  $0.02 \mu\text{g L}^{-1}$ . Significant differences in the concentrations of pigments, except in Neo, Zea, and Hex-Fuco, were determined between the two cruises. The concentrations of nearly all pigments, except Chl *b* and But-Fuco, were significantly higher in spring than in autumn ( $P < 0.05$ ). MgDVP, Pheide *a*, Cantha, DV-Chl *a*, and Phe *a* were not detected in the PRE during the two cruises.

The spatial distribution of Chl *a* and diagnostic pigments in spring and in autumn is presented in Figs. 4 and 5, respectively, while other pigments are not showed. Chl *a*, Chl *c*<sub>2</sub>, Fuco, Diadino, Diato, and  $\beta\beta$ -Car exhibited a similar distribution, i.e., higher in the northern or northwest estuary but lower in the south. Except Fuco, which is the characteristic pigment of

diatoms, Chl *a*, Chl *c*<sub>2</sub>, Diadino, Diato, and  $\beta\beta$ -Car were observed in many phytoplankton species. Their distributions were obviously influenced by diluted water. The highest values of Chl *a*, Fuco, Diadino, and  $\beta\beta$ -Car were observed at station A2, and those of Chl *c*<sub>2</sub> and Diato at stations F1 and F2. By contrast, Peri, the characteristic pigment of dinoflagellates, was mainly distributed in the northeast and south estuary. Chl *b*, Chl *c*<sub>3</sub>, Allo, Pras, Lut, Neo, Hex-Fuco, and But-Fuco were distributed at high concentrations in the southern part of the sampling region; these pigments were mainly found at station D3 or D5. The concentrations of Viola and Zea were high in the north and south, but low in the central part of the estuary.

Unlike in spring, Chl *a*, Chl *c*<sub>2</sub>, Fuco, Diadino, Diato, Allo, and But-Fuco showed high concentrations in the middle eastern and northeast parts of the sampling region, with the highest value in station B4. Similar to the pigments in spring, Chl *b*, Chl *c*<sub>3</sub>, Pras, and Zea in autumn were distributed in the southern part, with the highest value in station D4 or D2. Furthermore, Peri in autumn presented the same distribution as that in spring, whose high value was distributed both in the northeast and in the south.

Correlation analysis showed that Chl *a* in spring was significantly positively correlated with Fuco ( $r = 0.587$ ,  $P < 0.01$ ). In addition, Chl *a* and Fuco were significantly negatively correlated with salinity ( $r = -0.504$  and  $-0.768$ , respectively,  $P < 0.05$ ) but significantly positively correlated with nutrients ( $r = 0.444$ – $0.752$ ,  $P < 0.05$ ). By contrast, Hex-Fuco and But-Fuco were significantly positively correlated with salinity ( $r = 0.555$  and  $0.436$ , respectively,  $P < 0.05$ ) but significantly negatively correlated with nutrients ( $r = -0.491$  to  $-0.682$ ,  $P < 0.05$ ). Unlike in spring, Chl *a* in autumn was significantly positively correlated with Allo, Chl *b*, and Zea ( $r = 0.436$ – $0.753$ ,  $P < 0.05$ ). Allo, Chl *b*, and Zea were significantly positively correlated with salinity ( $r = 0.419$ – $0.598$ ,

**Figure 4** Spatial distributions of pigments in the PRE in spring [ $\mu\text{g L}^{-1}$ ].

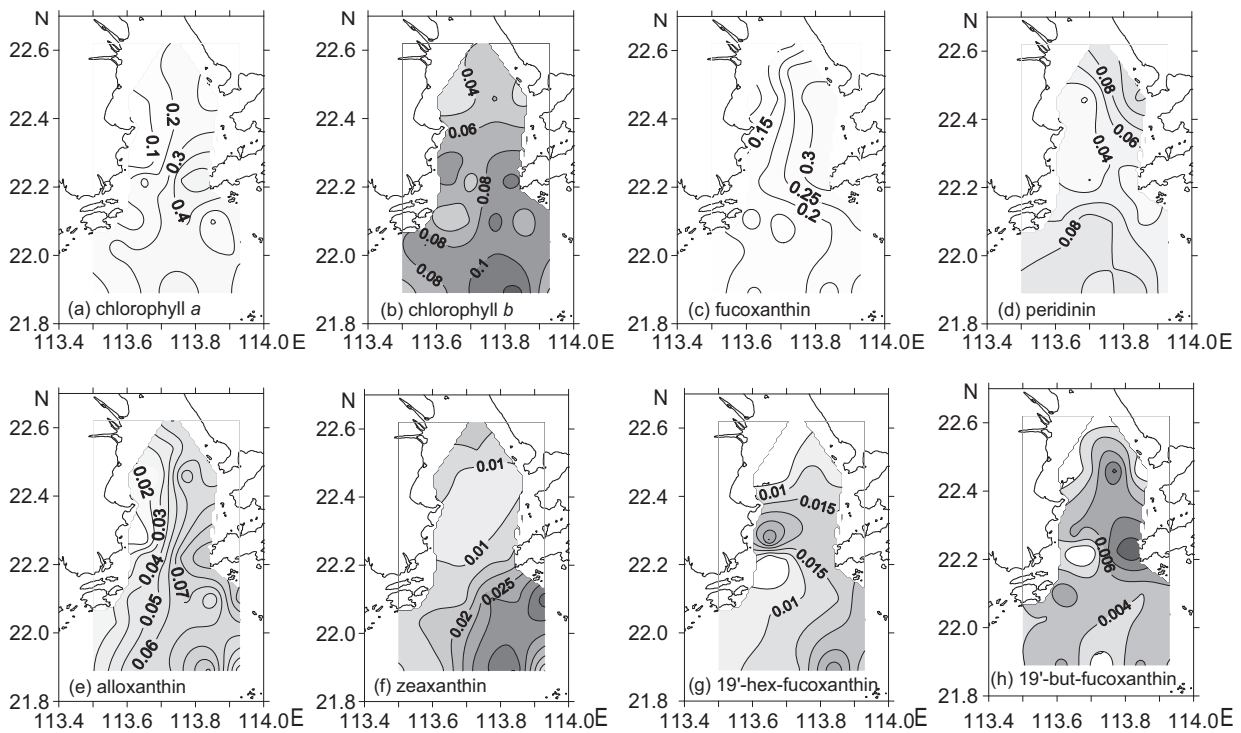


Figure 5 Spatial distributions of pigments in the PRE in autumn [ $\mu\text{g L}^{-1}$ ].

$P < 0.05$ ), whereas Chl *a*, Allo, Hex-Fuco, Chl *b*, and Zea were significantly negatively correlated with nitrate and silicate ( $r = -0.468$  to  $-0.625$ ,  $P < 0.05$ ).

### 3.3. Phytoplankton pigment indices

The mean of  $BP_m$  in spring was 85.4%, and ranged from 55.3% to 99.1%, which was higher than that in autumn with a mean of 64.1%. By contrast, the mean of  $BP_p$  in autumn (20.6%) was significantly higher than that in spring (3.3%). In spring,  $BP_m$  was higher in the area with salinity  $< 30$ , but  $BP_p$  and  $BP_n$  were higher in the area with salinity  $> 30$  (Fig. 6).  $BP_m$  generally increased but  $BP_p$  and  $BP_n$  reduced with the increase in nitrate, phosphate, and silicate. Similar to spring,  $BP_m$  increased but  $BP_n$  decreased with increasing nitrate and silicate. However, no relationship was found between  $BP_p$  and salinity or nutrients as well as between phosphate and any BP in autumn.

The PPC:PSC ratios in most stations of transects C and D in spring approached the unity linear relationship (red line, in Fig. 7), but were low in stations A1 to A4, B2, and F2. By comparison, the PPC:PSC ratios in all stations were under the unity line in autumn.

## 4. Discussion

### 4.1. Phytoplankton diversity and distribution in the PRE as revealed by pigments

High concentrations of Fuco and Peri during two cruises confirmed that diatoms and dinoflagellates were dominant, and the detected pigments, including Allo, Pras, Lut, Zea, Hex-Fuco, and But-Fuco, indicated the presence of cryptophytes,

prasinophytes, chlorophytes, cyanophytes, haptophytes, and pelagophytes. By contrast, DV-Chl *a* with an undetectable level implied that no *Prochlorococcus* was present during sampling time.

The distribution of pigments implies the spatial variations of phytoplankton. In spring, the high value of Chl *a* and Fuco suggested the existence of a diatom bloom in the north of the estuary. The distributions of Chl *b*, Allo, Pras, Lut, Hex-Fuco, and But-Fuco indicated that cryptophytes, chlorophytes, prasinophytes, haptophytes, and pelagophytes mainly existed in the south. The distributions of Peri and Zea indicated that dinoflagellates and cyanophytes basically existed both in the north and south but were low in the central part. Similar to spring, dinoflagellates in autumn were mainly distributed both in the northeast and in the south, while chlorophytes and cyanophytes were mainly distributed in the south. However, unlike in spring, diatoms, cryptophytes, and pelagophytes mainly existed in the middle-eastern and northeast parts of the estuary. The phytoplankton distribution found in the current study is consistent with those in previous studies (Harrison et al., 2008; Lu and Gan, 2015; Yin, 2003). Temperature, light, hydrodynamics, and nutrient supply are the major factors that control the spatial–temporal distribution of phytoplankton (Agawin et al., 2000; Marañón et al., 2007; Riegman et al., 1993). Lu and Gan (2015) found that the low river discharge leads to longer water residence time, satisfactory water column stability, and transparency, which are helpful for the diatom bloom in the upper PRE during the dry season. In the present study, higher salinity in spring indicated low river discharge, which may result in diatom bloom in the northern estuary during spring (Table 1). As for the spatial distribution, Li et al. (2013) and Zhang et al. (2013) reported that larger phytoplankton (e.g., diatom) are

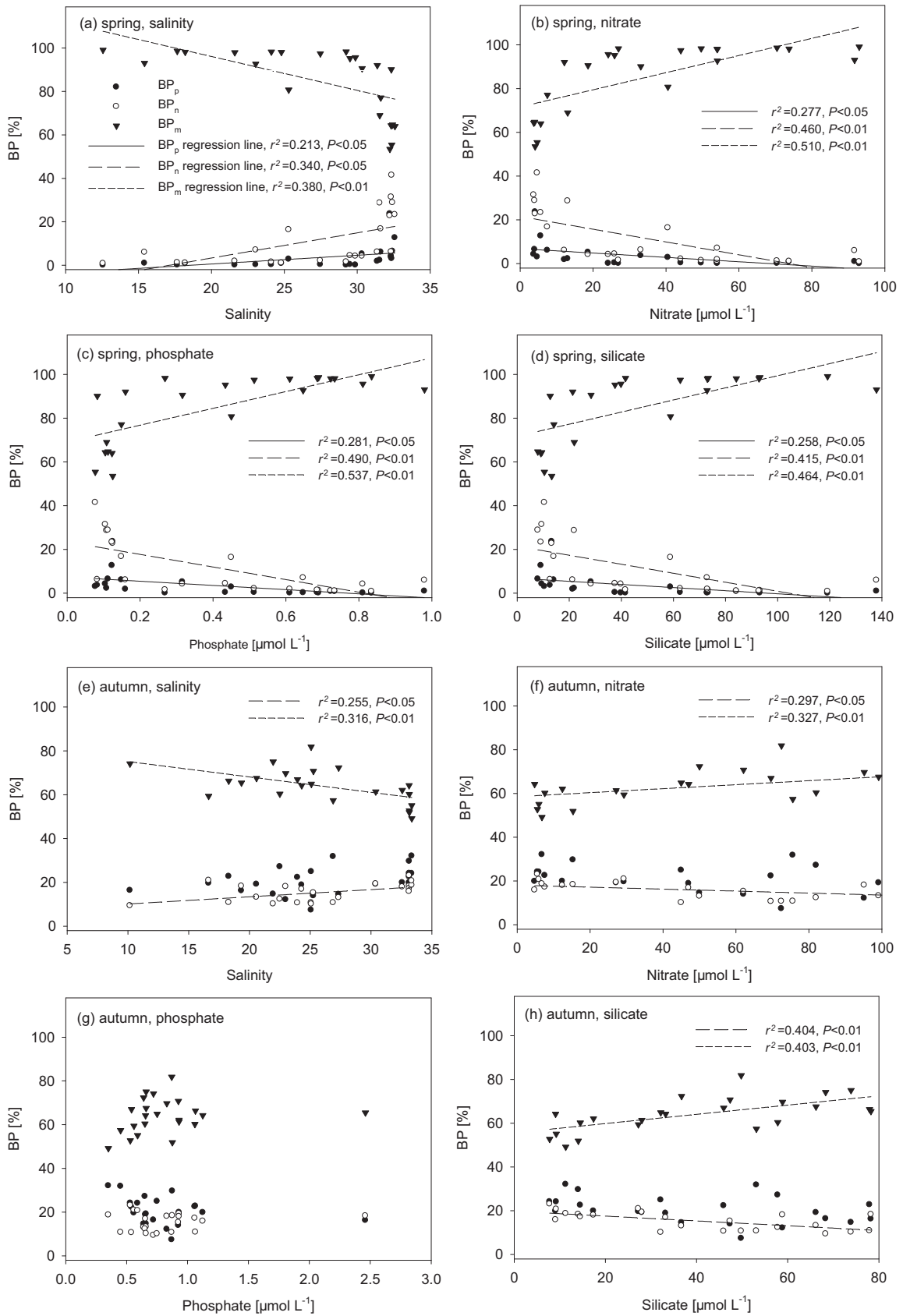
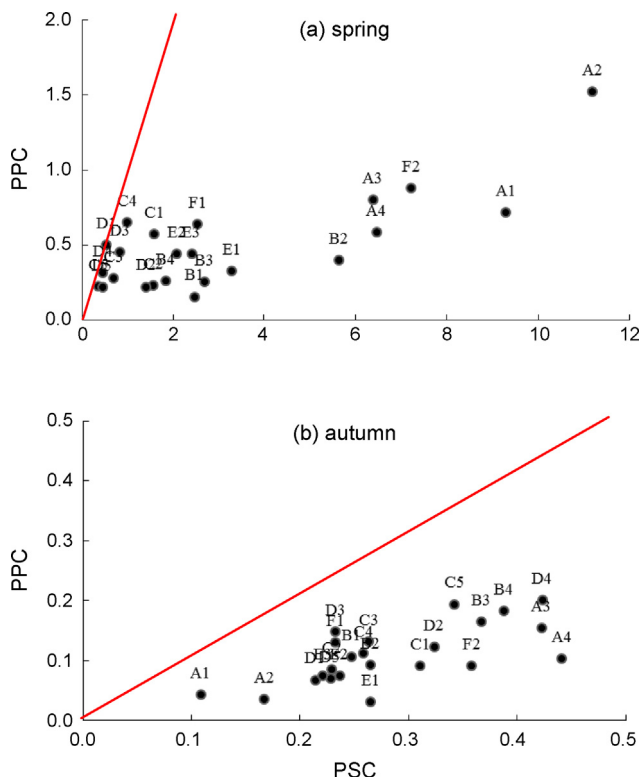


Figure 6 Relationship of BP with environmental variables in the PRE in spring and autumn.



**Figure 7** PPC vs. PSC by station numbers in the PRE in (a) spring and (b) autumn. The red line denotes the unity line, which indicates that PPC:PSC is 1. (For interpretation of the references to color in this figure legend, the reader is referred to the web version of this article.)

dominant in the upper PRE that has low salinity and high nutrient content, whereas the smaller ones (e.g., blue-green algae) are found in water with high salinity and low nutrient content. Stepwise multiple regression analysis indicated that Fuco positively correlated, whereas Hex-Fuco, Allo, Zea, and Chl *b* negatively correlated with PC 1, indicating that nutrients were the main environmental controlling factors (Table 3).

#### 4.2. Relationship of different phytoplankton groups as revealed by pigments with environmental factors

The biomass proportions derived from pigments suggest the size structure of phytoplankton. In this study, BP<sub>m</sub> was considerably higher than BP<sub>n</sub> and BP<sub>p</sub> in the area with salinity <30, and BP<sub>n</sub> increased, particularly in spring, despite the decrease in BP<sub>m</sub> in the area with salinity >30 (Fig. 6). Therefore, high BP<sub>m</sub> and BP<sub>n</sub> indicated the dominance of microphytoplankton and nanophytoplankton in the PRE. This result is consistent with previous investigations conducted through microscopy and flow cytometry (Qiu et al., 2010). In comparison, the increasing BP<sub>p</sub> in the area with salinity >30 in spring indicated that picophytoplankton became abundant (Fig. 6), and the increase in BP<sub>p</sub> in autumn suggested the abundance of picophytoplankton. Phytoplankton sizes are generally affected by environmental factors (Finkel et al., 2007,

**Table 3** Regression analysis of the principal component scores (as independent factors) for the diagnostic pigments in spring and autumn<sup>a</sup>.

Dependent factor	$R^2$	$F$	$\beta$	
			PC 1	PC 2
<b>Spring</b>				
Fuco	0.563**	12.880	0.609**	-0.438**
Peri	0.199	2.491	-0.085	0.438*
Allo	0.134	1.548	-0.306	0.201
Zea	0.104	1.336	-0.195	0.258
Chl <i>b</i>	0.203	2.544	-0.269	0.361
Hex-Fuco	0.607**	15.435	-0.751**	0.205
But-Fuco	0.551**	12.251	-0.741**	0.309
<b>Autumn</b>				
Fuco	0.027	0.274	-0.159	-0.036
Peri	0.154	1.825	-0.081	-0.384
Allo	0.397**	6.595	-0.615**	0.140
Zea	0.521**	10.888	-0.722**	-0.111
Chl <i>b</i>	0.484**	9.366	-0.541**	-0.437*
Hex-Fuco	0.301*	4.414	-0.516*	-0.188
But-Fuco	0.060	0.639	-0.181	-0.165

<sup>a</sup>  $R^2$ : regression coefficient;  $\beta$ :  $F$ -value of the full model and the standardized coefficient.

\*  $P < 0.05$ .

\*\*  $P < 0.01$ .

2009). Large phytoplanktons are generally developed in turbulent and high nutrient waters (Huete-Ortega et al., 2010; Margalef, 1978; Reul et al., 2006), whereas small phytoplanktons are developed in stratified and low nutrient waters (Chisholm, 1992; Kiørboe, 1993; Marañon, 2009). With the decrease in nutrient availability, phytoplankton typically change from a large species to small one (Roy et al., 2006); thus, microphytoplankton generally dominate areas in nutrient-rich conditions (Chen and Liu, 2010). By comparison, nanophytoplankton and picophytoplankton are abundant in nutrient-deficient waters (Roy et al., 2006; Thingstad, 1998), although they contribute to the total biomass in nutrient-rich coastal waters (Badylak and Phlips, 2004; Phlips et al., 1999). In the present study, BP<sub>n</sub> and BP<sub>p</sub> increased but BP<sub>m</sub> decreased with decreasing nutrient concentration in spring (Fig. 6). This result indicates that nutrient concentration influences phytoplankton distribution with different sizes. A previous study also reported that the abundance of picophytoplankton in the PRE is negatively correlated with inorganic nutrients (Zhang et al., 2013). This report implies that low nutrient concentrations in offshore areas promote the growth of picophytoplankton.

#### 4.3. Influence of environmental factors on PPC and PSC

Environmental and trophic conditions affect PPC and PSC, which function as indicators of the physiological condition of a phytoplankton community (Trees et al., 2000; Veldhuis and Kraay, 2004). Lutz et al. (2003) noted an increase in PPC at

high irradiance levels while the elevated proportion of PPC at low irradiance, and Barlow et al. (2007) found that PPC is dominated where nitrate concentrations are  $<0.007 \mu\text{mol L}^{-1}$ , but PSC is high at nitrate levels  $>0.007 \mu\text{mol L}^{-1}$ . As a result, intensive light and low nutrients increase the proportion of PPC, and consequently, the ratio of PPC:PSC (Moreno et al., 2012; Vijayan et al., 2009). In the present study, the nutrient concentration in the southern part was low in spring (Fig. 2); meanwhile, the average transparency was 1.98 m in transects C and D, which was considerably higher than that in transect A (0.2 m), inferring adequate light in transects C and D during spring. Therefore, adequate light and low nutrients may increase PPC:PSC ratios in the southern part (transects C and D) of the PRE in spring (Fig. 7).

By comparison, environmental variables between autumn and spring showed nonsignificant differences ( $P > 0.05$ ), except water temperature, which was significantly lower in spring than in autumn. Higher phytoplankton biomass and more samples of higher PPC:PSC ratio were observed during spring despite lower water temperature (Table 1, Fig. 7). These trends were probably due to the satisfactory water transparency in spring. Average transparency was 1.2 m during spring but was only 0.8 m during autumn (Table 1). Higher transparency may result in adequate light intensity, possibly causing high levels of the pigments and PPC:PSC ratios during spring. Zhang et al. (2014) also reported that turbidity and light are principal factors that affect phytoplankton biomass in the PRE. Therefore, the spatial–temporal distribution of PPC:PSC ratios provides information on the physiological condition of the phytoplankton community in the PRE as influenced by light, transparency, and nutrient conditions. On this basis, PPC:PSC ratio can be used as a classification tool for ecosystems because it can be related both to phytoplankton populations and to hydrography (Moreno et al., 2012).

## 5. Conclusion

Among the 22 pigments, 17 were detected using HPLC. Fuco was the most abundant accessory pigment. The detected pigments indicated the presence of diatoms, dinoflagellates, cryptophytes, prasinophytes, chlorophytes, cyanophytes, haptophytes, and pelagophytes. Most pigment levels were significantly higher in spring than in autumn, and different spatial distribution patterns were presented between the two seasons.

The salinity and nutrient levels influenced the distribution of phytoplankton functional types in the PRE.  $BP_m$  was higher during spring, whereas  $BP_p$  was higher during autumn.  $BP_m$  in spring was high in areas with salinity  $<30$ , whereas  $BP_p$  and  $BP_n$  were high in areas with salinity  $>30$ .  $BP_m$  increased whereas  $BP_p$  reduced with the increase in nutrient contents. By comparison,  $BP_p$  declined with the increase in nutrient contents during spring.

The PPC:PSC ratios in the southern estuary approached unity linear relationship during spring and were under the unity line during autumn. PPC:PSC ratios provide an estimate of the physiological condition of the phytoplankton community in the PRE as influenced by light, transparency, and nutrients conditions.

## References

- Agawin, N.R.S., Duarte, C.M., Agustí, S., 2000. Nutrient and temperature control of the contribution of picoplankton to phytoplankton biomass and production. *Limnol. Oceanogr.* 45 (3), 591–600.
- Aneeshkumar, N., Sujatha, C.H., 2012. Biomarker pigment signatures in Cochin back water system – a tropical estuary south west coast of India. *Estuar. Coast. Shelf Sci.* 99, 182–190.
- Badyaluk, S., Philips, E.J., 2004. Spatial and temporal patterns of phytoplankton composition in a subtropical coastal lagoon, the Indian River Lagoon, Florida, USA. *J. Plankton Res.* 26 (10), 1229–1247.
- Barlow, R.G., Aiken, J., Holligan, P.M., Cummings, D.G., Maritorena, S., Hooker, S., 2002. Phytoplankton pigment and absorption characteristics along meridional transects in the Atlantic Ocean. *Deep-Sea Res. Pt. I* 49 (4), 637–660.
- Barlow, R., Kyewalyanga, M., Sessions, H., Van den Berg, M., Morris, T., 2008. Phytoplankton pigments, functional types, and absorption properties in the Delagoa and Natal Bights of the Agulhas ecosystem. *Estuar. Coast. Shelf Sci.* 80 (2), 201–211.
- Barlow, R., Stuart, V., Lutz, V., Sessions, H., Sathyendranath, S., Platt, T., Kyewalyanga, M., Clementson, L., Fukasawa, M., Watanabe, S., Devred, E., 2007. Seasonal pigment patterns of surface phytoplankton in the subtropical southern hemisphere. *Deep-Sea Res. Pt. I* 54 (10), 1687–1703.
- Bulletin of Water Resources in the Pearl River Drainage, 2011. Commission of Water Resources of Pearl River, Ministry of Water Resources of the People's Republic of China, <http://www.pearlwater.gov.cn/xxcx/szygg/>.
- Bulletin of Water Resources in the Pearl River Drainage, 2012. Commission of Water Resources of Pearl River, Ministry of Water Resources of the People's Republic of China, <http://www.pearlwater.gov.cn/xxcx/szygg/>.
- Chen, B.Z., Liu, H.B., 2010. Relationships between phytoplankton growth and cell size in surface oceans: interactive effects of temperature, nutrients, and grazing. *Limnol. Oceanogr.* 55 (3), 965–972.
- Chisholm, S.W., 1992. Phytoplankton size. In: Falkowski, P.G., Woodhead, A.D. (Eds.), *Primary Productivity and Biogeochemical Cycles in the Sea*. Plenum Press, New York, 213–238.
- Finkel, Z.V., Sebbo, J., Feist-Burkhardt, S., Irwin, A.J., Katz, M.E., Schofield, O.M.E., Falkowski, P.G., 2007. A universal driver of macroevolutionary change in the size of marine phytoplankton over the Cenozoic. *Proc. Natl. Acad. Sci. U.S.A.* 104, 20416–20420.
- Finkel, Z.V., Vaillancourt, C.J., Irwin, A.J., Reavie, E.D., Smol, J.P., 2009. Environmental control of diatom community size structure varies across aquatic ecosystems. *Proc. R. Soc. B* 276, 1627–1634.
- Gibb, S.W., Barlow, R.G., Cummings, D.G., Rees, N.W., Trees, C.C., Holligan, P., Suggett, D., 2000. Surface phytoplankton pigment distributions in the Atlantic Ocean: an assessment of basin scale variability between 50°N and 50°S. *Prog. Oceanogr.* 45 (3–4), 339–368.
- Gibb, S.W., Cummings, D.G., Irigoien, X., Barlow, R.G., Fauzi, R., Mantoura, C., 2001. Phytoplankton pigment chemotaxonomy of northeastern Atlantic. *Deep-Sea Res. Pt. II* 48 (4–5), 795–823.
- Grasshoff, K., Erhardt, M., Kremling, K., 1983. *Methods of Seawater Analysis*. Verlag Chemie, Weinheim, 632 pp.
- Harrison, P.J., Yin, K.D., Lee, J.H.W., Gan, J.P., Liu, H.B., 2008. Physical–biological coupling in the Pearl River Estuary. *Cont. Shelf Res.* 28 (12), 1405–1415.
- He, B.Y., Dai, M.H., Zhai, W.D., Guo, X.H., Wang, L.F., 2014. Hypoxia in the upper reaches of the Pearl River Estuary and its maintenance mechanisms: a synthesis based on multiple year observations during 2000–2008. *Mar. Chem.* 167 (20), 13–24.
- Huang, L.M., Jian, W.J., Song, X.Y., Huang, X.P., Liu, S., Qian, P.Y., Yin, K.D., Wu, M., 2004. Species diversity and distribution for phytoplankton of the Pearl River estuary during rainy and dry seasons. *Mar. Pollut. Bull.* 49 (7–8), 588–596.

- Huete-Ortega, M., Marañón, E., Varela, M., Bode, A., 2010. General patterns in the size scaling of phytoplankton abundance in coastal waters during a 10-year time series. *J. Plankton Res.* 32 (1), 1–14.
- Jeffrey, S.W., Mantoura, R.F.C., Bjørnland, T., 1997. Data for the identification of 47 key phytoplankton pigments. In: Jeffrey, S.W., Mantoura, R.F.C., Wright, S.W. (Eds.), *Phytoplankton Pigments in Oceanography: Guidelines to Modern Methods*. Monographs on Oceanographic Methodology. UNESCO, Paris, 449–559.
- Jeffrey, S., Mantoura, R., Wright, S. (Eds.), 2005. *Phytoplankton Pigments in Oceanography. Guidelines to Modern Methods*. Monographs on Oceanographic Methodology, 2nd edn. UNESCO, Paris, 661 pp.
- Kjørboe, T., 1993. Turbulence, phytoplankton cell size, and the structure of pelagic food webs. *Adv. Mar. Biol.* 29, 1–72.
- Lerman, A., 1981. Control on river water composition and the mass balance of river systems. In: Martin, J.M., Burton, J.D., Eisma, D. (Eds.), *River Inputs to Ocean Systems. Proceedings of a SCOR/ACMRR/ECOR/IAHS/UNESCO/CMG/IABO/IAPSO Review and Workshop*, 26–30 March 1979, UNEP and UNESCO, Rome.
- Li, G., Lin, Q., Lin, J.D., Song, X.Y., Tan, Y.H., Huang, L.M., 2014. Environmental gradients regulate the spatial variations of phytoplankton biomass and community structure in surface water of the Pearl River estuary. *Acta Ecol. Sin.* 34 (2), 129–133.
- Li, L., Lu, S.H., Jiang, T., Li, X., 2013. Seasonal variation of size-fractionated phytoplankton in the Pearl River estuary. *Chin. Sci. Bull.* 58 (19), 2303–2314.
- Lu, Z.M., Gan, J.P., 2015. Controls of seasonal variability of phytoplankton blooms in the Pearl River Estuary. *Deep-Sea Res. Pt. II* 117, 86–96.
- Lutz, V.A., Sathyendranath, S., Head, E.J.H., Li, W.K.W., 2003. Variability in pigment composition and optical characteristics of phytoplankton in the Labrador Sea and the Central North Atlantic. *Mar. Ecol. Prog. Ser.* 260, 1–18.
- Marañón, E., 2009. Phytoplankton size structure. In: Steele, J.H., Turekian, K.K., Thorpe, S.A. (Eds.), *Encyclopedia of Ocean Sciences*. 2nd ed. Amsterdam, Elsevier, 445–452.
- Marañón, E., Cermeño, P., Rodríguez, J., Zubkov, M.V., Harris, R.P., 2007. Scaling of phytoplankton photosynthesis and cell size in the ocean. *Limnol. Oceanogr.* 52 (5), 2190–2198.
- Margalef, R., 1978. Life forms of phytoplankton as survival alternatives in an unstable environment. *Oceanol. Acta* 1 (4), 493–509.
- Moreno, D.V., Marrero, P., Morales, J., Llerandi García, C., Villagaría Úbed, M.G., Rueda, M.J., Llinás, O., 2012. Phytoplankton functional community structure in Argentinian continental shelf determined by HPLC pigment signatures. *Estuar. Coast. Shelf Sci.* 100, 72–81.
- Naik, R.K., Anil, A.C., Narale, D.D., Chitari, R.R., Kulkarni, V.V., 2011. Primary description of surface water phytoplankton pigment patterns in the Bay of Bengal. *J. Sea Res.* 65 (4), 435–441.
- Paerl, H.W., Valdes, L.M., Pinckney, J.L., Piehler, M.F., Dyble, J., Moisaner, P.H., 2003. Phytoplankton photopigments as indicators of estuarine and coastal eutrophication. *BioScience* 53 (10), 953–964.
- Phlips, E.J., Badylak, S., Lynch, T.C., 1999. Blooms of the picoplanktonic cyanobacterium *Synechococcus* in Florida Bay, a subtropical inner-shelf lagoon. *Limnol. Oceanogr.* 44 (4), 1166–1175.
- Qiu, D.J., Huang, L.M., Zhang, J.L., Lin, S.J., 2010. Phytoplankton dynamics in and near the highly eutrophic Pearl River Estuary, South China Sea. *Cont. Shelf Res.* 30 (2), 177–186.
- Reul, A., Rodríguez, J., Blanco, J.M., Rees, A.P., Burkill, P.H., 2006. Control of microplankton size structure in contrasting water columns of Celtic Sea. *J. Plankton Res.* 28 (5), 449–457.
- Riegman, R., Kuipers, B.R., Noordeloos, A.A.M., Witte, H.J., 1993. Size-differential control of phytoplankton and the structure of plankton communities. *Netherlands J. Sea Res.* 31, 255–265.
- Roy, R., Pratihary, A., Mangesh, G., Naqvi, S.W.A., 2006. Spatial variation of phytoplankton pigments along the southwest coast of India. *Estuar. Coast. Shelf Sci.* 69 (1–2), 189–195.
- Sieburth, J.M., Smetacek, V., Lenzen, J., 1978. Pelagic ecosystem structure: heterotrophic compartments of the plankton and their relationship to plankton size fractions. *Limnol. Oceanogr.* 23 (6), 1256–1263.
- Thingstad, T.F., 1998. Theoretical approach to structuring mechanisms in the pelagic food web. *Hydrobiologia* 363 (1–3), 59–72.
- Trees, C.C., Clark, D.K., Bidigare, R.R., Ondrusek, M.E., Mueller, J.L., 2000. Accessory pigments versus chlorophyll *a* concentrations within the euphotic zone: a ubiquitous relationship. *Limnol. Oceanogr.* 45 (5), 1130–1143.
- Veldhuis, M.J.W., Kraay, G.W., 2004. Phytoplankton in the subtropical Atlantic Ocean: towards a better assessment of biomass and composition. *Deep-Sea Res. Pt. I* 51 (4), 507–530.
- Vidussi, F., Claustre, H., Manca, B., Luchetta, A., Marty, J., 2001. Phytoplankton pigment distribution in relation to upper thermocline circulation in the eastern Mediterranean Sea during winter. *J. Geophys. Res.* 106 (C9), 19939–19956.
- Vijayan, A.K., Yoshikawa, T., Watanabe, S., Sasaki, H., Matsumoto, K., Saito, S.i., Takeda, S., Furuya, K., 2009. Influence on non-photosynthetic pigments on light absorption and quantum yield of photosynthesis in the western equatorial pacific and the subarctic north pacific. *J. Oceanogr.* 65 (2), 245–258.
- Wright, S.W., Jeffrey, S.W., 2006. Pigment markers for phytoplankton production. *The Handbook of Environmental Chemistry*, vol. 2, Part N. 71–104.
- Yin, K., 2003. Influence of monsoons and oceanographic processes on red tides in Hong Kong in the vicinity of the Pearl River Estuary. *Mar. Ecol. Prog. Ser.* 262, 27–41.
- Yin, K., Qian, P.Y., Chen, J.C., Hsieh, D.P., Harrison, P.J., 2000. Dynamics of nutrients and phytoplankton biomass in the Pearl River estuary and adjacent waters of Hong Kong during summer: preliminary evidence for phosphorus and silicon limitation. *Mar. Ecol. Prog. Ser.* 194, 295–305.
- Yin, K., Qian, P.Y., Chen, J.F., Huang, L., Zhang, J., Wu, M., 2004. Effect of wind events on phytoplankton blooms in the Pearl River Estuary during summer. *Cont. Shelf Res.* 24 (16), 1909–1923.
- Yin, K., Qian, P.Y., Wu, M.C.S., Chen, J.C., Huang, L.M., Song, X.Y., Jian, W.J., 2001. Shift from P to N limitation of phytoplankton growth across the Pearl River estuarine plume during summer. *Mar. Ecol. Prog. Ser.* 221, 17–28.
- Zapata, M., Rodríguez, F., Garrido, J.L., 2000. Separation of chlorophylls and carotenoids from marine phytoplankton: a new HPLC method using a reversed phase C8 column and pyridine-containing mobile phases. *Mar. Ecol. Prog. Ser.* 195, 29–45.
- Zhai, W., Dai, M., Cai, W.J., Wang, Y., Wang, Z., 2005. High partial pressure of CO<sub>2</sub> and its maintaining mechanism in a subtropical estuary: the Pearl River estuary, China. *Mar. Chem.* 93, 21–32.
- Zhang, X., Huang, X.P., Shi, Z., Ye, F., Liu, Q.X., 2013. Spatial and temporal variation of picophytoplankton in the Pearl River Estuary. *Acta Ecol. Sin.* 33 (7), 2200–2211, (in Chinese with English abstract).
- Zhang, X., Zhang, J.P., Huang, X.P., Huang, L.M., 2014. Phytoplankton assemblage structure shaped by key environmental variables in the Pearl River Estuary, South China. *J. Ocean Univ. China* 13 (1), 1–10.
- Zhao, H., 1990. *Evolution of the Pearl River Estuary*. Ocean Press, Beijing, (in Chinese).



ORIGINAL RESEARCH ARTICLE

# Distribution and invasiveness of a colonial ascidian, *Didemnum psammathodes*, along the southern Indian coastal water<sup>☆</sup>

H. Abdul Jaffar<sup>a,\*</sup>, A. Soban Akram<sup>a</sup>, M.L. Kaleem Arshan<sup>a</sup>,  
V. Sivakumar<sup>b</sup>, M. Tamilselvi<sup>c</sup>

<sup>a</sup> Department of Biotechnology, Islamiah College (Autonomous), Vaniyambadi, India

<sup>b</sup> Director of Research and Conservation, 4e India, NGO (Reg. No.: 188/2010), India

<sup>c</sup> Department of Zoology, V.V. Vanniaperumal College for Women, Virudhunagar, Tamilnadu, India

Received 28 March 2015; accepted 9 April 2016

Available online 28 April 2016

## KEYWORDS

Ascidians;  
Distribution;  
Invasion;  
South Indian coast;  
*Didemnum psammathodes*

**Summary** Ascidians are well known worldwide for their rapid invasions and also for the presence of potential biomedical molecules. Members of the family Didemnidae are widely distributed in tropical waters and they are reported to be among the families possessing rich bioactive compounds. *Didemnum psammathodes* has a cosmopolitan distribution in tropical waters. The growing evidence of multifarious potential and ever increasing invasion of this species accentuated the need for additional research into its diversity and distribution for sustainable utilization and conservation. The present study was intended to focus on distribution and invasiveness of colonial ascidian, *D. psammathodes*, along the southern Indian peninsular waters. The present data are based on our own observations made during 2012–2014 period and also on the published and unpublished records of the last 20 years. Out of 45 stations surveyed, *D. psammathodes* was encountered at a maximum of 41 stations and was found to be more abundant in Hare Island ( $n = 42$ ), North Break Water ( $n = 38$ ) and Vizhinjam bay ( $n = 32$ ). This species was

<sup>☆</sup> Financial support for this study was provided by the Department of Biotechnology, Ministry of Science and Technology, Government of India (grant number: BT/PR6801/AAQ/3/609/2012) to the principal investigator Dr. H. Abdul Jaffar Ali.

\* Corresponding author at: Department of Biotechnology, Islamiah College (Autonomous), Vaniyambadi 635752, India. Tel.: +91 9443528704; fax: +04174232619.

E-mail address: [jaffar.ascidian@gmail.com](mailto:jaffar.ascidian@gmail.com) (H. Abdul Jaffar).

Peer review under the responsibility of Institute of Oceanology of the Polish Academy of Sciences.



Production and hosting by Elsevier

<http://dx.doi.org/10.1016/j.oceano.2016.04.002>

0078-3234/© 2016 Institute of Oceanology of the Polish Academy of Sciences. Production and hosting by Elsevier Sp. z o.o. This is an open access article under the CC BY-NC-ND license (<http://creativecommons.org/licenses/by-nc-nd/4.0/>).

absent at four different stations. Catch per unit effort was higher (19.6) in Hare Island followed by NBW (16.0) and Vizhinjam bay (6.8). The highest number of colonies (136) was observed in calcareous stones, followed by embedded rocks (54) and molluscan shells (33). Hydrographical parameters showed no significant differences between the stations ( $p < 0.005$ ). It is concluded that *D. psammathodes* has the potential to invade most of the stations and its distribution was not influenced by hydrographical parameters rather than substrates.

© 2016 Institute of Oceanology of the Polish Academy of Sciences. Production and hosting by Elsevier Sp. z o.o. This is an open access article under the CC BY-NC-ND license (<http://creativecommons.org/licenses/by-nc-nd/4.0/>).

## 1. Introduction

Ascidians (also known as Tunicates) are a dominant and ever present group among benthic organisms in tropical and temperate regions (Goodbody, 1993; Hernandez-Zanuy and Carballo, 2001; Sahade et al., 1998). This group of animals have been acknowledged worldwide for the presence of potent secondary metabolites and rapid invasion. The colonial ascidian, *Didemnum vexillum*, first recorded in the 1980s along the coasts of North America was the first best example of an invasion and spreading. This species established a large population in numerous sites and overgrew many sessile plants and animals (Valentine et al., 2007), including other tunicates, resulting in considerable ecological and economic damage (Adams et al., 2011; Carman et al., 2010). The impact of non-indigenous ascidians on local species and habitats is currently being studied in several countries around the world (Bullard and Carman, 2009; Lambert and Lambert, 2003; Shenkar and Loya, 2009; Stachowicz et al., 2002a). On the other hand, ascidians have been proven to be a rich source of pharmacological compounds (Davidson, 1993; Haefner, 2003; Jain et al., 2008; Rinehart, 2000). Because of their high nutritive value of ascidians, some of them are used as food for man and feed for culturable species (Nanri et al., 1992; Nguyen, 2007; Randall, 1967; Tamilselvi and Abdul Jaffar Ali, 2013; Tapic Jopia and Toledo, 2007). Other ascidians have been used as flagship species for environmental monitoring (Abdul Jaffar Ali, 2004; Abdul Jaffar Ali et al., 2011, in press; Tamilselvi, 2008).

The increasing evidence of ascidians multifarious potential and their rapid invasion highlight the need for additional research of sustainable utilization, management and conservation of this group of animals. To date, limited studies have been carried out to report the invasive status of ascidians in Indian waters. Abdul Jaffar Ali et al. (2009) reported 34 non-indigenous ascidians from southern coast of the Indian peninsula and Tamilselvi et al. (2011) reported 22 non-indigenous ascidians from Thoothukudi coast of India. No study has been conducted on intercoastal spread of invasive ascidians. Such data are of great importance in terms of estimating the rate of invasion and possible effects on the native fauna in the natural environment.

Members of the family Didemnidae (class Ascidiacea, suborder Aplousobranchia) are widely distributed in tropical waters and are reported to possess chemically diverse novel compounds with potent biological activity (Carte, 1996; Davidson, 1993; Dunlap et al., 2011; Schmidt et al., 2013). This group has attracted increasing attention around the world for their potential invasion of marine communities.

Didemnids adapt to survive in a wide range of environmental variables (Bullard et al., 2007; Valentine et al., 2007). In recent past, interest in *Didemnum psammathodes* has heightened due to the presence of bioactive compounds with potent antibacterial and antifouling properties (Anand and Paterson, 2002; Ramasamy and Murugan, 2003; Sri Kumaran et al., 2011; Thakur, 2001).

In India, *D. psammathodes* was first documented along the Thoothukudi coast, by Renganathan (1981), and appeared in additional locations in Vizhinjam bay (Abdul Jaffar Ali and Sivakumar, 2007), Palk Bay (Karthikeyan et al., 2009) and the Gulf of Mannar (Meenakshi and Senthamarai, 2013). As with many species, the actual date of invasion is uncertain. The present study reveals the occurrence, distribution pattern, surface preference and intercoastal invasiveness of the colonial ascidian, *D. psammathodes*, along the southern Indian peninsula regions.

## 2. Material and methods

Studies were conducted during the 2012–2014 period covering all the seasons at 45 stations (Fig. 1) along the stretch of 110 km of southwest and 130 km of southeast coastlines of India. The survey was carried out on foot, via snorkelling and SCUBA diving in different habitats. Observations were made on different substrates available in the study areas. Description of each substrate is briefed below.

**Calcareous stones:** At stations 1, 6, 8, 9, 17, 18, 32, 34, 35, 36, 37, 38, 39 and 44, the calcareous stones of varying sizes ranging from 1 to 5 m<sup>3</sup> are laid down to break the sea water. These stones are considered here as artificial substrates. Observations were made on the undersides of the stones.

**Embedded rocks:** At stations 1, 5, 6, 13, 16, 17, 18, 22, 29 and 35, small to large boulders are embedded partially in shallow water regions and intertidal flats. The samplings were made at the submerged parts of the boulders.

**Mussel bed:** Stations 1, 2 and 3 are known for molluscan fishery. Molluscan beds of varying size are available at a depth of 10–15 m. Generally brown mussel, green mussel and some other bivalves are seasonally fished at these stations. Observations were made on shells of these molluscs via SCUBA diving.

**Hull of boat:** At harbour stations (1, 4, 33 and 42), the observations were made on a hull of a fishing boat and barges via snorkelling and SCUBA diving.

**Oyster cages:** At stations 1 and 33, oyster cages are installed at a depth of 4–5 m by the Central Marine

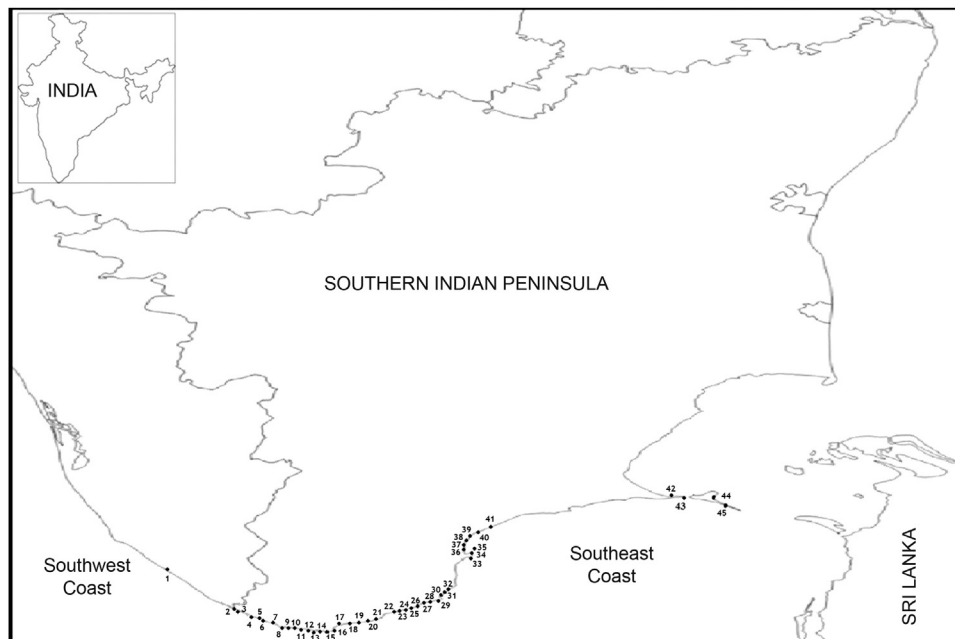


Figure 1 Map showing the study areas.

Fisheries Research Institute (CMFRI). The cages were observed for the presence of *D. psammathodes* during brushing.

**Cement blocks:** At stations 1, 4, 17, 33 and 42, harbour berths made of large sized cement blocks were sampled via snorkelling.

**Molluscan shells:** At stations 19, 30, 33 and 42, the samplings were made from broken and dead molluscan shells present in the shallow water region and intertidal flats.

**Coral pieces:** The stations 33 and 43 are known for coral reefs. Many dead coral pieces are found to occur in the shallow water and intertidal flats. They were also sampled.

**Sea weeds:** At station 40, large vegetation of sea weeds was observed for the occurrence of *D. psammathodes*.

All substrates (natural and artificial) at the surveyed sites were equally searched and when appropriate, small boulders and calcareous stones were overturned and examined. Since many ascidians have been trapped unintentionally during fishing at 15–20 m depth, fish landing centres were also visited to examine *D. psammathodes* from the fishing nets and trawl.

Hydrographic parameters such as temperature, salinity and pH were measured in situ using digital thermometer (Mextech), digital pH pen (Hanna-HI98107) and refractometer respectively. The dissolved oxygen in the water samples was measured using Water Quality Analyzer 301. Data of annual rainfall [mm] were obtained from meteorological departments of both states Tamilnadu and Kerala, India. Since search times differ at each site, the total number of *D. psammathodes* collected was standardized using catch per unit effort (CPUE). This measure was found by dividing the number of colonies observed by the number of person hours of search time (Mundo, 2009).

The data were analysed statistically by calculating mean and standard deviation for triplicates of the various

parameters investigated. Analysis of variance (one-way ANOVA) was used to evaluate the significance of differences between groups of measured parameters at different stations with the significance level set at  $p \leq 0.005$ .

### 3. Results

Occurrence and distribution of *D. psammathodes* on various substrates at different stations along the southern Indian coastal waters are represented in Table 1. In the present survey, a total of 316 colonies of *D. psammathodes* were observed along the southern Indian coastal waters at 45 stations.

The number of colonies ranged from 1 to 32 in southwest coast. Maximum number of colonies was observed at Vizhinjam bay ( $n = 32$ ) whereas no single colony was observed at Enayam. In southeast coast, *D. psammathodes* recruited majority of the stations (26) and the range varied between 2 and 42. The maximum number of colonies was observed at Hare Island ( $n = 42$ ), followed by the North Break Water (NBW) ( $n = 38$ ). *D. psammathodes* was absent in Thereapuram, Rameswaram and Dhanushkodi (Table 2).

Catch per unit effort (CPUE) for *D. psammathodes* ranged from 0.1 to 1.2 along the 18 stations of southwest coast and it was 6.8 at Vizhinjam bay. CPUE range was in between 0.1 and 4.4 along the 24 stations of southeast coast and it was higher (19.6) in Hare Island followed by NBW (16.0). CPUE was nil for four stations along the southwest and southeast coast of India.

Among the six available natural substrates in different stations encountered during the study, highest number of colonies (54) was recorded in embedded rocks followed by molluscan shells (33) and the low number of colonies was at sponges (11), whereas among the four artificial substrata, maximum number of colonies (136) was observed in calcareous stones followed by cement blocks (19), hull of boat (14) and oyster cages (9) (Fig. 2).

**Table 1** Occurrence and distribution of *Didemnum psammathodes* along the southern Indian coastal waters.

No.	Stations	Coordinates	Substrates	Occurrence	CM
<b>Southwest coast</b>					
1	Vizhinjam bay	8°22'55"N, 76°59'26"E	CS	x	HP
			ER	x	HP
			MB	x	SD
			HB	x	SN
			OC	x	SD
			CB	x	SN
2	Enayam	8°12'55.2"N, 77°11'31.9"E	MB	a	TC
3	Mel Midalam	8°12'45"N, 77°12'51"E	MB	x	TC
4	Colachel	8°8'17"N, 77°18'12.7"E	CB	x	HP
			HB	x	HP
5	Kadiyapattanam	8°8'4"N, 77°18'31"E	ER	x	HP
6	Muttom	8°8'17"N, 77°18'12.7"E	ER	x	HP
			CS	x	HP
7	Pillai Thoppu	8°7'38"N, 77°20'9"E	—	x	TC
8	Azhikkal	9°07'59.1"N, 76°27'44.3"E	CS	x	HP
9	Pozhikarai	8°6'26"N, 77°24'4"E	CS	x	HP
10	KesavanPuthenThurai	8°6'21"N, 77°24'34"E	—	x	TC
11	PuthenThurai	8°6'11"N, 77°25'4"E	—	x	TC
12	Sanguthurai	8°5'56.1"N, 77°25'26.7"E	—	x	TC
13	Pallam	8°5'58"N, 77°25'55"E	ER	x	HP
14	Mel Manakudi	8°5'29"N, 77°28'48"E	—	x	TC
15	Keel Manakudi	8°5'21"N, 77°29'22"E	—	x	TC
16	Kanyakumari	8°4'42.1"N, 77°33'5.4"E	ER	x	HP
17	China Muttom	8°5'47"N, 77°33'50"E	CS	x	HP
			ER	x	HP
			CB	x	HP
18	Leepuram	8°6'46"N, 77°33'19"E	ER	x	HP
			CS	x	HP
19	Arokiya Puram	8°7'9"N, 77°33'37"E	MS	x	HP
<b>Southeast coast</b>					
20	Kootapuli	8°8'50"N, 77°36'0"E	—	x	TC
21	Koodankulam	8°10'28"N, 77°42'19"E	—	x	TC
22	Uvari	8°16'40"N, 77°53'27"E	ER	x	HP
23	Kooduthalai	8°17'59"N, 77°55'37"E	—	x	TC
24	Periyathalai	8°20'7"N, 77°58'21"E	—	x	TC
25	Manapad	8°22'28"N, 78°3'34"E	—	x	TC
26	Kulasekharapatnam	8°24'1"N, 78°3'24"E	—	x	TC
27	Alanthalai	8°28'0"N, 78°5'58"E	—	x	TC
28	Amali Nagar	8°29'21"N, 78°7'22"E	—	x	TC
29	Tiruchendur	8°29'49"N, 78°7'32"E	ER	x	HP
30	Veerapandiapattanam	8°32'08.6"N, 78°7'17.0"E	MS	x	TC
31	Kayalpatnam	8°34'15"N, 78°7'15"E	—	x	TC
32	Punnakkayal	8°38'3"N, 78°6'50"E	CS	x	HP
33	Thoothukudi (Harbour)	8°45'14"N, 78°12'39"E	CS	x	HP
			HB	x	SD
			OC	x	SD
			CB	x	SD
			MS	x	HP
			CP	x	HP
34	North Break Water	8°46'24.3"N, 78°12'5.6"E	CS	x	HP

**Table 1** (Continued)

No.	Stations	Coordinates	Substrates	Occurrence	CM
35	Hare Island	8°46'36"N, 78°11'38"E	CS	x	HP
			ER	x	HP
36	Roch Park	8°48'59.3"N, 78°9'48.2"E	CS	x	HP
37	Inigo Nagar	8°47'22"N, 78°9'37"E	CS	x	HP
38	Collectors Bungalow	8°48'38"N, 78°9'53"E	CS	x	HP
39	Therespuram	8°48'59.3"N, 78°9'48.2"E	CS	a	HP
40	Vellapatti	9°7'7.6"N, 78°24'42.9"E	SW	x	HP
41	KeelaVaippar	8°59'54.8"N, 78°15'16.2"E	—	x	TC
42	Mandapam	9°17'29"N, 79°9'1.1"E	HB	x	HP
			CB	x	HP
43	Pamban	9°16'52.1"N, 79°11'53.5"E	MS	x	HP
			CP	x	HP
44	Rameswaram	9°17'2"N, 79°19'2"E	CS	a	HP
45	Dhanushkodi	9°12'42"N, 79°22'27"E	—	a	TC

Note: CM, collection method; CS, calcareous stones; ER, embedded Rocks; MB, mussel bed; HB, hull of boat; OC, oyster cages; CB, cement blocks; MS, molluscan shells; SW, sea weeds; CP, coral pieces; HP, hand picking; SD, SCUBA diving; SN, snorkelling; TC, trawl collection; x, present; a, absent.

**Table 2** Catch per unit effort (CPUE) per site.

S. no.	Stations	N	Time [min]	No. of person hours	Area [m <sup>2</sup> ]	CPUE
<b>Southwest coast</b>						
1	Vizhinjam bay	32	150	4.69	115	<b>6.8</b>
2	Enayam	0	30	0.00	60	0.0
3	Mel Midalam	6	30	5.00	60	1.2
4	Colachel	7	60	8.57	50	0.8
5	Kadiyapattanam	3	60	20.00	20	0.2
6	Muttom	7	80	11.43	70	0.6
7	Pillai Thoppu	2	30	15.00	—	0.1
8	Azhikkal	2	30	15.00	60	0.1
9	Pozhikarai	2	30	15.00	60	0.1
10	KesavanPuthenThurai	1	20	20.00	—	0.1
11	PuthenThurai	1	35	35.00	—	0.0
12	Sanguthurai	1	25	25.00	—	0.0
13	Pallam	2	50	25.00	65	0.1
14	Mel Manakudi	2	40	20.00	—	0.1
15	Keel Manakudi	2	25	12.50	—	0.2
16	Kanyakumari	5	60	12.00	60	0.4
17	China Muttom	12	120	10.00	75	1.2
18	Leepuram	5	30	6.00	80	0.8
19	Arokiya Puram	2	20	10.00	65	0.2
<b>Southeast coast</b>						
20	Kootapuli	4	40	10.00	—	0.4
21	Koodankulam	4	25	6.25	—	0.6
22	Uvari	6	60	10.00	80	0.6
23	Kooduthalai	2	30	15.00	—	0.1
24	Periyathalai	3	30	10.00	—	0.3
25	Manapad	3	60	20.00	—	0.2
26	Kulasekharapatnam	7	60	8.57	—	0.8
27	Alanthalai	7	30	4.29	—	1.6
28	Amali Nagar	5	30	6.00	—	0.8
29	Tiruchendur	12	90	7.50	80	1.6
30	Veerapandiapattanam	6	40	6.67	60	0.9
31	Kayalpatnam	3	30	10.00	—	0.3

Table 2 (Continued)

S. no.	Stations	N	Time [min]	No. of person hours	Area [m <sup>2</sup> ]	CPUE
32	Punnakkayal	5	40	8.00	85	0.6
33	Thoothukudi (Harbour)	20	90	4.50	225	4.4
34	North Break Water	38	90	2.37	120	<b>16.0</b>
35	Hare Island	42	90	2.14	160	<b>19.6</b>
36	Roch Park	10	60	6.00	70	1.7
37	Inigo Nagar	9	60	6.67	70	1.4
38	Collectors Bungalow	10	60	6.00	70	1.7
39	Therespuram	0	30	0.00	60	0.0
40	Vellapatti	4	40	10.00	80	0.4
41	KeelaVaippar	4	30	7.50	—	0.5
42	Mandapam	12	90	7.50	180	1.6
43	Pamban	6	40	6.67	120	0.9
44	Rameswaram	0	30	0.00	120	0.0
45	Dhanushkodi	0	30	0.00	—	0.0

Bold values signify the study areas Hare Island, North Break Water and Vizhinjam Bay recruited significantly higher number of colonies of *Didemnum psammathodes* species.

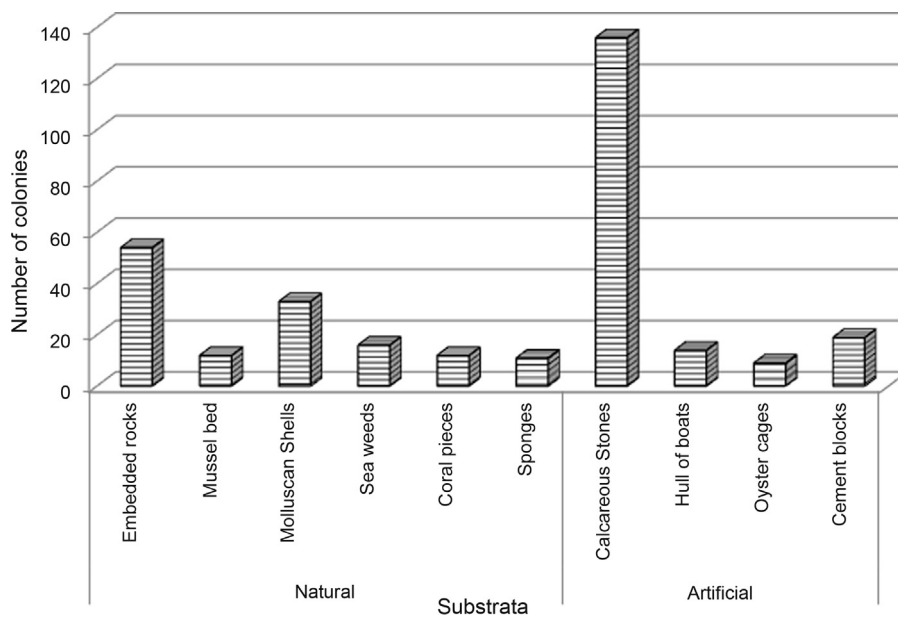


Figure 2 Number of colonies of *Didemnum psammathodes* observed on the various substrata.

Hydrographical parameters and number of colonies of *D. psammathodes* of southeast and southwest coasts of India are represented in Table 3. Temperature, salinity, dissolved oxygen and pH of the stations along the southwest coast ranged from 26.2 to 27.4°C, 30.1 to 31 ppt, 4.2 to 4.5 ml L<sup>-1</sup> and 7.2 to 7.6 respectively whereas, in the southeast coast the values ranged from 30.4 to 31°C, 34.1 to 35.2 ppt, 4.1 to 4.3 ml L<sup>-1</sup> and 7.7 to 7.9. Statistical analysis (one-way ANOVA) of these four parameters showed no significant differences between the different sites ( $p < 0.005$ ).

#### 4. Discussion

In the present survey, occurrence and distribution of *D. psammathodes* were investigated along the Arabian Sea, Indian Ocean and the Bay of Bengal. The maximum number of colonies was recorded at the southeast coast of

India. It could be correlated with the availability of structures, both natural (embedded rocks, seaweed, mussel bed, coral pieces, etc.) and man-made as well (stones, cement blocks, hulls of boat, oyster cages, etc.) (Fig. 2) which might have influenced the settlement of the ascidian.

The study on station-wise abundance of *D. psammathodes* revealed maximum record at Vizhinjam bay and Hare Island along the southwest and southeast coasts respectively. This could be attributed to the fact that these two stations are provided with numerous small-embedded rocks and loosely bound stones. Moreover, these stations experience very calm and low wave action, which facilitates *D. psammathodes* to encrust the substrata nearby. Colonies of *D. psammathodes* are found either single or in clumps (2–5 colonies), and sometimes as a very large mat. They are more commonly available in the immediate-sublittoral zone at approximately 1 m depth. In their natural habitat, majority of the colonies are located underneath stones and crevices of embedded

**Table 3** Hydrographical parameters of various stations along the southeast and southwest coast of India.

Stations	Temperature [°C]	Salinity [ppt]	DO [ml L <sup>-1</sup> ]	pH	N
Vizhinjam bay	27.0	30.7	4.4	7.6	32
Enayam	27.3	30.5	4.2	7.6	0
Mel Midalam	27.3	30.5	4.2	7.6	6
Colachel	27.4	30.1	4.3	7.6	7
Kadiyapattanam	27.0	31.0	4.5	7.6	3
Muttom	26.2	30.8	4.4	7.3	7
Pillai Thoppu	27.0	30.5	4.3	7.3	2
Azhikkal	27.0	30.5	4.3	7.3	2
Pozhikarai	27.0	30.5	4.3	7.3	2
KesavanPuthenThurai	27.0	30.5	4.3	7.3	1
PuthenThurai	27.0	30.5	4.3	7.3	1
Sanguthurai	27.0	30.5	4.3	7.4	1
Pallam	27.0	30.5	4.3	7.4	2
Mel Manakudi	26.8	30.5	4.3	7.2	2
Keel Manakudi	26.8	30.5	4.3	7.2	2
Kanyakumari	26.8	30.5	4.3	7.2	5
China Muttom	26.8	30.5	4.3	7.2	12
Leepuram	26.7	30.7	4.3	7.2	5
Arokiya Puram	26.7	30.7	4.3	7.2	2
Kootapuli	30.4	34.6	4.2	7.8	4
Koodankulam	31.0	35.2	4.3	7.9	4
Uvari	30.5	34.2	4.2	7.8	6
Kooduthalai	30.5	34.2	4.2	7.8	2
Periyathalai	30.5	34.2	4.2	7.8	3
Manapad	30.5	34.2	4.2	7.8	3
Kulasekharapatnam	30.5	34.2	4.2	7.8	7
Alanthalai	30.5	34.2	4.2	7.8	7
Amali Nagar	30.5	34.2	4.2	7.8	5
Tiruchendur	30.8	34.5	4.2	7.8	12
Veerapandiapattanam	30.8	34.5	4.2	7.8	6
Kayalpatnam	30.8	34.5	4.2	7.8	3
Punnakkayal	30.8	34.5	4.2	7.9	5
Thoothukudi (Harbour)	30.5	34.2	4.3	7.9	20
North Break Water	30.5	34.2	4.3	7.7	38
Hare Island	30.5	34.2	4.3	7.8	42
Roch Park	30.5	34.2	4.3	7.8	10
Inigo Nagar	30.5	34.2	4.3	7.8	9
Collectors Bungalow	30.5	34.2	4.3	7.8	10
Therespuram	30.5	34.2	4.3	7.8	0
Vellapatti	30.5	34.2	4.3	7.8	4
KeelaVaippar	30.5	34.2	4.3	7.8	4
Mandapam	30.2	34.1	4.1	7.8	12
Pamban	30.2	34.1	4.1	7.8	6
Rameswaram	30.2	34.1	4.1	7.7	0
Dhanushkodi	30.2	34.1	4.1	7.7	0
<b>Mean</b>	<b>29.0</b>	<b>32.7</b>	<b>4.3</b>	<b>7.6</b>	<b>7.0</b>

rocks. Shaded areas such as rock crevices and undersides tend to be favourable habitats for ascidians (Young and Chia, 1984). Ascidian larvae response to phototactic negative effect contributes to recruitment into these habitats (Svane and Dolmer, 1995; Svane and Young, 1989; Young and Chia, 1984).

Out of 45 stations, 16 stations, including Dhanushkodi, Enayam, Therespuram and Rameswaram, are sandy in nature and devoid of any substrata. In these stations, the sampling of

*D. psammathodes* was done by examining the fishing nets used for catching fishes from deep sea up to the depth of 15–20 m. The present observation confirmed the reports of Young (1989) and Tamilselvi et al. (2012) who reported that habitat stability is an important criterion for survivorship of an organism and sand movement adversely affects the settlement of its larvae.

Because of the uncertainty concerning the origin of this species, its status as non-indigenous species remains unclear.

Various levels of evidence suggest that this species is categorized into cryptogenic species (Abdul Jaffar Ali et al., 2009; Carlton, 1996). Since worldwide shipping facilitates the exotic species to invade the ports of various countries such as Japan, Malaysia, Indonesia, New Zealand, New South Wales (Central E coast), Queensland (Central E coast, Great Barrier Reef, NE coast), Victoria (Bass Strait), the western Indian Ocean, the Red Sea and India (Cariton and Geller, 1993; Hewitt et al., 2004; Monniot and Monniot, 1991, 1994), the invasiveness of this species into the Indian water could also be substantiated. In the previous report, this species was categorized as cryptogenic but based on the present observation, this species can be categorized as established cryptogenic based on various criteria proposed by Carlton (1996).

The occurrence of *D. psammathodes* was more common in harbour area, followed by fish landing centre nearby. This might be due to the connectivity of the ports, movement of ships and also the release of ballast water at the ports. Furthermore, the large number of boats with fouled hulls, especially fishing vessels that move from one harbour to another undoubtedly provide new breeding stock to recolonize the denuded surfaces and also enhance gene flow of *D. psammathodes* populations between the harbours. The increasing invasiveness of this species proved beyond doubt that the heavy traffic of fishing vessels and ship movements interlinking all the major ports and fishing harbours of southern India could probably pave the way for invasion of this non-native ascidian. Kott (2002), Abdul Jaffar Ali (2004) and Tamilselvi et al. (2011) reported that provisions of maritime and other installations associated with commercial harbour could have facilitated the settlement of ascidians species.

In the present study, hydrographical parameters in the southeast and southwest coasts of India showed slight variations but did not show any significant correlation with the number of colonies of *D. psammathodes*. On the contrary, the role of temperature in influencing *Didemnum* recruitment was suggested by Stachowicz et al. (2002b). Carlton (2000) recorded that the given temperature and species composition significantly impacted temperate subtidal communities and cumulative impact of these factors may facilitate the future invasion. As adult ascidians are sedentary in nature, its abundance and distribution of species are highly influenced by the larval behaviour rather than physical disturbance, predation and competition (Svane and Young, 1989). Along with these factors, the substrate features also determine the composition of ascidians (Tamilselvi and Abdul Jaffar Ali, 2013).

Worldwide distribution of *D. psammathodes* is often explained by its high dispersive capability and also by certain aspects of their life cycle including motility of larval, budding, colony fragmentation, etc. The short-lived larvae released from a colony facilitate the dispersal of the species over short distances. The larvae also settle close to the parental colony (Tamilselvi et al., 2011; Yund and Stires, 2002). The present survey also revealed the rapid invasion and spread of *D. psammathodes* along the southern Indian coastal waters. The distribution and abundance of *D. psammathodes* are determined by availability of diverse substrates, heavy traffic and intercoastal movement of ships and fishing vessels and also life-history traits.

Since the search time differs at each site, the total number of *D. psammathodes* collected was standardized

using catch per unit effort (CPUE). Higher CPUE at Hare Island and NBW could possibly occur because this species formed the colonies at undersides of loosely bound and embedded rocks close to surface of the water and collection did not take as long compared to searching underneath boulders and rock crevices in Muttom, Kadiyapattanam and Kanyakumari regions of Tamilnadu, India.

To conclude, *D. psammathodes* has strong potential to invade most of the stations along southern Indian coastal waters at a significantly greater rate and its distribution is not influenced by hydrographical parameters but by substrates. Owing to ever changing coastal diversity and topography of the collection spots, a special attention should be given to the biofoulers such as ascidians. This study will definitely be very helpful for researchers, coastal planners, port authorities, coastal thermal plants and atomic power plants in proper management. Since there is no concrete solution to prevent and/or eradicate bioinvasion, *D. psammathodes* can be better utilized in a positive way by preparing supplementary feed for culturable organisms and to isolate the novel lead molecules as reported by earlier studies.

## Acknowledgements

We would like to express our deep gratitude to Mr. L.M. Muneer Ahmed, B.Sc., Secretary and Dr. K. Prem Nazeer, Principal of Islamiah College (Autonomous), Vaniyambadi, Tamilnadu, India for their generous support and providing a great research environment.

## References

- Abdul Jaffar Ali, H., 2004. Comparative study on ecology of *Phallusia nigra* Savigny 1816 from Tuticorin (southeast coast) and Vizhinjam (southwest coast). (Ph.D. thesis). Manonmaniam Sundaranar Univ., Tirunelveli.
- Abdul Jaffar Ali, H.A., Sivakumar, V., 2007. Occurrence and distribution of ascidians in Vizhinjam bay (southwest coast of India). *J. Exp. Mar. Biol. Ecol.* 342 (1), 189–190.
- Abdul Jaffar Ali, H.A., Sivakumar, V., Tamilselvi, M., 2009. Distribution of alien and cryptogenic ascidians along the southern coasts of Indian peninsula. *World J. Fish Mar. Sci.* 1 (4), 305–312.
- Abdul Jaffar Ali, H., Tamilselvi, M., Sivakumar, V. Non-indigenous ascidians in V.O. Chidambaram port, Thoothukudi, India. *Indian J. Geo-Mar. Sci.* in press.
- Abdul Jaffar Ali, H., Tamilselvi, M., Sivakumar, V., Zaman, G.M.H., Muthu Mohamed, H.S., 2011. Marine ascidian biodiversity – a promising resource for bioactive compounds. *Suppl. Adv. Biotech.* 10 (10), 26–32.
- Adams, C.M., Shumway, S.E., Whitlatch, R.B., Getchis, T., 2011. Biofouling in marine molluscan shellfish aquaculture: a survey assessing the business and economic implications of mitigation. *J. World Aquac. Soc.* 42 (2), 242–252.
- Anand, T., Paterson, J.K., 2002. Antimicrobial activity in the tissue extracts of five species of *Cypraea* spp. (Mollusca: Gastropoda) and an ascidian *Didemnum psammathodes* (Tunicata: Didemnidae). *Indian J. Mar. Sci.* 31 (3), 239–242.
- Bullard, S.G., Carman, M.R., 2009. Current Trends in Invasive Ascidian Research. *Invasive Species: Detection, Impact and Control.* Nova Sci. Publ., New York, 217 pp.
- Bullard, S.G., Lambert, G., Carman, M.R., Byrnes, J., Whitlatch, R. B., Ruiz, G., Miller, R.J., Harris, L., Valentine, P.C., Collie, J.S., Pederson, J., McNaught, D.C., Cohen, A.N., Asch, R.G., Dijkstra, J., Heinonen, K., 2007. The colonial ascidian *Didemnum* sp. A:

- current distribution, basic biology and potential threat to marine communities of the northeast and west coasts of North America. *J. Exp. Mar. Biol. Ecol.* 342 (1), 99–108.
- Cariton, J.T., Geller, J.B., 1993. Ecological roulette: the global transport of nonindigenous marine organisms. *Science* 261 (5117), 78–82.
- Carlton, J.T., 1996. Pattern, process, and prediction in marine invasion ecology. *Biol. Conserv.* 78 (1–2), 97–106.
- Carlton, J.T., 2000. Global change and biological invasions in the oceans. In: Hobbs, R.J., Mooney, H.A. (Eds.), *Invasive Species in a Changing World*. Island Press, Covelo, CA, 31–53.
- Carman, M.R., Morris, J.A., Karney, R.C., Grunden, D.W., 2010. An initial assessment of indigenous and invasive tunicates in shellfish aquaculture of the North American east coast. *J. Appl. Ichthyol.* 26 (S2), 8–11.
- Carte, B.K., 1996. Biomedical potential of marine natural products. *Bioscience* 46 (4), 271–286.
- Davidson, B.S., 1993. Ascidians: producers of amino acid derived metabolites. *Chem. Rev.* 93 (5), 1771–1791.
- Dunlap, W.C., Long, P.F., Jaspars, M., 2011. Biomedicinals from the microbial metagenomes of marine invertebrates. In: de Bruijn, F. J. (Ed.), *Handbook of Molecular Microbial Ecology*, vol. II: Metagenomics in Different Habitats. Wiley Blackwell, Hoboken, New Jersey, pp. 517–544.
- Goodbody, I., 1993. The ascidian fauna of a Jamaican lagoon: thirty years of change. *Rev. Biol. Trop.* 41 (10), 35–38.
- Haefner, B., 2003. Drugs from the deep: marine natural products as drug candidates. *Drug Discov. Today* 8 (12), 536–544.
- Hernandez-Zanuy, A.C., Carballo, A.C., 2001. Distribution and abundance of ascidian assemblages in Caribbean reef zones of the Golfo de Batabano (Cuba). *Coral Reefs* 20 (2), 159–162.
- Hewitt, C.L., Willing, J., Bauckham, A., Cassidy, A.M., Cox, C.M.S., Jones, L., Wotton, D.M., 2004. New Zealand marine biosecurity: delivering outcomes in a fluid environment. *New Zeal. J. Mar. Freshw. Res.* 38 (3), 429–438.
- Jain, R., Sonawane, S., Mandrekar, N., 2008. Marine organisms: potential source for drug discovery. *Curr. Sci. India* 94 (3), 292 pp.
- Karthikeyan, M.M., Ananthan, G., Balasubramanian, T., 2009. Antimicrobial activity of crude extracts of some ascidians (Urochordata: Ascidiacea), from Palk Strait (Southeast Coast of India). *World J. Fish Mar. Sci.* 1 (4), 262–267.
- Kott, P., 2002. A complex didemnid ascidian from Whangamat, New Zealand. *J. Mar. Biol. Assoc. UK* 82 (4), 62–628.
- Lambert, C.C., Lambert, G., 2003. Persistence and differential distribution of nonindigenous ascidians in harbours of the Southern California Bight. *Mar. Ecol. Prog. Ser.* 259, 145–161.
- Meenakshi, V.K., Senthamarai, S., 2013. Diversity of ascidians from the Gulf of Mannar. In: Venkataraman, K., Sivaperuman, C., Raghunathan, C. (Eds.), *Ecology and Conservation of Tropical Marine Faunal Communities*. Springer, Berlin, Heidelberg, 213–229.
- Monniot, C., Monniot, F., 1991. Discovery of a new lineage among the deep sea ascidians: a carnivorous Ascidiidae. *C. R. Acad. Sci. Ser. III* 312 (8), 383–388.
- Monniot, C., Monniot, F., 1994. Additions to the inventory of eastern tropical Atlantic ascidians: arrival of cosmopolitan species. *Bull. Mar. Sci.* 54 (1), 71–93.
- Mundo, G.M., 2009. Phylogenetic and phylogeographic study of the New Zealand endemic sea tunicate *Cnemidocarpa nisiotis*. (Master thesis). School Biol. Sci., Univ. Canterbury, Christchurch, New Zealand, 136 pp.
- Nanri, K., Ogawa, J., Nishikawa, T., 1992. Tunic of a pyurid ascidian *Microcosmus hartmeyeri* Oka is eaten locally in Japan. *Nanki Seibutu* 34 (2), 135 pp.
- Nguyen, T.T.T., 2007. Aquaculture of sea-pineapple, *Halocynthia roretzi* in Japan. *Aquac. Asia* XII (2), 21–23.
- Ramasamy, M., Murugan, A., 2003. Chemical defense in ascidians *Eudistoma viride* and *Didemnum psammathodes* in Tuticorin, southeast coast of India: bacterial epibiosis and fouling deterrent activity. *Indian J. Mar. Sci.* 32 (4), 337–339.
- Randall, J.E., 1967. Food habits of reef fishes of the West Indies. *Stud. Trop. Oceanogr.* 5, 665–847.
- Renganathan, T.K., 1981. On the occurrence of colonial ascidian, *Didemnum psammathodes* (Sluiter, 1985) from India. *Curr. Sci. India* 50 (20), 922 pp.
- Rinehart, K.L., 2000. Antitumour compounds from tunicates. *Med. Res. Rev.* 20 (1), 1–27.
- Sahade, R., Tatian, M., Kowalke, J., Kuhne, S., Esna, G.B., 1998. Benthic faunal associations on soft substrates at Potter Cove, King George Island, Antarctica. *Polar Biol.* 19 (2), 85–91.
- Schmidt, E.W., Donia, M.S., McIntosh, J.A., Fricke, W.F., Ravel, J., 2013. Origin and variation of tunicate secondary metabolites. *J. Nat. Prod.* 75 (2), 295–304.
- Shenkar, N., Loya, Y., 2009. Non-indigenous ascidians (Chordata: Tunicata) along the Mediterranean coast of Israel. *Mar. Biodivers. Rec.* 2 (e166), 1–7.
- Sri Kumaran, N., Bragadeeswaran, S., Meenakshi, V.K., 2011. Evaluation of antibacterial activity of crude extracts of ascidian *Didemnum psammathodes* Sluiter, 1895 against isolated human and fish pathogens. *Asian Pac. J. Trop. Biomed.* 1 (1), S90–S99.
- Stachowicz, J.J., Fried, H., Osman, R.W., Whitlatch, R.B., 2002a. Biodiversity, invasion resistance, and marine ecosystem function: reconciling pattern and process. *Ecology* 83 (9), 2575–2590.
- Stachowicz, J.J., Terwin, J.R., Whitlatch, R.B., Osman, R.W., 2002b. Linking climate change and biological invasions: ocean warming facilitates nonindigenous species invasions. *Proc. Natl. Acad. Sci. U.S.A.* 99 (24), 15497–15500.
- Svane, I., Dolmer, P., 1995. Perception of light at settlement: a comparative study of two invertebrate larvae, a *Scyphozoa* planula and a simple ascidian tadpole. *J. Exp. Mar. Biol. Ecol.* 187 (1), 51–61.
- Svane, I., Young, C.M., 1989. The ecology and behaviour of ascidian larvae. *Oceanogr. Mar. Biol. Annu. Rev.* 27, 45–90.
- Tamilselvi, M., 2008. Ecological studies on ascidians of Tuticorin coast. (Ph.D. thesis). Manonmaniam Sundaranar Univ., Tirunelveli, India.
- Tamilselvi, M., Abdul Jaffar Ali, H., 2013. Exploration of untapped resource of ascidians along the Thoothukudi coast of India. *Mult. Res. J. VVV. Coll.* 1 (1), 139–145.
- Tamilselvi, M., Sivakumar, V., Abdul Jaffar Ali, H., Thilaga, R.D., 2011. Distribution of alien tunicates (Ascidians) in Tuticorin coast, India. *World J. Zool.* 6 (2), 164–172.
- Tamilselvi, M., Sivakumar, V., Abdul Jaffar Ali, H., Thilaga, R.D., 2012. Diversity and seasonal variations of class Ascidiacea in Thoothukudi coast, India. *Int. J. Environ. Sci.* 3 (3), 1097–1105.
- Tapic Jopia, C., Toledo, N.B., 2007. *Pesqueria de Pyura chilensis* (Molina 1782) (Tunicata, Ascidiacea, Pyuridae). *Investigacion situacion pesquerias bentonicas 2006*. Instit. Fomento Pesquero (IFOP). Valparaíso 66 pp., (in Spanish).
- Thakur, N.L., 2001. Studies on some bioactivity aspects of selected marine organisms. (Ph.D. thesis). Goa Univ., Goa.
- Valentine, P.C., Carman, M.R., Blackwood, D.S., Hefferon, E.J., 2007. Ecological observations on the colonial ascidian *Didemnum* sp. in a New England tide pool. *J. Exp. Mar. Biol. Ecol.* 342 (1), 109–122.
- Young, C.M., 1989. Distribution and dynamics of an intertidal ascidian pseudopopulation. *Bull. Mar. Sci.* 45 (2), 288–303.
- Young, C.M., Chia, F.S., 1984. Microhabitat-associated variability in survival and growth of subtidal solitary ascidians during the first 21 days after settlement. *Mar. Biol.* 81 (1), 61–68.
- Yund, P.O., Stires, A., 2002. Spatial variation in population dynamics in a colonial ascidian (*Botryllus schlosseri*). *Mar. Biol.* 141 (5), 955–963.



Available online at [www.sciencedirect.com](http://www.sciencedirect.com)

ScienceDirect

journal homepage: [www.elsevier.com/locate/oceano](http://www.elsevier.com/locate/oceano)



ORIGINAL RESEARCH ARTICLE

# Determination of antibiotic residues in southern Baltic Sea sediments using tandem solid-phase extraction and liquid chromatography coupled with tandem mass spectrometry

Grzegorz Siedlewicz<sup>a,\*</sup>, Marta Borecka<sup>b</sup>, Anna Białk-Bielińska<sup>b</sup>, Kinga Sikora<sup>c</sup>, Piotr Stepnowski<sup>b</sup>, Ksenia Pazdro<sup>a</sup>

<sup>a</sup> Department of Marine Chemistry and Biochemistry, Institute of Oceanology, Polish Academy of Sciences, Sopot, Poland

<sup>b</sup> Department of Environmental Analysis, Faculty of Chemistry, University of Gdańsk, Gdańsk, Poland

<sup>c</sup> Physicochemical Laboratories, Faculty of Chemistry, University of Gdańsk, Gdańsk, Poland

Received 14 January 2016; accepted 22 April 2016

Available online 7 May 2016

## KEYWORDS

Antibiotic residues;  
Sediments;  
SPE;  
LC–MS/MS;  
Baltic Sea

**Summary** The main objective of this study was to adapt analytical procedures for determining antibiotic residues in solid and aquatic samples to marine sediments and to investigate the occurrence of 9 sulfonamides, trimethoprim and 2 quinolones in southern Baltic Sea sediments. The analytical procedure was applied to sediment samples characterized as sand and silty sand. The validation results showed that a sensitive and efficient method applying tandem solid-phase extraction (SPE) and liquid chromatography coupled with tandem mass spectrometry (LC–MS/MS) was obtained. Analytes were determined in the lower  $\text{ng g}^{-1}$  range with good accuracy and precision. The proposed analytical procedure was applied to the analysis of 13 sediment samples collected from the Baltic Sea along the Polish coast. Concentrations of antibiotic residues in environmental samples were calculated based on external matrix-matched calibration. Residues of nine out of twelve of the above antibiotics were detected in sediment samples in a concentrations of up to  $419.2 \text{ ng g}^{-1}$  d.w. (dry weight). Sulfamethoxazole and sulfachloropyridazine were the most frequently detected compounds (58% of the analyzed samples). The

\* Corresponding author at: Department of Marine Chemistry and Biochemistry, Institute of Oceanology, Polish Academy of Sciences, ul. Powstańców Warszawy 55, 81-712 Sopot, Poland. Tel.: +48 587311938; fax: +48 585512130.

E-mail address: [gsiedlewicz@iopan.gda.pl](mailto:gsiedlewicz@iopan.gda.pl) (G. Siedlewicz).

Peer review under the responsibility of Institute of Oceanology of the Polish Academy of Sciences.



Production and hosting by Elsevier

<http://dx.doi.org/10.1016/j.oceano.2016.04.005>

0078-3234/© 2016 Institute of Oceanology of the Polish Academy of Sciences. Production and hosting by Elsevier Sp. z o.o. This is an open access article under the CC BY-NC-ND license (<http://creativecommons.org/licenses/by-nc-nd/4.0/>).

occurrence frequency of trimethoprim was 42% and it was always detected simultaneously with sulfamethoxazole. Preliminary studies on the spatial distribution of the analyzed antibiotics indicate a high level of antibiotics occurring in the Pomeranian Bay and close to the mouths of Polish rivers. The study is the first one to demonstrate the occurrence of antibiotic residues in sediments of the Polish coastal area. The obtained results suggest that sediment can be an important secondary source of antibiotic residues in the marine environment.

© 2016 Institute of Oceanology of the Polish Academy of Sciences. Production and hosting by Elsevier Sp. z o.o. This is an open access article under the CC BY-NC-ND license (<http://creativecommons.org/licenses/by-nc-nd/4.0/>).

## 1. Introduction

At the end of the second half of the twentieth century scientists started to treat pharmaceutical residues as environmental contaminants (Daughton and Ternes, 1999; Hirsch et al., 1999). The development and common use of sensitive analytical instruments like liquid or gas chromatographs coupled with mass spectrometers allowed the detection of trace concentrations of these compounds in different environmental matrices (Kot-Wasik et al., 2007; Mutavdžić-Pavlović et al., 2007). Special attention should be paid to antibiotic residues. In 2002, Wise estimated the world use of antibiotics at between 100 and 200 thousand tonnes per year. According to data published by Boeckel et al. (2014), global consumption of antibiotic drugs increased by 36% between 2000 and 2010. The main sources of antibiotics in the environment are animal farms, agriculture, and urban, municipal and hospital wastewaters (Boxall, 2008a; Hörsing et al., 2011; Kümmerer, 2008a; Łuczkiwicz et al., 2013; Minh et al., 2009; Sarmah et al., 2006). These bioactive compounds have only been detected in low concentrations in environmental samples, nonetheless, given their important, continuous input and only partial degradation, they are considered as 'pseudo-persistent' pollutants (Khetan and Collins, 2007). Prolonged exposure of organisms to antibiotic residues may strongly affect bacterial populations and induce biological effects in non-target organisms, potentially disrupting ecosystem processes (Arnold et al., 2014; Capone et al., 1996; González-Pleiter et al., 2013; Halling-Sørensen et al., 1998; Kotlarska et al., 2015; Kümmerer, 2008b; Molander et al., 2009; Nikolaou et al., 2007). Therefore, it has become of great importance to evaluate concentration levels of antibiotic residues and to understand their environmental fate.

Many studies have demonstrated that antibiotic residues are widespread in treated wastewaters, soils, groundwaters, river and lake water and sediments (Boxall et al., 2002; Kemper, 2008; Li et al., 2012; Sacher et al., 2001; Vazquez-Roig et al., 2012; Yang et al., 2010). The availability of data on antibiotic concentrations and their ecotoxicological properties in marine waters is still limited, while seas can be seen as the final sink of the most persistent antibiotic residues (Chen and Zhou, 2014; Claessens et al., 2013; McEneff et al., 2014). Once discharged into coastal waters, antimicrobial residues, like other contaminants, can undergo biotic and abiotic transformations (including degradation), sorb to suspended particulate matter and sediment, or accumulate in the tissues of organisms (Gaw et al., 2014; Ramirez et al., 2009). The fate of antibiotic residues varies depending on the physicochemical properties of compounds and

matrices, in addition to environmental parameters also playing an important role. Freshwater and marine ecosystems differ significantly in terms of physicochemical conditions e.g. salinity, pH and organic matter content. Therefore, the conclusions generated for freshwater ecosystems on the environmental fate of antibiotics may not necessarily be transferable to marine environments (Weigel et al., 2002). The mobility of compounds greatly depends on water solubility, the octanol–water partitioning coefficient, and  $pK_a$  values governed by their chemical structure. Antibiotics are mostly hydrophilic compounds and should be present with relatively high frequency and concentrations in marine waters. This statement can be confirmed by several studies reporting the presence of these emerging contaminants in seawater (Borecka et al., 2013, 2015; Na et al., 2011; Nödler et al., 2014; Wille et al., 2010; Zhang et al., 2013). However, Bu et al. (2013) suggest that antibiotics could also accumulate in sediments, which could thus serve as a sink and secondary source of antibiotics in the aquatic environment. Several complex processes can be involved in the sorption mechanism of antibiotics in sediments. These comprise not only hydrophobicity but also cation bridging, cation exchange, hydrogen bonding and surface complexation (Kim and Carlson, 2005). All these factors may play important roles in retaining antibiotic residues on a sediment matrix. The sorption of antibiotics like sulfonamides is also governed by the property to ionize numerous compounds from this class depending on the pH of a medium. The  $\log K_{ow}$  coefficients of ionizing compounds change considerably in a pH range around the  $pK_a$  (Mutavdžić-Pavlović et al., 2012).

According to data published by Gaw et al. (2014) and Pazdro et al. (2016), until now only around twenty studies have evaluated the presence of antibiotics residues in marine sediments. Their presence has been reported in some coastal regions of the Pacific (mainly in China) and Atlantic Ocean (Beretta et al., 2014; Lara-Martín et al., 2014; Moreno-González et al., 2015; Na et al., 2013; Shi et al., 2014; Stewart et al., 2014; Yang et al., 2010; Yang et al., 2011; Zhou et al., 2011). As shown above, the information about spatial and seasonal distribution of antibiotic residues concentrations in many coastal areas is still very limited. This is particularly true for the Baltic Sea, a shallow inland sea with a large catchment area. There are only a few publications concerning the occurrence of pharmaceuticals in the Baltic Sea region and these are limited to water and fish (Beck et al., 2005; Borecka et al., 2013, 2015; HELCOM, 2010; Nödler et al., 2014). Borecka et al. (2013, 2015) reported the presence of antimicrobials from the sulfonamide and quinolone groups as well as trimethoprim, at concentrations

of up to  $\text{ng L}^{-1}$  in southern Baltic Sea waters. Apart from our preliminary study reporting the detection of hydrophilic antibiotics from the tetracyclines class in sediments from the Gulf of Gdańsk (Siedlewicz et al., 2014), to our knowledge, no study has been performed with regard to antibiotic residues in the sediments of the Baltic Sea.

The small amount of data available for marine sediments is also caused by the fact that the analysis of such a complex matrix is a very demanding task. The number of papers on the analytical methods of antibiotics residues determination in solid matrices is significant, but there is still a need for improvements in analytical procedures, aiming at reliable identification and quantification of these compounds in marine sediments (Białk-Bielińska et al., 2016). Moreover, the simultaneous analysis of compounds with quite different physicochemical properties in complex solid matrices like marine sediments also poses several problems (Mutavdžić-Pavlović et al., 2012).

The main objectives of the study were: (1) to adapt existing analytical extraction procedures for determining antibiotic residues concentrations in solid and aquatic samples to the analysis of Baltic sediments (Babić et al., 2006; Majka, 2010) and (2) to perform, by applying adapted, validated methods, preliminary studies on the concentration levels and spatial distribution of nine sulfonamides, trimethoprim and two quinolones in sediments from the southern Baltic Sea. The choice of target antibiotics was made due to their vast production and consumption worldwide (Dzierżawski and Cybulski, 2012; Kümmerer, 2008c; Sarmah et al., 2006). The target compounds represent a variety of structures and are characterized by different physicochemical properties (e.g. water solubility,  $\text{pK}_a$  values, hydrolytic stability) (Mutavdžić-Pavlović et al., 2012). Moreover their presence in southern Baltic surface waters has been observed (Borecka et al., 2013, 2015).

## 2. Material and methods

### 2.1. Chemicals and materials

Sulfathiazole (ST), sulfapyridine (SP), sulfamerazine (SRZ), sulfamethazine (SMZ), sulfamethiazole (SMT), sulfachloropyridazine (SCP), sulfamethoxazole (SMX), sulfisoxazole (SSX), sulfadimethoxine (SDM), trimethoprim (TMP), oxolinic acid (OA) and enrofloxacin (ENR) standards were purchased from Sigma-Aldrich (Germany). Methanol (MeOH) and acetonitrile (ACN) (HPLC grade) were obtained from Merck (Germany). Ammonium chloride ( $\text{NH}_4\text{Cl}$ ), disodium ethylenediamine tetraacetate ( $\text{Na}_2\text{EDTA}$ ), ammonium acetate ( $\text{CH}_3\text{COONH}_4$ ), acetic acid ( $\text{CH}_3\text{COOH}$ ) (all of analytical reagent grade) and filter paper were purchased from POCH (Poland). Milli-Q water was obtained from the Milli-Q water purification system (Millipore, Germany). Oasis HLB cartridges (Waters, Ireland) with 500 mg of packing material, a 6 mL reservoir, as well as Discovery DSC-SAX (Sigma-Aldrich) (500 mg/6 mL) cartridges were used for sample preparation. For sample processing, an SPE 12 position vacuum manifold (Phenomenex, Germany) was used.

Standard stock solutions of each compound were prepared in methanol at a concentration of  $100 \mu\text{g mL}^{-1}$  and stored at  $-18^\circ\text{C}$ . Stability tests show a minimum 6-month degradation

resistance of the solutions under the presented conditions. Working solutions of pharmaceuticals were prepared before analysis by diluting the stock solution in  $\text{ACN:H}_2\text{O}$  (10:90, v/v) and stored at  $4^\circ\text{C}$ . To prepare calibration curves, the working solution was diluted with mobile phase A to an appropriate concentration.

### 2.2. Sediment sampling and sample characterization

Surface sediment samples were collected during the cruise of r/v Oceania in April 2010 and during the cruise of s/y Task in July 2010 using Reineck or Niemistö corers. The location of 10 sampling sites is shown in Fig. 1. During sampling, parameters of near bottom waters, such as temperature ( $T$ ), pH, salinity ( $S$ ) and dissolved oxygen concentration ( $\text{O}_2$ ), were measured for all samples. Water parameter measurements were performed using a multimeter (Hach-Lange, HQ40D). The surface layer of sediment (0–5 cm) was retrieved, frozen ( $-18^\circ\text{C}$ ) in pre-cleaned glass jars and transported to the laboratory. Sediment samples were homogenized, freeze-dried (Labconco, 091118527 D) and used for chemical analyses. For each lyophilized sediment sample, a grain size analysis was performed. The sediment particle size was analyzed using meshes (% of grain  $< 0.063 \text{ mm}$ ), and the sediment type was classified according to the Shepard classification (1954) modified by Piekarek-Jankowska (2010). The organic matter content in sediments was measured by loss on ignition (LOI). Dry and homogenous samples of the sediments were weighed before and after heating for 5 h at  $550^\circ\text{C}$  (Ciborowski, 2010). Details of sampling sites and selected sediment characteristics are given in Table 1.

### 2.3. Sample preparation

The extraction procedure of the sediment samples consisted of two steps: (a) extraction of the analytes from the sediment by sonification and (b) the enrichment and clean-up of the extract applying SPE. The samples were extracted adopting the method used by Majka (2010) and clean-up procedure was performed adopting the method described by Babić et al. (2006). The extraction and the clean-up details are briefly described below.

In the case of the development of the method modification, before extraction 2.5 mL of a working solution of a mixture of antibiotics was spiked into the sediment to reach a final concentration in the sediment of  $5 \mu\text{g g}^{-1}$  d.w. and kept in the dark at room temperature overnight to reach equilibrium, then the excess of the solvent was evaporated at room temperature.

Two grams of homogenized sediment sample were weighed in 30 mL polypropylene centrifuge tubes and subjected to the extraction. The procedure proposed by Majka (2010) for the analysis of 12 sulfonamides in soils and sediments consisted of extraction with 5 mL of a  $\text{NH}_4\text{Cl}:\text{MeOH}$  (1:1, v/v) mixture and 0.5 mL 0.1 M EDTA.  $\text{NH}_4^+$  ions can increase the desorption efficiency by replacing antibiotic cations in a sediment matrix. Furthermore, a water solution of  $\text{NH}_4\text{Cl}$  enhances phase separation. The EDTA is added to prevent the analytes from complexing with metal ions (Lalumera et al., 2004). In this study, during the development

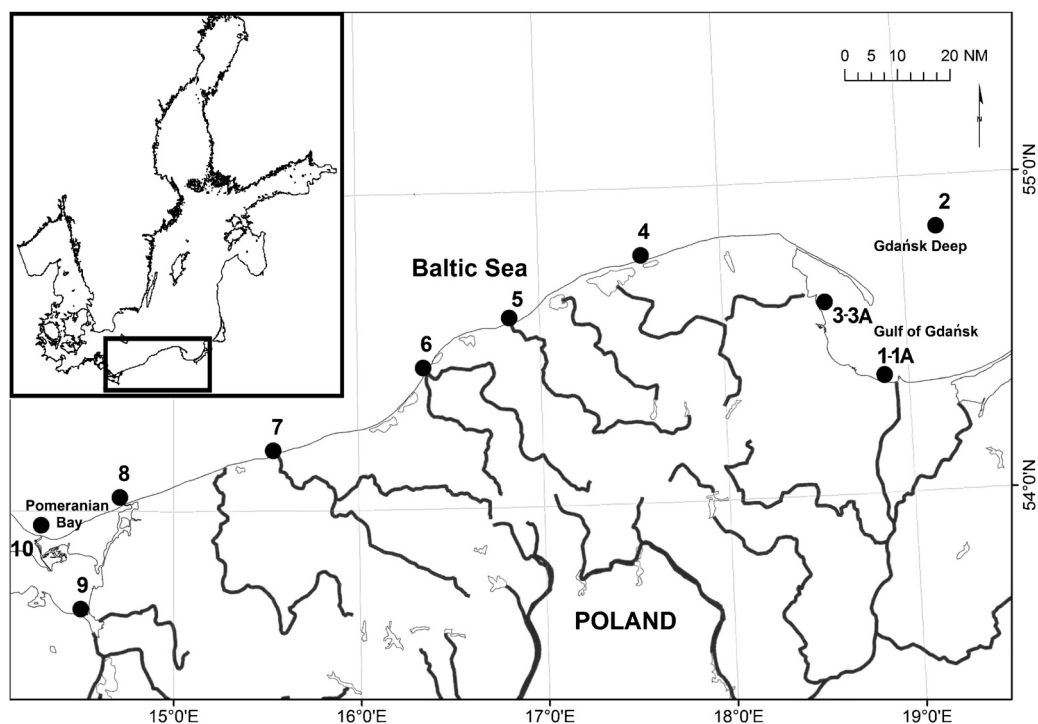


Figure 1 Locations of sampling sites.

of the method, different solutions and volumes of  $\text{NH}_4\text{Cl}$  or citrate/phosphate buffer (McIlvaine buffer) were used to test the extraction efficiency of antibiotics from the spiked sediment. The McIlvaine buffer was applied earlier in the extraction of tetracyclines from the Baltic Sea sediments (Siedlewicz et al., 2014). Eventually, according to the best recovery results, the extraction mixture consisted of methanol, supersaturated  $\text{NH}_4\text{Cl}$  and 0.1 M EDTA. 10 mL of methanol, 10 mL of supersaturated  $\text{NH}_4\text{Cl}$  water solution and 2 mL of 0.1 M EDTA were added to each tube. The samples were mixed on a vortex mixer for 1 min. The samples were then sonicated for 20 min and mixed on a vortex for 20 h in darkness in a cold place (different mix times were tested, and 20 h showed the best recoveries for all analytes). The samples were then centrifuged at 4000 rpm for 10 min. The supernatant from each tube was filtered using paper filter and collected in a glass flask. The extraction was repeated three times without the 20 h vortex stage. The supernatants were combined and 1440 mL of Milli-Q water (to dilute the organic solvent) were added before the clean-up step.

The clean-up procedure was based on the method of Babić et al. (2006) for wastewater samples, where a 60 mg OASIS HLB column was used and the following consecutive steps were performed: pre-conditioning: 5 mL MeOH, 5 mL  $\text{H}_2\text{O}$  pH = 4, washing: 2 mL 2% MeOH, elution:  $2 \times 5$  mL MeOH. In this study, the procedure was modified by using tandem SPE Discovery SAX – Oasis HLB, instead of single OASIS HLB SPE and the elimination of sample acidification. The application of strong anion exchange SPE – Discovery SAX, allowed the removal of negatively charged compounds like humic and fulvic acids, and therefore, a decrease in matrix effects.

Briefly, Discovery SAX (6 mL, 500 mg) and Oasis HLB (6 mL, 500 mg) were set up in tandem for the clean-up of the aqueous sediment extracts. Each tandem column was preconditioned with 8 mL of methanol and 10 mL of Milli-Q

water. Each extract was passed through the tandem cartridge at a flow rate of  $6 \text{ mL min}^{-1}$ , without allowing the cartridge to dry out. After sample loading, the SAX cartridge was removed and the HLB cartridge was rinsed with 8 mL of 2% methanol. The HLB cartridge was then air-dried under a vacuum for about 20 min. The target compounds were eluted with 8 mL of methanol. The eluate was evaporated to dryness under a gentle nitrogen stream, and stored at  $-80^\circ\text{C}$  until LC–MS/MS analysis. Just prior to LC–MS/MS, the residue was re-dissolved in 1 mL of mobile phase A, vortexed, centrifuged to remove particles and transferred to vials.

#### 2.4. LC–MS/MS analysis

The instrumental analysis method was performed, according to the method developed by Biatk-Bielińska et al. (2009) for the determination of 12 sulfonamides in soil samples. Chromatographic separations were performed using an Agilent 1200 Series LC system (Agilent Technologies Inc., Santa Clara, USA) with an Agilent Eclipse XDB C18 column (150 mm  $\times$  4.6 mm, 5  $\mu\text{m}$  particle size) (Agilent Technologies Inc., Santa Clara, USA).  $\text{H}_2\text{O}:\text{ACN}$  (90:10, v/v, 1 mM  $\text{NH}_4\text{Ac}/\text{AcH}$ , pH 3.56) (A) and 100% ACN (B) were used as mobile phases. The flow rate was  $0.3 \text{ mL min}^{-1}$ . The gradient program started with 0% of mobile phase B, which was increased to 64% within 15 min. The injection volume was 50  $\mu\text{L}$ . The mass spectrometric measurements were carried out on an HCT Ultra ion trap mass spectrometer (Bruker Daltonics, Bremen, Germany) equipped with an electrospray ionization source. For data acquisition, EsquireControl software was used. The source temperature was  $350^\circ\text{C}$ . Nitrogen was employed as the nebulizer gas (30 psi) and the dry gas ( $10 \text{ L min}^{-1}$ ). The capillary voltage was  $-4 \text{ kV}$ . Helium (99.999%) was used as the collision gas in the ion trap. The best conditions for isolating the precursor ion were determined. Ions were acquired in the multiple reaction

**Table 1** Location and characteristics of the sampling sites and the sediments collected from the southern Baltic Sea.

Station number/ sediment type	Sampling site	Sampling date	Coordinates	Depth [m]	LOI [%]	Fraction < 0.063 mm content [%]	S [PSU]	T [°C]	pH	O <sub>2</sub> [mg dm <sup>-3</sup> ]	SPM [mg dm <sup>-3</sup> ]
1 sand	Mouth of the Vistula, close to	April 2010	54°22.423	13	0.39	0.4	6.9	12.4	9.01	9.87	27.2
1A sand	WWTP 'Gdańsk Wschód' outlet	July 2010	18°52.093		0.36	0.9	4.9	13.2	8.84	10.90	17.4
2 silty sand	Gdańsk Deep	April 2010	54°49.085 19°17.147	111	20.72	28.9	11.9	7.2	7.32	2.17	80.3
3 sand	WWTP 'Gdynia Dębogórze'	April 2010	54°36.798	10	0.81	1.7	7.0	15.4	8.72	10.41	11.9
3A sand	outlet	July 2010	18°33.712		0.47	1.4	6.9	19.2	8.27	10.92	5.5
4 sand	Mouth of the Łeba river	April 2010	54°47.209 17°33.971	13	0.26	0.5	7.1	10.7	8.75	10.31	4.5
5 sand	Mouth of the Stupia river	April 2010	54°36.027 16°50.161	18	0.48	1.4	6.8	15.2	9.17	10.15	3.4
6 sand	Mouth of the Wieprza river	April 2010	54°26.897 16°21.595	10	0.99	0.7	6.2	10.2	8.89	10.12	5.3
7 sand	Mouth of the Parsęta river	April 2010	54°11.534 15°32.361	11	0.20	2.7	6.2	14.2	8.72	10.26	4.6
8 sand	Mouth of the Dziwna river	April 2010	54°02.703 14°42.626	10	0.18	0.2	6.7	13.2	8.62	10.15	7.4
9 silty sand	Szczecin Lagoon	April 2010	53°41.387 14°30.217	6	11.83	10.9	0.3	19.0	9.35	8.70	130.1
10 sand	Mouth of the Świna river	April 2010	53°57.315 14°17.253	10	0.77	1.5	5.6	12.1	8.46	9.60	62.1

LOI, loss on ignition; S, salinity; SPM, suspended particulate matter content; WWTP, wastewater treatment plant.

monitoring mode. After this, the full scan MS mode was used to record the product ion. For each compound, the fragmentation amplitude and isolation width were also optimized manually to increase the sensitivity and selectivity of the method and to select the three most intensive and characteristic fragmentation ions for qualitative analysis. For quantitative analysis, the ion of the highest intensity was selected. Analyses were performed in the positive mode for all compounds. The optimized MS/MS conditions are shown in Table 2.

## 2.5. Analytical procedure validation

The developed SPE-LC-MS/MS method was validated using sediment samples at eleven spiking levels (0.5, 1, 2, 5, 10, 20, 50, 100, 200, 500, 1000 ng g<sup>-1</sup> d.w. of sediment). The sediments were spiked with a mixture of external standards of antibiotics. Each concentration was analyzed 5 times. Validation parameters such as linearity, method detection limit (MDL), method quantification limit (MQL), precision and accuracy of the whole procedure were determined. The

**Table 2** Retention time, precursor and product ion used for LC–MS/MS analyses.

Compound	Retention time [min]	Precursor ion with isolation width	Product ions	Fragmentation amplitude [V]
ST	15.9	256 ± 2.0	<b>156</b>	0.55
			108	0.60
			92	0.65
SP	16.6	250 ± 0.9	<b>156</b>	0.50
			184	0.60
			108	0.55
SRZ	17.4	265 ± 2.0	<b>190</b>	0.65
			174	0.60
			156	0.55
SMZ	19.1	279 ± 1.9	<b>204</b>	0.60
			124	0.55
			156	0.55
SMT	19.3	271 ± 2.0	<b>156</b>	0.60
			108	0.70
			92	0.60
SCP	22.4	285 ± 2.0	<b>156</b>	0.65
			108	0.60
			92	0.65
SMX	23.8	254 ± 2.0	<b>156</b>	0.65
			188	0.65
			147	0.50
SSX	24.5	268 ± 2.0	<b>156</b>	0.70
			113	0.65
			108	0.65
SDM	26.5	311 ± 2.0	<b>156</b>	0.60
			245	0.60
			218	0.65
TMP	14.9	291 ± 2.0	<b>230</b>	0.90
			261	0.90
			123	0.90
OA	24.7	262 ± 2.0	<b>244</b>	0.75
			216	1.05
			234	1.05
ENR	16.9	360 ± 2.0	<b>316</b>	0.85
			245	0.75
			342	0.75

ST, sulfathiazole; SP, sulfapyridine; SRZ, sulfamerazine; SMZ, sulfamethazine; SMT, sulfamethiazole; SCP, sulfachloropyridazine; SMX, sulfamethoxazole; SSX, sulfisoxazole; SDM, sulfadimethoxine; TMP, trimethoprim; OA, oxolinic acid; ENR, enrofloxacin. Product ion selected for quantitative analysis marked in bold.

calibration curves were constructed by plotting peak areas against analyte concentrations. Linearity was determined for the whole range of concentrations, but for better accuracy of the results two concentration ranges were applied (0.5–50 and 50–1000 ng g<sup>-1</sup> d.w.). The method detection limit was calculated as three times the standard deviation of the lowest acceptable concentration of analytes (Białk-Bielińska et al., 2009; Taverniers et al., 2004). The method quantification limit was set as three times the MDL value. The precision was determined as a coefficient of variation (CV) for the repeated measurements for each spiking level. The accuracy was calculated as the agreement between the measured and known concentrations of each sample analyzed in the applied linear ranges. The validation of the whole analytical procedure was applied to the two types of sediment samples from the Baltic Sea. For this purpose, sediments differing in granulometry and organic matter content were analyzed (silty sand from station 2 – Gdańsk Deep – with high organic matter content, sand from station 3A – WWTP 'Gdynia Dębogórze' outlet – with low organic matter content). Sediments used as blank samples were burned at 450°C for 8 h to eliminate organic contaminants and analyzed in the same way as other samples. Antibiotic residue concentrations in environmental samples were calculated based on an external matrix-matched calibration.

## 2.6. Statistical analysis

Linear regression analysis was used to evaluate the influence of environmental factors on the distribution of frequently detected antibiotic residues. A level of  $p < 0.05$  was considered statistically significant. The statistical analysis was performed using Statistica 10 software (Stat Soft<sup>®</sup>, Poland).

## 3. Results and discussion

### 3.1. Method development

The target antibiotic residues are present in the environment in low concentrations, which, together with the complexity of the sediment-like matrix, makes their reliable determination difficult. Sample preparation is therefore a key step in analysis. In this study sediment samples were extracted and cleaned up adopting the modified analytical method developed by Majka (2010) and Babić et al. (2006). The extraction procedure described by Majka (2010) (MSc thesis in Polish language) included the application of supersaturated NH<sub>4</sub>Cl, 0.1 M EDTA and methanol for the extraction of sulfonamides from soils and sediments. The modification of the extraction method used in this study consisted of increasing the volume of methanol, supersaturated NH<sub>4</sub>Cl and 0.1 M EDTA compared to the original extraction procedure. The application of the clean-up procedure described by Babić et al. (2006) for wastewater analyses resulted in low recoveries, ranging from 8% for SSX in the Baltic silty sands to 154% for SMZ in the sand sediments. Subsequently, the SPE clean-up procedure was modified. The main part of the modification concerned the use of tandem coupled SPE columns and an increased volume of solvent used for column conditioning and purification. The step of the acidification of the sample was also eliminated. The modified method was characterized by higher accuracy than the starting procedure.

The proposed analytical procedure was applied to two types of sediment samples from the Baltic Sea. The sediments used in the validation procedure (from station 2 – silty sand and station 3A – sand) were almost completely free from antibiotic residues. Only in sample 3A, was SCP concentration < MQL level, and it was taken into account in the calculation of the validation parameters. The validation parameters of the whole analytical procedure for sand and silty sand are presented in Table 3.

The MDL values were very low for both types of sediments. For the sand, the values were generally lower (MDL = 0.15–1.86 ng g<sup>-1</sup> d.w.) than the values for the silty sand (MDL = 0.23–10.2 ng g<sup>-1</sup> d.w.). The method detection limit and method quantification limit for the target compounds were similar to, or lower than, the values of these parameters reported in the literature (Löffler and Ternes, 2003; Na et al., 2013; Xu et al., 2014; Zhou et al., 2011). However, Shi et al. (2014) obtained lower limit of detection (LOD) values for some target compounds ranging from 0.05 ng g<sup>-1</sup> d.w. for SP to 0.1 ng g<sup>-1</sup> d.w. for SMX. Similarly, Chen and Zhou (2014) described the limit of quantification (LOQ) of their target antibiotic in the range of 0.01–0.5 ng g<sup>-1</sup> d.w. The higher MDL and MQL values observed for Baltic sediments were probably caused by matrix effects. For example, Gdańsk Deep sediments are characterized by a high content of organic matter and accumulated persistent organic pollutants, heavy metals or anionic surfactants (Hampel et al., 2012; Konat and Kowalewska, 2001; Szefer et al., 1995). Those compounds can affect the ionization efficiency (Caban et al., 2012; Van De Steene and Lambert, 2008; Zhou et al., 2011). Furthermore, the strong sorption properties of OA and ENR could be a reason for their high MDL/MQL values in silty sand type sediments (Kümmerer, 2008a, 2008c; Le-Minh et al., 2010). The calibration curves obtained for all compounds were linear in the assayed range, with the correlation coefficients  $r \geq 0.98$ . Linear concentration ranges were applied for most of the compounds except OA and ENR in silty sand. For these analytes the accuracy of spiking levels located beyond the linear range (presented in Table 3) increased or decreased enormously. The calibration curves were proved to be linear within the range of the linear regression parameters of both the matrix-matched and standard calibration curves. The accuracy of the method was expressed as the mean recoveries with standard deviations (SD) of spiked antibiotics in the sediment matrix. Good accuracies, ranging from 89 to 119%, were obtained for the two spiking levels in both sediment types assayed. This accuracies are very satisfactory compared to the methods described in the literature, where the reported accuracy for sulfonamides and quinolones were in the range of 51–141% (Chen and Zhou, 2014; Luo et al., 2011; Na et al., 2013; Raich-Montiou et al., 2007). However, some accuracies of target compounds were relatively high. At the lowest spiking level of OA in sand sediment and the highest spiking level of ST, SP, SRZ and SMT, in silty sand, the standard deviations obtained were higher than 20%. The physicochemical properties of the target substances and the influence of the matrix may affect the accuracy (Caban et al., 2012; Zhou et al., 2011). According to Kim and Carlson (2005) cation exchange, cation bridging, surface complexation and hydrogen bonding may play important role in retaining pharmaceuticals on a solid matrix. Białk-Bielińska et al. (2012) and Maszkowska

**Table 3** Validation results for the entire analytical procedure (SPE-LC-MS/MS) applied to determination of 12 antibiotics in Baltic sediments.

Compound	Sand					Silty sand				
	Range	$R^2$	MDL [ng g <sup>-1</sup> d.w.]	MQL [ng g <sup>-1</sup> d.w.]	Accuracy [%] Mean (SD) (n = 5)	Range	$R^2$	MDL [ng g <sup>-1</sup> d.w.]	MQL [ng g <sup>-1</sup> d.w.]	Accuracy [%] Mean (SD) (n = 5)
ST	0.5–50	1.000	0.38	1.14	96.5 (12.9)	0.5–50	1.000	0.43	1.29	100.5 (9.4)
	50–1000	1.000			95.1 (18.4)	50–1000	0.975			101.0 (21.0)
SP	0.5–50	1.000	0.19	0.57	91.2 (16.9)	1–50	0.999	0.77	2.31	93.9 (9.5)
	50–1000	0.999			109.9 (9.6)	50–100	0.999			92.1 (28.2)
SRZ	0.5–50	1.000	0.25	0.75	94.1 (11.1)	0.5–50	1.000	0.23	0.69	100.8 (6.6)
	50–1000	0.999			107.7 (7.8)	50–1000	0.999			102.5 (22.9)
SMZ	1.0–50	0.999	0.49	1.47	103.4 (9.8)	1–50	1.000	0.59	1.77	90.5 (15.6)
	50–1000	0.984			112.1 (12.6)	50–1000	0.999			109.0 (11.9)
SMT	1–50	1.000	0.79	2.37	101.4 (6.3)	0.5–50	0.999	0.88	2.64	103.8 (11.7)
	50–1000	0.999			88.8 (17.7)	50–1000	0.985			118.8 (23.4)
SCP	0.5–50	1.000	0.15	0.45	97.6 (6.1)	0.5–50	1.000	0.37	1.11	105. (17.2)
	50–1000	1.000			100.2 (3.0)	50–1000	0.999			104.3 (9.5)
SMX	0.5–20	1.000	0.31	0.93	99.3 (4.4)	1–50	1.000	0.83	2.49	101.3 (7.2)
	50–1000	1.000			95.9 (16.9)	50–1000	0.999			104.8 (8.2)
SSX	0.5–50	0.999	0.26	0.78	101.1 (12.2)	2–100	0.984	0.58	1.74	96.5 (11.8)
	50–1000	0.999			107.9 (12.0)	100–1000	1.000			104.8 (8.4)
SDM	0.5–50	0.999	0.53	1.59	103.5 (6.6)	1–50	1.000	0.54	1.62	98.7 (10.6)
	50–1000	0.999			104.8 (7.8)	50–1000	0.984			106.0 (14.9)
TMP	0.5–50	1.000	0.34	1.02	103.1 (11.7)	0.5–50	1.000	0.34	1.02	102.7 (9.2)
	50–1000	0.984			103.8 (12.3)	50–1000	0.984			102.3 (16.6)
OA	2–50	0.999	1.86	5.58	108.7 (24.5)	50–1000	0.999	10.2	30.6	113.8 (12.7)
	50–1000	0.984			104.5 (16.7)					
ENR	2–50	0.985	1.22	3.66	98.5 (18.7)	2–200	0.999	1.38	4.14	97.7 (18.6)
	50–1000	1.000			101.8 (4.0)					

*n*, number of replicates; MDL, method detection limit; MQL, method quantification limit;  $R^2$ , determination coefficient; SD, standard deviation; ST, sulfathiazole; SP, sulfapyridine; SRZ, sulfamerazine; SMZ, sulfamethazine; SMT, sulfamethiazole; SCP, sulfachloropyridazine; SMX, sulfamethoxazole; SSX, sulfisoxazole; SDM, sulfadimethoxine; TMP, trimethoprim; OA, oxolinic acid; ENR, enrofloxacin.

et al. (2013) reported a strong dependence between the sorption/desorption of selected sulfonamides and the organic carbon content in soils. In the light of these investigations it can be assumed that similar dependencies could be a reason for the difference in accuracies observed for analyzed types of Baltic sediments. Matrix effects like ion suppression and/or ion enhancement are ubiquitous during LC–MS/MS analysis, due to ionization competition between eluting compounds in a chromatographic system (Na et al., 2011; Van De Steene and Lambert, 2008). To reduce high values of the standard deviation and to fully determine the influence of the sample matrix on the obtained results, the use of internal, isotope-labelled standards is recommended (Löffler and Ternes, 2003; Na et al., 2011; Yang et al., 2010). However, these were not applied at this stage. The exact values of matrix effects were not calculated as they were compensated by working with a matrix-matched calibration. Studies on matrix effects in different types of Baltic sediments will be continued in future research applying isotope-labelled analogues. This approach was demonstrated to be the most advantageous approach for an accurate determination of target compounds in environmental complex samples (Na et al., 2013). The selection of an internal standard has to be based on its similarity to the compounds of interest, with regard to chemical structure, mass spectrometric response, chromatographic retention time and matrix effect (ion suppression or enhancement) (Bayen et al., 2013). However, the commercial availability of reference standards is still low, thus according to the literature satisfactory results can be obtained using only one or two internal standards to correct for all compounds (Wille et al., 2012).

In the applied method, the precision (CV) values were in general less than 20%. The sediment matrix and the properties of some target analytes could explain the differences in the validation parameters between both types of sediments. Analyses of the blank samples, in which none of the analyzed compounds were detected, in comparison with spiked sediment samples showed that the method also exhibited good selectivity.

The obtained validation results showed that a sensitive and efficient extraction procedure and analytical method, applying tandem SPE and LC–MS/MS, has been developed to determine 12 antibiotics in Baltic sediments. The described procedure allows the determination of 9 sulfonamides, 2 quinolones and trimethoprim in Baltic sediments down to the lower  $\text{ng g}^{-1}$  range, with good accuracy and precision.

### 3.2. Results of the real samples analysis

The proposed analytical procedure was applied to the analysis of 12 sediment samples collected from the southern Baltic Sea. Environmental samples were analyzed in duplicate, and the reported data are the average of the two analyses. The detected compounds together with their concentrations are shown in Table 4. Nine of the twelve target antibiotics were detected in the sediment samples. Among the analyzed antibiotics, SMX and SCP were the most frequently detected (58%) in sediment samples. The occurrence frequency of TMP was 42% and it was detected in the samples simultaneously with SMX. SMT, SRZ, SSX and SDM were found in the monitored area but only in single samples. No residues of SP, OA, ENR were detected in any of the samples analyzed.

The concentrations of the analyzed antibiotics ranged from <MDL to  $419 \text{ ng g}^{-1}$  d.w. for sulfonamides and from <MDL to  $2.46 \text{ ng g}^{-1}$  d.w. for TMP. The highest concentrations were observed for SMX up to  $419.2 \text{ ng g}^{-1}$  d.w. Compounds observed sporadically were found at low concentrations, with one exception – SMT. In the case of SMT, notable concentrations were observed ( $12.85$  and  $20.84 \text{ ng g}^{-1}$  d.w.).

This preliminary study has demonstrated for the first time the occurrence of the analyzed compounds in sediments collected in the Polish coastal area. It is worth noting that very little information is available on the concentrations of antibiotic residues in marine sediments. Most of the available data has been reported for Asian coastal seas. In general, the maximum concentrations of sulfonamides in marine sediments in other geographical areas were lower than in the present study. For example, Na et al. (2013), investigating the

**Table 4** Occurrence of target compounds in sediment samples collected from the southern Baltic Sea.

Sampling station	Concentration, mean value (SD) [ $\text{ng g}^{-1}$ d.w.]											
	ST	SP	SRZ	SMZ	SMT	SCP	SMX	SSX	SDM	TMP	OA	ENR
1	n.d.	n.d.	n.d.	n.d.	n.d.	n.d.	11.12 (0.42)	n.d.	n.d.	<MQL	n.d.	n.d.
1A	<MQL	n.d.	<MQL	1.76 (0.23)	n.d.	1.07 (0.32)	2.34 (0.61)	<MQL	<MQL	2.46 (0.12)	n.d.	n.d.
2	n.d.	n.d.	n.d.	n.d.	n.d.	n.d.	n.d.	n.d.	n.d.	n.d.	n.d.	n.d.
3	n.d.	n.d.	n.d.	n.d.	n.d.	0.54 (0.04)	7.83 (0.40)	n.d.	n.d.	<MQL	n.d.	n.d.
3A	n.d.	n.d.	n.d.	n.d.	n.d.	<MQL	n.d.	n.d.	n.d.	n.d.	n.d.	n.d.
4	n.d.	n.d.	n.d.	<MQL	n.d.	0.55 (0.06)	67.24 (5.32)	n.d.	n.d.	<MQL	n.d.	n.d.
5	1.77 (0.03)	n.d.	n.d.	n.d.	20.84 (0.52)	n.d.	n.d.	n.d.	n.d.	n.d.	n.d.	n.d.
6	n.d.	n.d.	n.d.	n.d.	12.85 (0.23)	n.d.	n.d.	n.d.	n.d.	n.d.	n.d.	n.d.
7	n.d.	n.d.	n.d.	<MQL	n.d.	0.47 (0.23)	275.8 (13.1)	n.d.	n.d.	1.74 (0.03)	n.d.	n.d.
8	n.d.	n.d.	n.d.	n.d.	n.d.	<MQL	185.7 (5.4)	n.d.	n.d.	n.d.	n.d.	n.d.
9	n.d.	n.d.	n.d.	n.d.	n.d.	<MQL	n.d.	n.d.	n.d.	n.d.	n.d.	n.d.
10	n.d.	n.d.	n.d.	n.d.	n.d.	n.d.	419.2 (2.6)	n.d.	n.d.	n.d.	n.d.	n.d.

n.d. not detected (<MDL below method detection limit), <MQL below method quantification limit, ST, sulfathiazole; SP, sulfapyridine; SRZ, sulfamerazine; SMZ, sulfamethazine; SMT, sulfamethiazole; SCP, sulfachloropyridazine; SMX, sulfamethoxazole; SSX, sulfisoxazole; SDM, sulfadimethoxine; TMP, trimethoprim; OA, oxolinic acid; ENR, enrofloxacin; SD, standard deviation.

occurrence of 20 antibiotics in the coastal areas of Dalian (China), reported different patterns in the maximum concentration and frequency of sulfonamides: ST, SRZ and SMZ were at maximum levels in the range of 1.8–3.7 ng g<sup>-1</sup>, whereas SMT, SCP, SMX, SSX and SDM were not detected in any sediment sample, despite some of them being present in seawater. Seasonal variations in the detection frequency of ST, SP, SRZ, SMZ, SMX and ENR, and a maximum concentration range of <LOQ to 9.1 ng g<sup>-1</sup>, were observed by Shi et al. (2014) in the Yangtze Estuary. In the same area, Yang et al. (2011) observed SMX in water but not in sediments. Low levels of SMZ and ENR, and an absence of SMX, were also observed by Liang et al. (2013) in sediments of the Pearl River Estuary. In sediments of the Mar Menor Lagoon (Spain), the concentration of SMX was <LOD and that of TMP was <LOQ (Moreno-González et al., 2015). Low concentrations (<1 ng g<sup>-1</sup>) of SMT and TMP were measured in sediments around Auckland in New Zealand (Stewart et al., 2014). Higher concentrations of SMX, TMP and OA than reported in this article have been detected in sediment collected near aquacultures. Le and Munekage (2004) observed levels of these compounds in the range of 1.8–820 µg g<sup>-1</sup> in Viet Nam shrimp ponds, where these antibiotics are popular components of shrimp feed (Le and Munekage, 2004). The authors also observed higher concentrations of antibiotic residues in sediments than in water samples in the vicinity of these shrimp farms (Le and Munekage, 2004).

The observed levels of sulfonamides and trimethoprim in the collected sediments were higher than those reported for Baltic seawaters (Borecka et al., 2013; Nödler et al., 2014) and Polish river waters (Gbylik-Sikorska et al., 2014). The spatial distribution of the analyzed antibiotics indicates a high level of antibiotics occurring in the Pomeranian Bay and in the mouths of rivers. The highest SMX levels were found at station 10 (Pomeranian Bay) close to the mouth of the Świna river (station 10 – 419.2 ng g<sup>-1</sup> d.w.). A high level of SMX was also observed close to the mouths of the Parsęta river (station 7 – 275.75 ng g<sup>-1</sup> d.w.) and the Dziwna river (station 8 – 185.70 ng g<sup>-1</sup> d.w.). To exclude the influence of artificial interference resulting in the detection of high concentrations of SMX, the analyses of samples from stations 7, 8 and 10 were repeated by independent analysts. In the case of the Gulf of Gdańsk, samples collected in summer from the station in the

mouth of the Vistula, close to the Wastewater Treatment Plant (WWTP) 'Gdańsk Wschód' outlet (1A), were characterized by the highest frequency of antibiotics. These results were quite different from those for samples collected from the same place in April (1), where only SMX and TMP were detected. Samples collected in April and June (stations 3 and 3A), near to the WWTP 'Gdynia Dębogórze' outlet, demonstrated much lower antibiotic frequency than stations 1 and 1A. There was only one sample – collected from the Gdańsk Deep station – where none of the analytes were detected.

The presence of SMX and TMP most probably results from their application in medicine (commonly used together in the ratio 5:1) (Chang et al., 2008). The main source of these compounds in the investigated samples may be wastewaters from WWTPs. Łuczkiwicz et al. (2013) proved that the removals of TMP and SMX in Gdańsk WWTP were only in the range of 7–38% and 47–65% respectively. Another source of compounds like SCP or SMZ may be used in livestock, further surface runoff from soil, and final discharge to the sea (Xu et al., 2014). The results from station 10 (mouth of the Świna river), which show high concentrations of SMX, were very surprising and may be caused by different factors like, for example, the impact of the Odra and Świna rivers or the city of Świnoujście (a point source of pollution). Such phenomena were also observed by Nödler et al. (2014) for caffeine in the Cape Arcona area (western Baltic Sea). It is suggested that, as this location includes popular tourist destination places, the detected concentrations may be attributed to tourist activities. The influence of tourist activity on pharmaceutical levels was also observed by Moreno-González et al. in the Mar Menor lagoon (western Mediterranean Sea) (Moreno-González et al., 2015). The mouth of the Świna river has a high shipping throughput and the coast nearby is a popular tourist attraction, so the high level of pollution may be caused by tourists and sewage dumping by ships near the sampling location. This hypothesis about tourist activity influencing contamination could also explain the higher frequency of antibiotic residue occurrence at station 1A in the coastal area of the Gulf of Gdańsk in summer compared to spring. However, to verify this hypothesis, a greater volume of data would be necessary.

**Table 5** The Pearson linear correlation between environmental parameters and SMX, TMP, SCP (measurable intensity) in sediment samples collected from the southern Baltic Sea.

Compound	LOI [%]	<0.063 mm [%]	S [PSU]	T [°C]	pH	O <sub>2</sub> [mg dm <sup>-3</sup> ]	SPM [mg dm <sup>-3</sup> ]
SMX	0.1144 <i>n</i> = 7 <i>p</i> = 0.807	0.4279 <i>n</i> = 7 <i>p</i> = 0.338	-0.2815 <i>n</i> = 7 <i>p</i> = 0.541	-0.1220 <i>n</i> = 7 <i>p</i> = 0.794	-0.8012* <i>n</i> = 7 <i>p</i> = 0.030	-0.6280 <i>n</i> = 7 <i>p</i> = 0.131	0.5374 <i>n</i> = 7 <i>p</i> = 0.213
TMP	-0.3975 <i>n</i> = 5 <i>p</i> = 0.508	0.3444 <i>n</i> = 5 <i>p</i> = 0.570	-0.9619* <i>n</i> = 5 <i>p</i> = 0.009	0.2067 <i>n</i> = 5 <i>p</i> = 0.739	-0.1127 <i>n</i> = 5 <i>p</i> = 0.857	0.7057 <i>n</i> = 5 <i>p</i> = 0.183	-0.0761 <i>n</i> = 5 <i>p</i> = 0.903
SCP	-0.1373 <i>n</i> = 7 <i>p</i> = 0.769	-0.1323 <i>n</i> = 7 <i>p</i> = 0.777	-0.0939 <i>n</i> = 7 <i>p</i> = 0.841	-0.4345 <i>n</i> = 7 <i>p</i> = 0.330	0.3111 <i>n</i> = 7 <i>p</i> = 0.497	0.5496 <i>n</i> = 7 <i>p</i> = 0.201	-0.0665 <i>n</i> = 7 <i>p</i> = 0.887

*n*, number of samples; LOI, loss on ignition; S, salinity; SPM, suspended particulate matter content; SMX, sulfamethoxazole; TMP, trimethoprim; SCP, sulfachloropyridazine.

\* *p* < 0.05.

Statistical analyses showed that SMX concentrations correlate with bottom water parameters like pH (Table 5). Białk-Bielińska et al. (2012) confirmed that sulfadimethoxine and sulfaguanidine had lower  $K_d$  values with increasing pH. The inverse Pearson correlation between TMP and the salinity of bottom waters may be caused by the dilution of this compound in marine waters (Liang et al., 2013; Zhang et al., 2012). No significant correlation existed between the concentrations of the target compounds and the sediment properties, which is in contrast with the situation for persistent organic pollutants (POPs). The content of POPs, which are hydrophobic compounds, in sediments, in general, strongly correlates with organic matter content and fine grain content (Pazdro, 2004). Although the obtained results indicate that the sediment composition is not the determining factor in the retention of the analyzed antibiotics, it should be remembered that the number of samples is low for statistical analyses and that a larger database would help in drawing conclusions. Due to the hydrophilic properties of the target antibiotics, sorption on sediment particles is more complex than that of hydrophobic organic contaminants (Beretta et al., 2014). Antibiotics like sulfonamides or trimethoprim are generally persistent in the marine environment and are sparingly adsorbed by sediment due to their physicochemical properties (Benotti and Brownawell, 2009; Boxall, 2008b; Hektoen et al., 1995; Sukul and Spittler, 2006; Thiele-Bruhn, 2003; Tolls, 2001). On the other hand, quinolones are easily photodegraded and strongly adsorbed by solid matrices (Khetan and Collins, 2007; Kümmerer, 2008a, 2008c; Le-Minh et al., 2010; Zhang et al., 2012). García-Galán et al. (2010) concluded that the high presence of some antibiotic residues in the environment has more to do with the high quantities employed than with physicochemical properties such as the solubility of the compound in water. This could be the reason why SMX, TMP and SCP were detected more frequently than OA, ENR or other sulfonamides.

#### 4. Conclusions

A reliable method for the simultaneous determination of sulfonamides, trimethoprim and selected quinolones has been developed. Nevertheless, the employment of isotope-labelled internal standards should be considered in the future research to further compensate for matrix effects. The obtained method has been applied to analyze the Baltic Sea sediments. This preliminary study demonstrates for the first time the occurrence of antibiotic residues in the southern Baltic Sea. The obtained results suggest that sediment can be an important sink and, in some cases, a secondary source of antibiotic residues like sulfamethoxazole, sulfachloropyridazine or trimethoprim in the marine environment. Consequently, the studies will be continued to establish a more extensive database of the occurrence of antibiotic residues in the southern Baltic Sea and to identify factors governing their spatial and temporal distribution.

#### Acknowledgements

This work was supported by the National Science Centre of Poland under grant DEC-2011/01/N/ST10/06977 and the Institute of Oceanology of the Polish Academy of Sciences under statutory activity task no. II. 2.

#### References

- Arnold, K.E., Brown, A.R., Ankley, T.G., Sumpter, J.P., 2014. Medicating the environment: assessing risks of pharmaceuticals to wildlife and ecosystem. *Phil. Trans. R. Soc. B* 369 (1656), 1–11, <http://dx.doi.org/10.1098/rstb.2013.0569>.
- Babić, S., Ašperger, D., Mutavdžić, D., Horvat, A.J.M., Kaštelan-Macan, M., 2006. Solid phase extraction and HPLC determination of veterinary pharmaceuticals in wastewater. *Talanta* 70 (4), 732–738, <http://dx.doi.org/10.1016/j.talanta.2006.07.003>.
- Bayen, S., Zhang, H., Desai, M.M., Ooi, S.K., Kelly, B.C., 2013. Occurrence and distribution of pharmaceutically active and endocrine disrupting compounds in Singapore's marine environment: influence of hydrodynamics and physical-chemical properties. *Environ. Pollut.* 182, 1–8, <http://dx.doi.org/10.1016/j.envpol.2013.06.028>.
- Beck, I.C., Bruhn, R., Gandrass, J., Ruck, W., 2005. Liquid chromatography–tandem mass spectrometry analysis of estrogenic compounds in coastal surface water of the Baltic Sea. *J. Chromatogr. A* 1090 (1–2), 98–106, <http://dx.doi.org/10.1016/j.chroma.2005.07.013>.
- Benotti, M.J., Brownawell, B.J., 2009. Microbial degradation of pharmaceuticals in estuarine and coastal seawater. *Environ. Pollut.* 157 (3), 994–1002, <http://dx.doi.org/10.1016/j.envpol.2008.10.009>.
- Beretta, M., Britto, V., Tavares, T.M., da Silva, S.M.T., Pletsch, A.L., 2014. Occurrence of pharmaceutical and personal care products (PPCPs) in marine sediments in the Todos os Santos Bay and the north coast of Salvador, Bahia, Brazil. *J. Soil. Sedim.* 14 (7), 1278–1286, <http://dx.doi.org/10.1007/s11368-014-0884-6>.
- Białk-Bielińska, A., Kumirska, J., Borecka, M., Caban, M., Paszkiewicz, M., Pazdro, K., Stepnowski, P., 2016. Selected analytical challenges in the determination of pharmaceuticals in drinking/marine waters and soil/sediment samples. *J. Pharmaceut. Biomed.* 121, 271–296, <http://dx.doi.org/10.1016/j.jpba.2016.01.016>.
- Białk-Bielińska, A., Kumirska, J., Palavinskas, R., Stepnowski, P., 2009. Optimization of multiple reaction monitoring mode for the trace analysis of veterinary by LC-MS/MS. *Talanta* 80 (2), 947–953, <http://dx.doi.org/10.1016/j.talanta.2009.08.023>.
- Białk-Bielińska, A., Maszkowska, J., Mroziak, W., Bielawska, A., Kotodziejska, M., Palavinskas, R., Stepnowski, P., Kumirska, J., 2012. Sulfadimethoxine and sulfaguanidine: their sorption potential on natural soils. *Chemosphere* 86 (10), 1059–1065, <http://dx.doi.org/10.1016/j.chemosphere.2011.11.058>.
- Boeckel, T.P., van Gandra, S., Ashok, A., Caudron, Q., Grenfell, B.T., Levin, S.A., Laxminarayan, R., 2014. Global antibiotic consumption 2000 to 2010: an analysis of national pharmaceutical sales data. *Lancet Infect. Dis.* 14 (8), 742–750, [http://dx.doi.org/10.1016/S1473-3099\(14\)70780-7](http://dx.doi.org/10.1016/S1473-3099(14)70780-7).
- Borecka, M., Białk-Bielińska, A., Siedlewicz, G., Kornowska, K., Kumirska, J., Stepnowski, P., Pazdro, K., 2013. A new approach for the estimation of expanded uncertainty of results of an analytical method developed for determining antibiotics in seawater using solid-phase extraction disks and liquid chromatography coupled with tandem mass spectrometry technique. *J. Chromatogr. A* 1304, 138–146, <http://dx.doi.org/10.1016/j.chroma.2013.07.018>.
- Borecka, M., Siedlewicz, G., Haliński, Ł.P., Sikora, K., Pazdro, K., Stepnowski, P., Białk-Bielińska, A., 2015. Contamination of the southern Baltic Sea waters by the residues of selected pharmaceuticals: method development and field studies. *Mar. Pollut. Bull.* 94 (1–2), 62–71, <http://dx.doi.org/10.1016/j.marpolbul.2015.03.008>.
- Boxall, A.B., 2008a. Fate and transport of veterinary medicines in the soil environment. In: Aga, D.S. (Ed.), *Fate of Pharmaceuticals in the Environment and in Water Treatment Systems*. CRC Press, Boca Raton, 123–137.

- Boxall, A.B., 2008b. Fate of veterinary medicines applied to soils. In: Kümmerer, K. (Ed.), *Pharmaceuticals in the Environment: Sources, Fate, Effects and Risk*. Springer, Berlin, 103–119, [http://dx.doi.org/10.1007/978-3-540-74664-5\\_8](http://dx.doi.org/10.1007/978-3-540-74664-5_8).
- Boxall, A.B., Blackwell, P., Cavallo, R., Kay, P., Tolls, J., 2002. *The sorption and transport of a sulphonamide antibiotic in soil systems*. *Toxicol. Lett.* 131 (1–2), 19–28.
- Bu, Q., Wang, B., Huang, J., Deng, S., Yu, G., 2013. Pharmaceuticals and personal care products in the aquatic environment in China: a review. *J. Hazard. Mater.* 262, 189–211, <http://dx.doi.org/10.1016/j.jhazmat.2013.08.040>.
- Caban, M., Migowska, N., Stepnowski, P., Kwiatkowski, M., Kumirska, J., 2012. Matrix effects and recovery calculations in analyses of pharmaceuticals based on the determination of  $\beta$ -blockers and  $\beta$ -agonists in environmental samples. *J. Chromatogr. A* 1258, 117–127, <http://dx.doi.org/10.1016/j.chroma.2012.08.029>.
- Capone, D.G., Weston, D.P., Millera, V., Shoemaker, C., 1996. Antibacterial residues in marine sediments and invertebrates following chemotherapy in aquaculture. *Aquaculture* 145 (1–4), 55–75, [http://dx.doi.org/10.1016/S0044-8486\(96\)01330-0](http://dx.doi.org/10.1016/S0044-8486(96)01330-0).
- Chang, H., Hu, J., Asami, M., Kunikane, S., 2008. Simultaneous analysis of 16 sulfonamide and trimethoprim antibiotics in environmental waters by liquid chromatography-electrospray tandem mass spectrometry. *J. Chromatogr. A* 1190 (1–2), 390–393, <http://dx.doi.org/10.1016/j.chroma.2008.03.057>.
- Chen, K., Zhou, J.L., 2014. Occurrence and behavior of antibiotics in water and sediments from the Huangpu River, Shanghai, China. *Chemosphere* 95, 604–612, <http://dx.doi.org/10.1016/j.chemosphere.2013.09.119>.
- Ciborowski, T., 2010. *Organic matter*. In: Bolatek, J. (Ed.), *Physical, Biological and Chemical Studies on Marine Sediments*, Wyd. UG, Gdańsk, 287–290, (in Polish).
- Claessens, M., Vanhaecke, L., Wille, K., Janssen, C.R., 2013. Emerging contaminants in Belgian marine waters: single toxicant and mixture risks of pharmaceuticals. *Mar. Pollut. Bull.* 71 (1–2), 41–50, <http://dx.doi.org/10.1016/j.marpolbul.2013.03.039>.
- Daughton, C.G., Ternes, T.A., 1999. *Pharmaceuticals and personal care products in the environment: agents of subtle changes*. *Environ. Health Perspect.* 107 (6), 907–938.
- Dzierżawski, A., Cybulski, W., 2012. *The need for rational use of antibiotics in veterinary practice*. *Życie Weterynar.* 87 (4), 316–321, (in Polish).
- García-Galán, M.J., Villagrasa, M., Diaz-Cruz, M.S., Barceló, D., 2010. LC-QqLIT MS analysis of nine sulfonamides and one of their acetylated metabolites in the Llobregat River basin. Quantitative determination and qualitative evaluation by IDA experiments. *Anal. Bioanal. Chem.* 397 (3), 1325–1334, <http://dx.doi.org/10.1007/s00216-010-3630-y>.
- Gaw, S., Thomas, K.V., Hutchinson, T.H., 2014. Sources, impacts and trends of pharmaceuticals in the marine and coastal environment. *Phil. Trans. R. Soc. B* 369 (1656), 1–11, <http://dx.doi.org/10.1098/rstb.2013.0572>.
- Gbylik-Sikorska, M., Posyniak, A., Mirowska, K., Gajda, A., Bładek, T., Śniegocki, T., Żmudzki, J., 2014. Occurrence of veterinary antibiotics and chemotherapeutics in fresh water, sediment, and fish of the rivers and lakes in Poland. *B. Vet. I. Pulawy* 58 (3), 399–404, <http://dx.doi.org/10.2478/bvip-2014-0062>.
- González-Pleiter, M., Gonzalo, S., Rodea-Palomares, I., Leganés, F., Rosal, R., Boltes, K., Marco, E., Fernández-Piñas, F., 2013. Toxicity of five antibiotics and their mixtures towards photosynthetic aquatic organisms: implications for environmental risk assessment. *Water Res.* 47 (6), 2050–2064, <http://dx.doi.org/10.1016/j.watres.2013.01.020>.
- Halling-Sørensen, B., Nielsen, S.N., Lanzky, P.F., Ingerslev, F., Holten Lützhøft, H.C., Jørgensen, S.E., 1998. Occurrence, fate and effects of pharmaceutical substances in the environment – a review. *Chemosphere* 36 (2), 357–393, [http://dx.doi.org/10.1016/S0045-6535\(97\)00354-8](http://dx.doi.org/10.1016/S0045-6535(97)00354-8).
- Hampel, M., Mauffret, A., Pazdro, K., Blasco, J., 2012. Anionic surfactant linear alkylbenzene sulfonates (LAS) in sediments from the Gulf of Gdańsk (southern Baltic Sea, Poland) and its environmental implications. *Environ. Monit. Assess.* 184 (10), 6013–6023, <http://dx.doi.org/10.1007/s10661-011-2399-6>.
- Hektoen, H., Berge, J.A., Hormazabal, V., Yndestad, M., 1995. Persistence of antibacterial agents in marine sediments. *Aquaculture* 133 (3–4), 175–184, [http://dx.doi.org/10.1016/0044-8486\(94\)00310-K](http://dx.doi.org/10.1016/0044-8486(94)00310-K).
- HELCOM, 2010. Hazardous substances in the Baltic Sea – an integrated thematic assessment of hazardous substances in the Baltic Sea, Baltic Sea Environment Proceedings No. 120B, <http://www.helcom.fi/Lists/Publications/BSEP120B.pdf> (accessed: 5 December 2015).
- Hirsch, R., Ternes, T., Haberer, K., Kratz, K.L., 1999. Occurrence of antibiotics in the aquatic environment. *Sci. Total Environ.* 225 (1–2), 109–118, [http://dx.doi.org/10.1016/S0048-9697\(98\)00337-4](http://dx.doi.org/10.1016/S0048-9697(98)00337-4).
- Hörsing, M., Ledin, A., Grabic, R., Fick, J., Tysklind, M., la Cour, J.J., Andersen, H.R., 2011. Determination of sorption of seventy-five pharmaceuticals in sewage sludge. *Water Res.* 45 (15), 4470–4482, <http://dx.doi.org/10.1016/j.watres.2011.05.033>.
- Kemper, N., 2008. Veterinary antibiotics in the aquatic and terrestrial environment. *Ecol. Indic.* 8 (1), 1–13, <http://dx.doi.org/10.1016/j.ecolind.2007.06.002>.
- Khetan, K., Collins, T.J., 2007. Human pharmaceuticals in the aquatic environment: a challenge to green chemistry. *Chem. Rev.* 107 (6), 2319–2364, <http://dx.doi.org/10.1021/cr020441w>.
- Kim, S.C., Carlson, K., 2005. LC-MS<sup>2</sup> for quantifying trace amounts of pharmaceutical compounds in soil and sediment matrices. *TrAC-Trends Anal. Chem.* 24 (7), 635–644, <http://dx.doi.org/10.1016/j.trac.2005.04.006>.
- Konat, J., Kowalewska, G., 2001. Polychlorinated biphenyls (PCBs) in sediments of the southern Baltic Sea. *Sci. Total Environ.* 280 (1–3), 1–15, [http://dx.doi.org/10.1016/S0048-9697\(01\)00785-9](http://dx.doi.org/10.1016/S0048-9697(01)00785-9).
- Kot-Wasik, A., Dębska, J., Namieśnik, J., 2007. Analytical techniques in studies of the environmental fate of pharmaceutical and personal-care products. *TrAC-Trends Anal. Chem.* 26 (6), 557–568, <http://dx.doi.org/10.1016/j.trac.2006.11.004>.
- Kotlarska, E., Łuczkiwicz, A., Pisowacka, M., Burzyński, A., 2015. Antibiotic resistance and prevalence of class 1 and 2 integrons in *Escherichia coli* isolated from two wastewater treatment plants, and their receiving waters (Gulf of Gdansk, Baltic Sea, Poland). *Environ. Sci. Pollut. Res.* 22 (3), 2018–2030, <http://dx.doi.org/10.1007/s11356-014-3474-7>.
- Kümmerer, K., 2008a. *Antibiotics in the environment*. In: Kümmerer, K. (Ed.), *Pharmaceuticals in the Environment: Sources, Fate, Effects and Risk*. Springer, Berlin, 75–93.
- Kümmerer, K., 2008b. *Effects of antibiotics and virustatics in the environment*. In: Kümmerer, K. (Ed.), *Pharmaceuticals in the Environment: Sources, Fate, Effects and Risk*. Springer, Berlin, 223–244.
- Kümmerer, K., 2008c. *Pharmaceuticals in the environment – a brief summary*. In: Kümmerer, K. (Ed.), *Pharmaceuticals in the Environment: Sources, Fate, Effects and Risk*. Springer, Berlin, 3–22.
- Lalumera, G.M., Calamari, D., Galli, P., Castiglioni, S., Crosa, G., Fanelli, R., 2004. *Preliminary investigation on the environmental occurrence and effects of antibiotics used in aquaculture in Italy*. *Chemosphere* 54 (5), 661–668.
- Lara-Martín, P., González-Mazo, E., Petrovic, M., Barceló, D., Brownawell, B.J., 2014. Occurrence, distribution and partitioning of nonionic surfactants and pharmaceuticals in the urbanized Long Island Sound Estuary (NY). *Mar. Pollut. Bull.* 85 (2), 710 pp., <http://dx.doi.org/10.1016/j.marpolbul.2014.01.022>.
- Le, T.X., Munekage, Y., 2004. Residues of selected antibiotics in water and mud from shrimp ponds in mangrove areas in Viet Nam. *Mar. Pollut. Bull.* 49 (11–12), 922–929.

- Le-Minh, N., Khan, S.J., Drewes, J.E., Stuetz, R.M., 2010. Fate of antibiotics during municipal water recycling treatment processes. *Water Res.* 44, 4295–4323.
- Li, W., Shi, Y., Gao, L., Liu, J., Cai, Y., 2012. Occurrence of antibiotics in water, sediments, aquatic plants, and animals from Baiyangdian Lake in North China. *Chemosphere* 89 (11), 1307–1315, <http://dx.doi.org/10.1016/j.chemosphere.2012.05.079>.
- Liang, X.M., Chen, B., Nie, X., Shi, Z., Huang, X., Li, X., 2013. The distribution and partitioning of common antibiotics in water and sediment of the Pearl River Estuary, South China. *Chemosphere* 92 (11), 1410–1416, <http://dx.doi.org/10.1016/j.chemosphere.2013.03.044>.
- Löffler, D., Ternes, T.A., 2003. Determination of acidic pharmaceuticals, antibiotics and ivermectin in river sediment using liquid chromatography-tandem mass spectrometry. *J. Chromatogr. A* 1021 (1–2), 133–144, <http://dx.doi.org/10.1016/j.chroma.2003.08.089>.
- Luczkiewicz, A., Felis, E., Ziemińska, A., Gnida, A., Kotlarska, E., Olańczuk-Neyman, K., Górska-Surmacz, J., 2013. Resistance of *Escherichia coli* and *Enterococcus* spp. to selected antimicrobial agents present in municipal wastewater. *J. Water Health* 11 (4), 600–612, <http://dx.doi.org/10.2166/wh.2013.130>.
- Luo, Y., Xu, L., Rysz, M., Wang, Y., Zhang, H., Alvarez, P.J., 2011. Occurrence and transport of tetracycline, sulfonamide, quinolone, and macrolide antibiotics in the Haihe River Basin, China. *Environ. Sci. Technol.* 45 (5), 1827–1833, <http://dx.doi.org/10.1021/es104009s>.
- Majka, M., 2010. Development of methods for the isolation of sulfonamides from soils and preliminary analysis of processes of sorption. (MSc thesis). Univ. Gdańsk (in Polish).
- Maszkowska, M., Kotodziejaska, M., Białk-Bielińska, A., Mrozik, W., Kumirska, J., Stepnowski, P., Palavinskas, R., Krüger, O., Kalbe, U., 2013. Column and batch tests of sulfonamide leaching from different types of soil. *J. Hazard. Mater.* 260, 468–474, <http://dx.doi.org/10.1016/j.jhazmat.2013.05.053>.
- McEneff, G., Barron, L., Kelleher, B., Paull, B., Quinn, B., 2014. A year-long study of the spatial occurrence and relative distribution of pharmaceutical residues in sewage effluent, receiving marine waters and marine bivalves. *Sci. Total Environ.* 476–477, 317–326, <http://dx.doi.org/10.1016/j.scitotenv.2013.12.123>.
- Minh, T.B., Leung, H.W., Loi, I.H., Chan, W.H., So, M.K., Mao, J.Q., Choi, D., Lam, J.C., Zheng, G., Martin, M., Lee, J.H., Lam, P.K., Richardson, B.J., 2009. Antibiotics in the Hong Kong metropolitan area: ubiquitous distribution and fate in Victoria Harbour. *Mar. Pollut. Bull.* 58 (7), 1052–1062, <http://dx.doi.org/10.1016/j.marpolbul.2009.02.004>.
- Molander, L., Gerstrand, M., Rudén, C., 2009. WikiPharma – a freely available, easily accessible, interactive and comprehensive database for environmental effect data for pharmaceuticals. *Regul. Toxicol. Pharmacol.* 55 (3), 367–371, <http://dx.doi.org/10.1016/j.yrtph.2009.08.009>.
- Moreno-González, R., Rodríguez-Mozaz, S., Gros, D., Barceló, M., León, V.M., 2015. Seasonal distribution of pharmaceuticals in marine water and sediment from a Mediterranean coastal lagoon (SE Spain). *Environ. Res.* 138, 326–344, <http://dx.doi.org/10.1016/j.envres.2015.02.016>.
- Mutavdžić-Pavlović, D.M., Babić, B., Horvat, A.J.M., Kaštelan-Macan, M., 2007. Sample preparation in analysis of pharmaceuticals. *TrAC-Trends Anal. Chem.* 26 (11), 1062–1875, <http://dx.doi.org/10.1016/j.trac.2007.09.010>.
- Mutavdžić-Pavlović, D.M., Pinušić, T., Periša, M., Babić, S., 2012. Optimization of matrix solid-phase dispersion for liquid chromatography tandem mass spectrometry analysis of 12 pharmaceuticals in sediments. *J. Chromatogr. A* 1258, 1–15, <http://dx.doi.org/10.1016/j.chroma.2012.08.025>.
- Na, G., Fang, X., Cai, Y., Ge, L., Zong, H., Yuan, X., Yao, Z., Zhang, Z., 2013. Occurrence, distribution, and bioaccumulation of antibiotics in coastal environment of Dalian, China. *Mar. Pollut. Bull.* 69 (1–2), 233–237, <http://dx.doi.org/10.1016/j.marpolbul.2012.12.028>.
- Na, G., Gu, J., Ge, L., Zhang, P., Wang, Z., Liu, Ch., Zhang, L., 2011. Detection of 36 antibiotics in coastal waters using high performance liquid chromatography-tandem mass spectrometry. *Chin. J. Oceanol. Limnol.* 29 (5), 1039–1102, <http://dx.doi.org/10.1007/s00343-011-0225-1>.
- Nikolaou, A., Meric, S., Fatta, D., 2007. Occurrence patterns of pharmaceuticals in water and wastewater environments. *Anal. Bioanal. Chem.* 387 (4), 1225–1234, <http://dx.doi.org/10.1007/s00216-006-1035-8>.
- Nödler, K., Voutsas, D., Licha, T., 2014. Polar organic micropollutants in the coastal environment of different marine systems. *Mar. Pollut. Bull.* 85 (1), 50–59, <http://dx.doi.org/10.1016/j.marpolbul.2014.06.024>.
- Pazdro, K., 2004. Persistent organic pollutants in sediments from the Gulf of Gdańsk. *Ann. Environ. Prot.* 6, 63–76.
- Pazdro, K., Borecka, M., Siedlewicz, G., Białk-Bielińska, A., Stepnowski, P., 2016. Analysis of the residues of pharmaceuticals in marine environment: state-of-the-art, analytical problems and challenges. *Curr. Anal. Chem.* 12 (3), 202–226, <http://dx.doi.org/10.2174/1573411012666151009193536>.
- Piekarek-Jankowska, H., 2010. Sediments classification. In: Boletek, J. (Ed.), *Physical, Biological and Chemical Studies on Marine Sediments*, Wydawnictwo Uniwersytetu Gdańskiego, Gdańsk, 287–290, (in Polish).
- Raich-Montiou, J., Folch, J., Compano, R., Granados, M., Prat, M.D., 2007. Analysis of trace sulfonamides in surface water and soil sample by liquid chromatography-fluorescence. *J. Chromatogr. A* 1172 (2), 186–193, <http://dx.doi.org/10.1016/j.chroma.2007.10.010>.
- Ramirez, A.J., Brain, R.A., Usenko, S., Mottaleb, M.A., O'Donnell, J. G., Stahl, L.L., Wathen, J.B., Snyder, B.D., Pitt, J.L., Perez-Hurtado, P., Dobbins, L.L., Brooks, B.W., Chambliss, C.K., 2009. Occurrence of pharmaceuticals and personal care products in fish: results of a national pilot study in the United States. *Environ. Toxicol. Chem.* 28 (12), 2587–2597, <http://dx.doi.org/10.1897/08-561.1>.
- Sacher, F., Lange, F.T., Brauch, H.J., Blankenhorn, I., 2001. Pharmaceuticals in groundwaters: analytical methods and results of a monitoring program in Baden-Württemberg, Germany. *J. Chromatogr. A* 938 (1–2), 199–210, [http://dx.doi.org/10.1016/S0021-9673\(01\)01266-3](http://dx.doi.org/10.1016/S0021-9673(01)01266-3).
- Sarmah, A., Meyer, M., Boxall, B., 2006. A global perspective on the use, sales, exposure pathways, occurrence, fate and effects of veterinary antibiotics (VAs) in the environment. *Chemosphere* 65 (5), 725–759.
- Shepard, E.P., 1954. Nomenclature based on sand-silt-clay relation. *J. Sedim. Petrol.* 24 (3), 151–158.
- Shi, H., Yang, Y., Liu, M., Yan, C., Yue, H., Zhou, J., 2014. Occurrence and distribution of antibiotics in the surface sediments of the Yangtze Estuary and nearby coastal areas. *Mar. Pollut. Bull.* 83 (1), 317–323, <http://dx.doi.org/10.1016/j.marpolbul.2014.04.034>.
- Siedlewicz, G., Pazdro, K., Borecka, M., Kornowska, K., Białk-Bielińska, A., Stepnowski, P., 2014. Determination of tetracyclines residues in the Gulf of Gdansk (Southern Baltic Sea) sediments using a tandem solid-phase extraction with liquid chromatography coupled with tandem mass spectrometry. In: Zieliński, T., Pazdro, K., Dragan-Górska, A., Weydman, A. (Eds.), *Insights on Environmental Changes: Where the World is Heading*. Springer International Publishing, Switzerland, 33–48.
- Stewart, M., Olsen, G., Hickey, C.W., Ferreira, B., Jelić, A., Petrović, M., Barceló, D., 2014. A survey of emerging contaminants in the estuarine receiving environment around Auckland, New Zealand. *Sci. Total Environ.* 468–469, 202–210, <http://dx.doi.org/10.1016/j.scitotenv.2013.08.039>.
- Sukul, P., Spiteller, M., 2006. Sulfonamides in the environment as veterinary drugs. *Rev. Environ. Contam. Toxicol.* 187, 67–101, [http://dx.doi.org/10.1007/0-387-32885-8\\_2](http://dx.doi.org/10.1007/0-387-32885-8_2).

- Szefer, P., Glasby, G.P., Pempkowiak, J., Kaliszan, R., 1995. Extraction studies of heavy-metal pollutants in surficial sediments from the southern Baltic Sea off Poland. *Chem. Geol.* 120 (1–2), 111–126, [http://dx.doi.org/10.1016/0009-2541\(94\)00103-F](http://dx.doi.org/10.1016/0009-2541(94)00103-F).
- Taverniers, I., De Loose, M., Bockstaele, E., 2004. Trends in quality in the analytical laboratory. II. Analytical method validation and quality assurance. *TrAC-Trends Anal. Chem.* 23 (8), 535–551, <http://dx.doi.org/10.1016/j.trac.2004.04.001>.
- Thiele-Bruhn, S., 2003. Pharmaceutical antibiotics compounds in soils – a review. *J. Plant Nutr. Soil Sci.* 166 (2), 145–167, <http://dx.doi.org/10.1002/jpln.200390023>.
- Tolls, J., 2001. Sorption of veterinary pharmaceuticals in soils: a review. *Environ. Sci. Technol.* 35 (17), 3397–3406, <http://dx.doi.org/10.1021/es0003021>.
- Van De Steene, J.C., Lambert, W.E., 2008. Comparison of matrix effects in HPLC-MS/MS and UPLC-MS/MS analysis of nine basic pharmaceuticals in surface waters. *J. Am. Soc. Mass Spectrom.* 19 (5), 713–718, <http://dx.doi.org/10.1016/j.jasms.2008.01.013>.
- Vazquez-Roig, P., Andreu, V., Blasco, C., Picó, Y., 2012. Risk assessment on the presence of pharmaceuticals in sediments, soils and waters of the Pego-Oliva Marshlands (Valencia, eastern Spain). *Sci. Total Environ.* 440, 24–32, <http://dx.doi.org/10.1016/j.scitotenv.2012.08.036>.
- Weigel, S., Kuhlmann, J., Hühnerfuss, H., 2002. Drugs and personal care products as ubiquitous pollutants: occurrence and distribution of clofibric acid, caffeine and DEET in the North Sea. *Sci. Total Environ.* 295 (1–3), 131–141, [http://dx.doi.org/10.1016/S0048-9697\(02\)00064-5](http://dx.doi.org/10.1016/S0048-9697(02)00064-5).
- Wille, K., De Brabander, H.F., De Wulf, E., Van Caeter, P., Janssen, C.R., Vanhaecke, L., 2012. Coupled chromatographic and mass spectrometric techniques for the analysis of emerging pollutants in the aquatic environment. *TrAC-Trends Anal. Chem.* 35, 87–108, <http://dx.doi.org/10.1016/j.trac.2011.12.003>.
- Wille, K., Noppe, H., Verheyden, K., Vanden Bussche, J., De Wulf, E., Van Caeter, P., Janssen, C.R., De Brabander, H.F., Vanhaecke, L., 2010. Validation and application of an LC-MS/MS method for the simultaneous quantification of 13 pharmaceuticals in seawater. *Anal. Bioanal. Chem.* 397 (5), 1797–1808, <http://dx.doi.org/10.1007/s00216-010-3702-z>.
- Wise, R., 2002. Antimicrobial resistance: priorities for action. *J. Antimicrob. Chemother.* 49 (4), 585–596, <http://dx.doi.org/10.1093/jac/49.4.585>.
- Xu, J., Zhang, Y., Zhou, C., Guo, C., Wang, D., Du, P., Luo, Y., Wan, J., Meng, W., 2014. Distribution, sources and composition of antibiotics in sediment, overlying water and pore water from Taihu Lake, China. *Sci. Total Environ.* 497–498, 267–273, <http://dx.doi.org/10.1016/j.scitotenv.2014.07.114>.
- Yang, J.F., Ying, G.G., Zhao, J.L., Tao, R., Su, H.C., Chen, F., 2010. Simultaneous determination of four classes of antibiotics in sediments of the Pearl Rivers using RRLC-MS/MS. *Sci. Total Environ.* 408 (16), 424–432, <http://dx.doi.org/10.1016/j.scitotenv.2010.03.049>.
- Yang, Y., Fu, J., Peng, H., Hou, L., Liu, M., Zhou, J.L., 2011. Occurrence and phase distribution of selected pharmaceuticals in the Yangtze Estuary and its coastal zone. *J. Hazard. Mater.* 190 (1–3), 588–596, <http://dx.doi.org/10.1016/j.jhazmat.2011.03.092>.
- Zhang, R., Tang, J., Li, J., Cheng, Z., Chaemfa, C., Liu, D., Zheng, Q., Song, M., Luo, C., Zhang, G., 2013. Occurrence and risks of antibiotics in the coastal aquatic environment of the Yellow Sea, North China. *Sci. Total Environ.* 450–451, 197–204, <http://dx.doi.org/10.1016/j.scitotenv.2013.02.024>.
- Zhang, R., Zhang, G., Zheng, Q., Tang, J., Chen, Y., Xu, W., Zou, Y., Chen, X., 2012. Occurrence and risks of antibiotics in the Laizhou Bay, China: impacts of river discharge. *Ecotoxicol. Environ. Safe.* 80, 208–215, <http://dx.doi.org/10.1016/j.ecoenv.2012.03.002>.
- Zhou, L., Ying, G., Zhao, J., Yang, J., Wang, L., Yang, B., Liu, S., 2011. Trends in the occurrence of human and veterinary antibiotics in the sediments of the Yellow River, Hai River and Liao River in northern China. *Environ. Pollut.* 159 (7), 1877–2188, <http://dx.doi.org/10.1016/j.envpol.2011.03.034>.



Available online at [www.sciencedirect.com](http://www.sciencedirect.com)

ScienceDirect

journal homepage: [www.elsevier.com/locate/oceano](http://www.elsevier.com/locate/oceano)



SHORT COMMUNICATION

# Position, swimming direction and group size of fin whales (*Balaenoptera physalus*) in the presence of a fast-ferry in the Bay of Biscay<sup>☆</sup>

Ana S. Aniceto<sup>a,b,\*</sup>, JoLynn Carroll<sup>b,1</sup>, Michael J. Tetley<sup>c,2</sup>,  
Cock van Oosterhout<sup>a,3</sup>

<sup>a</sup> Department of Biological Sciences, University of Hull, Kingston upon Hull, UK

<sup>b</sup> ARCEX (Research Centre of Arctic Petroleum Exploration), UiT The Arctic University, Department of Geology, Tromsø, Norway

<sup>c</sup> Whale and Dolphin Conservation Society (WDCS), Critical Habitats and MPAs Programme, Chippenham, UK

Received 23 September 2014; accepted 19 February 2016

Available online 12 March 2016

## KEYWORDS

Fin whales;  
Ship strikes;  
Behavior

**Summary** We analyze group size, swimming direction and the orientation of fin whales relative to a fast ferry in the Bay of Biscay. Fin whale groups ( $\geq 3$  individuals) were on average closer to the vessel than single individuals and pairs ( $F_{1,114} = 4.94$ ,  $p = 0.028$ ) and were more often observed within a high-risk angle ahead of the ferry (binomial probability:  $p = 7.60 \times 10^{-11}$ ). Also, small groups tend to swim in the opposite direction (heading of  $180^\circ$ ) of the ferry at the starboard side (binomial test:  $p = 6.86 \times 10^{-5}$ ) and at the portside (binomial test:  $p = 0.0156$ ). These findings provide valuable information to improve shipping management procedures in areas at high risk for collisions.

© 2016 Institute of Oceanology of the Polish Academy of Sciences. Production and hosting by Elsevier B.V. This is an open access article under the CC BY-NC-ND license (<http://creativecommons.org/licenses/by-nc-nd/4.0/>).

<sup>☆</sup> This project was performed under ORCA's "Go Large" campaign (funded by the Esmée Fairbairn Foundation) that aimed to raise public awareness regarding collisions between ships and whales. Dr. Cock van Oosterhout is funded by ELSA, the Earth and Life Systems Alliance. Dr. Michael Tetley, acting Coordinator for the Atlantic Research Coalition (ARC) of cetacean ferry surveys, is funded by the John Ellerman Foundation and ORCA. This article was prepared for submission while A.S. Aniceto was engaged in a PhD program associated with the research Centre for Arctic Exploration (ARCEX), funded by the Research Council of Norway (project #228107) together with 10 academic and 8 industry partners.

\* Corresponding author at: Akvaplan-niva AS, Fram Centre, 9296 Tromsø, Norway. Tel.: +47 77 75 03 73.

E-mail address: [asa@akvaplan.niva.no](mailto:asa@akvaplan.niva.no) (A.S. Aniceto).

<sup>1</sup> Present address: Akvaplan-niva AS, Fram Centre, 9296 Tromsø, Norway.

<sup>2</sup> Present address: Montague House, Gilesgate, Durham DH1 2LF, UK.

<sup>3</sup> Present address: School of Environmental Sciences, University of East Anglia, Norwich Research Park, Norwich NR4 7TJ, UK.

Peer review under the responsibility of Institute of Oceanology of the Polish Academy of Sciences.



<http://dx.doi.org/10.1016/j.oceano.2016.02.002>

0078-3234/© 2016 Institute of Oceanology of the Polish Academy of Sciences. Production and hosting by Elsevier B.V. This is an open access article under the CC BY-NC-ND license (<http://creativecommons.org/licenses/by-nc-nd/4.0/>).

## 1. Introduction

During recent decades there has been a rapid expansion in shipping traffic with a corresponding increased impact to biodiversity at a global scale (Flagella and Abdulla, 2005; IUCN, 2009; Panigada et al., 2008). For large vertebrates, such as cetaceans, ships pose a risk in terms of discharges that may release contaminants into the ocean, noise pollution that can affect marine mammal distributions and behavior, and direct physical harm caused by collisions (Evans, 2003; Laist et al., 2001; Mayol et al., 2008; McGilivray et al., 2009; Panigada and Leaper, 2010). Previous studies have shown the impact of ship-related events on the distribution and behavior of many cetacean species, including North Atlantic right whales (*Eubalaena glacialis*), fin whales (*Balaenoptera physalus*) and sperm whales (*Physeter macrocephalus*) (Evans, 2003; Laist et al., 2001; Mayol et al., 2008; McGilivray et al., 2009; Panigada and Leaper, 2010; Panigada et al., 2008).

The vulnerability of a given species to ship traffic mainly depends on their behavior and on the spatial-temporal characteristics of shipping traffic in a given area (David, 2002; Evans, 2003). For North Atlantic right whales, mortalities due to ship collisions have led to a significant decline in their populations (Jensen and Silber, 2004; Kraus et al., 2005; Laist et al., 2001; Nowacek et al., 2004). It has been hypothesized that the observed slow recovery in population numbers for these whales is due to the cumulative effects of several anthropogenic factors (Jensen and Silber, 2004; Kraus et al., 2005; Laist et al., 2001; Nowacek et al., 2004).

On a global scale, the fin whale is the most commonly recorded species to collide with ships (David, 2002; Laist et al., 2001). Yet contrary to other baleen whales, fin whales are fast swimmers (Laist et al., 2001; Panigada et al., 2006). This suggests that fin whales have the physical capability to avoid colliding with ships; albeit, if the vessel is detected in sufficient time for the whale to change course and/or swim away from the vessel. The high occurrence of these accidents may be related to aspects of this species' behavior rather than swimming speed. For example, cetaceans engaging in activities such as feeding or breeding have been shown to be less responsive to vessel approach (Dolman et al., 2006; Richardson et al., 1995).

The Bay of Biscay is navigated by fast ferries that connect England, France and Spain (Kiszka et al., 2007; ORCA, 2013). We performed a monthly monitoring program in the Bay of Biscay on board a commercial fast ferry in order to understand behavioral patterns of fin whales in relation to ships. Our aim was to identify factors that affect the risk of collisions between fin whales and fast ferries, considering that fin whales are the most recorded species hit by ships (David, 2002; Laist et al., 2001).

The Bay of Biscay is an ideal location for this study because it is an area with both high diversity and abundance of cetacean species and heavy ship traffic. Fin whales are present in the Bay mainly during the spring and summer months. In this study, groups of four observers performed monthly monitoring of fin whales (group size, swimming direction, orientation and positions) from a 21 m high steering house. Through this assessment of the data collected during the surveys, we examine the behavior of fin whales

and evaluate the implications for future management decisions in relation to ship collisions.

## 2. Material and methods

We study group size, swimming direction, orientation and positions of 228 fin whales relative to a commercial fast ferry with routine operations in the Bay of Biscay. Opportunistic observations were made on board of the *Brittany Ferries'* largest ferryboat – *MV Pont-Aven* (184.60 m) during the Portsmouth & Plymouth to Santander crossing (Fig. 1). No observations were performed during crossings over the English Channel given the low abundance of fin whales in those areas (ORCA, 2013). Given an average travel speed of 25 knots and the large size of the ship, the *MV Pont-Aven* ferry is among the group of vessels that has a high probability of involvement in severe or fatal ship–whale strike events (Laist et al., 2001; Panigada et al., 2006; Vanderlaan and Taggart, 2007).

Data on group size, swimming direction, orientation and positions was collected during monthly surveys from August 2006 to October 2008. Each monthly survey was conducted for 3 consecutive days (representing a return trip Plymouth-Santander-Portsmouth). Surveys were carried out from dawn to dusk from a 21.75 m high steering house, in sea states of 4 or less (based on the Beaufort Sea State table). Observations collected during winter months (November to March) were not analyzed due to the scarcity of data. In winter, fin whales are not present in the Bay of Biscay as they migrate to more southern locations. The study generated data for a total of 39 survey days.

Groups of fin whales were highly conspicuous even at a far distance. The data recorded for each sighting of an individual or group of whales included date, time of the day (GMT), GPS coordinates, distance, group size, angle at which animals were spotted and their heading (using an angle board – 0° to 360°) (see for example Littaye et al., 2004). Observations were recorded along a linear transect between 45°56.3'N–4°29.6'W and 43°41.2'N–3°49.4'W. Following the suggestions of Weinrich et al. (2010), in that detection of cetaceans is enhanced by the presence of trained and dedicated observers, the observation team consisted of four trained observers positioned on the navigation bridge. No observations were collected between 90° and 270° due to access restrictions on the navigation bridge. The search for cetaceans was therefore limited to scanning ahead of the ship (9° to either side of the bow). Scanning was performed using the naked eye and binoculars while species identification and distance measurements were performed with binoculars (Steiner® reticle binoculars of 7x50).

Perception bias (bias due to observer's inability to detect an animal when it is present) can influence the amount of data acquired during surveys. Perception bias by observers is due, for example, to long observation times and insufficient training. Although bias by observers cannot be ruled out completely in studies of marine mammals, several precautions were taken in the present study to minimize it. Firstly, all observations were made within a 4 km distance of the ship. Given the height of the navigation bridge, this distance was also the visible range to the horizon, which was estimated to be around 10 km (ORCA, 2013). In addition,

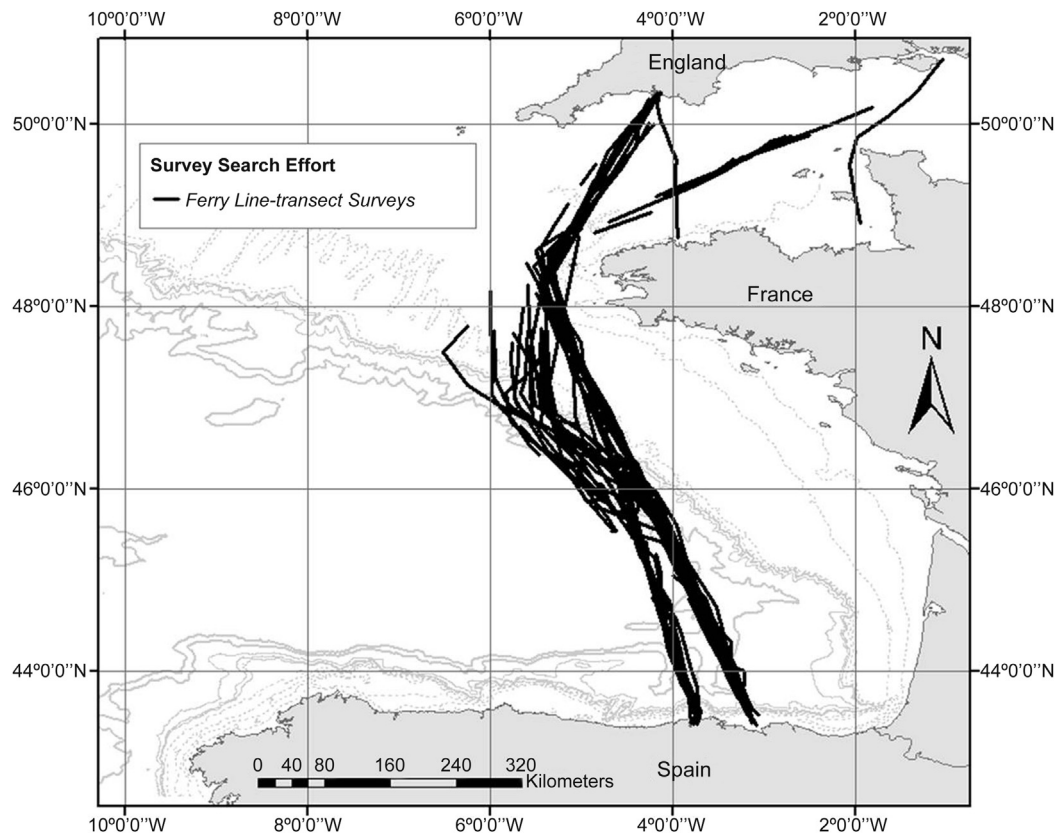


**Figure 1** Survey effort of transects performed in the Bay of Biscay. Survey effort of transects between England (top) and Spain (bottom), crossing the Continental Shelf (200 m) to the Gascogne Gulf (4000 m).

the observers changed positions every 30 min, and observations were terminated after 4–5 h to avoid fatigue-related bias.

A General Linear Model (GLM) was formulated to analyze the relationship between whales and the response variable, distance from the ship. The variables, observer and presence/absence of calves, were included in the model as random factors. Covariates in the GLM were date, time of day and group size. In addition to the GLM, binomial tests were performed on the variables swimming direction (heading) and angle of identification (orientation) of whales relative to ship's orientation. Orientation measurements were made at first surfacing, while heading measurements were recorded as the angle between the first and second time the whale was observed surfacing. Heading measurements were recorded among four values ( $0^\circ$ , on the ferry route;  $90^\circ$ , starboard;  $180^\circ$ , opposite the ship route;  $270^\circ$ , portside). All statistical tests were conducted using Minitab 12.1.

### 3. Results

A total of 228 fin whales (in 129 groups) were observed along an estimated total transect length of 4537 km surveyed during this study. We analyzed which factors explained significant variation in the animals' distance to the ship using a GLM. No significant variation was explained by the observer ( $F_{12,114} = 0.72$ ,  $p = 0.734$ ), presence/absence of calves ( $F_{1,114} = 0.97$ ,  $p = 0.327$ ) and time of day

( $F_{1,114} = 0.36$ ,  $p = 0.551$ ). However, the group size did explain significant variation ( $F_{1,114} = 4.94$ ,  $p = 0.028$ ), with large groups of fin whales ( $N \geq 3$  individuals) being recorded significantly closer to the ship than small groups (i.e. pairs and singletons). Furthermore, whereas the headings of large groups were random relative to the ship (binomial test:  $p = 0.109$ ), headings of small groups appeared not to be random (Fig. 2). Closer inspection of the data showed that small groups tended to swim in the opposite direction (heading of  $180^\circ$ ) of the ferry at the starboard side (18 out of 33 observations, binomial test:  $p = 6.86 \times 10^{-5}$ ) and at the portside (26 of the 38 whales, binomial test:  $p = 0.0156$ ). As a result, the distance between these small groups of whales and the ferry generally decrease during surveys. Fin whale sightings recorded at the front starboard side (between  $0^\circ$  and  $45^\circ$ ;  $N = 107$ ) are similar to the number of sightings made at the front portside (between  $270^\circ$  and  $360^\circ$ ;  $N = 116$ ) (binomial test:  $p = 0.296$ ) (Fig. 2). However, significantly more individuals were observed in the quadrant in front of the ship's bow ( $315\text{--}360^\circ$  and  $0\text{--}45^\circ$ ;  $N = 169$ ) than in the remaining quadrants of the port ( $270\text{--}15^\circ$ ) and starboard ( $45\text{--}90^\circ$ ) sides combined ( $N = 54$ ) (binomial probability:  $p = 7.60 \times 10^{-11}$ ).

### 4. Discussion

In this 26-month study of fin whale behavior, we examined orientation (position relative to a Bay of Biscay commercial

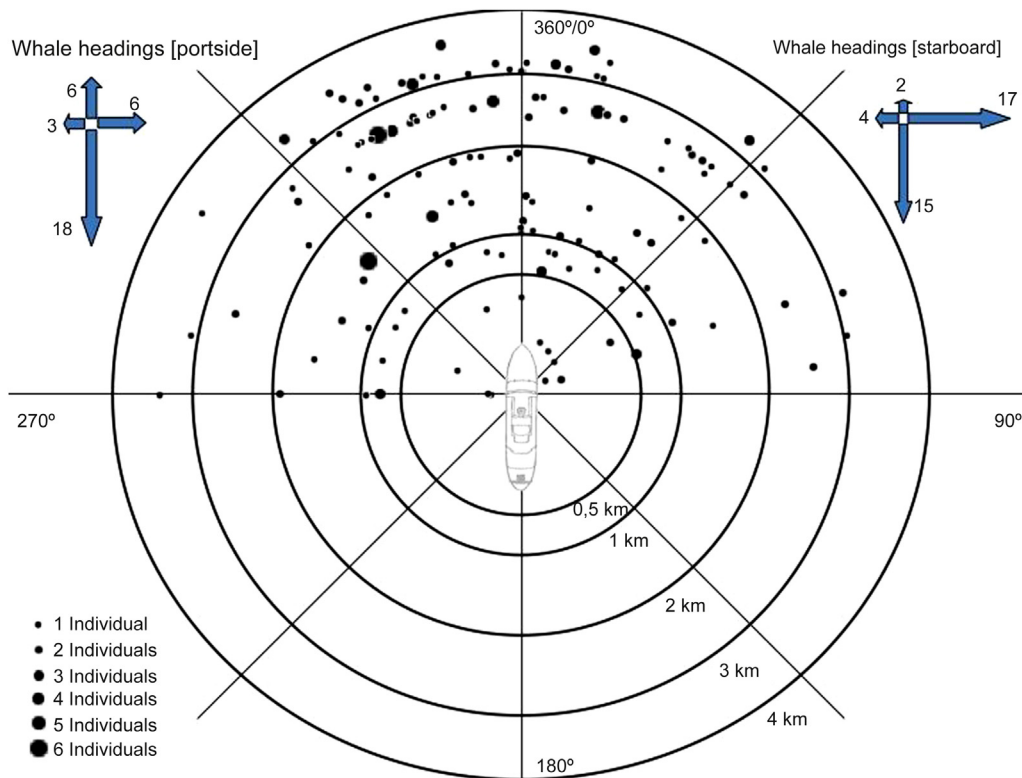


**Figure 2** Fin whale sightings around *MV Pont-Aven*. The position of fin whales (dots) and heading (block arrows) in relation to the position of the ferry during surveys in the Bay of Biscay from August 2006 to October 2008.

fast ferry), group size and swimming direction (heading). We examine possible factors leading to the observed patterns and discuss the implications for risk reduction of collisions with ships. The results of this study provide insight on fin whale behavior (orientation, group size and swimming direction) and how information generated through this study may be further developed to support shipping and whale conservation management decisions.

#### 4.1. Orientation

The heading of small groups towards the oncoming ship was found not to be random. This suggests that the animals are aware of the presence of the ship and as a result alter their swimming routes. Previous studies on the difference of detections between dedicated observers and ship operators has shown that operators have shorter reaction times in detecting whales in the vicinity of the vessel (Weinrich et al., 2010). At high speed the ability to detect and subsequently avoid whales at distance is thus further hindered. This, together with the possibility for animals to cross the vessels' path creates situations of increased risk of collision. The assistance of whale observers during ferry operations and speed reduction could help in reducing such risk (Panigada et al., 2006; Weinrich et al., 2010).

Additionally, in this study significantly more animals were recorded in the quadrant in front of the ship's bow (from 315–360° and 0–45°), ( $N = 169$ ) than on either side (270–315° and 45–90°) ( $N = 54$ ). We cannot exclude that

observers had a greater tendency to survey the sea straight ahead, however, the bow of large vessels can create an acoustic shadow, making vessel sounds indistinguishable from background environmental noise (Gerstein et al., 2002, 2009). This can limit the whales' capabilities of detecting oncoming vessels and explain why there were significantly more sightings in the front of the bow.

#### 4.2. Group size

Our data indicate that large groups of fin whales ( $\geq 3$  individuals) in the Bay of Biscay remain significantly closer to a ferry compared to small groups (single individuals or pairs of individuals). This finding is in accordance with previous studies showing that whales in active groups have a reduced attentiveness, and as a result, are less likely to respond to the presence of a ship. The resulting lack of awareness of nearby vessels may be due to masking of sensory cues (David, 2002; Jahoda et al., 1996; Richardson et al., 1995), or alternatively less vigilant state in accordance with the "group-size" effect (Elgar, 1989). Cetaceans engaged in biologically important activities, such as feeding have been shown to be less responsive and may not be able to detect environmental sounds (Dolman et al., 2006; Panigada et al., 2006). Given that generally, fin whales are found in pairs or traveling individually and that fin whales are present in the Bay of Biscay for feeding purposes, it is possible that groups detected in this location are indeed conducting collective foraging or socializing, which will thus further hinder their

abilities to be vigilant of their surroundings. Other explanations for this reduced attentiveness include the effect of noise propagating from larger vessels such as tankers and container ships. Noise may also impact a cetacean's sensory cues (McKenna et al., 2012) putting them at greater risk for ship strikes (McKenna et al., 2012). The fact that large groups in this study were found to be significantly closer to the ship than small groups is therefore consistent with previous studies on masking effects and whale proximity to vessels (David, 2002; Jahoda et al., 1996; Richardson et al., 1995).

#### 4.3. Swimming direction

Swimming direction was measured as the heading of an animal or animals relative to the ferry. Unlike large groups, small groups showed headings that were significantly different from a random distribution, and tended to swim in opposite direction of the movement of the ferry. We interpret these observations as further evidence that fin whale swimming directions may be influenced by the presence of the ferry. This corroborates previous work in the Mediterranean Sea, that documented interruptions in feeding activities by fin whales in the presence of vessels (Jahoda et al., 2003). Though changes in behavior were not documented in the present study, the fact that fin whales in the Bay of Biscay tend to swim in the opposite direction relative to the ferry's path (maintaining a parallel position), suggests that this finding may be related to a behavioral response. However, additional (unidentified) biological factors such as migratory patterns or prey availability may also play an important role in the swimming direction of fin whales relative to ferries. Though further work is necessary to explore this hypothesis, these results highlight the need for telemetry and disturbance studies to provide more detail in fin whale behavioral reactions to large vessels.

#### 4.4. Management implications

Several authors have suggested that ferry speeds are highly relevant for assessing collision risk (Carrillo and Ritter, 2010; Gende et al., 2011; IWC, 2009; Mayol et al., 2008; McGilivray et al., 2009; Panigada and Leaper, 2010; Panigada et al., 2006; Silber et al., 2010; Van Waerebeek and Leaper, 2007; Weinrich, 2004). The present study suggests that this risk is also warranted for fin whales in the Bay of Biscay. Hence, we reiterate suggestions made in the literature that speed reduction is an important management measure that should be taken into consideration by shipping authorities (Panigada et al., 2006; Vanderlaan and Taggart, 2007).

#### Acknowledgements

This study is part of a long-term observation project of fin whale presence and behavior in the vicinity of a fast ferry. We thank Richard C. Bull from the Charity Organisation Cetacea (ORCA) who provided the monthly survey data on cetaceans. We would also like to thank Brittany Ferries for the use of *MV Pont-Aven* as the research platform for this study. We thank three anonymous reviewers for their valuable comments which have greatly improved the manuscript. Dylan Walker, at the time of the study also a member of

the science board of ORCA, provided additional guidance and orientation of protocol during the surveys.

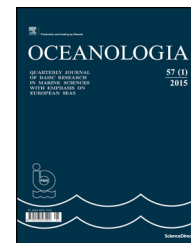
#### References

- Carrillo, M., Ritter, F., 2010. Increasing numbers of ship strikes in the Canary Islands: proposals for immediate action to reduce risk of vessel–whale collisions. *J. Cetacean Res. Manage.* 11 (2), 131–138.
- David, L., 2002. Disturbance to Mediterranean cetaceans caused by vessel traffic. In: Notarbartolo di Sciara, G. (Ed.), *Cetaceans of the Mediterranean and Black Seas: State of Knowledge and Conservation Strategies*. Report to the ACCOBAMS Secretariat, Monaco, February 2002, Section 11, 21 pp.
- Dolman, S., Williams-Grey, V., Asmutis-Silvia, R., Isaac, S., 2006. *Vessel collisions and cetaceans: what happens when they don't miss the boat*. WDCS Sci. Rep., Chippenham, UK, 25 pp.
- Elgar, M.A., 1989. Predator vigilance and group size in mammals and birds: a critical review of the empirical evidence. *Biol. Rev. Camb. Philos. Soc.* 64 (1), 13–33, <http://dx.doi.org/10.1111/j.1469-185X.1989.tb00636.x>.
- Evans, P.G.H., 2003. Shipping as a possible source of disturbance to cetaceans in the ASCOBANS region. In: ASCOBANS 4th Meeting of the Parties. Agenda Item 9.2: Interactions with shipping, Document MOP4/Doc. 17(S).
- Flagella, M.M., Abdulla, A.A., 2005. Ship ballast water as a main vector of maritime introductions in the Mediterranean Sea. *WMU J. Marit. Affairs* 4 (1), 95–104, <http://dx.doi.org/10.1007/BF03195066>.
- Gende, S.M., Hendrix, A.N., Harris, K.R., Eichenlaub, B., Nielsen, J., Pyare, S., 2011. A Bayesian approach for understanding the role of ship speed in whale–ship encounters. *Ecol. Appl.* 21 (6), 2232–2240, <http://dx.doi.org/10.1890/10-1965.1>.
- Gerstein, E.R., Blue, J.E., Forsythe, S.E., 2002. Ship strikes and whales: shadows, mirrors and paradoxes. *J. Acoust. Soc. Am.* 112 (5), 2430, <http://dx.doi.org/10.1121/1.4779972>.
- Gerstein, E.R., Gerstein, L.A., Forsythe, S.E., 2009. Parametric projectors protecting marine mammals from vessel collisions. *J. Acoust. Soc. Am.* 125 (4), 2689, <http://dx.doi.org/10.1121/1.4784279>.
- IUCN, 2009. *Risks from Maritime Traffic to Biodiversity in the Mediterranean Sea: Identification Issues and Possible Responses*. IUCN Centre for Mediterranean Cooperation, Malaga, Spain, 26 pp.
- IWC, 2009. *Ship Strikes Working Group: Fourth Progress Report to the Conservation Committee*. In: 61st Annual Meeting of the IWC Report, IWC/61/CC11 Agenda item 4.1. International Whaling Commission, 11 pp.
- Jahoda, M., Airoldi, S., Azzellino, A., Biassoni, N., Borsani, J.F., Cianfanelli, L., Lauriano, G., Notarbartolo di Sciara, G., Panigada, S., Vallini, C., Zanardelli, M., 1996. Behavioural reactions to biopsy-darting on Mediterranean fin whales. In: Evans, P.G.H. (Ed.), *European Res. Cetac.* 10. Proceedings of the Tenth Annual Conference of the European Cetacean Society. 11–13 March 1996, Lisbon, Portugal, 43–47, 34 pp.
- Jahoda, M., Lafortuna, C.L., Biassoni, N., Almirante, C., Azzellino, A., Panigada, S., Zanardelli, M., Notarbartolo di Sciara, G., 2003. Mediterranean fin whales (*Balaenoptera physalus*) response to small vessels and biopsy sampling assessed through passive tracking and timing of respiration. *Mar. Mammal Sci.* 19 (1), 96–110, <http://dx.doi.org/10.1111/j.1748-7692.2003.tb01095.x>.
- Jensen, A.S., Silber, G.K., 2004. Large whale ship strike database. US Department of Commerce, NOAA Technical Memorandum. NMFS-OPR, 37 pp.
- Kiszka, J., Macleod, K., Van Canneyt, O., Walker, D., Ridoux, V., 2007. Distribution, encounter rates, and habitat characteristics of toothed cetaceans in the Bay of Biscay and adjacent waters

- from platform-of-opportunity data. ICES J. Mar. Sci. 64 (5), 1033–1043, <http://dx.doi.org/10.1093/icesjms/fsm067>.
- Kraus, S.D., Brown, M.W., Caswell, H., Clark, C.W., Fujiwara, M., Hamilton, P.K., Kenney, R.D., Knowlton, A.R., Landry, S., Mayo, C. A., McLellan, W.A., Moore, M.J., Nowacek, D.P., Pabst, D.A., Read, A.J., Rolland, R.M., 2005. North Atlantic right whales in crisis. *Science* 309 (5734), 561–562, <http://dx.doi.org/10.1126/science.1111200>.
- Laist, D.W., Knowlton, A.R., Mead, J.G., Collet, A.S., Podesta, M., 2001. Collisions between ships and whales. *Mar. Mammal Sci.* 17 (1), 35–75, <http://dx.doi.org/10.1111/j.1748-7692.2001.tb00980.x>.
- Littaye, A., Gannier, A., Laran, S., Wilson, J.P.F., 2004. The relationship between summer aggregation of fin whales and satellite-derived environmental conditions in the northwestern Mediterranean Sea. *Rem. Sens. Environ.* 90 (1), 44–52, <http://dx.doi.org/10.1016/j.rse.2003.11.017>.
- Mayol, P., Capoulade, F., Beaubrun, P., 2008. Limiting the risks of collision between commercial vessels and large cetaceans. In: REPCET (Real time plotting of cetaceans) – Presentation of the System. Souffleurs d'Ecume – Scientific Association for the Protection of Nature, 6 pp.
- McGilivray, P.A., Schwehr, K.D., Fall, K., 2009. Enhancing AIS to improve whale–ship collision avoidance and maritime security. In: MTS/IEEE OCEANS Conference Proceedings, Biloxi, USA, 1–8.
- McKenna, M.F., Ross, D., Wiggins, S.M., Hildebrand, J.A., 2012. Underwater radiated noise from modern commercial ships. *J. Acoust. Soc. Am.* 131 (1), 92–103, <http://dx.doi.org/10.1121/1.3664100>.
- Nowacek, D.P., Johnson, M.P., Tyack, P.L., 2004. North Atlantic right whales (*Eubalaena glacialis*) ignore ships but respond to alerting stimuli. *Proc. Biol. Sci.* 271 (1536), 227–231, <http://dx.doi.org/10.1098/rspb.2003.2570>.
- ORCA, 2013. Large whales of the Bay of Biscay and whale strike risk. Organisation Cetacea Report Ship Strike Tool Kit, 16 pp.
- Panigada, S., Leaper, R., 2010. Ship strikes in the Mediterranean Sea: assessment and identification of conservation and mitigation measures. Report to the Scientific Committee of the International Whaling Commission SC/61/BC2. International Whaling Commission, 5 pp.
- Panigada, S., Pavan, G., Borg, J.A., Galil, B.S., Vallini, C., 2008. Biodiversity impacts of ship movement, noise, grounding and anchoring. In: Abdulla, A., Linden, O. (Eds.), *Maritime Traffic Effects on Biodiversity in the Mediterranean Sea: Review of Impacts, Priority Areas and Mitigation Measures*. IUCN Centre for Mediterranean Cooperation, Malaga, Spain, 10–41.
- Panigada, S., Pesante, G., Zanardelli, M., Capoulade, F., Gannier, A., Weinrich, M.T., 2006. Mediterranean fin whales at risk from fatal ship strikes. *Mar. Pollut. Bull.* 52 (10), 1287–1298, <http://dx.doi.org/10.1016/j.marpolbul.2006.03.014>.
- Richardson, W.J., Greene Jr., C.R., Malme, C.I., Thomson, D.H., 1995. Zones of noise influence. In: Richardson, W.J., Greene, Jr., C.R., Malme, C.I., Thomson, D.H. (Eds.), *Marine Mammals and Noise*. Academic Press, Elsevier, San Diego, CA, 325–386, <http://dx.doi.org/10.1016/B978-0-08-057303-8.50013-6>.
- Silber, G.K., Slutsky, J., Bettridge, S., 2010. Hydrodynamics of a ship/whale collision. *J. Exp. Mar. Biol. Ecol.* 391 (1–2), 10–19, <http://dx.doi.org/10.1016/j.jembe.2010.05.013>.
- Van Waerebeek, K., Leaper, R., 2007. Report from the IWC Vessel Strike Data Standardization Group. IWC Document SC/59/BC12. International Whaling Commission, Anchorage, May 2007, 6 pp.
- Vanderlaan, A.S.M., Taggart, C.T., 2007. Vessel collisions with whales: the probability of lethal injury based on vessel speed. *Mar. Mammal Sci.* 23 (1), 144–156, <http://dx.doi.org/10.1111/j.1748-7692.2006.00098.x>.
- Weinrich, M.T., 2004. A review of worldwide collisions between whales and fast ferries. Report to the Scientific Committee of the International Whaling Commission SC/56/BC9. International Whaling Commission, 8 pp.
- Weinrich, M., Pekarčík, C., Tackaberry, J., 2010. The effectiveness of dedicated observers in reducing risks of marine mammal collisions with ferries: a test of the technique. *Mar. Mammal Sci.* 26 (2), 460–470, <http://dx.doi.org/10.1111/j.1748-7692.2009.00343.x>.

Available online at [www.sciencedirect.com](http://www.sciencedirect.com)

ScienceDirect

journal homepage: [www.elsevier.com/locate/oceano](http://www.elsevier.com/locate/oceano)

## SHORT COMMUNICATION

# The inflow in the Baltic Proper as recorded in January–February 2015

Daniel Rak\*

*Institute of Oceanology, Polish Academy of Sciences, Sopot, Poland*

Received 18 November 2015; accepted 1 April 2016

Available online 22 April 2016

## KEYWORDS

Inflow;  
Baltic Sea;  
Salinity;  
Temperature;  
Stagnation

**Summary** Inflowing saline waters of the Major Baltic Inflow (MBI) in 2014 were recorded in the Baltic Proper in January 2015. After 12 years of stagnation, this inflow brought highly saline (about 20) waters into the Bornholm Basin. As in the previous inflow in January 2003, saltwater moved in the near-bottom layer with a current speed of approx.  $25 \text{ cm s}^{-1}$ . This paper presents data collected in January and February 2015 and compares them to earlier records from 2000 to 2014. © 2016 Institute of Oceanology of the Polish Academy of Sciences. Production and hosting by Elsevier Sp. z o.o. This is an open access article under the CC BY-NC-ND license (<http://creativecommons.org/licenses/by-nc-nd/4.0/>).

## 1. Introduction

Since the 1980s stagnation without any inflow has become the usual state in the deep waters of the Baltic Sea (Dahlin et al., 1993; Jakobsen, 1995; Liljebladh and Stigebrandt, 1996; Matthäus and Lass, 1995). However, extreme non-periodic saltwater inflow events, exchanging water between the North Sea and the Baltic, occur at different intervals, ranging

from a few years to about a decade (Franck et al., 1987; Matthäus and Franck, 1992). The occurrence of inflows depends mainly on atmospheric forcing, and over 90% of such events take place during late autumn (Matthäus and Franck, 1992). Until the 1980s the longest period without an inflow event was about 3 years; thereafter, however, a decade elapsed between the major inflows observed in 1983, 1993 and 2003 (Franck et al., 1987; Piechura and Beszczyńska-Möller, 2004). Already over 11 years had passed since the last such event in January 2003. Measurements carried out by the Institute of Oceanology, Polish Academy of Sciences (IO PAN) in January 2015 revealed record-high salinities in the deep layers of the Baltic Proper.

Large inflows ( $100\text{--}250 \text{ km}^3$ ), usually carrying highly saline waters (salinity 17–23 PSU), represent the most important mechanism by which the deep waters of the Baltic Sea are displaced and renewed (Franck et al., 1987; Matthäus and Franck, 1992). The inflows propagate over the bottom but still substantially mix with the overlying surface water (Burchard et al., 2005; Stigebrandt and Gustafsson, 2003).

*E-mail address:* [rak@iopan.gda.pl](mailto:rak@iopan.gda.pl).

\* Correspondence to: Institute of Oceanology, Polish Academy of Sciences, Powstańców Warszawy 55, P.O. Box 148, 81-712 Sopot, Poland. Tel.: +48 58 7311906; fax: +48 58 551 21 30.

*E-mail address:* [rak@iopan.gda.pl](mailto:rak@iopan.gda.pl).

Peer review under the responsibility of Institute of Oceanology of the Polish Academy of Sciences.



Production and hosting by Elsevier

<http://dx.doi.org/10.1016/j.oceano.2016.04.001>

0078-3234/© 2016 Institute of Oceanology of the Polish Academy of Sciences. Production and hosting by Elsevier Sp. z o.o. This is an open access article under the CC BY-NC-ND license (<http://creativecommons.org/licenses/by-nc-nd/4.0/>).

Small inflows (10–20 km<sup>3</sup>) are insufficient to displace the deep waters and, because of their much lower density, are eventually trapped between the halocline and bottom water on their pathway (Matthäus, 2006; Stigebrandt, 2001). Large and medium-sized inflows are extremely important to the ecosystem, because they oxygenate the deep basins of the Baltic Sea (Matthäus and Lass, 1995).

The main aim of this paper is to describe the recent saltwater inflow from the North Sea into the Baltic Proper as recorded after passing the Danish Straits and the Arkona Basin.

## 2. Material and methods

### 2.1. Study area

The high-resolution hydrographic transects used in this paper were obtained using a towed profiling CTD (Conductivity, Temperature, Depth) system. The main transect (Fig. 1) ran along the axis of deep basins, starting from the Arkona Basin (AB), through the Bornholm Deep (BD) and the Stupsk Furrow (SF), and ending in the Gdańsk Deep (GD).

Since 2000 repeated hydrographic measurements, focused on monitoring the origin of waters flowing into the southern Baltic, have been made in different seasons (at least 4 times per year) during regular cruises of *r/v 'Oceania'* (Fig. 2). This paper focuses on measurements made during two cruises in 2015 (on January 5–9 and February 23–27).

### 2.2. Field data

The profiling system consisted of a CTD probe (Seabird 49) suspended in a steel frame towed on a cable behind the vessel (Paka et al., 2006). To ensure measurements of high quality, the temperature and conductivity sensors were calibrated annually by the manufacturer. The suspension

system maintained the probe in a horizontal position during profiling, the steel frame protected it from mechanical damage, while a chain fixed below the frame reduced the risk of bottom contact. To obtain a profile, the CTD system was lowered and raised between the surface and bottom by releasing or hauling in a towing cable. The horizontal resolution of about 200–500 m was obtained at a constant ship speed of approx. 4 knots for a basin with a typical depth of 60–120 m. With the CTD probe operating at a frequency of 10 Hz, the vertical resolution of the towed measurements was about 30 measurements per metre. Since 2013, high-resolution profiles of dissolved oxygen concentration have been obtained along the hydrographic transects with the Rinko-I sensor mounted on the towed system.

The velocity and direction of sea currents were recorded continuously using the vessel-mounted Acoustic Doppler Current Profiler (RDI ADCP 150 kHz), set up with a cell width of 4 m.

Data provided by the International Council of the Exploration of the Sea (ICES) were used to extend the Bornholm Deep distribution of temperature and salinity. ICES Oceanographic database, Extractions January 1978–December 1995; Hydrological data. ICES, Copenhagen.

## 3. Results

During the recent inflow, the temperature distribution along the main transect was slightly different from the typical winter situation in the last decade (Rak and Wieczorek, 2012) in that the waters in the Bornholm Deep and Stupsk Furrow in January 2015 were slightly warmer (about 10°C) than the surrounding ones (Fig. 3). This warm layer was about 10 m thick in the Bornholm Deep and almost twice as thick in the Stupsk Furrow. In the Stupsk Furrow the warm layer was formed by the waters previously occupying the deep layer of the Bornholm Deep, which were raised to 50 m depth and in consequence were able to pass over the Stupsk Sill at the

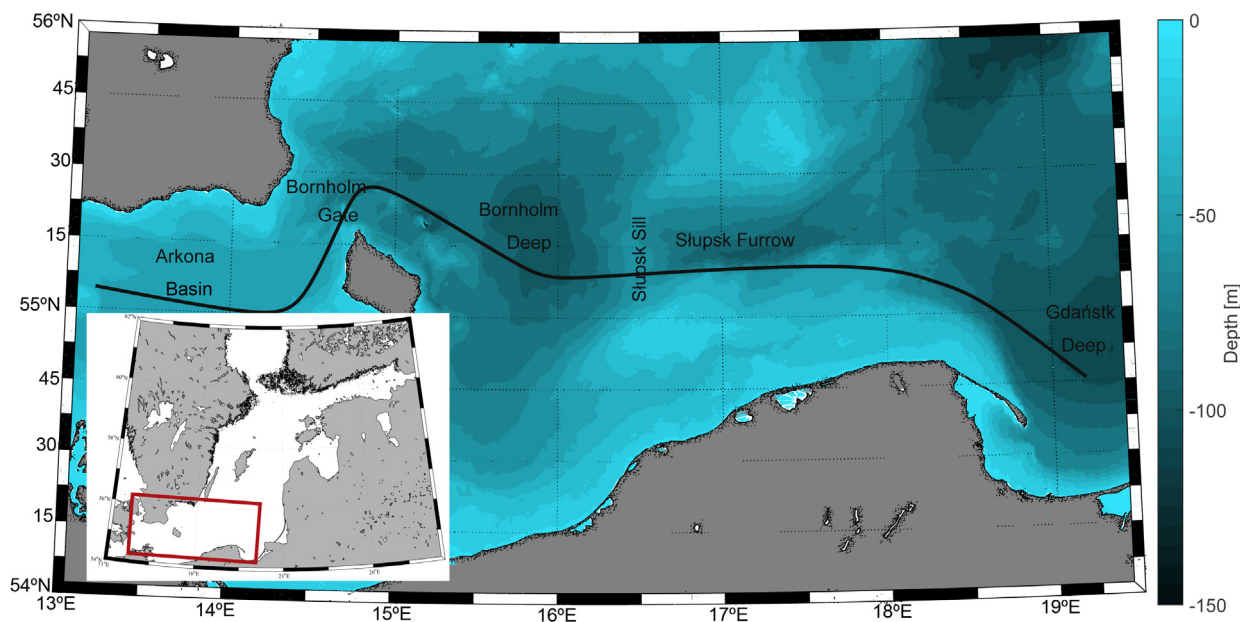


**Figure 1** Location of measurements. The main hydrographic transect along the deep basins of the Baltic Proper (2000–2014) is shown as a black line.

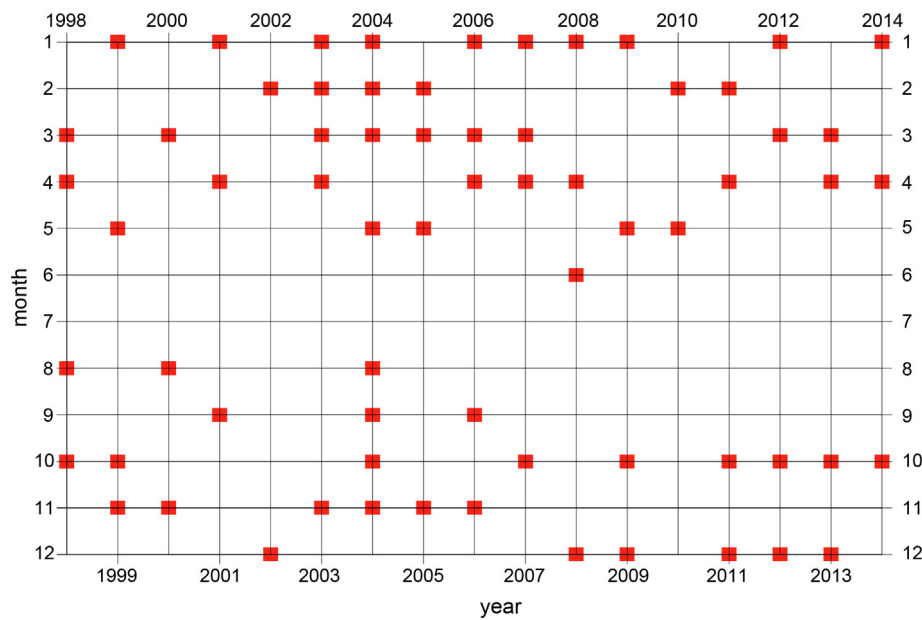


Figure 2 Distribution of r/v Oceania cruises in 1998–2014.

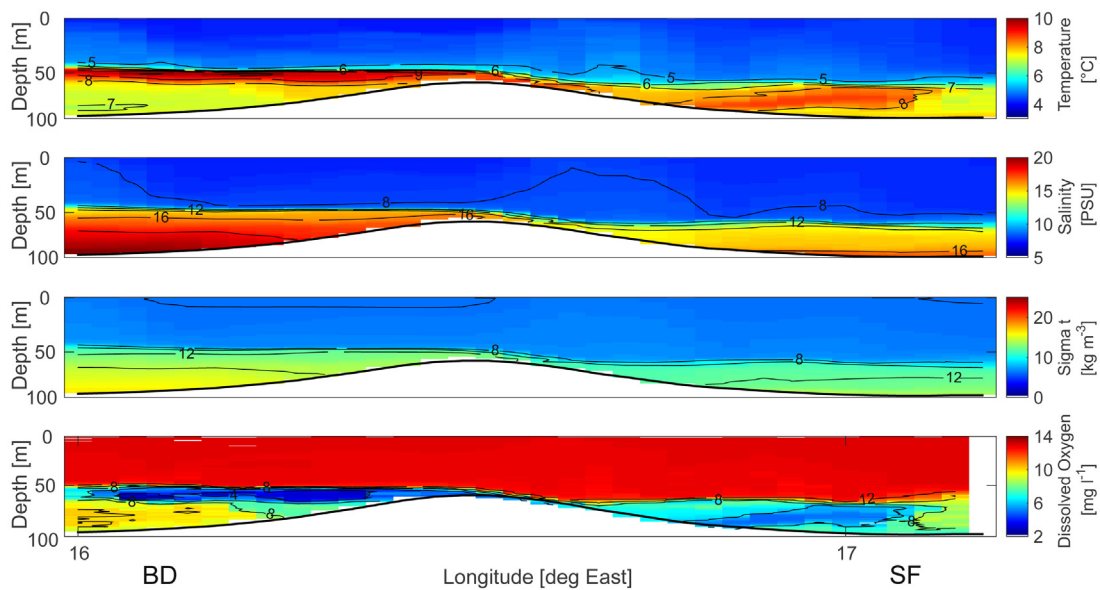


Figure 3 Distribution of temperature, salinity, density and oxygen concentration on the main transect along the axis of the deep basins in the Stupsk Sill area on January 5–9, 2015. BD, the Bornholm Deep; SF, the Stupsk Furrow.

thermocline depth. The thermocline observed along the main section in the Bornholm Basin and Stupsk Furrow was shifted down to a depth of 45–60 m, resulting in an isothermal upper layer with a temperature of about 5°C. Most likely this can be ascribed to the coupled effect of thermal convection due to the positive (upward) heat flux and wind forcing.

The salinity distribution in the upper layers of the Bornholm Deep and Stupsk Furrow was similar to the situation observed in earlier years (Rak and Wiczorek, 2012) with a slightly higher salinity of about 8 PSU measured in relatively small areas (Fig. 3). At the same time, strong rises in salinity to about 20 and 17 PSU in the Bornholm Deep and Stupsk Furrow, respectively, were found in the layer beneath the

halocline owing to the recent inflow that had carried extremely saline waters into both basins.

The water originating from the major inflow in 2014 was dense enough to propagate over the bottom layer of the Bornholm Deep, as shown by the density distribution measured in January 2015 (Fig. 3). When the inflow entered the Bornholm Basin, it partially mixed with local waters and pushed them to the halocline depth. After reaching the Stupsk Sill the inflow waters continued over the bottom and crossed the sill into the Stupsk Furrow.

Oxygen concentrations of about 12 mg l<sup>-1</sup> were recorded in the surface mixed layer (Fig. 3), while in the near-bottom layer of the Bornholm Basin values were lower by

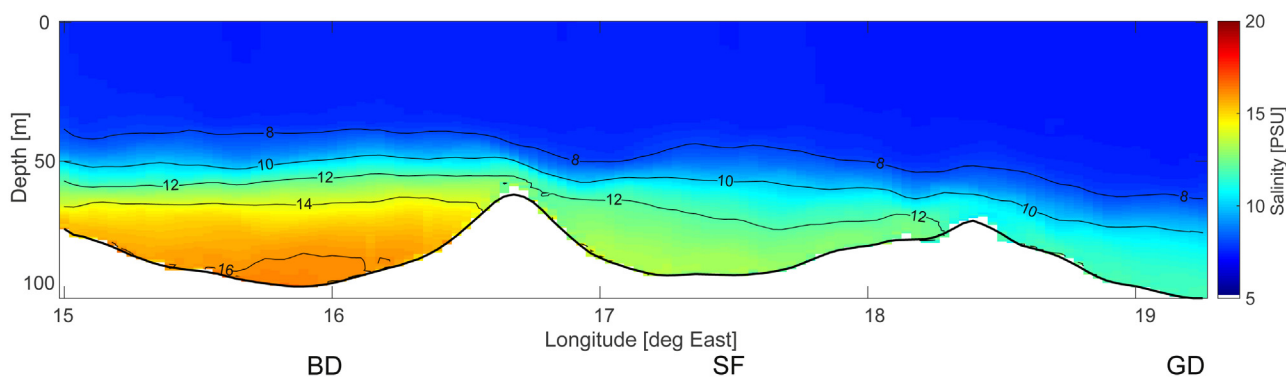


**Figure 4** Mean salinity on the main transect, represented by the average of nine cruises in October–November in 2000–2013. BD, the Bornholm Deep; SF, the Stupsk Furrow; GD, the Gdańsk Deep.

$4 \text{ mg l}^{-1}$ . The Bornholm Deep anoxic waters recorded in January were pushed up towards the halocline and, on crossing the Stupsk Sill, mixed with the inflow waters. There was a difference in near-bottom oxygen concentration of about  $6 \text{ mg l}^{-1}$  between the areas to the west and east of the Stupsk Furrow.

The salinity distribution in January 2015 was compared to the long-term mean salinity, represented by an average of 9 transects in October–November in 2000–2013 (Fig. 4). The mean salinity distribution in the Baltic Proper was characterized by a slightly deeper halocline in the Bornholm Deep and generally lower salinities than those measured during the 2014 inflow. In the mean situation the halocline is about 5 m deeper than during the recent inflow, which prevents the more saline waters from flowing over the Stupsk Sill. The salinities of the surface layers in the Bornholm Deep and Stupsk Furrow are similar. In the Baltic Proper the largest differences between the mean salinity and the salinity (up to ca 4 PSU) measured during the recent inflow were found in the layer beneath the halocline in the Bornholm Deep and Stupsk Furrow.

The steeper temperature gradient between the surface and bottom layer measured in February 2015 (Fig. 5a) can most probably be attributed to the coupled effect of thermal convection, wind mixing and subsequent cooling of the upper layer. The temperature at the thermocline depth in the Bornholm Deep has remained high since January.

The saline waters that passed through the Stupsk Furrow were recorded in the Gdańsk Deep in February (Fig. 5a). Extremely high salinities of about 20, 16 and 14 PSU were recorded in the Bornholm Basin, Stupsk Furrow and Gdańsk Deep, respectively, after dense and highly saline water originating from the 2014 inflow propagated eastwards along the axis of the main basins. The upward shift of the halocline observed in the Gdańsk Deep was very probably due to the prevailing cyclonic circulation in the basin, or an effect of internal wave.

In February 2015 the near-bottom oxygen concentration was slightly lower in the Bornholm Basin (by approx.  $2 \text{ mg l}^{-1}$ ) than the value measured in January (Fig. 5a). However, the oxygen concentration in the previously anoxic bottom layer increased by  $4 \text{ mg l}^{-1}$  as a result of mixing processes. Two months later, the water layer beneath the halocline in the Stupsk Furrow had become largely homogeneous. Despite the

higher near-bottom oxygen concentration during the inflow, anoxic waters persisted in the Gdańsk Deep until February.

For the measured currents (Fig. 5b), the surface and near-bottom layers were blanked (8 m from the surface and 18% of the total depth from the bottom) owing to the removal of side-lobe effects. In general, moderate current speeds of about  $30 \text{ cm s}^{-1}$  along the axis of the deep basins prevailed along the most of the transect. Current speeds up to  $25 \text{ cm s}^{-1}$  with associated velocity error of  $0.4 \text{ cm s}^{-1}$  were measured in the layer beneath the halocline in the Bornholm Gate. Flows were also faster at the base of the eastern, leeward side of the Stupsk Sill.

Fig. 6 shows the temporal variability of the mean temperature and salinity in the Bornholm Basin, averaged in the layer below 70 m. The mean salinity recorded in the Bornholm Basin in January 2015 had a record-high value in the time series combined from IO PAN data from repeated cruises and the ICES database. Compared to the inflow in February 2003, the maximum salinity observed in the Bornholm Basin in 2014 was 1 PSU higher. The temperature during the recent inflow was similar to that recorded during other early winter cruises (January).

#### 4. Discussion

The inflow of extremely saline waters from the North Sea started to pass through the Bornholm Gate in December 2014 (Mohrholz et al., 2015), bringing more saline waters into the deeper parts of the Baltic Proper. That extreme event created strong vertical and horizontal gradients of salinity and temperature in the studied areas of the southern Baltic Sea. The water from this inflow crossing the Bornholm Basin had a mean salinity of about 20 PSU, a mean temperature of about  $8^\circ\text{C}$ , a mean potential density of  $17 \text{ kg m}^{-3}$  and a mean oxygen concentration of  $10 \text{ mg l}^{-1}$ . The salinities recorded in January 2015 were the highest in the 16-year long IO PAN record of repeated measurements in the Baltic Proper (Rak and Wieczorek, 2012). In the Bornholm Deep the saltwater influx mixed with and raised the adjacent waters, creating a layer of warm, anoxic waters beneath the halocline. This water body, previously occupying the Bornholm Deep, had originated from a minor inflow in August 2014 (Anderson, 2014). Therefore, the water pushed into the Stupsk Furrow

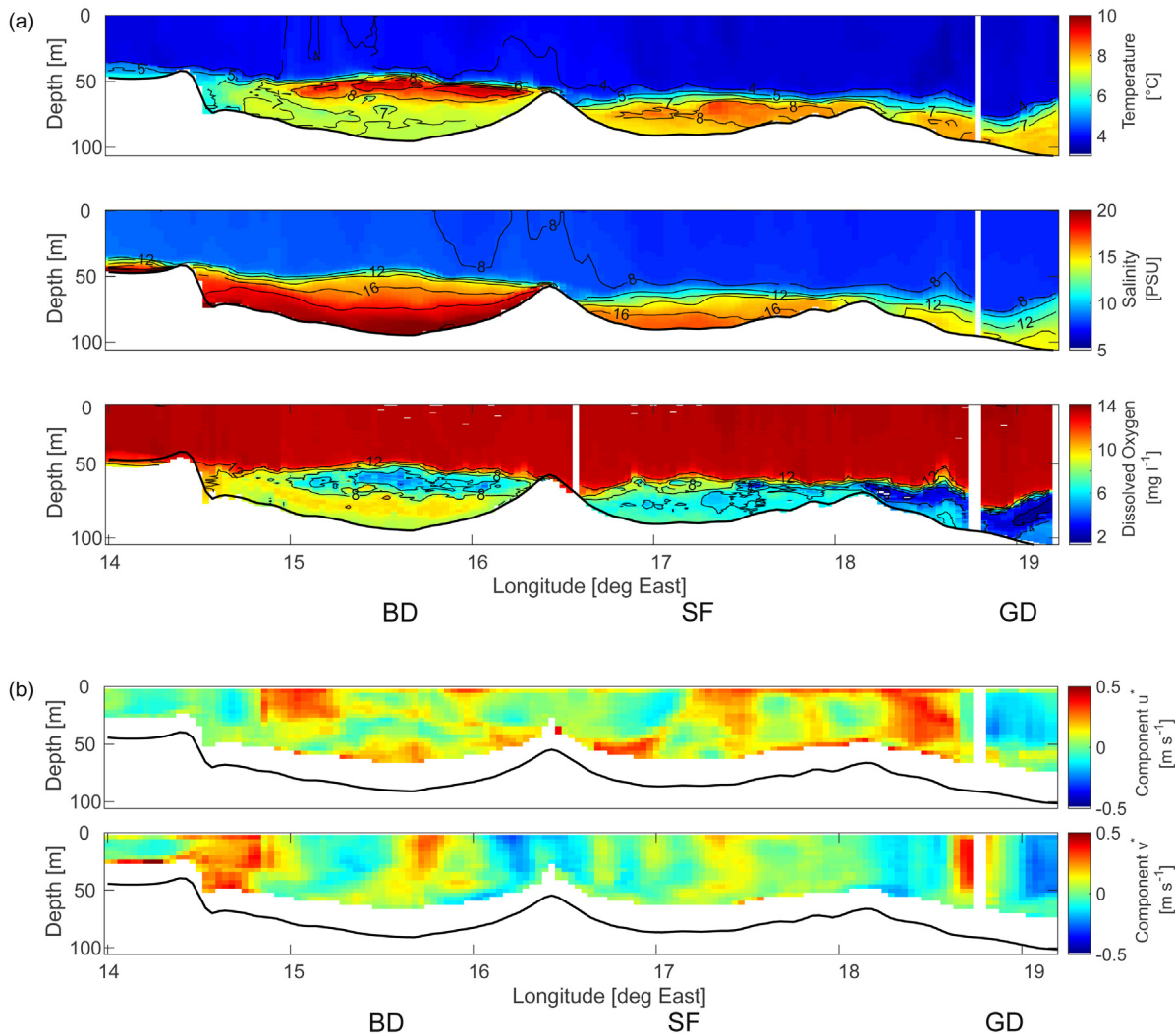


**Figure 5** (a) Distribution of temperature, salinity and oxygen concentration on the main transect along the axis of the deep basins in the Baltic Proper on February 23–27, 2015. The vertical white lines represent missing data. (b) The distribution of flow velocity components ( $u^*$  parallel and  $v^*$  perpendicular to the profile) on the main transect along the axis of the deep basins in the Baltic Proper on February 23–27, 2015. The positive values of  $u^*$  indicate direction of flow component along the transect (Fig. 1) from the West to East. The vertical white lines represent missing data. BD, the Bornholm Deep; SF, the Stupsk Furrow; GD, the Gdańsk Deep.

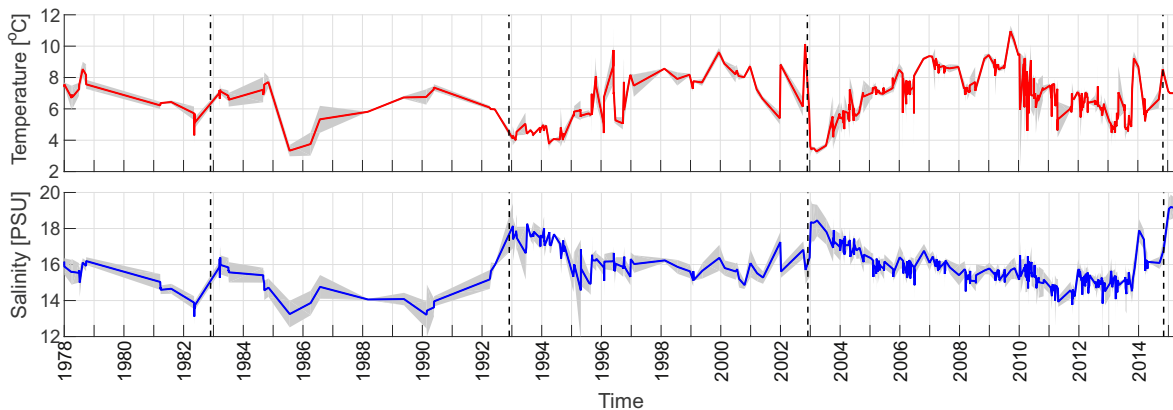


**Figure 6** Temperature and salinity averaged between 14.77 and 16.3°E in the layer below 70 m in the Bornholm Basin in 1978–2015. The mean (line) and standard deviation (shaded area) of the temperature and salinity are based on individual cruises. The IO PAN data were extended by data from the ICES database ([www.ices.dk/](http://www.ices.dk/)).

was warmer by 4°C and less saline by 3 PSU than the water in the Bornholm Deep originating from the 2015 inflow.

As during the previous inflow, the inflowing water moved over the sea bed with a speed of at least 25 cm s<sup>-1</sup>. As shown by different authors (Feistel et al., 2003; Fischer and Matthäus, 1996; Franck et al., 1987; Matthäus and Franck, 1992) the barotropic inflows are characterized by:

- forced mainly by sea level differences;
- caused by constant strong westerly winds, preceded by easterly winds;
- the inflowing waters are usually rich in oxygen;
- carry significant amounts of salt up to about 2 Gt (Lass and Mohrholz, 2003; Mohrholz et al., 2006);
- they occur mainly in autumn and winter.

Until the 1980s the average interval between successive inflows was about 3 years, but this period extended to 10 years in 1983–2003. In the last two decades large barotropic inflows have been less frequent, whereas weak and moderate inflows have taken place more often (Meier, 2006). The last two inflows in 1993 and 2003 are well-studied phenomena, both by observation (the 1993 inflow: Jakobsen, 1995; Matthäus and Lass, 1995; the 2003 inflow: Feistel et al., 2003; Piechura and Beszczyńska-Möller, 2004) and by hydrodynamic modelling (the 1993 inflow: Andrejev et al. 2002; Huber et al., 1994; Lehmann, 1995; Meier and Döscher, 2003; the 2003 inflow: Lehmann et al., 2004; Meier et al., 2004). The extensive (ca 200 km<sup>3</sup>) inflow in 2003 of extremely low temperature (about 1–2°C) reached all basins in the Baltic Proper (Feistel et al., 2003). Ventilation of the Karlsö Deep (south-west of Gotland) took place 2 years after the inflow event, while the Bornholm and Eastern Gotland Basins were already returning to stagnation (Feistel et al., 2006). According to the latest observations (Mohrholz et al., 2015) the 2014 MBI, the total oxygen transport into the Baltic Sea was estimated at 2.04 × 10<sup>6</sup> t. Waters with an oxygen concentration of about 10 mg l<sup>-1</sup> were recorded in the Bornholm Deep in January 2015, but 2 months later the oxygen concentration was 2 mg l<sup>-1</sup> less. The amount of oxygen pushed into the Gdańsk Deep in February was not yet sufficient to eliminate anoxia from the near bottom layer. The near bottom waters of the Gotland Deep were sufficiently well oxygenated to eliminate hydrogen sulphide in March 2015 (<http://www.io-warnemuende.de/suboxic-and-anoxic-regions-in-the-baltic-sea-deep-waters.html>).

## 5. Summary

- In January 2015, after 12 years of stagnation, highly saline and well-oxygenated waters, originating from the major inflow in 2014, were found in the Bornholm Deep, Stupsk Furrow and Gdańsk Deep.
- Record-high salinities in the entire 16-year long period of IO PAN repeated observations were recorded in the Bornholm Basin (about 20 PSU). In 2015 the salinity in the Bornholm Basin was 1 PSU higher compared to the previous inflow in 2003.
- In January 2015 the older waters, previously occupying the deep layer of the Bornholm Deep, were raised to 50 m

depth and in consequence were able to pass over the Stupsk Sill at the thermocline depth.

- Instantaneous values of the current component along the inflow axis of about 25 cm s<sup>-1</sup> were measured in the inflowing waters propagating over the sea bed in the Bornholm Deep.
- The concentration of dissolved oxygen of about 10 mg l<sup>-1</sup>, measured in January 2015 in the deep layer of the Bornholm Deep, decreased after 1 month by 1 mg l<sup>-1</sup>.
- The amount of oxygen pushed into in the Gdańsk Deep in February 2015 was not yet sufficient to eliminate the anoxia in the near-bottom layer.

## References

- Anderson, L., 2014. Cruise report from R/V Aranda week 32, 2014, [http://www.smhi.se/en/publications/cruise-reports-from-the-marine-monitoring?page=1&query=&filter=auto\\_time\\_years%3A2014](http://www.smhi.se/en/publications/cruise-reports-from-the-marine-monitoring?page=1&query=&filter=auto_time_years%3A2014) (accessed: 08. 03.2016).
- Andrejev, O., Myrberg, K., Mälkki, P., Perttilä, M., 2002. Three-dimensional modelling of the main Baltic inflow in 1993. *Environ. Chem. Phys.* 24 (3), 156–161.
- Burchard, H., Lass, H.U., Mohrholz, V., Umlauf, L., Sellschopp, J., Fiekas, V., Bolding, K., Arneborg, L., 2005. Dynamics of medium-intensity dense water plumes in the Arkona Basin, Western Baltic Sea. *Ocean Dynam.* 55 (5), 391–402, <http://dx.doi.org/10.1007/s10236-005-0025-2>.
- Dahlin, S., Fonselius, H., Sjöberg, B., 1993. The changes of the hydrographic conditions in the Baltic proper due to 1993 major inflow to the Baltic Sea. In: ICES Statutory Meeting. Dublin, ICES, 1993/C:58, 14 pp.
- Feistel, R., Nausch, G., Hagen, E., 2006. Unusual Baltic inflow activity in 2002–2003 and varying deep-water properties. *Oceanologia* 48 (5), 21–35.
- Feistel, R., Nausch, G., Matthäus, W., Hagen, E., 2003. Temporal and spatial evolution of the Baltic deep water renewal in spring 2003. *Oceanologia* 45 (4), 623–642.
- Fischer, H., Matthäus, W., 1996. The importance of the Drogden Sill in the Sound for major Baltic inflows. *J. Mar. Syst.* 9 (3–4), 137–157.
- Franck, H., Matthäus, H., Sammler, R., 1987. Major inflows of saline water into the Baltic Sea during the present century. *Gerlands Beitr. Geophys.* 96 (6), 517–531.
- Huber, K., Kleine, E., Lass, H.U., Matthäus, W., 1994. The major Baltic inflow in January 1993 – measurements and modeling results. *Dt. Hydrogr. Z.* 46, 103–114.
- Jakobsen, F., 1995. The major inflow to the Baltic Sea during January 1993. *J. Mar. Syst.* 6 (3), 227–240.
- Lass, H.U., Mohrholz, V., 2003. On dynamics and mixing of inflowing salt water in the Arkona Sea. *J. Geophys. Res.* 108 (C2), 3042, <http://dx.doi.org/10.1029/2002JC001465>.
- Lehmann, A., 1995. A three-dimensional baroclinic eddy-resolving model of the Baltic Sea. *Tellus A* 47, 1013–1031, <http://dx.doi.org/10.1034/j.1600-0870.1995.00206.x>.
- Lehmann, A., Lorenz, P., Jacob, D., 2004. Modelling the exceptional Baltic Sea inflow events in 2002–2003. *Geophys. Res. Lett.* 31 (21), L21308, <http://dx.doi.org/10.1029/2004GL020830>.
- Liljebadh, B., Stigebrandt, A., 1996. Observations of deepwater flow into the Baltic Sea. *J. Geophys. Res.* 101 (C4), 8895–8911.
- Matthäus, W., 2006. The history of investigation of salt water inflow into the Baltic Sea – from the early beginning to recent results. *Mar. Sci. Rep.* 65, 1–74.
- Matthäus, W., Franck, H., 1992. Characteristics of major Baltic inflows – a statistical analysis. *Cont. Shelf Res.* 12 (12), 1375–1400.

- Matthäus, W., Lass, H.U., 1995. The recent salt inflow into the Baltic Sea. *J. Phys. Oceanogr.* 25 (2), 280–286.
- Meier, H.E.M., 2006. Baltic Sea climate in the late twenty-first century: a dynamical downscaling approach using two global models and two emission scenarios. *Clim. Dynam.* 27 (1), 39–68, <http://dx.doi.org/10.1007/s00382-006-0124-x>.
- Meier, H.E.M., Broman, B., Kjellström, E., 2004. Simulated sea level in past and future climates of the Baltic Sea. *Climate Res.* 27 (1), 59–75, <http://dx.doi.org/10.3354/cr027059>.
- Meier, H.E.M., Döscher, R., 2003. A multiprocessor coupled ice-ocean model for the Baltic Sea: application to salt inflow. *J. Geophys. Res.* 108 (C8), 3273, <http://dx.doi.org/10.1029/2000JC000521>.
- Mohrholz, V., Dutz, J., Kraus, G., 2006. The impacts of exceptionally warm summer inflow events on the environmental conditions in the Bornholm Basin. *J. Mar. Syst.* 60 (3–4), 285–301.
- Mohrholz, V., Naumann, M., Nausch, G., Krüger, S., Gräwe, U., 2015. Fresh oxygen for the Baltic Sea – an exceptional saline inflow after a decade of stagnation. *J. Mar. Syst.* 148, 152–166, <http://dx.doi.org/10.1016/j.jmarsys.2015.03.005>.
- Paka, V., Golenko, N., Korzh, A., 2006. Distinctive features of water exchange across the Stupsk Sill (a full-scale experiment). *Oceanologia* 48 (S), 37–54.
- Piechura, J., Beszczyńska-Möller, A., 2004. Inflow waters in the deep regions of the southern Baltic Sea – transport and transformations. *Oceanologia* 46 (1), 113–141.
- Rak, D., Wieczorek, P., 2012. Variability of temperature and salinity over the last decade in selected regions of the southern Baltic Sea. *Oceanologia* 54 (3), 339–354, <http://dx.doi.org/10.5697/oc.54-3.339>.
- Stigebrandt, A., 2001. Physical oceanography of the Baltic Sea. In: *A Systems Analysis of the Baltic Sea*. Springer-Verlag, Berlin, Heidelberg, 19–74.
- Stigebrandt, A., Gustafsson, B., 2003. The response of the Baltic Sea to climate change – theory and observations. *J. Sea Res.* 49 (4), 243–256.